INFORMATION TO USERS

This manuscript has been reproduced from the microfilm master. UMI films the text directly from the original or copy submitted. Thus, some thesis and dissertation copies are in typewriter face, while others may be from any type of computer printer.

The quality of this reproduction is dependent upon the quality of the copy submitted. Broken or indistinct print, colored or poor quality illustrations and photographs, print bleedthrough, substandard margins, and improper alignment can adversely affect reproduction.

In the unlikely event that the author did not send UMI a complete manuscript and there are missing pages, these will be noted. Also, if unauthorized copyright material had to be removed, a note will indicate the deletion.

Oversize materials (e.g., maps, drawings, charts) are reproduced by sectioning the original, beginning at the upper left-hand corner and continuing from left to right in equal sections with small overlaps.

Photographs included in the original manuscript have been reproduced xerographically in this copy. Higher quality 6" x 9" black and white photographic prints are available for any photographs or illustrations appearing in this copy for an additional charge. Contact UMI directly to order.

UMI®

ELECTRON TRANSFER WITHIN VARIOUS ORGANOMETALLIC SPECIES

By

C. ED WHITTLE

A DISSERTATION PRESENTED TO THE GRADUATE SCHOOL OF THE
UNIVERSITY OF FLORIDA IN PARTIAL FULLFILLMENT OF THE
REQUIREMENTS FOR THE DEGREE OF DOCTOR OF PHILOSOPHY

UNIVERSITY OF FLORIDA

2001

UMI Number: 3009980

UMI®

Dedicated to my parents with gratitude for their love and support

ACKNOWLEDGEMENTS

This dissertation represents the work that I have accomplished while at the University of Florida. It reflects my efforts in the lab while here at UF. It also demonstrates that with a lot of support and guidance, a good-ol'-boy from Kentucky who typically tries to find the easiest, least stressful road (the path with the lowest activation barrier) who often oversimplifies many things, can produce quality work. Within this short acknowledgement, I hope to thank some of the people who have pushed me and given me the support and guidance I truly needed to get through this.

First, I cannot thank my organic chemistry professor, advisor and friend at Western Kentucky University enough. Dr. Robert Holman was the reason that I even became a chemistry major in undergraduate school. Everyone at WKU used to say "don't take Holman for organic, he is way too hard." It wasn't that he was hard, it was that he expected you to know what you were doing. I think that the best attribute that a professor can have is that he cares. Dr. Holman really does.

Then there are my parents. I have to say that everything that I am today was instilled in me by my parents (good and bad, although much more good than bad). They made growing up fun and were always there in good and bad times to offer support and more. I don't think that I will ever feel that I have repayed what they have given me. They have shown me that it is not what you have, but who you have.

iii

My dearest wife has put up with me for seven years. For that, everyone should thank her. She brightens my day and makes everything else go away when I am in her presence. I cannot wait until we are finally completely together so that she is the first thing I see when I wake up every morning and the last thing I see when I go to sleep. I know that it has been so hard on her these past two years living in different states and I hope that I can make it up to her in the many years to come.

I must also thank my advisor here at UF, Dr. Kirk Schanze. He made me a much better chemist that I ever thought I could be. He has been very understanding and very helpful in my life and in my science. But most of all I must thank him for allowing me to work independently over these past years. Many "bosses" would not have let me do that.

Finally, I must thank several groups here in the UF chemistry department. First, the Enholm group (Maria, Jennifer, Schwin, Paul, even Jim) have all been great friends over the years. Next, the Wright group (Buck, the red-neck; Ravi, mad bomber; and Claude, the New Yorker) provided great entertainment over the past two years. And finally, the entire Schanze group (Yin, Yao, Ed (not me), Yiting, Kevin (I guess), Joanne, Keith, Jiang, Chunyan, Shengxia, Benjamin, and Ksenija) who are all great lab-mates. I have to also give a big "thanks" to Yibing Shen who always went above and beyond what was asked or expected of him. I thank everyone.

TABLE OF CONTENTS

vi

LIST OF FIGURES

Figure

x

Abstract of Dissertation Presented to the GraduateSchool
of the University of Florida in Partial Fulfillment of the
Requirements for the Degree of Doctor of Philosophy

ELECTRON TRANSFER WITHIN VARIOUS ORGANOMETALLIC SPECIES

By

C. Ed Whittle

May 2001

Chairman: Kirk S. Schanze
Major Department: Chemistry

This work comprises several aspects of electron transfer in various different systems. The first chapter gives a brief and general background of electron transfer and various aspects of the energy gap law, and then details several different π-conjugated systems and their applications in organic chemistry. Each of the following chapters has a separate introduction explains previous work in detail specific to the individual chapter.

The second chapter discusses the mechanistic aspects of cyclizations induced by inter- and intra-molecular electron transfer processes in aminyl cation radicals. A system was devised in which an amine, when electron transfer forming an aminyl radical cation, cyclizes onto an alkene. This system is investigated thoroughly in this chapter. Return electron transfer usually occurs stepwise. However, in this study, the photophysical data obtained implies dissociative return electron transfer.

xiii

The third chapter discusses the synthesis and photophysics of a series of bipyridyl platinum bisacetylides. This study incorporates both bipyridyl and acetylide ligands in a platinum complex and it has been seen that relatively long lived, highly luminescent states occur upon excitation. In order to fully investigate this luminescent state, two series of bipyridyl platinum bisacetylides were synthesized and characterized. The two systems vary the electron donating ability of the substituents on the bipyridyl and acetylide ligands to determine the effect on the bipyridyl based MLCT emission.

The final two chapters deal with the synthesis and photophysical characterization of various macrocycles based on platinum acetylide bonds. The first of these two chapters discusses the synthesis of platinum squares by self-assembly. It is demonstrated in this chapter that these squares exhibit quite long lived luminescent excited states that, unlike the platinum acetylides of the third chapter, are $^3\pi,\pi^*$ based emission. In order for self assembly of macrocycles to be high yielding, the cyclization step must be highly reversible so that "self-healing" can occur finally yielding the thermodynamic product (the macrocycle). The strength of the platinum acetylide bond limits "self-healing" and thus the yield of macrocyclic product was limited. The final chapter details the development of a method to keep the terminal acetylene ends in close proximity, thus increasing the likelihood that formation of the macrocycle would occur. This was accomplished by linking the sides to a central benzene ring through ester bonds, thus increasing the localized concentration of the terminal acetylenes. The macrocycle formed, as with the squares of Chapter 4, exhibit long-lived $^3\pi,\pi^*$ luminescent excited states. Full photophysical characterization is then employed.

CHAPTER 1
INTRODUCTION

Photoinduced Electron Transfer

The definition of a chromophore is, simply put, a molecule that absorbs light. The idea that a chromophore can and will absorb discrete energy was first realized in the early part of the twentieth century.[1-9] Until that time, it was believed that a chromophore would absorb a continuum of energies. This absorption of light energy actually promotes a molecule from, for example, the ground state to its first excited singlet state. The energy that a chromophore will absorb is the light energy that corresponds to the energy gap between two electronic energy levels. For the example above, the energy difference between the S_0 and S_1 energy levels corresponds to the energy of light that the chromophore will absorb.

To further illustrate this point, let us consider the simple organic molecule benzophenone. The absorption spectrum of benzophenone in cyclohexane exhibits an absorption band possessing a maximum wavelength of 260 nm. This band corresponds to one type of $S_0 \rightarrow S_1$ transition, a $\pi \rightarrow \pi^*$ transition. The energy required for this transition in benzophenone is 110 kcal/mol.[2] This amount of energy is, in fact, enough energy to break a H-H bond. One might expect some chemical change to occur, however, no chemical change does occurs in this molecule because the energy is rapidly dissipated into the vibrational energy of the solvent.

1

2

After the absorption of light energy, the molecule is in an excited state. This excited state may facilitate a photoinduced electron transfer instead of dissipating its energy to the surrounding solvent molecules. Photoinduced electron transfer is an electron transfer from an excited state donor molecule to a ground state acceptor molecule, or conversely, an electron transfer from an excited state acceptor molecule to a ground state donor molecule.

Figure 1-1 illustrates this point. In the figure are the electronic energy levels of an electron donor (D) and electron acceptor (A). The arrows represent photoinduced electron transfer in the gas phase between two different redox pairs where EA is the electron affinity of the acceptor molecule and IP is the ionization potential of the donor molecule. For the figure at the top, the ground state of the acceptor molecule is depicted on the left, and the excited state of the same acceptor molecule is depicted on the right. It can be seen that for the ground state acceptor molecule, energy transfer is uphill in energy from the donor molecule to acceptor molecule. However, in the acceptor's excited state, electron transfer is downhill in energy from the donor to the acceptor. The lower figure demonstrates the opposite case. Here, the ground state of the donor molecule is located on the left and the excited state of the donor molecule is on the right. Again, it can be seen that electron transfer is uphill in energy when the donor molecule is in the ground state. When the donor molecule is in the excited state, however, electron transfer is downhill in energy and therefore favorable.
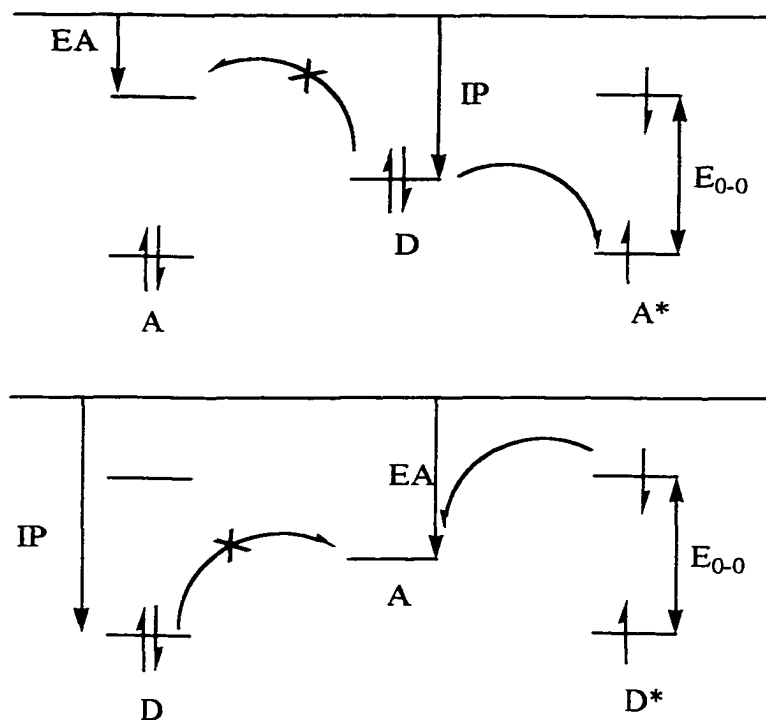
Figure 1-1. The energetic considerations for the possibility of photoinduced electron transfer in the gas phase. A* and D* are the excited acceptor and donor, respectively

The following equations used to determine the free energy of the electron transfer process can be derived from Figure 1-1:[3]

$$\Delta H^{\circ}_{FET}(\text{gas phase}) = IP - EA - E_{0\text{-}0} \tag{1-1}$$

$$\Delta G^{\circ}_{FET}(\text{soln. phase}) = E^{\circ}_D - E^{\circ}_A - E_{0\text{-}0} \tag{1-2}$$

$$\Delta G^{\circ}_{BET}(\text{soln. phase}) = E^{\circ}_A - E^{\circ}_D \tag{1-3}$$

ΔH°_{FET} is the enthalpy of forward electron transfer from the excited state donor to the ground state acceptor or from the ground state donor to the excited state acceptor; ΔG°_{FET} is the free energy for back electron transfer in the redox pair to return back to the ground state donor and acceptor; E°_D and E°_A are the oxidation potential of the donor and

reduction potential of the acceptor, respectively, and E_{0-0} is the energy difference between the ground state and excited state of the chromophore.

For equations (1-2) and (1-3), which correspond to electron transfer systems in solution phase, IP is replaced by E°_D and E_A is replaced by Ea. Typically, the excited state of electron donor or acceptor is a stronger reductant or oxidant, respectively, than its ground state. This is due to the energy difference between the ground and excited states (E_{0-0}). The reduction potential of the excited state electron acceptor and the oxidation potential of the excited state donor in solution phase are defined as follows:

$$*E^{\circ}_A \;=\; E^{\circ}_A \;+\; E_{0-0} \tag{1-4}$$

$$*E^{\circ}_D \;=\; E^{\circ}_D \;-\; E_{0-0} \tag{1-5}$$

In general, the excited state reduction potential of organic and inorganic molecules is 1.5 to 3.5 eV more positive than the ground state reduction potential because excited state triplet and singlet energies are typically 1.5 to 3.5 eV above the ground state.[4]

Marcus Theory of Electron Transfer

Kinetic considerations

A description of electron transfer may be presented by using a reaction coordinate based on the potential energy surfaces of the reactants and products. This can be done because electron transfer is a simple, weak interaction process in which there are neither bonds formed or bonds broken. Figure 1-2 illustrates the reaction coordinate mentioned above. This system is derived from the semi-classical treatment of electron transfer by Marcus and later elaborated by Hush and Sutin.[10-17] Electron transfer may be defined as

the crossing from the well of the reactants' potential energy surface (D,A: D is the

electron donor and A is the electron acceptor) to the well of the products' potential

energy surface (D$^+$,A$^-$: D$^+$ is the oxidized donor; and A$^-$ is the reduced acceptor). Marcus

developed an analysis of the electron transfer process based on parabolic surfaces to

relate the rate to the activation energy:[10]

$$k_{ET} = A\ \kappa_n \tag{1-6}$$

$$A = \nu_n\ k_{el} \tag{1-7}$$

$$\kappa_n = \exp(-\Delta G^{\neq}/RT) \tag{1-8}$$

$$\Delta G^{\neq} = (\lambda/4)\ (1 + \Delta G^{\circ}/\lambda)^2 \tag{1-9}$$

$$\lambda = \lambda_{in} + \lambda_{out} \tag{1-10}$$

$$k_{ET} = A\ \exp[-(\lambda/4RT)\ (1 + \Delta G^{\circ}/\lambda)^2] \tag{1-11}$$
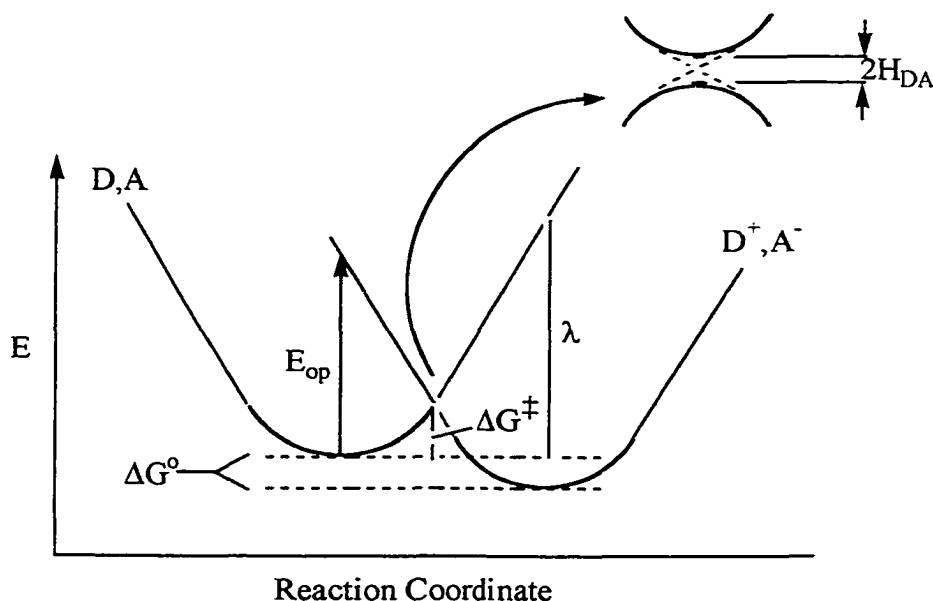
Figure 1-2. The potential energy surfaces for the reactants (D,A) and products (D$^+$,A$^-$) which describe electron transfer.

In Figure 1-2, the x-coordinate is the nuclear configuration that defines displacements in the nuclear coordinates of the system. There are two types of nuclear coordinates. The first is inner-sphere coordinates that comprise the bond lengths and bond angles of the reactants. The second is the outer-sphere coordinates that specify the arrangement of the solvent surrounding the reactants and products. The vertical axis is the free energy displacements from the local minima.

Quantum mechanical rules dictate that on the timescale of electron transfer the nuclei of the donor and acceptor cannot move. According to the Franck-Condon Principle,[8] electron transfer can only occur at the point where the reactant and product surfaces cross, because this is where the two states are iso-energetic. Figure 1-2 illustrates that electron transfer occurs at the crossing point of the (D,A) and (D$^+$,A$^-$) energy curves. The transition state at the crossing point leading to electron transfer corresponds to the lowest energy pathway available in the nuclear configuration of the system.

For equation 1-6, the term A in depends on the nature of the electron transfer reaction (e.g., bimolecular or intramolecular); κ_n is called the nuclear factor. The term A can be expressed as the product of v_n (the effective nuclear vibrational frequency) and k_{el} (the electronic factor which ranges from 0 to 1) as in equation 1-7.

Electron transfer consists of electron movement between orbitals. An electron may flow from a singly or doubly occupied molecular orbital of the donor to a fully vacant or half vacant orbital of the acceptor. Therefore, the orbital overlap between the occupied and unoccupied orbitals must play an important role in electron transfer. The orbitals act like conductors of the electron. Structural and environmental factors that

influence their mutual separation, orientation and symmetry, or restrict their freedom of movement to find the most favorable spatial symmetry, or restrict their freedom of movement to find the most favorable spatial orientation, can profoundly influence the rate of electron transfer. When k_{el} is 1 the term A is equal to v_n; conversely, when $k_{el} \ll$ 1 the term A is given by v_{el} where v_{el} is the electron hopping frequency which is directly related to the nature and the overlap of the occupied and unoccupied orbitals involved in electron transfer.

According to Marcus Theory, the initial thermally equilibrated nuclear geometry of the reactants and surrounding solvent molecules undergoes reorganization in the stages preceding electron transfer. This brings the reactants and surrounding solvent molecules into the high energy, distorted and non-equilibrium geometry of the transition state. At the transition state, electron transfer takes place rapidly. During this brief moment, the nuclear geometry of the transition state remains fixed. Following electron transfer, nuclear relaxation rapidly establishes the thermally equilibrated product state. The nuclear factor κ_n in equation 1-6 is related to the activation energy $\Delta G^{\neq}$ by equation 1-8 to 1-10, where ΔG^o is the standard free energy of reaction, l is the total reorganizational energy composed of vibrational (λ_{in} for the inner sphere barrier) and solvational (λ_{out} for the outer sphere barrier) components. λ_{in} is the free energy change associated with the nuclear bond length changes within the reactant molecules, and it can be estimated from a classical model provided the knowledge of bond lengths and force constants in the reacting molecules before and after electron transfer is available. λ_{out} is the free energy change associated with the slow changes in the polarization of the surrounding solvent molecules prior to electron transfer, and is generally calculated form a classical model

developed by Marcus and Hush.[9] λ_{out} depends on solvent polarity, separation of the redox sites, and on the shape of the reacting molecules.

Marcus Inverted Region

One of the most surprising features of the Marcus Theory is the behavior it predicts in the highly exoergic $\Delta G°$ region, known as the Marcus Inverted Region first described in 1960. The reaction rate is predicted to decrease as -$\Delta G°$ exceeds λ. Initially, the existence of the inverted region was approached with skepticism since it directly conflicted with linear free energy relationships. In fact, not until the middle of the 1980's did experimental evidence surface to support its existence.

The origin of the Marcus inverted region can be understood by following the crossing point as the exothermicity of the reaction becomes more negative shown in figure 1-3. Inspection of equation 1-6 shows that k_{ET} will increase as -$\Delta G°$ increases, reaching a maximum value when -$\Delta G° = \lambda$. When -$\Delta G°$ becomes larger than λ, k_{ET} will decrease. Thus a plot of log (k_{ET}) vs. -$\Delta G°$ should have the shape of a parabola. Figure 3 depicts three regions predicted by Marcus Theory.[10] The far left figure shows the normal region where reactions are thermally activated. The middle figure shows the activationless region where the -$\Delta G° = \lambda$ and the electron transfer reactions are very exothermic. Therefore, for moderately exothermic reactions the rate of electron transfer will increase, but for strongly exothermic reactions as shown in the right figure their rate of electron transfer is predicted to decrease.

Energy Gap Law

An important class of physical processes is the simple non-radiative decay of an electronic excited state without any chemical reaction. Characteristics of this type of reaction are small internal bond displacements and small rearrangements of the external medium. Since non-radiative decay processes are so important, the theory is well advanced. The result of the study of the large energy separation between the initial and final states is the energy gap law. This, simply put, states that the nonradiative decay rate is found to decrease exponentially with increasing energy separation. There have been several different derivations of this relationship that vary only slightly in the resulting equations. The interesting feature of the energy gap law is that the equations are set with terms that are experimentally measurable, making testing of the law quite simple.

A better definition of the energy gap law is that for a series of related excited states based on the same chromophore, radiationless decay rates are determined largely by vibrational overlap between the ground and excited states. The extent of vibrational coupling is determined by the magnitude of vibrational wave function overlap between the $v = 0$ levels in the excited state and highly vibrationally excited isoenergetic levels of the ground state. The value of the non-radiative decay rate (k_{nr}) is given approximately by the equation derived by Englman and Jortner:

$$k_{nr} = (2\pi V^2/\hbar)(1/2\pi\hbar\omega_M\Delta E)^{\frac{1}{2}}\exp(-S)\ \exp(-\gamma\Delta E/\hbar\omega_M) \tag{1-12}$$

Where ΔE is the internal energy gap between the upper and lower states, ω_M is the frequency of the deactivating mode(s), V is the electron tunneling matrix element, γ and S are defined by equations 1-13 and 1-14 respectively:

$$\gamma = \ln (2\Delta E/\Sigma\hbar\omega_j\Delta_j2) - 1 \qquad\qquad (1\text{-}13a)$$

$$\gamma \sim \ln (2\Delta E/\hbar\omega_M\Delta_M^2) - 1 \qquad\qquad (1\text{-}13a)$$

$$S = \tfrac{1}{2}\Sigma\Delta_j^2 \qquad\qquad (1\text{-}14)$$

Where Δ_j is the dimensionless fractional displacement between the equilibrium nuclear configuration of the ground and excited state for the complex's jth normal mode. Equation 1-13a can only be simplified to equation 1-13b if the critical high-frequency mode M undergoes substantial distortion in the excited state.

When one compares a series of excited states, equation 1-12 can be simplified to equation 1-15 if variations in V and S are relatively small and assuming $\Delta E \sim E_{em}$.

$$\ln k_{nr} = (\ln \beta - S) - (\gamma E_{em}/\hbar\omega_M) \qquad\qquad (1\text{-}15)$$

Since $\ln \beta$ and γ are weakly varying functions of ΔE, it can be predicted on the basis of equation 1-15 that if the assumptions made above are appropriate, a linear relationship should exist between $\ln k_{nr}$ and E_{em}.

The assumption that variations in V are relatively small for excited states is vital to the use of equation 1-15. V will not be constant, and appears in the intercept as $\ln V^2$. According to equation 1-12, variations of V on the order of 30–100 cm^{-1} must be too small to affect the linear relationship between $\ln k_{nr}$ and E_{em}.

A E$_{em}$

ħω$_1$

E$_0$

Δv$_{1/2}$

Intensity →

B E$_0$

Δv$_{1/2}$

ħω$_2$

E$_{00}$

fwhm

hb

← Energy
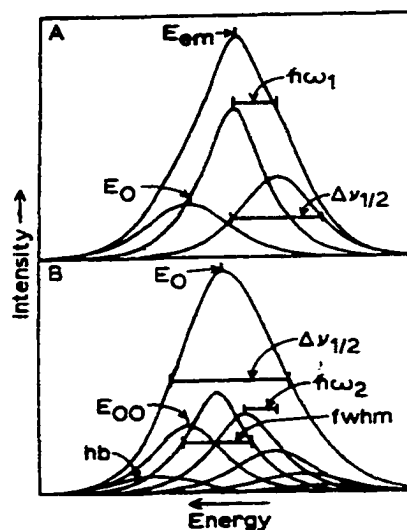
Figure 1-3. Definition of spectral fitting parameters. The complete spectrum is fit to a series of bands with spacing ħω[1]. The band shapes have a half-width of Δv$_{1/2}$ and the first maximum peak occurs at E$_0$ with the peak maximum of the entire spectrum at E$_{em}$.

Line shape analysis of emission spectrum often becomes important in obtaining important experimental values. One method entails using two vibrational modes with ħω$_1$ ~ 1300 cm^{-1} and ħω$_2$ = 300 cm-1. The Franck-Condon envelopes can be calculated by standard formulas where a Boltzman population in the lower frequency mode is used, and it is assumed that the vibrational frequencies of the ground and excited states are the same. Thus, the relative peak intensity can be readily defined by the temperature and the displacements in the two vibrational modes as measured by the Huang-Rhys factors (S$_{1,2}$). The individual vibronic peaks can be represented with Gaussian bandshapes that have equivalent values for full width half maximum (fwhm) and are centered on their transition energies. Values of S$_1$, S$_2$, fwhm, ħω$_1$, and E$_{00}$ can then be varied until the best-fit spectrum is obtained.

The basic formula used in the line shape analysis described above is given in equation 1-16.

$$I_{\upsilon,\upsilon*}^{em} = (64\pi^4 c/3\hbar)N_{\upsilon*}(\nu_{\upsilon,\upsilon*})^3 <d>^2 \Pi \mid <\chi_{j,\upsilon} \mid \chi_{j,\upsilon*}> \mid^2 \qquad (1\text{-}16)$$

Where $I_{\upsilon,\upsilon*}^{em}$ is the emission intensity between the vibronic states υ and $\upsilon*$ which occurs at frequency $\nu_{\upsilon,\upsilon*}$, and $N_{\upsilon*}$ is the number of molecules in the $\upsilon*$ vibronic level or excited state. $<d>$ is the transition dipole moment integral between υ and $\upsilon*$, and $\chi_{j,\upsilon}$ is the vibrational wave function for mode j in the vibronic state υ.

π-Conjugated Polymers

During the past decade the number of π-conjugated π-polymers investigated as advanced materials for electronic and photonic applications has developed rapidly, and has cased an ever increasing interest from both academic and industrial research laboratories. The inherent synthetic flexibility, potential ease of processing, and the possibility of tailoring characteristic properties to accomplish a desired function makes them promising candidates for manifold applications in materials science. Thus, they are used as laser dyes,[11] scintillators,[12] light-emitting diodes (LED's)[13], piezoelectric and pyroelectric materials[14], photoconductors,[15] and are investigated for optical data storage,[16] optical switching and signal processing,[17] as well as in nonlinear optical (NLO) applications.[18]

There are several classes of π-conjugated polymers (Figure 1-4). These π-conjugated polymers are often referred to as and are, strictly speaking, a subclass of "rigid rod" polymers and "molecular wires". The reason for terming these polymers "molecular wires" is because an exciton or photo-excited electron can easily travel

through the electron cloud created along the polymer backbone by extended π-conjugation.[18] For the purposes of the work presented in this dissertation, only a couple of classes will be detailed in this introduction: 1) phenylenevinylene (PPV) and aryleneethynylene-based (PPE) polymers and 2) polymers of the same type that incorporate a metal either along or directly in the polymer backbone.

etc.
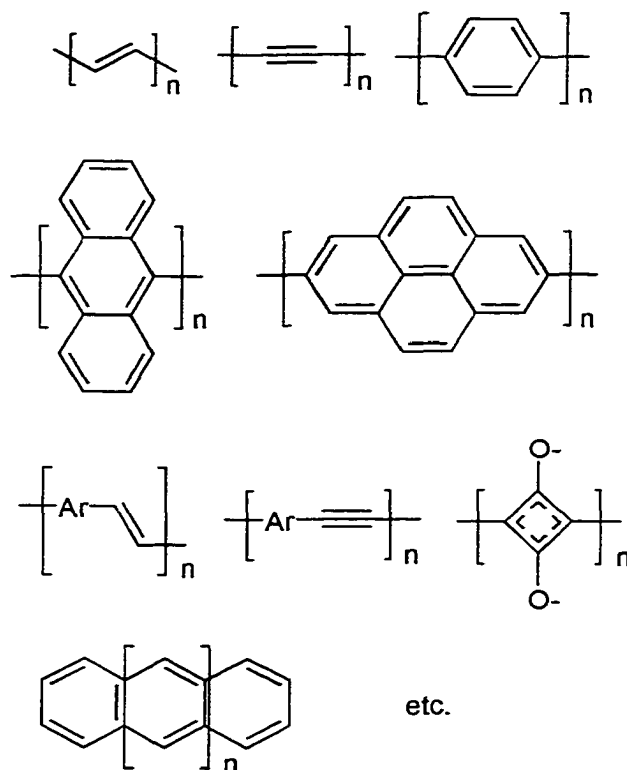
Figure 1-4. Various π-conjugated polymers.

The concept of π-conjugated polymers acting as molecular wires was extensively studied by Rothberg[19] in his work with PPV polymers. The ground state absorption spectrum that is typically seen for PPV films are a broad band centered around 400 nm and the emission spectrum is characterized by an intense fluorescence at around 540 nm. The excited state energies, specifically the triplet excited state, are very difficult to

measure for PPV and most other π-conjugated polymers due to the absence of

phosphorescence. However, the energy can be determined via indirect methods such as

triplet-triplet energy transfer quenching studies. This method was employed by

Monkman and coworkers[20] to determine the triplet energy for poly(2-methoxy-5-(2-

ethyl-hexyloxy)-p-phenylenevinylene) (MEH-PPV) and a value of 1.27 eV (29.3

kcal/mol) was calculated. Previously, an estimate of the triplet excited state energies for

PPV molecules between 1.2 and 1.4 eV (27.7 – 32.3 kcal/mol) was reported[21].

Monkman's calculated value agrees quite well with previous estimates.

One PPV polymer that has received considerable attention and is often used in

photophysical studies is poly(2,5-bis(2-ethylhexyloxy)-p-phenylenevinylene (BEH-

PPV).[22] Another PPV polymer incorporates a bipyridine sub-unit, which reasons for will

be discussed later in this section (Figure 1-5).[23] The absorption spectrum of the BEH-

PPV polymer exhibits a 504 nm band while the emission spectrum shows a sharp 560 nm

emission band. There is also a broad singlet excited state absorption in the transient

absorption spectrum of this PPV. The PPV with the bipyridine sub-unit incorporated into

the backbone shows a blue shift with respect to the BEH-PPV polymer in both the

absorption and emission spectrum (438 and 510 nm, respectively). This blue shift can be

explained by the fact that the bipyridine units in the polymer effectively break the

conjugation because they two rings are twisted out of plane with the rest of the polymer.

The transient absorption spectrum of the bipyridine incorporated polymer is shown in

Figure 1-6. This spectrum displays the broad excited-state absorption band discussed

previously as well as a bleaching of the ground state π,π* absorption.
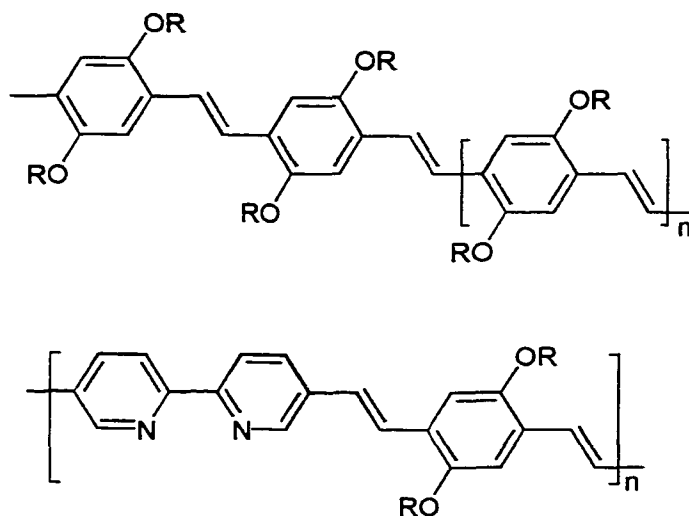
Figure 1-5. BEH-PPV (top) and 2,2'-bipyridine containing BEH-PPV (bottom) (R = CH₂CH(C₂H₅)C₄H₉)

(R = $CH_2CH(C_2H_5)C_4H_9$)
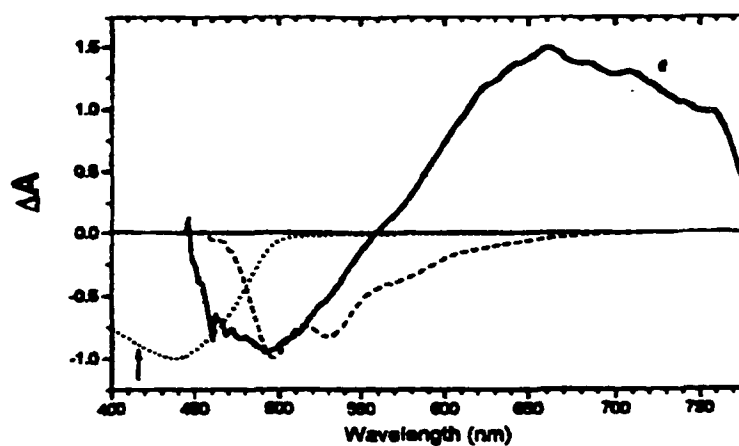
Figure 1-6. Transient Absorption spectrum (solid line) of singlet excited state of 2,2'-bipyridine containing PPV.

PPE polymers, depicted in Figure 1-7, are similar to PPV, but substitute ethynyl groups in place of the vinyl groups. These polymers have been studied by Davey et al.,[24] Le Moigne et al.,[25] and Swager et al.[26] The ethynyl groups add rigidity as compared to PPV polymers. The added rigidity typically allows for higher emission quantum yields

due to the decrease in non-radiative decay rates. This fact makes them more suitable for

conjugated polymer applications. Typical absorption and emission spectra are depicted

in figure 1-8. The absorption spectra is characterized by a strong absorption band at 448

nm that is assigned as a π,π^* transition of the conjugated backbone. The emission

spectrum exhibits a sharp emission band with a maximum at 482 nm.
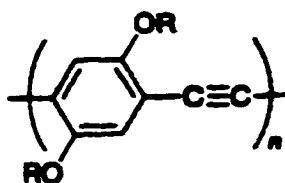
Figure 1-7. Example PPE polymer.
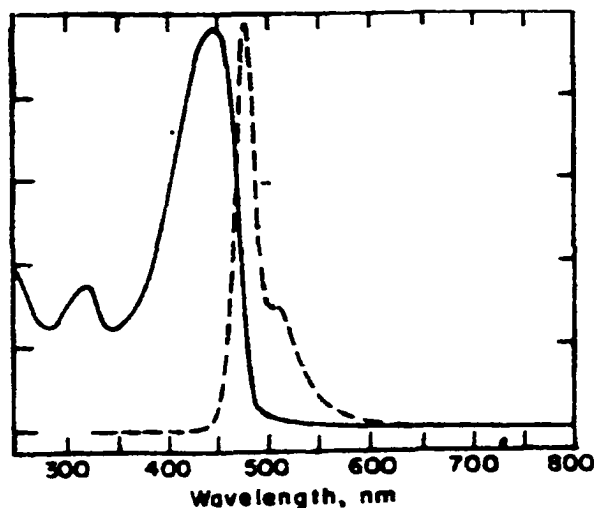
Figure 1-8. Typical absorption and emission spectra of PPE polymers.

Swager and coworkers have studied various different PPE polymers,[26-30] one of

which is depicted in Figure 1-9. As can be seen from this diagram, varying amounts of

the anthracene chromophore is incorporated into the polymer backbone. The absorption

and emission spectra of a polymer where x = 0.17 is depicted in Figure 1-10. The

interesting features that differ from that of other typical PPE polymers is that the

absorption spectrum features a new absorption band that corresponds to absorption by the anthracene sub-unit. The emission spectra also have new fluorescence bands that also correspond to the anthracene moiety. Also, the emission from the polymer is dramatically reduced. This suggests that the exciton was trapped by the anthracene sub-unit. This was the first time that it was seen that the excited state properties of the polymer could be altered or tuned systematically. In order to further investigate this effect, models were synthesized such that the anthracene moiety is only on the end group. This model also exhibited marked emission from the anthracene suggesting very efficient energy transfer along the polymer backbone.
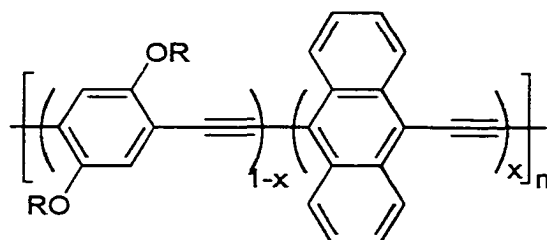
Figure 1-9. Structure of PPE that incorporates anthracene into the backbone.
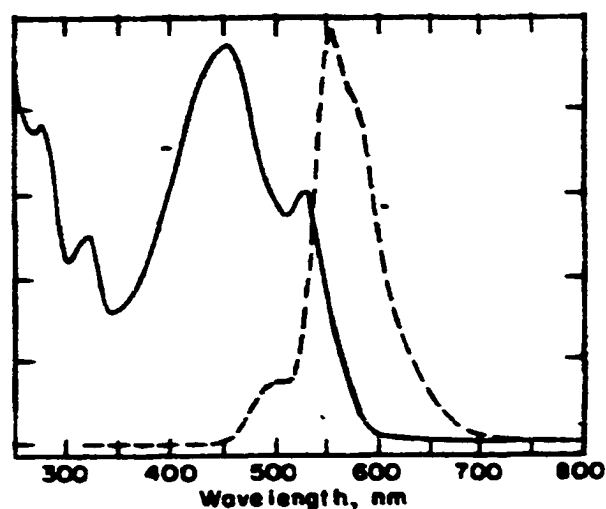
Figure 1-10. Absorption and emission spectra of the anthracene containing PPE.

It was thought that incorporation of an inorganic MLCT (metal-to-ligand charge transfer) chromophore into the polymer backbone could lead to greater ease of control of the excited state properties of these π-conjugated polymers. The inorganic chromophores have excited states that can be easily tuned by ligand substitution. Yamamoto and coworkers were the first to introduce MLCT chromophores into π-conjugated polymers in their study of poly-2,2'-bipyridine. The bipyridine repeat unit allows easy ligation of a variety of metals.

Work by Wasielewski and coworkers use PPV polymers that incorporate 2,2'-bipyridine in the polymer backbone, as described earlier (Figure 1-5) as sensors for various ions. In the un-complexed form, the π,π* absorption band lies around 450 nm. When a solution of the 2,2'-bipyridine containing PPV is titrated with nickel(II), zinc(II), or palladium(II), the π,π* band red-shifts between 50 and 100 nm depending on the metal ion. This red shift is caused by the extension of the π-conjugation length upon complexation of the bipyridine units (making them coplanar see Figure 1-11). The increase in conjugation length not only changes the absorption spectrum, but a shift in the emission spectrum is also seen. This can be attributed to a lowering of the LUMO.
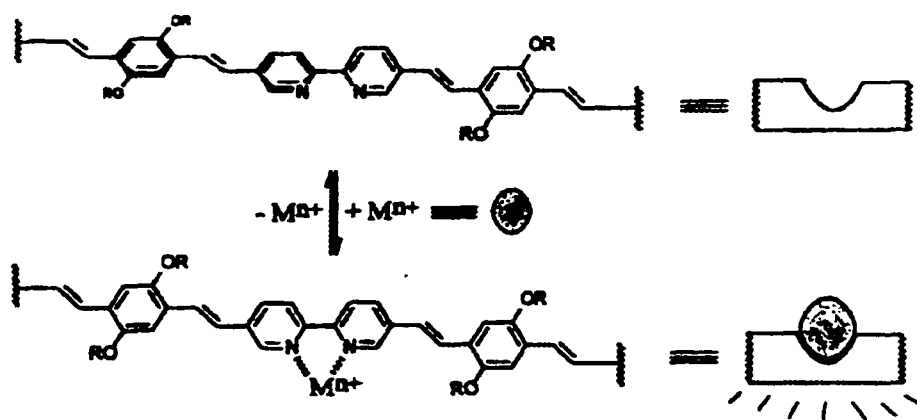
Figure 1-11. Metal complexation showing conformational change.

Another method of introducing a metal into a polymer is to actually incorporate the metal directly into the polymer backbone as opposed to along the side of the polymer chain. The aryleneethynylene-based polymers that contain $Pd[P(C_4H_9)_3]_2$ or $Pt[P(C_4H_9)_3]_2$ shown in Figure 1-12 have been studied by Wittmann and coworkers. The ground state absorption of these polymers exhibits an intense 380 nm singlet and a weaker 510 nm triplet absorption. This is considerably red shifted from the model monomer compounds spectrum suggesting a clear increase in delocalization across the π orbitals in the polymer backbone.
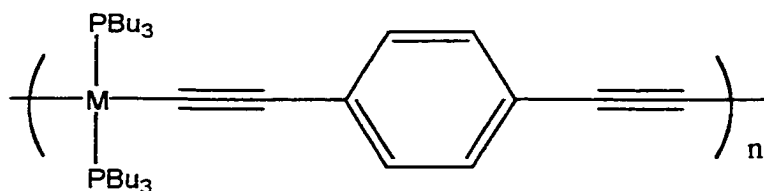
Figure 1-12. Incorporation of metal into aryleneethynylene-based polymer
(M = Pd or Pt)

CHAPTER 2
AMINYL CATION-RADICAL CYCLIZATION VIA PHOTOINDUCED INTRA- AND INTER-MOLECULAR ELECTRON TRANSFER

Introduction

Aminyl Radical Reactions

The use of radical based chemistry is of great importance in many areas of synthetic chemistry. A primary understanding of the absolute and relative rate constants of these radical reactions is important in the design of synthetic pathways and for mechanistic studies. There is an abundance of information on the kinetics of simple alkyl radical reactions providing a kinetic scale that has proved invaluable to the synthetic community. However, until fairly recent work by Newcomb and co-workers[53], there has not been such a kinetic scale for nitrogen centered dialkylaminyl radical reactions. Setting up a kinetic scale for these reactions would become quite useful as recently there has been several synthetic conversions carried out using dialkylaminyl radicals. Dialkylaminyl radicals can be produced in a number of manners such as chain reactions of N-chloro or bromoamines,[55] direct formation from N-hydroxypyridine-d(1H)-thione derivatives (PTOC carbamates) and sulfenamides,[56] addition of carbon radicals to imines,[57] and ring openings of radicals formed from α-(haloalkyl)aziridines (Figure 2-1).[58]

20

Prior to the work of Newcomb, the only kinetic information available came from one kinetic ESR study by Maeda and Ingold[59] who studied the ring opening of N-cyclobutylpropylaminyl radical at low temperatures and a laser

Figure 2-1. Formation of aminyl radicals

Figure 2-2. Early aminyl radical studies

flash photolysis (LFP) study of the cyclization of the 5,5-diphenyl-4-pentene-1-butylamine system (Figure 2-2). Newcomb set out to establish a kinetic scale for a series of dialkylaminyl radical reactions.[60] The first work utilized a competition study and direct observation by LFP to investigate the cyclization rate of N-methyl-5,5-diphenyl-4-

pentenaminyl radical (Figure 2-3). The first competition studies of the trapping of the radical formed upon production of a carbamoyloxyl radical followed by subsequent decarboxylation looked at the relative ratios of cyclized and acyclic products. It was found that in the
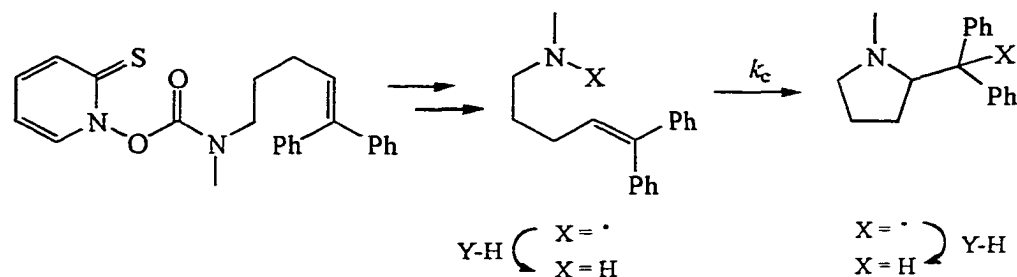
Figure 2-3. Newcomb's first cyclization study

presence of Bu$_3$SnH, the aminyl radical cyclized in yields of up to 95%. The determination of absolute rate constants for cyclization and trapping of the acyclic radical were determined by LFP. Upon cyclization, a diphenylmethyl radical, which has a characteristic absorption with a λ_{max} at ca. 330 nm, is formed. This radical was observed to grow in with time (Figure 2-4) yielding a rate constant for cyclization (k_{cyc}) at 25°C of 4 x 10^5s^{-1}.[61]

To further expand upon the study described in the previous paragraph, Newcomb designed several systems that would give a series of dialkylaminyl radical reactions with increasing unimolecular reactivity (Figure 2-5).[61] All systems again utilized the PTOC carbamate and were designed such that upon reaction they would produce benzylic or diphenylalkyl radicals (λ_{max} ca. 315 and 330 nm, respectively). Direct unimolecular determination of the kinetics of the reactions was again determined via LFP. Due to instrument limitations, the kinetics of three of the reactions could not be determined in

this manner. Fragmentation of **2-1** was too slow to observe, and the ring opening of **2-5** and **2-6** were too fast to observe (ring opened product was observed at even the
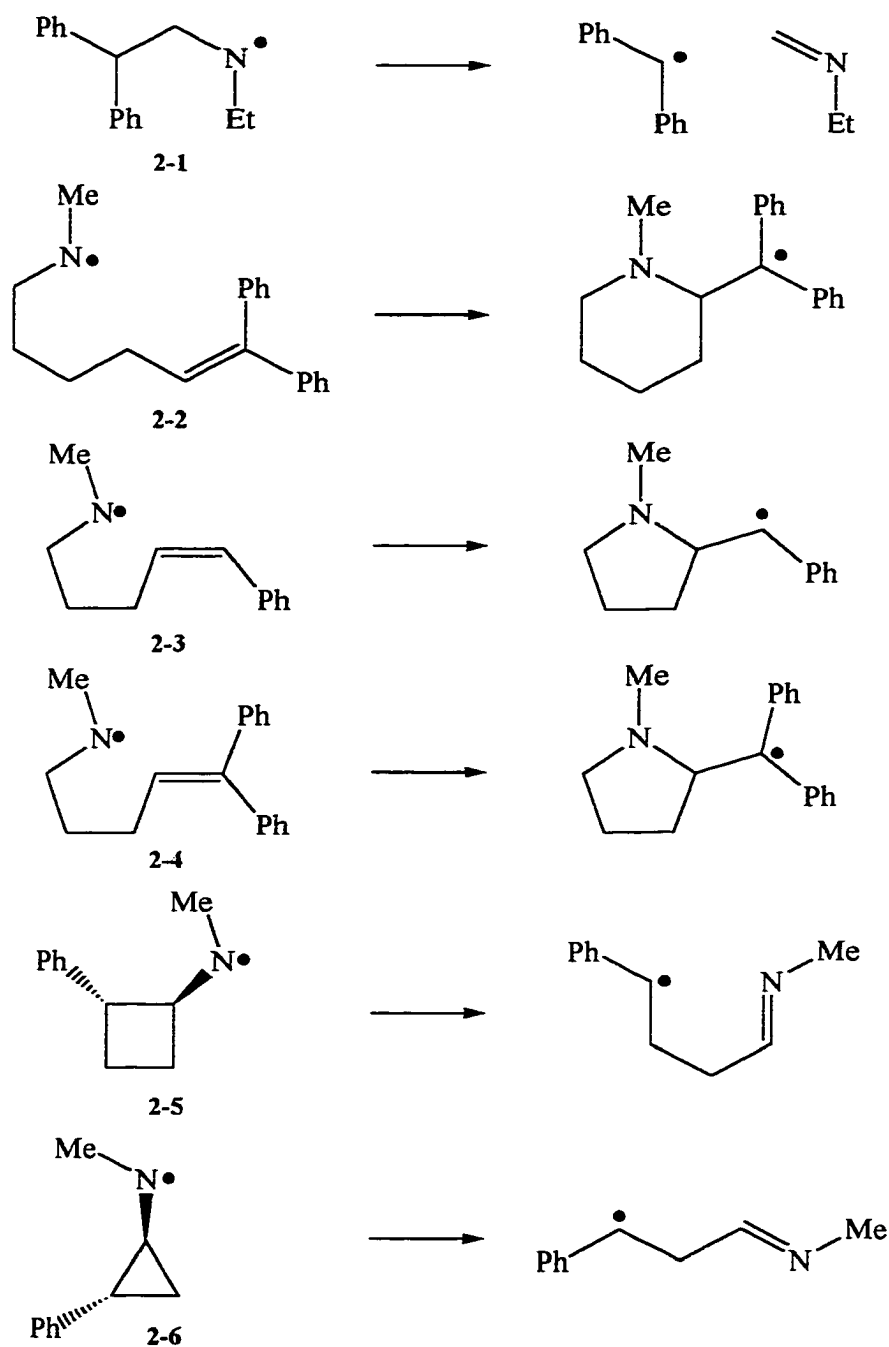
Figure 2-5. Systems studied by Newcomb to set up kinetic scale

earliest times). Results of these studies are tabulated in Table 2-1 and compared to the analogous carbon centered radicals.

Dialkylaminium Cation Radicals

Like the aminyl radicals described in the previous section, aminium radical cations play an important role in synthesis. These radical cations can

Table 2-1. Rate constants for various rearrangements

Structure	Rate (s^{-1})		
	X = N	X = NH+	X = CH
(structure: Ph, Ph, Et, X·)	$< 1 \times 10^4$	2×10^7	---
(structure: Me, X·, Ph, Ph)	7×10^3	4×10^7	2×10^5
(structure: Me, X·, Ph, Ph)	3.2×10^5	1×10^{10}	2×10^7
(structure: Me, X, cyclopropyl, Ph)	7.2×10^{11}	---	3×10^{11}

be produced in a number of ways such as chemical, electrochemical, and photochemical electron transfer reactions of amines. They have also been proposed as intermediates in biological oxidations of amines by enzymes. Because of their importance, a fundamental understanding of the kinetics of the reactions of aminium radical cations is necessary.

There have been several kinetic studies on anilinium,[62] dialkylaminium,[63] and

trialkylaminium radical cations[64] as well as radical cations of NADH analogs.[65]

In another study by Newcomb and co-workers,[66] an attempt to develop a kinetic

scale for dialkyaminium radical cation reactions was conducted. The dialkylaminium

radical cation kinetics were studied by LFP methods. By irradiation of PTOC-

carbamates with 355 nm light, dialkylaminyl radicals were produced. These radicals

were then protonated to produce dialkylaminyl radical cations. This study looked at the

fragmentation of N-ethyl-2,2-diphenylethylaminium radical cation 2-7, and the

cyclizations of N-methyl-6,6-diphenyl-5-hexenaminium 2-8 and N-methyl-5,5-diphenyl-

4-pentenaminium 2-9 radical cations (Figure 2-6). It was found that the reactions of

these radical cations were several orders of magnitude faster than the analogous

dialkylaminyl radical reactions the results of which are tabulated in Table 2-1.
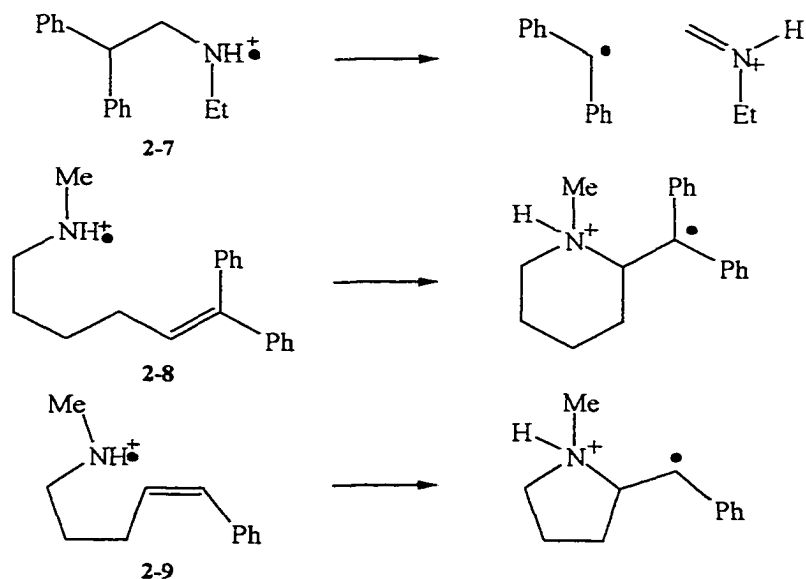
Figure 2-6. Fragmentation and cyclization of aminium cation radicals

Metal-Organic Dyads

A metal-organic dyad is a supramolecular assembly consisting of a transition metal complex that serves as a light absorbing chromophore and an organic electron donor or acceptor. The most studied metal-organic dyads contain a metal with a d^6 electronic configuration which has a lowest excited state arising from a metal to ligand charge transfer (MLCT) transition that involves promotion of a metal centered d electron into a ligand based π^* level. This can lead to two possible events, which separates metal-organic dyads into two categories (Types 1 and 2).[67-74] Type 1 metal-organic dyads contain an electron acceptor covalently attached to the d^6 metal chromophore. In this type of dyad, forward electron transfer occurs when the promoted electron from MLCT is donated to a π^* orbital of the organic acceptor. Back electron transfer occurs when an electron in the π^* orbital of the organic acceptor moves back to the d-shell of the transition metal (Figure 2-7a). Type 2 metal-organic dyads contain an electron donor covalently attached to the d^6 metal chromophore. In this type of dyad, forward electron transfer occurs when an electron from a π orbital of the organic donor is transferred to the "hole" left in the d-shell of the transition metal from MLCT. Back electron transfer is a charge recombination reaction between an organic radical anion and an organic radical cation (Figure 2-7b).

A) Type 1 Dyad   **B) Type 2 Dyad**

$$^{-\bullet}\text{*L-M(d}^5)\text{-A}$$
$$\text{MLCT}$$

+hv ↑ │ FET → $\text{L-M(d}^5)\text{-A}^{-\bullet}$

BET ↙

$$\text{L-M(d}^6)\text{-A}$$

$$^{-\bullet}\text{*L-M(d}^5)\text{-D}$$
$$\text{MLCT}$$

+hv ↑ │ FET → $^{-\bullet}\text{L-M(d}^6)\text{-D}^{+\bullet}$

BET ↙

$$\text{L-M(d}^6)\text{-D}$$
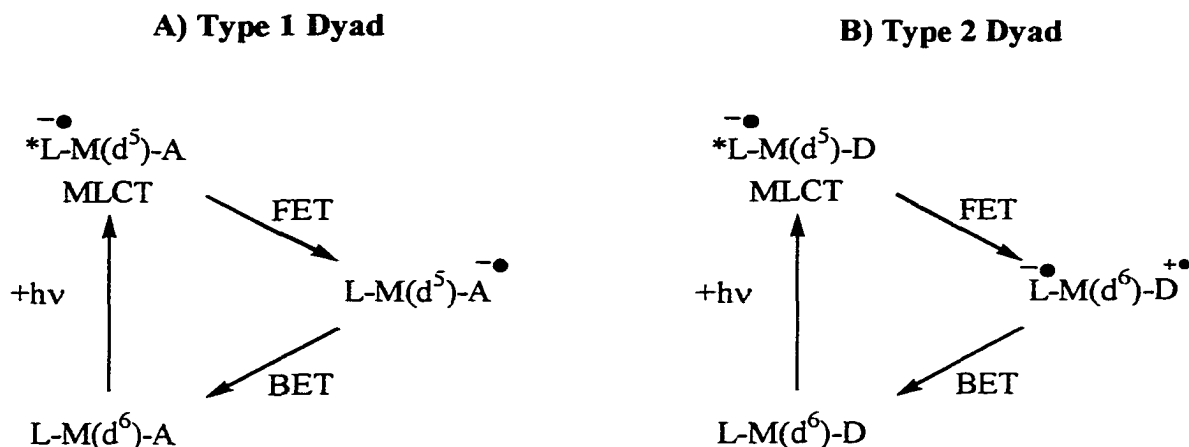
Figure 2-7. Type 1 and Type 2 Dyads

As an example of Type 2 dyads, Schanze and coworkers[75] investigated a series of

Re-based acceptor-donor complexes with emphasis on understanding driving force and

solvent dependence on the rates of forward and back electron transfer (k_{fet} and k_{bet},

respectively). The transition metal chromophore in this case is (diimine)Re^I(CO)$_3$. The

organic donor is N,N-dimethylaniline linked to the chromophore through a short amide

linkage (Figure 2-8). By changing the diimine ligand, the electron demand was altered

and thus the driving force of forward and back electron transfer (ΔG_{FET} and ΔG_{BET},

respectively). The system was also studied by varying the solvent from methylene

chloride to dimethylformamide and finally to acetonitrile. Photoexcitation of the $d\pi$ (Re)

-> π* (diimine) MLCT initiated FET from the dimethylaniline to the MLCT excited state

generating a ligand-to-ligand charge transfer (^{3}LLCT) excited state which decays by back

electron transfer through the ^{1}LLCT state. By using fluorescence lifetime measurements

and nanosecond transient absorption spectroscopy, the mechanism and kinetics were

established. If was found that the rate of forward electron transfer was strongly

dependent on ΔG_{FET} and solvent polarity ranging from 10^7 s^{-1} to $>10^9$ s^{-1}. However, the

rate of back electron transfer showed a weak inverted dependence on ΔG_{BET} ranging from 10^7 s^{-1} to 5×10^8 s^{-1}, and also shows no solvent dependence.
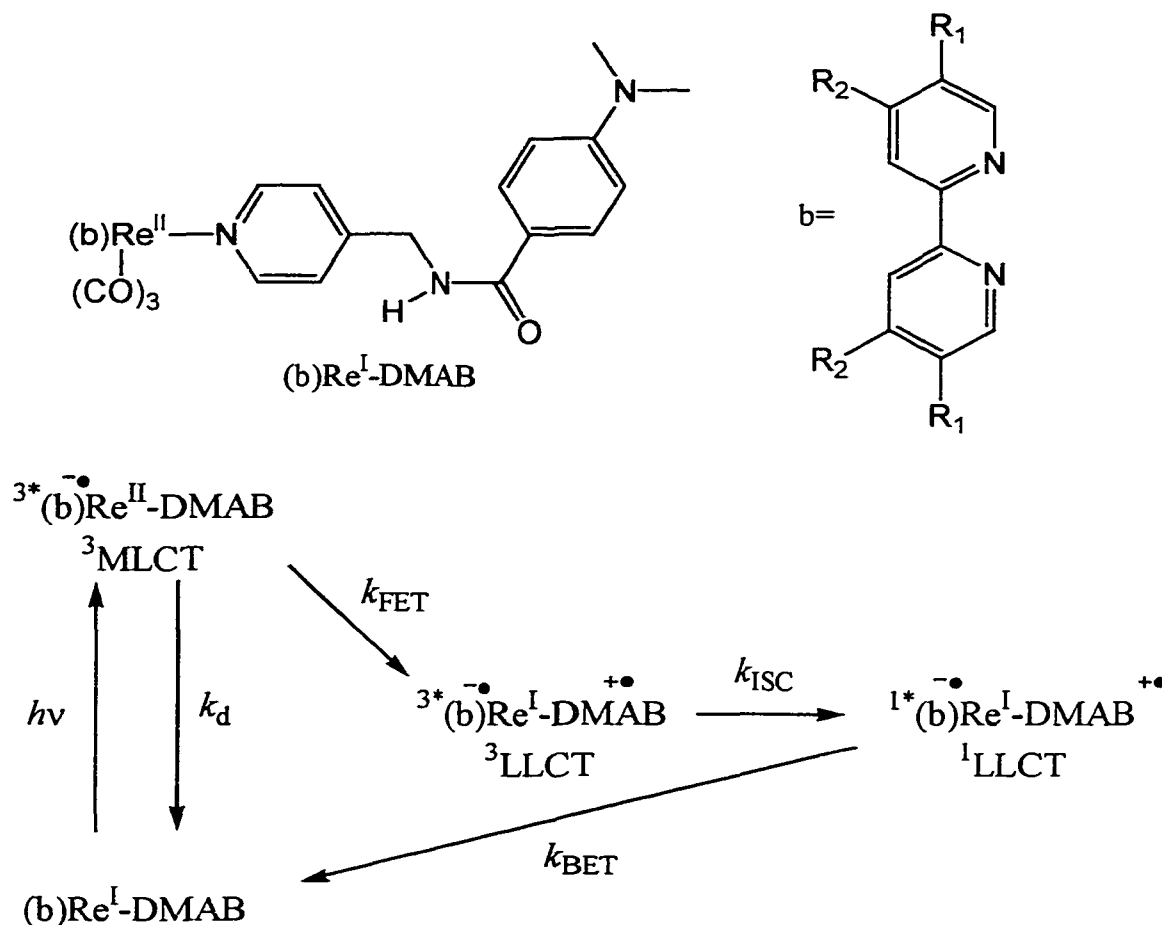
Figure 2-8. Example of Type 2 Dyad

Scope of Present Study

Based on the work by Newcomb regarding dialkylaminium radical cations and the Schanze group's previous studies on metal-organic dyads, aminium radical cations seemed to be an interesting system to study the dynamics of electron transfer. The objectives were two fold: 1) to establish the mechanism for the formation and decay

pathways of the charge-separated excited state and to quantify the kinetic processes involved in the charge-separated excited state based on the mechanism established, 2) use reactions as possible probes or clocks for intramolecular electron transfer. During the investigation, the project changed direction when it was realized that electron transfer and bond making were reversible. This led to studies on a similar system where the amine group is linked to the rhenium photo-oxidant.

In most studies of this type, the chemical reaction is irreversible, i.e. bond cleavage, and the product quantum yields can provide information on the dynamics of electron transfer. However, if the electron transfer triggered reaction has no bond cleavage or other irreversible reaction, the product will return to the ground state with no observable change and thus making the system difficult to study. Therefore, some feature must be built into the system, which allows the intermediates to be detected. So, to study the proposed process (Figure 2-9), a similar system is used as that employed by

R' = H or Ph
R" = Me or (bpy)Re ^{I}(CO)$_3$

R' = H or Ph
R" = Me or (bpy)Re ^{II}(CO)$_3$

R' = H or Ph
R" = Me or (bpy)Re ^{II}(CO)$_3$
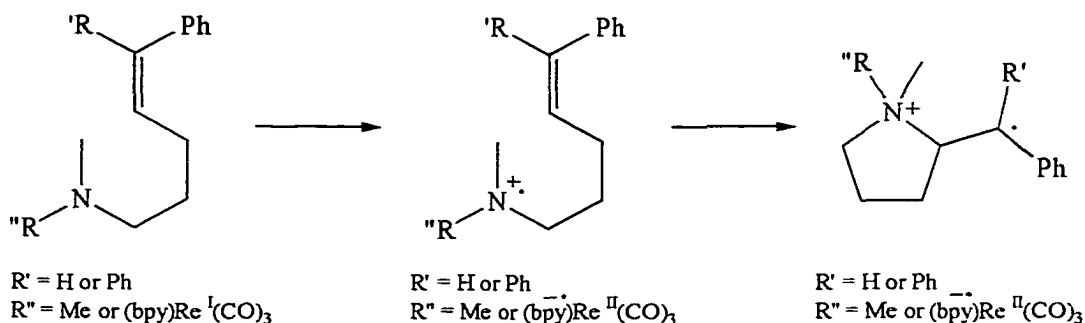
Figure 2-9. Proposed system

Newcomb whereby if cyclization occurs, a distonic radical cation is formed which features a benzylic or diphenylmethyl radical which as stated earlier has a characteristic absorbance band with a λ_{max} ca. 330 nm. This feature allows LFP techniques to be used to detect these transient species. The compounds studied in this chapter are N,N-

dimethyl-5,5-diphenyl-4-pentenamine (**A-5**), N,N-dimethyl-5-phenyl-4-pentenamine (**A-5mp**), [(bpy)Re(CO)$_3$(1-(N-methyl-N-pyridylmethylamino)-5,5-diphenyl-4-pentene)$^+$] [PF$_6^-$] (**Re-A5**), and [(bpy)Re(CO)$_3$(1-(N-methyl-N-pyridylmethylamino)-5-phenyl-4-pentene)$^+$][PF$_6^-$] (**Re-A5mp**) (see Figure 2-10 for structures).
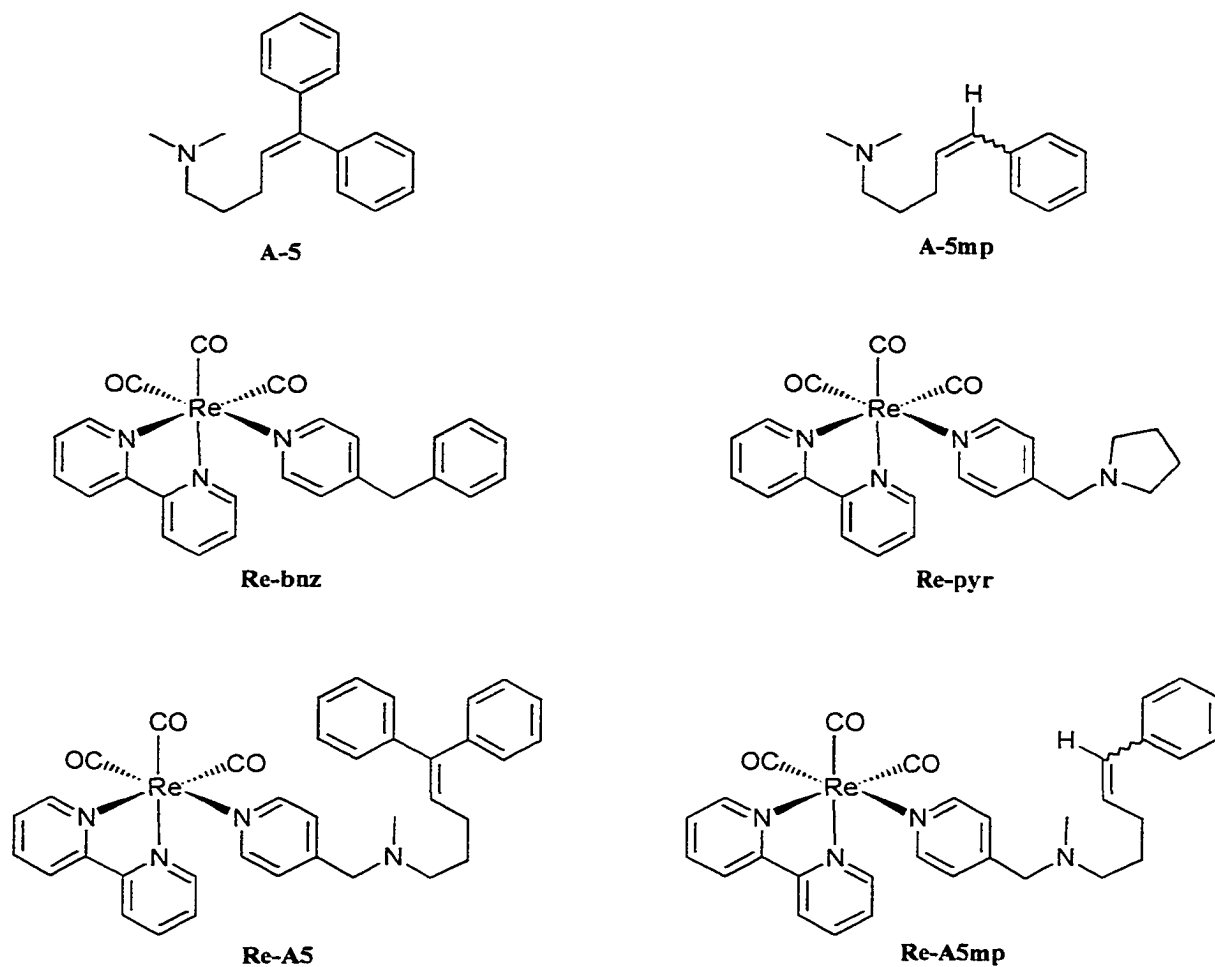
Figure 2-10. Relevant structures

Results

Bimolecular Systems

In an attempt measure the cyclization rates for the radical cations of **A-5** and **A-5mp** (depicted in Figure 2-10), several investigations were attempted. The results of which are discussed in detail below.

Quenching Studies

To determine the quenching efficiency of **A-5** on the rhenium photo-oxidant, a series of Stern-Volmer experiments were carried out (Figure 2-11, Equation 2-1). Two stock solutions of the Re photo-oxidant ($[(bpy)Re(CO)_3(py)^+][PF_6^-]$) in acetonitrile

$$^*Re^+ + A5 \xrightarrow{k_q} Re^0 + \overset{+\bullet}{A5}$$
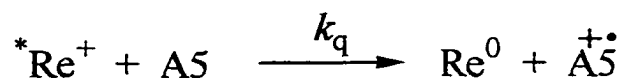
Figure 2-11. Quenching of Re photooxidant where Re = $[(bpy)Re(CO)_3(py)^+][PF_6^-]$

$$\frac{\tau^0}{\tau} = 1 + k_q \tau^0 [Q] \tag{2-1}$$

and methylene chloride were prepared. Several concentrations of **A-5** ranging from 0 to 0.02 M were prepared using the Re stock solutions. Emission lifetimes were determined for each of the air-saturated solutions varying concentrations. The plot of τ_0/τ versus [**A-5**] was found to be linear in every multiple trial (Figure 2-12). The slopes of the lines from the Stern-Volmer plots yields a quenching rate constant of 6.0×10^8 $M^{-1}s^{-1}$ in acetonitrile and 1.3×10^9 $M^{-1}s^{-1}$ in methylene chloride. Thus, at a concentration of 20 mM in acetonitrile, **A-5** quenches >75% of the excited states of the Re complex excited

states. Experiments to determine the quenching efficiency of A-5mp were completed in an analogous fashion with similar results ($k_q = 5.7 \times 10^8$ $M^{-1}s^{-1}$ in CH_3CN).

There is the possibility that the alkene portion of the molecule might quench the excited state through energy transfer. To test for this, a quenching experiment with 1,1-diphenylethylene (DPE) was performed. Concentrations were varied up to [DPE] = 0.03 M, and no quenching was observed. With this in mind, a two point quenching experiment was performed with β-methylstyrene at 0.01 M that showed a quenching of the excited state lifetime from 115 ns to 70 ns. This gives the possibility that quenching arises from energy transfer and not electron transfer. This result will be addressed in the section describing the steady-state photochemistry experiments.
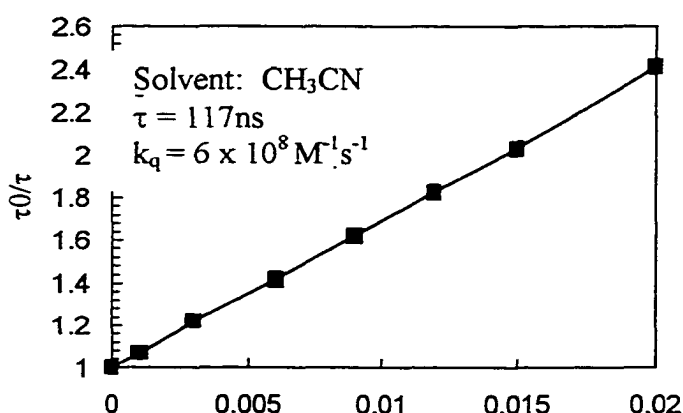
Figure 2-12: Stern-Volmer Quenching study on the quenching efficiency of A-5 on [(bpy)Re(CO)3(py)$^+$][PF6$^-$] in air saturated CH_3CN

Transient Absorption Studies

With the quenching efficiency now in hand, an attempt to determine the rate of cyclization for **A-5** by transient absorption (TA) spectroscopy was performed. A solution that was 20 mM A-5 and 5×10^{-5} M [(bpy)Re(CO)3(py)$^+$][PF6$^-$] was studied at several timescales. The shortest timescale TA spectrum is depicted in Figure 2-14. It can be

seen that even at the earliest times, there is an absorption band at ca. 330 nm, which is

attributed to absorption by the diphenylalkyl radical. This is accompanied by the decay

of a metal-to-ligand charge transfer (MLCT) state at ca. 370 nm. Because the

diphenylalkyl radical is present at the earliest time, it can be assumed that the rate of

radical cation cyclization must be much greater than pseudo-first order rate of forward

electron transfer, thus $k_{cyc} > 10^8 \text{ s}^{-1}$.
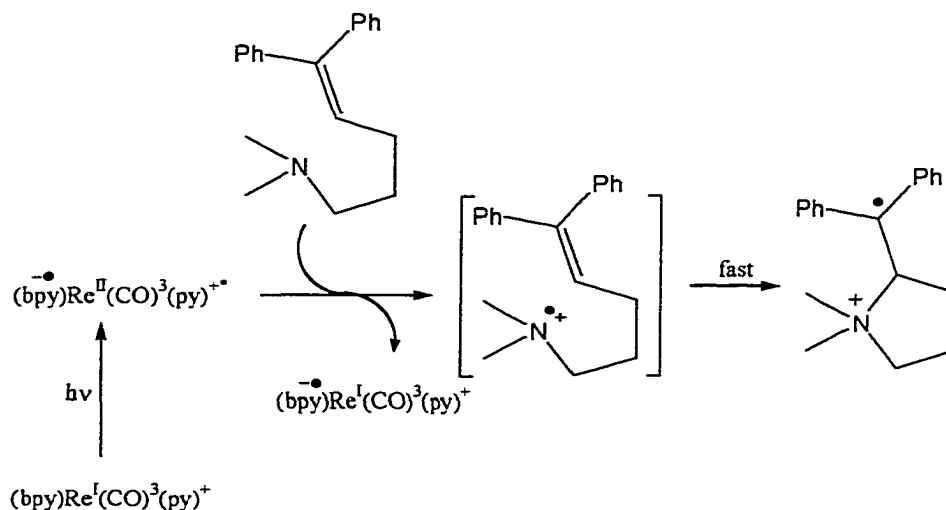
Figure 2-13. Structure that produces absorption band at ca. 330 nm.
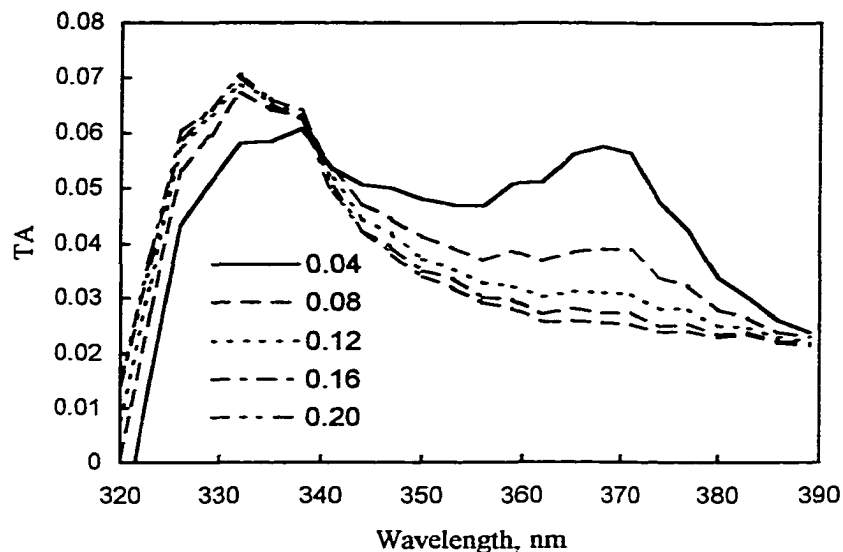
Figure 2-14. Transient absorption spectrum of (bpy)Re(CO)₃(py) in the presence of 20 mM A5 on short timescale. Legend indicates time delay after the laser pulse (ns).

The TA spectrum was obtained again on a longer timescale and is shown in

Figure 2-15. The band at ca. 330 nm is again attributed to the diphenylalkyl radical of

the cyclized radical cation. The entire spectrum is a mixture of absorption by the reduced

metal complex and the cyclized distonic radical cation. This transient decays uniformly

at all wavelengths, and follow equal concentration, second-order kinetics. This indicates

that the pair decays by back electron transfer.
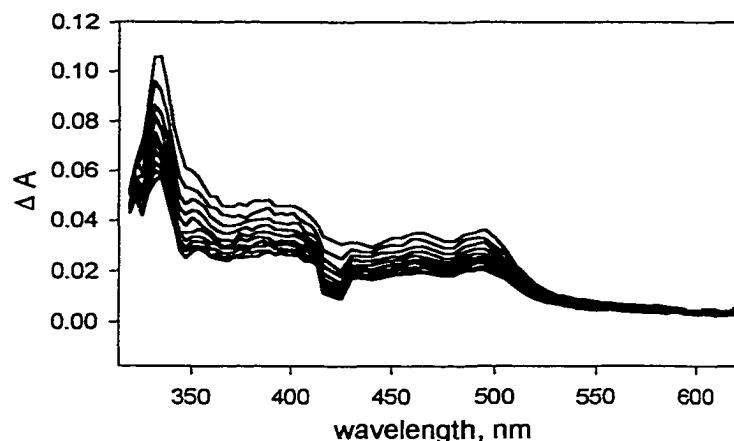
Figure 2-15:   Transient absorption spectrum of (bpy)Re(CO)₃(py) in the
presence of 20 mM A5 from 0 ns (highest ΔA) to 40 μs (lowest
ΔA)after the laser pulse.

TA spectroscopy was also used to determine the yields of free radical ions formed

by electron transfer quenching. A stock solution of the rhenium photo-oxidant at 5×10^{-5}

M in acetonitrile was prepared and used as an actinometer. A 20 mM solution of A-5 in

the stock solution containing the rhenium photo-oxidant was prepared and argon

degassed for 30 minutes in a 50 mL flow cell. A strong absorption band at 330 nm again

dominates the spectrum obtained. The yield of the formation of free radical ions can be

determined by using Equation 2-2. Where C_{*Re} is the initial concentration of MLCT

excited state produced by the laser excitation of the actinometer solution; C_{Re0} is the

concentration of reduced complex formed in the sample solution of the complex and A-5;

η_q is the fraction of MLCT excited states that are quenched by A-5 (for this system, $\eta_q =$

1); ΔA^{490nm}_{Re0} is the difference absorptivity at 490 nm in the sample solution; $\Delta\varepsilon^{490nm}_{Re0}$

is the difference molar absorptivity at 490 nm for the reduced complex, (bpy⁻

)Re^I(CO)₃(py); ΔA^{370nm}_{*Re} is the difference absorptivity at 370 nm immediately following

the laser pulse in the complex actinometer solution; and $\Delta\varepsilon^{370}{}_{\bullet Re}=11900\ M^{-1}cm^{-1}$.

Multiple trials were performed and the results are tabulated in Table 2-5.

$$\Phi_{esc} = \frac{1}{\eta_q}\frac{C_{Re^0}}{C_{\bullet Re}} = \frac{(\Delta A^{490\,nm}_{Re^0} / \Delta\varepsilon^{490\,nm}_{Re^0})}{(\Delta A^{370\,nm}_{\bullet Re} / \Delta\varepsilon^{370\,nm}_{\bullet Re})} \qquad (2\text{-}2)$$

Table 2-4. Yield of free ions.

Solvent	[A-5] (mM)	[Re] (M)	Yield
CH_3CN	20	5×10^{-5}	0.61
CH_3CN	20	5×10^{-5}	0.65
CH_3CN	20	5×10^{-5}	0.69
CH_3CN	20	5×10^{-5}	0.71
CH_3CN	20	5×10^{-5}	0.70
THF	25	6×10^{-5}	0.70
$MeCl_2$	25	6.5×10^{-5}	0.38

^{1}H NMR Studies

All ^{1}H NMR spectra were obtained on either a GE VXR-300 MHz or Gemini-300 MHz spectrometer. All solution were made in CD_3CN (0.1% v/v TMS) and kept in the dark until use.

In order to show that there were no processes other than radical cation formation, cyclization, and back electron transfer, a quantitative steady state photolysis experiment was performed. Aberchrome 540 was used as the actinometer to determine the intensity of the light produced by the Hg-Xe arc lamp as it undergoes a simple ring closure reaction upon irradiation (Figure 2-16) with a quantum yield of 0.20 .
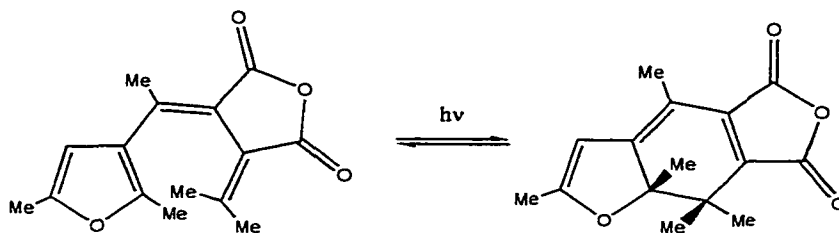
Figure 2-16. Aberchrome 540 isomerization

A 0.7 mL aliquot of a 20mM [(bpy)Re(CO)$_3$(py)$^+$][PF$_6^-$]/50 mM **A-5** (>95% quenching) solution in CD$_3$CN was then placed in a sealable NMR tube. The tube was degassed via a freeze/pump/thaw method, which entails repeatedly freezing the sample in liquid nitrogen, evacuating the tube via high vacuum pump, and then allowing the tube to thaw. The ^{1}H NMR spectrum of the sample was then taken. The sample was irradiated for 5 hours, which would be enough time for any distinguishing changes to be visible via NMR should any other efficient reaction be taking place. After the irradiation time, the ^{1}H NMR spectrum was again taken. The two spectra show little to no change, which indicates that any other processes that might be taking place are inefficient.

To show isomerization of the double bond in the **A-5mp** compound from cis to trans (Figure 2-17), a 0.7 mL sample of a 20mM [(bpy)Re(CO)$_3$(py)$^+$][PF$_6^-$]/50 mM **A-5mp** solution in CD$_3$CN was irradiated with a 450 watt Hg-Xe arc lamp for varying time intervals for 3 hours. Between the time intervals, the ^{1}H NMR spectrum (Figure 2-18) was taken. The signals from the cis and trans alkene protons (δ = 5.82 and 6.41, respectively) were monitored for changes and show an increase in the amount of trans alkene proton signal (δ = 6.41) and a decrease in the amount of cis alkene proton signal (δ = 5.82) suggesting a bond rotation. This can occur through electron transfer/

cyclization/bond-rotation as shown in Figure 2-17 or, as noted before, through energy

transfer directly to the double bond.
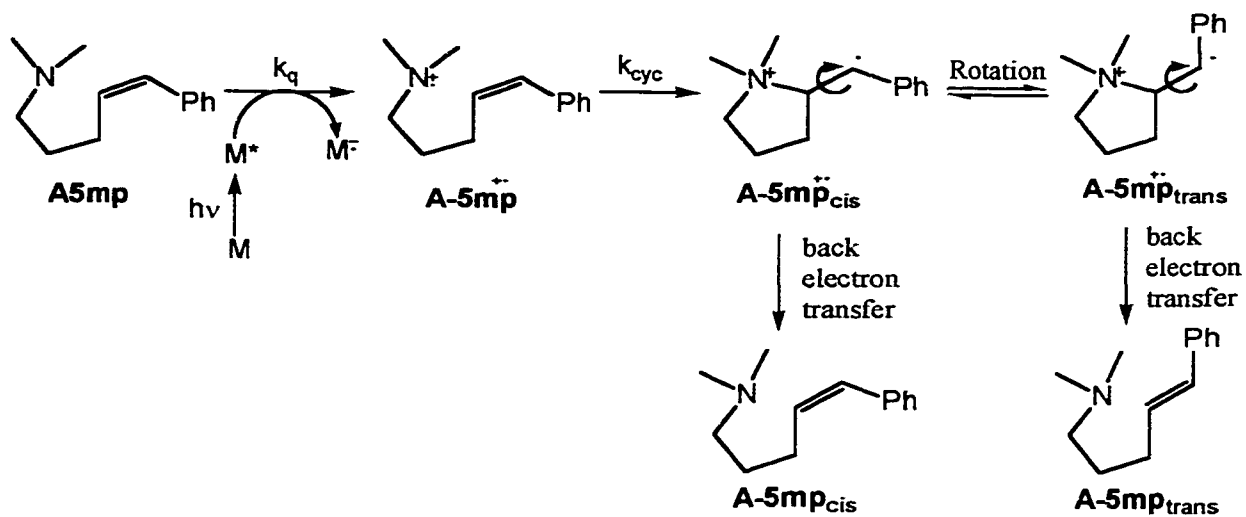
Figure 2-17. Bond rotation of A-5mp

both   trans   cis

t = 3 hrs

δ

0.81   0.55   0.28

both

trans   cis   t = 0

δ

1.88 0.87   1.00
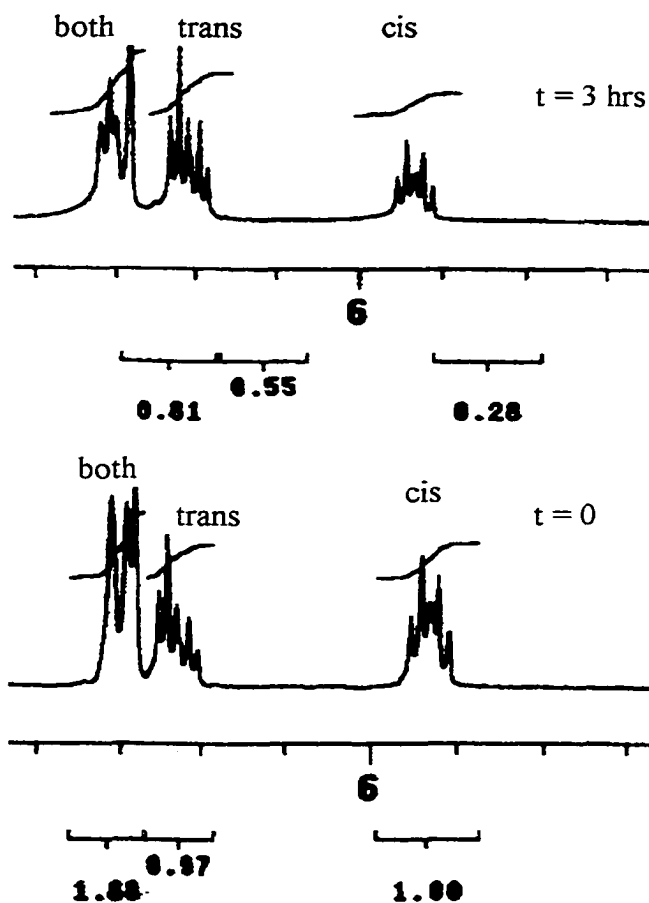
Figure 2-18. ^{1}H NMR spectra of **A-5mp** in the presence of (bpy)Re(CO)$_3$(py) monitoring the alkene protons. Bottom spectrum: 0 irradiation (shows mostly cis isomer). Top spectrum: 3 hrs irradiation (shows growth of trans isomer). In each spectrum, cis signals at δ = 5.82 and 6.60; trans signals at δ = 6.41 and 6.60)

Because the trans-β-methylstyrene quenched the excited state of the rhenium

photo-oxidant, it was necessary to perform a similar experiment as described above to

determine if and how much bond rotation can take place here. The same conditions were

used as above (20mM [(bpy)Re(CO)$_3$(py)$^+$][PF$_6^-$]/50 mM trans-β-methylstyrene in

CD$_3$CN). The sample was irradiated for several hours, taking ^{1}H NMR spectra at varying

time intervals to monitor the change in the signal from trans protons and any cis that

forms upon energy transfer. The results are shown in Figure 2-19. It is obvious that energy transfer is taking place and that isomerization of the initially 100% trans double bond to the cis isomer is occurring. It is important to note here that in this case, the amount of trans is decreasing while the amount of cis is increasing. In the case of **A-5mp**, the opposite occurs.

(bpy)Re(CO)₃py + β-
methylstyrene
time = 0 min

6.6   6.4   6.2   6.0   5.8   5.6   5

1.00

1.26

(bpy)Re(CO)₃py + β-
methylstyrene
time = 5 hr

.8   6.6   6.4   6.2   6.0   5.8   5.6   5.

1.00

0.18

1.01

(bpy)Re(CO)₃py + β-
methylstyrene
time = 12 hr

6.7   6.6   6.5   6.4   6.3   6.2   6.1   6.0   5.9   5.8   5.7   5.6   ppm

1.00   0.76

0.41
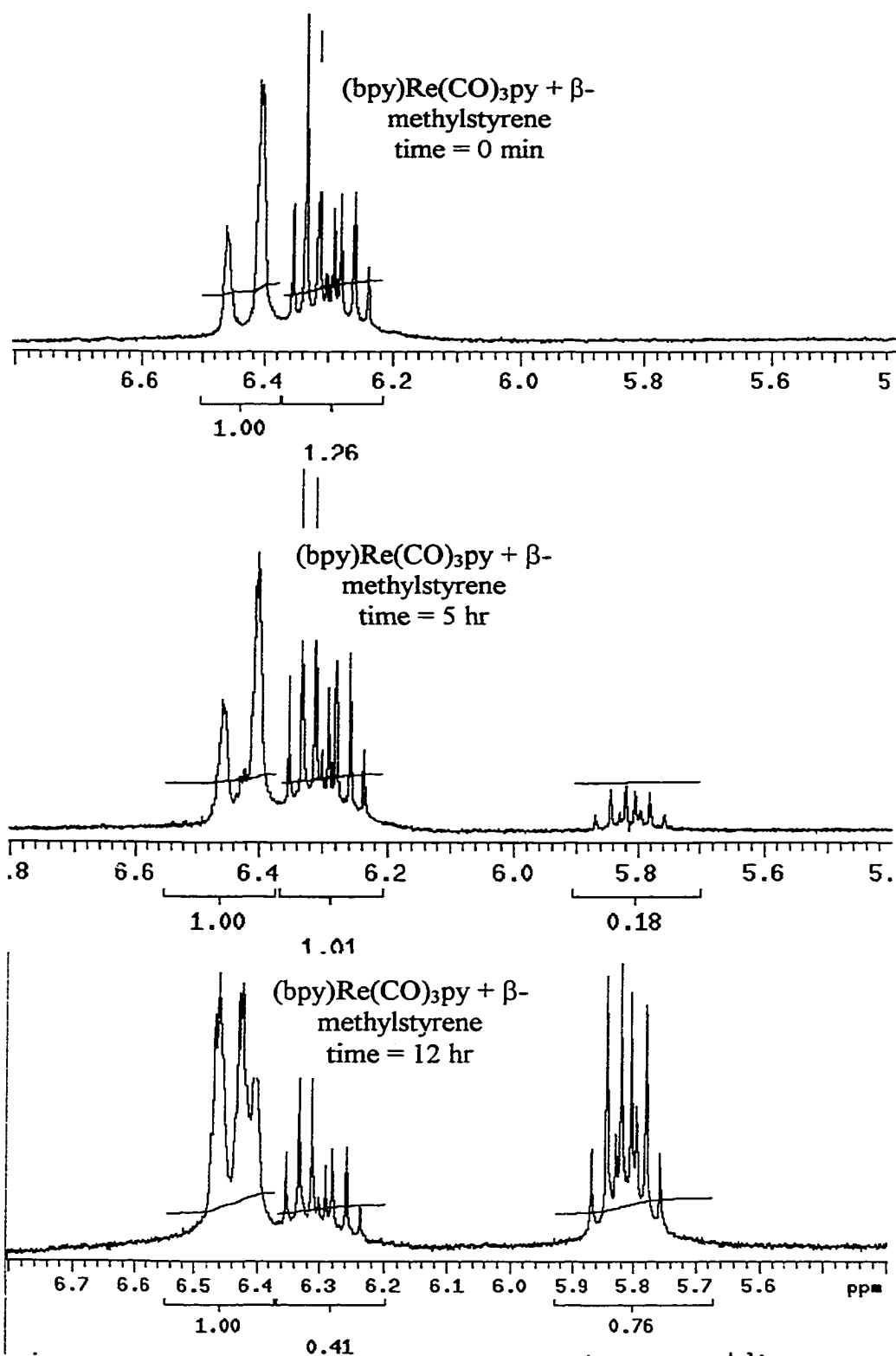
Figure 2-19. ¹H NMR spectra of trans-β-methylstyrene in the presence of (bpy)Re(CO)₃(py) monitoring the alkene protons.

42

Covalently Linked Studies

After the work on the bimolecular systems of the previous section, it was determined that there were three possible pathways for return electron transfer. The three ways are shown in Figure 2-20. 1) The cyclic distonic radical cation can simply ring open to the aminyl radical cation, which can then simply undergo return electron transfer with the reduced rhenium species. 2) Direct return electron transfer to the cyclic distonic radical cation could occur yielding an ylide which would then simply fragment a N-C bond to return to the ground state. 3) Return electron transfer to the cyclic distonic radical cation and bond fragmentation could occur in a concerted fashion (also known as dissociative return electron transfer or DRET). All of the data suggests that DRET is the most likely pathway. In an attempt to establish further evidence for DRET and to possibly determine the rate of the initial radical cation cyclization, complexes were synthesized which tethered A-5 and A-5mp directly to the rhenium center through a pyridine linkage as well as two model compounds for comparison (Re-A5, Re-A5mp, Re-bnz, and Re-py, Figure 2-10).
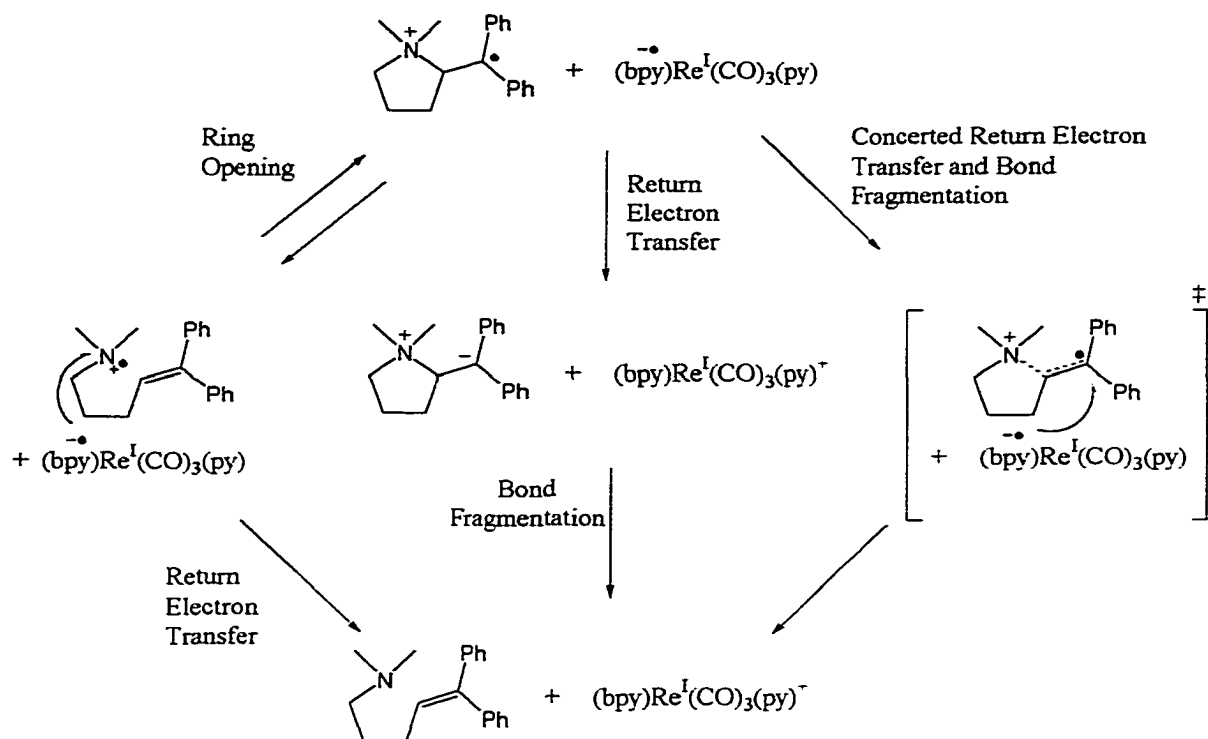
Figure 2-20. Possible pathways for return electron transfer

Emission Lifetime and Quenching Studies

The emission lifetime was determined for each of the complexes. Emission light was selected by using a P-10 600 nm emission filter. Lifetimes were calculated by the analysis of the experimental decays with DECAN, a rate-fitting program that allows for deconvolution of the instrument response function. The decays of Re-bnz and Re-pyr were fit with single component parameters, while Re-A5 and Re-A5mp were fit with two component parameters. Lifetimes of the rhenium-donor (Re-D) complexes are tabulated in Table 2-5.

Table 2-5. Emission and transient lifetimes

Compound	Component	τ_{em} (ns)	τ_{ta} (ns)
Re-bnz	---	210	210
Re-pyr	---	45	50
Re-A5	A	45 (0.92)*	50
	B	110 (0.08)*	150
Re-A5mp	A	45 (0.95)*	50
	B	100 (0.05)*	120

*Note: For the emission lifetimes, the amplitudes are shown in parenthesis.

Transient Absorption Spectra

Nanosecond transient absorption (TA) studies were carried out on each of the compounds in order to gain spectroscopic and kinetic information on excited states and reactive intermediates involved in the photochemistry. The program SPECFIT, a program designed to perform global kinetic analysis of time-resolved data, was used to determine the decay rates/lifetimes from each of the spectra.

Solutions of each of the Re-D complexes were made with a concentration of ~ 5 x 10^{-5} M. Each solution was argon degassed for 30 minutes and sealed in the cell. The spectra obtained from each sample are depicted in Figure 2-21. All spectra are qualitatively essentially the same, showing an absorption band from ~325 to 390 nm with a peak absorption at about 375 nm and a broad band from 400 to 500 nm. The two model compounds (Re-bnz and Re-pyr) upon global kinetic analysis show single component fits while the Re-D complexes (Re-A5 and Re-A5mp) show two component fits. The results of the global fits are shown compared to the emission lifetime data from above in Table 2-5.
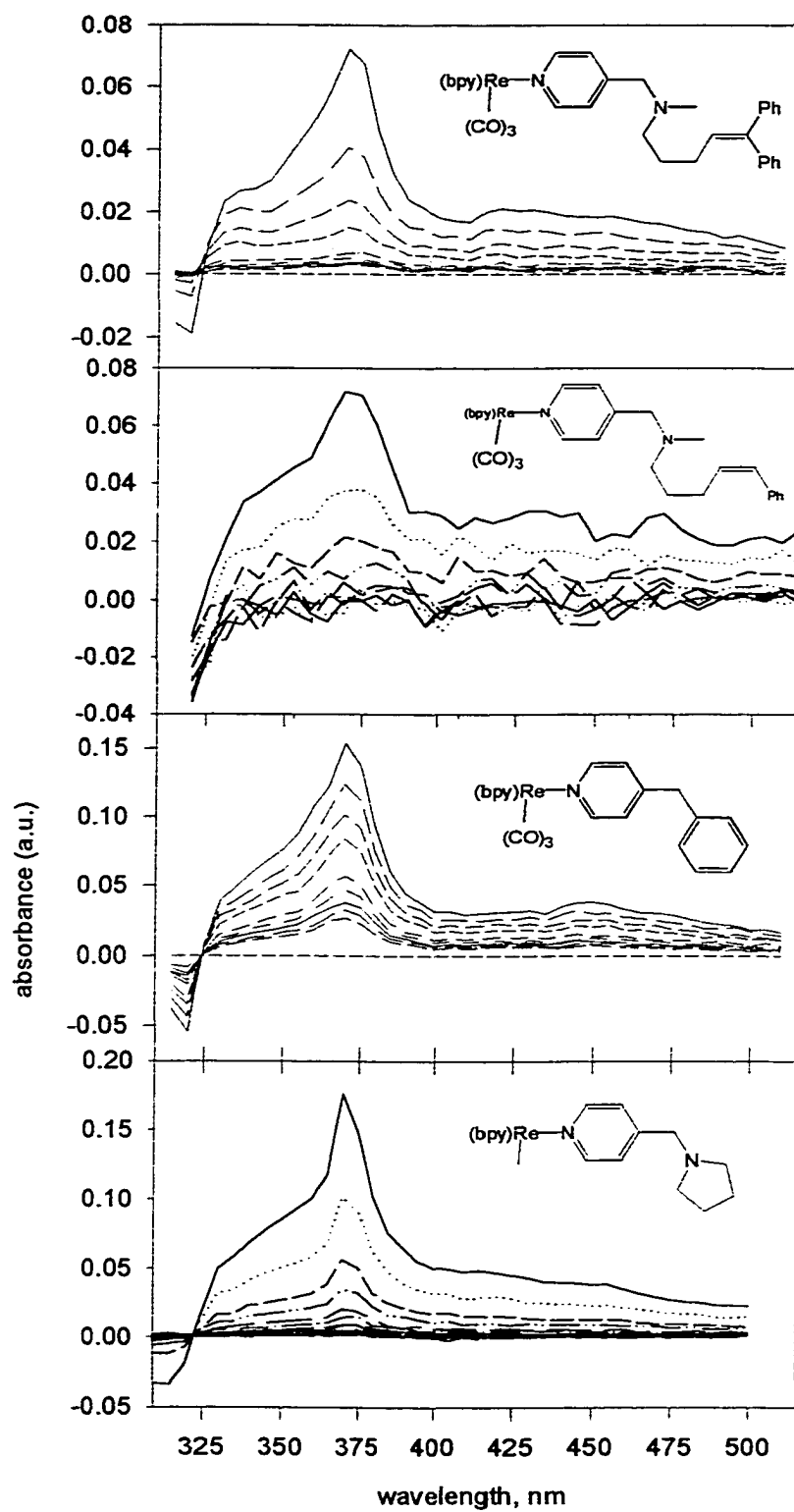
Figure 2-21. Transient absorption spectra of Re-A5, Re-A5mp, Re-bnz, and Re-pyr. Transients are in 40 ns intervals.

^{1}H NMR Studies

A similar experiment as those described for **A-5** and **A-5mp** was performed on the **Re-A5mp** complex where a solution of 4 mg of **Re-A5mp** was dissolved in 0.7 mL of CD_3CN was freeze/pump/thaw degassed in a sealable NMR tube. The tube was then irradiated at various time intervals. Again, between the irradiation times, the NMR spectrum (Figure 2-22) was taken monitoring the cis and trans alkene proton signals. Similar results were found as in the **A-5mp** study above. At time 0, the spectrum shows ~70% of the cis isomer and ~30% of the trans isomer. After 6 hours, an equilibrium point was found showing ~35% of the cis isomer and 65% or the trans isomer.
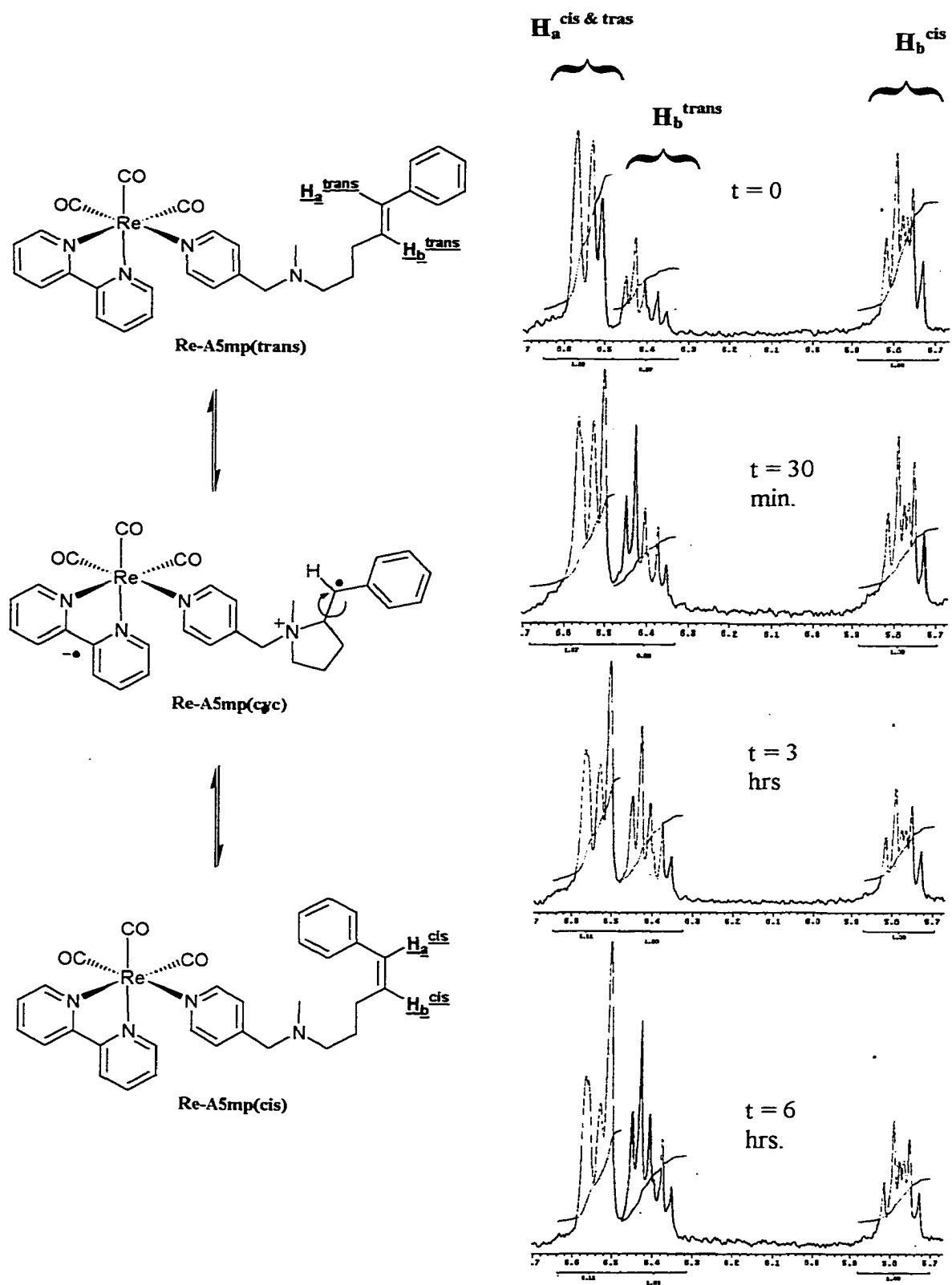
Figure 2-22. 1H spectra showing cis to trans isomerization of Re-A5mp

Discussion

Bimolecular studies

In order to relate the photophysical and photochemical results to the rate of the

photochemically induced cyclization that is observed in **A-5** and **A-5mp**, a kinetic model

must be, developed (Figure 2-23). Using the model presented in this scheme, the

photochemical reaction is proposed to occur via the following sequence: (1) initial

photoexcitation of the Re-photo-oxidant to the luminescent MLCT excited state; (2)

intermolecular donor (**A-5** or **A-5mp**) to metal electron transfer (with rate k_{fet}) to produce

the aminium radical cation; (3) reversible cyclization to form the distonic pyrolidinium

radical cation (with rate k_{cyc}); (4) back electron transfer prior to cyclization; (5) charge

recombination or back electron transfer after cyclization.
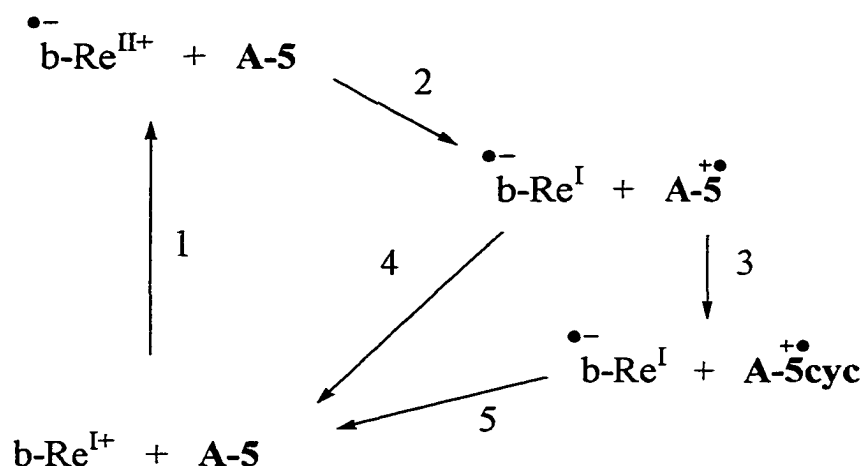
Figure 2-23. Proposed mechanism

The TA spectrum obtained of **A-5** with the Re photo-oxidant shows a strong band

with a 330 nm maximum even at the earliest times. This, based on literature data, can be

ascribed to the diphenyl methyl radical, which can only form via the ring closing of the

aminyl radical cation with the alkene, analogous to 5-hexenyl radical systems. All other

absorption bands can be attributed to the reduced rhenium species. This, along with the fact that the yield studies show a high yield of around 0.70, it can be assumed that electron transfer is taking place.

Further evidence for electron transfer and subsequent cyclization is seen when looking at the **A-5mp** system. Upon irradiation of **A-5mp** in the presence of the Re photo-oxidant, it is seen that the cis and trans proton signal ratios change in the ^{1}H NMR spectra reaching an equilibrium. Because β-methylstyrene also shows cis-trans isomerization in a similar experiment, there are two possible pathways that can result in this isomerization; 1) triplet energy sensitized bond rotation (energy transfer), 2) rotation about the C-C bond after cyclization of the aminyl radical cation (**A-5mp$^{+\cdot}$**) formed by electron transfer from the excited state of the metal, to the cyclized radical cation (**A-5mp$_{cyc}^{+\cdot}$**, Figure 2-16). The data suggests that **A-5mp** isomerizes through the second method (electron transfer/cyclization/bond rotation). This conclusion stems from three facts: 1) isomerization of β-methylstyrene can only occur through energy transfer, 2) the final equilibrium ratio of cis and trans isomers of β-methylstyrene overwhelmingly favors the cis isomer, and 3) the final equilibrium of cis and trans isomers of **A-5mp** favors the trans isomer. Energy transfer reactions would always favor the cis; however, **A-5mp** favors the trans and thus must isomerize from the cyclized radical ion.

Several attempts to resolve the rate of cyclization (k_{cyc}) for the original **A-5**/Re photo-oxidant system have been made; however, our instrument capabilities have limited us and thus we estimate that the cyclization occurs with a rate that is greater than or equal to 2×10^7 s^{-1} (instrument's limit). A mechanism of this entire process is proposed from this initial data and is shown in Figure 2-23. The Re complex is excited by light, yielding

Re*. A-5 then donates an electron from the lone pair of the nitrogen producing the Re radical anion and A-5$^{+\cdot}$. Upon this initial electron transfer, the aminyl radical cation can then cyclize with the intermolecular double bond forming a five membered quaternary amine structure with an exocyclic diphenyl-methyl radical (A-5cyc$^{+\cdot}$). This diphenyl-methyl radical absorbs strongly in the 330 nm region of the UV spectrum.

One of the more interesting pieces of data was obtained upon a kinetic analysis of the spectrum showed that the return electron transfer occurred extremely fast with a rate constant ca. 7×10^9 $M^{-1}s^{-1}$. As stated earlier, there are three possible pathways for return electron transfer (Figure 2-19). It would normally be assumed that back electron transfer from the reduced metal to the cyclized aminyl radical cation would first form an anion at the diphenyl methyl, which would then kick in and break the N$^+$-C bond (Figure 2-24).
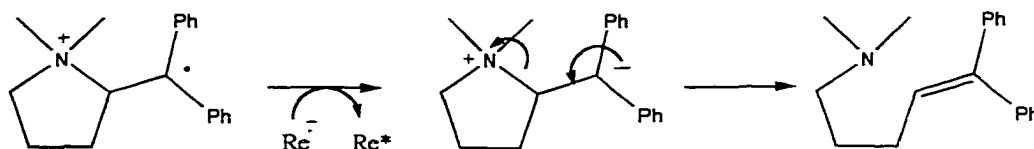
Figure 2-24. Formation of anion via BET

However, this rapid decay back to the ground state implicates dissociative return electron transfer (DRET). DRET can only be possible if electron transfer from the reduced metal to the cyclized aminyl radical cation and the N-C bond fragmentation occur concertedly.

DRET is further supported by the first steady state ^{1}H NMR study on A-5/Re photo-oxidant photolysis. Because the spectrum before irradiation and the spectrum after irradiation show little difference, other possible reactions can be ruled out. If other

modes of back electron transfer were taking place such as an anion being formed on the diphenyl methyl unit by electron transfer from the radical anion of the metal species, one would assume that this anion would be reactive enough to do further chemistry. Since no other chemistry is observed through the NMR spectra, DRET is likely the only process that can take place.

Unimolecular studies

In order to further study the kinetics of this amino-ethylene system, the A-5 and A-5mp moieties were covalently linked to the rhenium through a mono-dentate pyridine (Re-A5 and Re-A5mp, Figure 2-4). The objectives in doing so are two fold. First, in hopes to speed up the initial electron transfer in order to build up a larger concentration of the uncyclized A-5 radical cation so that the rate of cyclization could be further resolved. Second, to have better evidence for the DRET mechanism described earlier.

Again, in order to relate the photophysical and photochemical results to the rate of the photochemically induced cyclization observed for Re-A5 and Re-A5mp, a kinetic model must be developed (Figure 2-25). According to the proposed kinetic model, there is first an initial photoexcitation to the luminescent MLCT excited state. This is followed by irreversible intramolecular donor ligand to metal electron transfer (rate = k_{FET}) to produce the LLCT state. Next, reversible cyclization occurs forming a pyrolidinium radical cation (rate = k_{cyc}) followed by charge recombination via dissociative return electron transfer (rate = k_{DRET}). It is important to note that forward electron transfer competes with decay of the MLCT excited state via normal radiative and nonradiative decay pathways (rate = k_d), and cyclization competes with decay of the LLCT state via back electron transfer (rate = k_{BET})
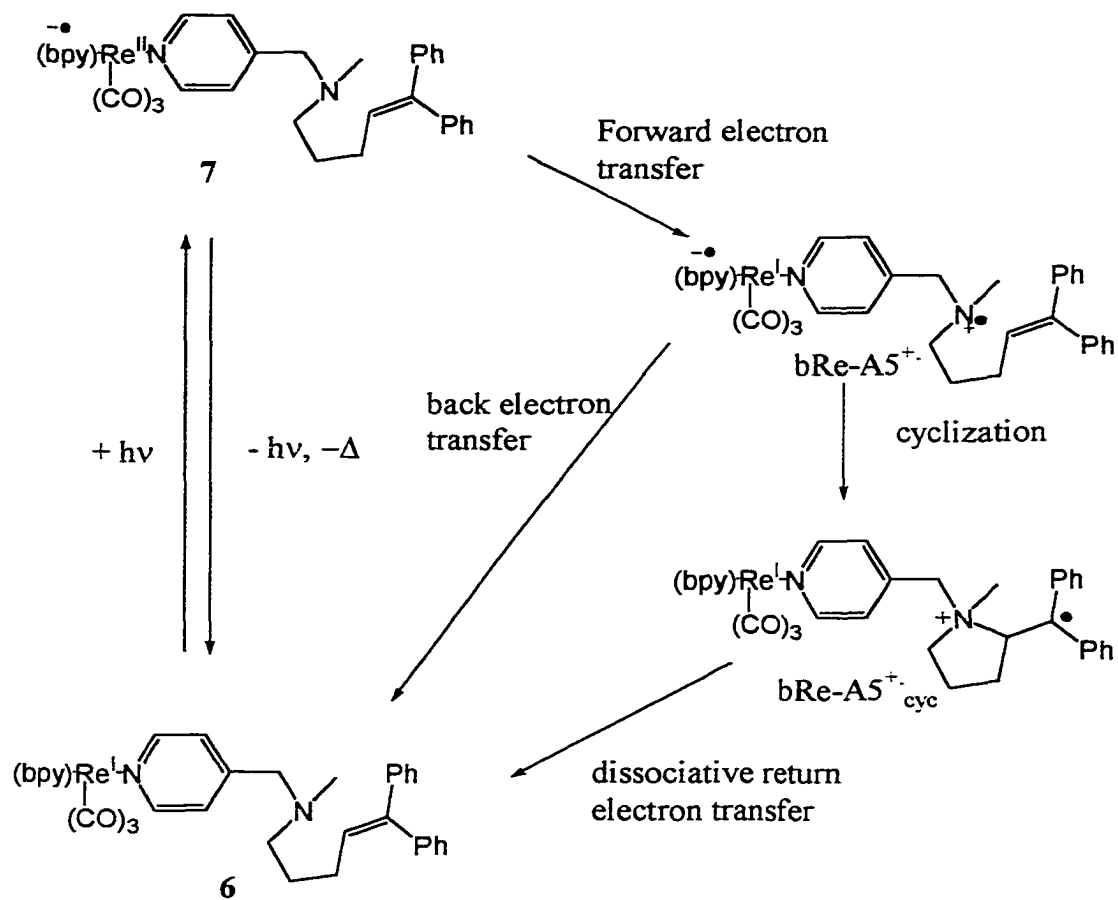
Figure 2-25. Proposed photochemical mechanism

Along with Re-A5 and Re-A5mp, model compounds Re-bnz and Re-pyr (Figure 2-4) were also needed to further understand the processes associated with the Re-A5 and Re-A5mp. First, Re-bnz was chosen because this species can only exhibit metal to ligand charge transfer (1→2), followed by simple decay of the excited state (2→1) as shown in Figure 2-26a. This gives a base from which to build. The next model chosen was Re-pyr. This complex adds another pathway for deactivation. Along with the normal modes (4→3), there is also the availability of the lone pair on nitrogen for electron donation (4→5) followed by charge recombination (5→3), as shown in Figure 2-26b. By studying

these two compounds and understanding the kinetics of the processes they

$$*\text{(bpy)Re}^{II}\text{-bnz} \qquad\qquad *\text{(bpy)Re}^{II}\text{-pyr}$$

2 $\qquad\qquad\qquad\qquad$ **4** $\qquad k_{4\to5}$

A $\qquad h\nu \;\; \Big\updownarrow\; k_{2\to1} \qquad$ **B** $\qquad h\nu \;\; \Big\updownarrow\; k_{4\to3} \qquad \text{(bpy)Re}^{I}\text{-pyr}$

5

$k_{5\to3}$

$$\text{(bpy)Re}^{I}\text{-bnz} \qquad\qquad \text{(bpy)Re}^{I}\text{-pyr}$$

1 $\qquad\qquad\qquad\qquad$ **3**
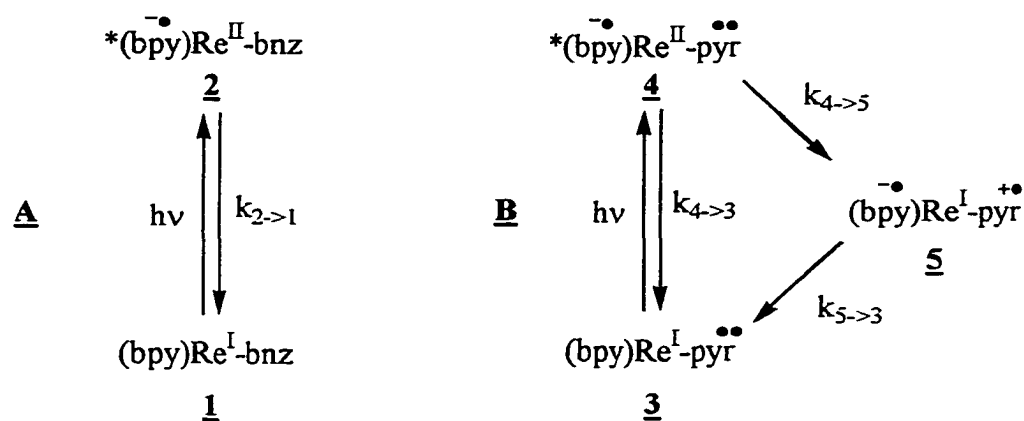
Figure 2-26. Mechanism for **Re-bnz** and **Re-pyr**

exhibit, a better understanding of the mechanism and kinetics of **Re-A5** can be

developed. As seen in Figure 2-27, **Re-A5** not only exhibits the excitation pathway

identical to both the model compounds (6→7 vs. 1→2 and 3→4), electron donation to

form an aminium radical cation as in Re-pyr (7→8 vs. 4→5), but has still another

pathway where the aminium radical cation can rearrange (8→9).

$$*\text{(bpy)Re}^{II}\text{-A5}$$

7 $\qquad k_{7\to8}$

$$\text{(bpy)Re}^{I}\text{-A5}$$

8

$h\nu \;\; \Big\updownarrow\; k_{7\to6} \qquad\qquad\qquad k_{8\to9}$

$k_{8\to6} \qquad \text{(bpy)Re}^{I}\text{-A5}_{cyc}$

9

$$\text{(bpy)Re}^{I}\text{-A5} \qquad k_{9\to6}$$

6
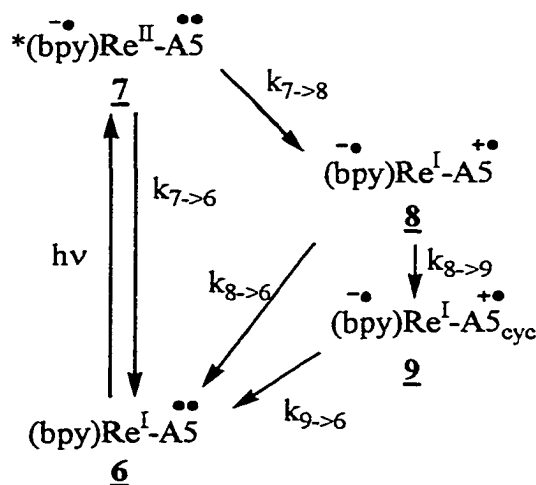
Figure 2-27. Mechanism for **ReA5**

54

Nanosecond transient absorption experiments on these complexes, at first glace, show little evidence for the cyclization of the **A-5** ligand. However, upon further inspection and comparison with the model compounds, it is clearly evident that cyclization is taking place, albeit not as prevalent in the bimolecular studies. The TA spectrum of Re-bnz, being that only electron transfer from the metal to the diimine can take place, shows only the MLCT state absorption. SPECFIT analysis gives a lifetime of 210 ns with a single component fit.

The TA spectrum of **Re-pyr** (Figure 2-19) qualitatively looks much like that of **Re-bnz**, indicating the absorption is due to the MLCT state. The only exception is that the decay is much faster as evident by the lifetime of 50 ns, again determined by a single component fit. To explain this one must look at Figure 2-24b, which illustrates that after formation of the MLCT state (4), there are two pathways of decay. The first is through normal modes of decay as seen in **Re-bnz**, and the second is through electron transfer from the donor pyrollidine ligand. It is this second process that is much faster than the normal modes seen in **Re-bnz** and thus the rate determining step for deactivation ($1/\tau = k_{4\rightarrow3} + k_{4\rightarrow5}$). Since the normal modes of deactivation are much slower than that of electron transfer from the amine, the rate constant for forward electron transfer can be taken as the inverse of the observed lifetime (τ_{obs}=50 ns, $k_{4\rightarrow5} = 2 \times 10^7$ s^{-1} (Equation 2-4)). The fact that there seems to be no build up of 5, and studies on similar amine systems have placed a lower limit for the rate of back electron transfer ($k_{5\rightarrow3}$) around 1×10^8 s^{-1}, leads to the assumption that Re-pyr would show similar rates, thus implying that $k_{5\rightarrow3} > 1 \times 10^8$ s$^{-1} >> k_{4\rightarrow5}$.

Again, the TA spectrum of **Re-A5** (Figure 2-19) looks qualitatively the same as that of Re-bnz and Re-pyr. This implies that the majority of what is being observed is again decay from the MLCT state. There are, however, subtle, but significant differences between the spectra of the model complexes and that of **Re-A5**. Most notably is the slightly enhanced absorption band at 330 nm. Specfit analysis of this transient absorption data confirmed this point by yielding an excellent fit to two components with lifetimes ca. 50 ns and 150 ns, which corresponds to decay rates of 2×10^7 s^{-1} and 6×10^6 s^{-1}, respectively. The calculated spectrum of each is depicted in Figure 2-28, where the first component with an observed lifetime of 50 ns has the same shape as the two model compounds. This component must correspond to the MLCT state, which, like that of Re-pyr, has two modes of decay. When comparing this MLCT state to that of Re-pyr, it is clear that they have the same lifetime, which confirms that the rate of forward electron transfer is 2×10^7 s^{-1}. In the calculated spectrum of the second component, there is a relatively strong absorption band around 330 nm, which likely arises from the diphenyl-methyl radical (Ph$_2$C$^{\cdot}$-R). This suggests that the second component corresponds to the cyclized charge-transfer state, and that this state decays with a rate of $1/\tau = 6 \times 10^6$ s^{-1}. All lifetimes correspond to those obtained via emission lifetime experiments and are tabulated in Table 2-5.

56
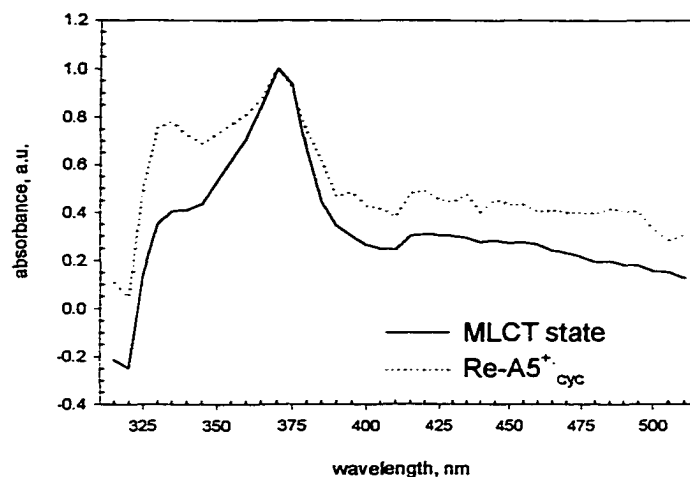
Figure 2-28. Spectral analysis showing two components

To interpret this data and apply it to Figure 2-23, it is easiest to describe the entire

process again and redisplay in Figure 2-29. Starting at the ground state, excitation yields

the MLCT state. At this point there are two pathways: (1) normal radiative and

nonradiative decay (rate = k_d), and (2) forward electron transfer (rate = k_{FET}) yielding the

aminium radical cation. Because of the close relation of **Re-bnz** to **Re-A5**, it can be

assumed that the decay rate found for **Re-bnz** can approximate the normal radiative and

non-radiative decay rate of **Re-A5**, thus placing a value on $k_d = 4.8 \times 10^6$ s^{-1}. Again,

because of the close relationship between **Re-pyr** and **Re-A5**, it can be assumed that the

forward electron transfer rate for Re-pyr approximates the rate of forward electron

transfer, placing a value on $k_{FET} = 2 \times 10^7$ s^{-1}.

At this point, the aminium radical cation has two competitive paths to take: back

electron transfer and cyclization. The study of the model compound **Re-pyr** indicates

that back electron transfer occurs faster that forward electron transfer with a rate likely

greater than 10^8 s^{-1} ($k_{BET}>10^8$ s^{-1}). Because the absorption due to the diphenylmethyl

radical is present at even the earliest times, we are not able to place an absolute rate

constant for the cyclization. However, since cyclization competes with back electron

transfer, and there is no build up of the diphenylmethyl radical, it can only be concluded that back electron transfer is faster than the cyclization. This places an upper limit of 1×10^8 s^{-1} for k_{cyc}. It is also known from the bimolecular studies that the cyclization is also faster than forward electron transfer, which places a lower limit on kcyc at 2×10^7 s^{-1}. Therefore, k_{cyc} falls in the range of 1×10^8 s^{-1} and 2×10^7 s^{-1}, placing the rate ca. 5×10^7 s^{-1}. Since it would be uphill in energy for the cyclized species to return to the acyclic radical cation, the only means of decay is dissociative return electron transfer. Since it has been determined that the second component in the transient absorption spectrum of **Re-A5** is likely due to the cyclized radical cation, the rate for DRET (k_{DRET}) can be given as 6×10^6 s^{-1}.
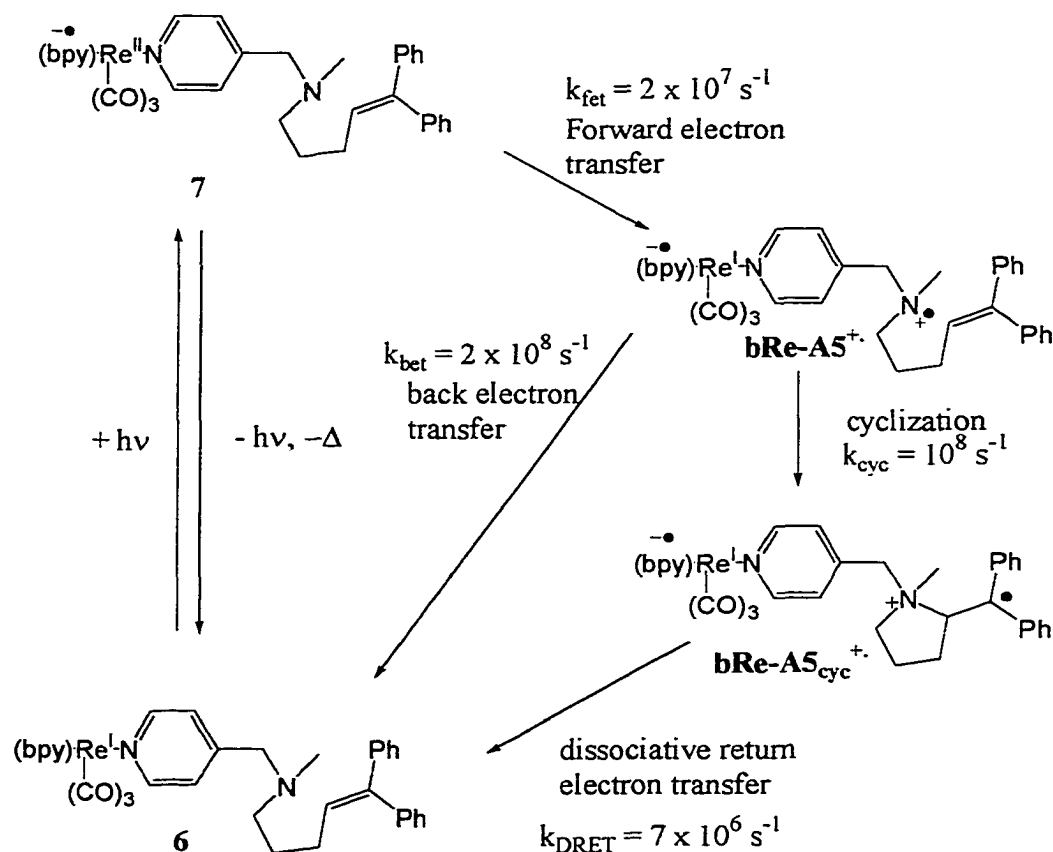
Figure 2-29. Entire mechanism and approximate rates for intramolecular radical ion cyclization

58

Experimental

Transient Absorption Spectroscopy

All TA experiments were carried out using the third harmonic of a Nd:YAG laser (355 nm, 10 ns fwhm, 5-10 mJ/pulse) to excite into the Re→bpy MLCT absorption band. These experiments were carried out in an argon degassed recirculating cell to minimize the possibility of photodegredation during data acquisition. Global kinetic fits were obtained utilizing the SPECFIT program, which uses singular value decomposition to obtain orthogonal (transient absorption) spectral eigenvectors. The temporal evolution of the spectral eigenvectors is then fitted to a user-defined kinetic model using the Levenburg-Marquadt algorithm.

Steady-State Aberchrome 540 Actinometry:

Aberchrome 540 (6.5 mg, 0.025 mmol) was dissolved in 5 mL of toluene. A 0.5 mL aliquot was diluted to 2 mL and the absorption spectrum of this solution was obtained and showed no absorbance at 500 nm. Next, 0.5 mL of the solution was pipetted into each of five NMR tubes. One tube was irradiated for 20 minutes with a 450 W arc lamp with filters selected to allow 366 nm light to reach the solution. After this time, the solution was transferred to a 2 mL volumetric flask and diluted with toluene. The absorption spectrum was then obtained of this diluted solution. A new band in the absorption spectrum had grown in at 500 nm. Another NMR tube was irradiated for 10 minutes and the dilution procedure described above was performed. Again, the absorption spectrum was obtained of this diluted solution. The band at 500 nm was half as intense as that of the previous solution. This was repeated several times varying irradiation times.

Plotting the absorbance versus time yielded a slope of 1.197×10^{-3} s^{-1}. Using

equation 2-3, where A/t is the slope of the line, V is the volume, N_A is avagadro's

number, P is the quantum yield and e is the extinction coefficient at 494 nm, it was

determined that the intensity, I, was 8.79×10^{14} photons/s. By dividing the number of

moles of A-5 by the intensity of the light it was determined that for 0.7 mL of a 50 mM

solution of A-5, a time of 6.66 hours of irradiation was required to convert all of the

compound to a photo-product, assuming a quantum yield of unity.

$$I = \frac{A \times V \times N_A}{t \times \Phi \times \varepsilon} \qquad (2\text{-}3)$$

Emission Lifetime

Emission lifetimes were determined by time-correlated single photon counting on

a PRA (Photochemical Research Associates) system. The excitation source was a

hydrogen-filled spark gap preset at a repetition frequency of 3×10^4 Hz. Emission light

was selected by using a P-10 600 nm emission filter. Lifetimes were calculated by the

analysis of the experimental decays with DECAN, a rate-fitting program that allows for

deconvolution of the instrument response function.

Synthesis:

A synthetic scheme for all products is shown in Figure 2-30.

PhMgBr
THF

1a X=Cl
1b X=H

2a Y=Ph
2b Y=H

HOTs

MeNH₂ or
Me₂NH

Z

Me

A5 Y=Ph, Z=Me
A5mp Y=H, Z=Me
4a Y=Ph, Z=H
4b Y,Z=H

3a Y=Ph
3b Y=H

NaCNBH₃

hv

Me

5a Y=Ph
5b Y=H

Me

6a Y=H

(CO)₃

ReA5 Y=Ph
ReA5mp Y=H
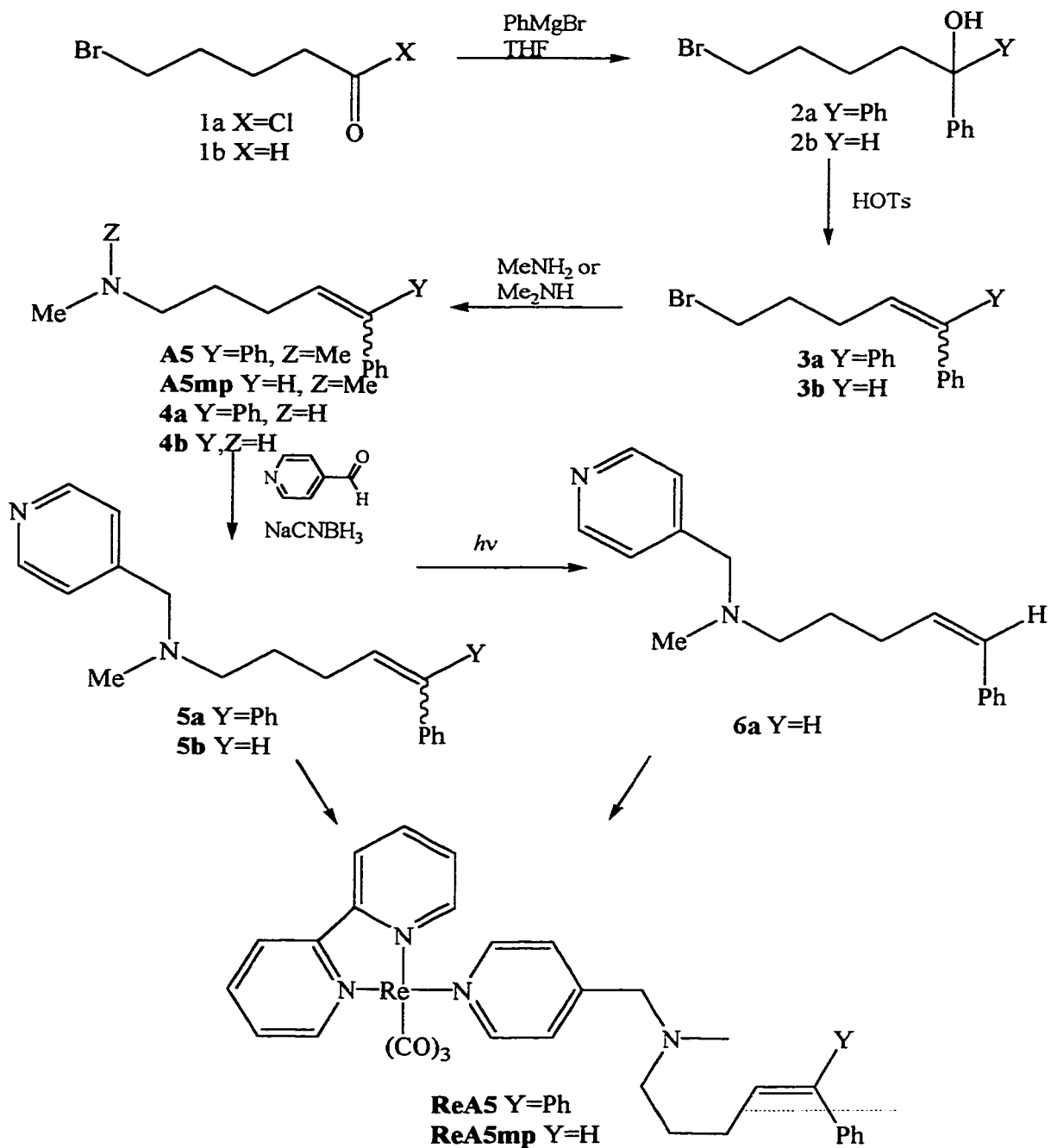
Figure 2-30. Synthesis

5-Bromo-1,1-diphenyl-1-pentanol. To an oven dried, nitrogen flushed flask charged with 100 mmol of phenylmagnesium bromide, 5-bromo-pentanoyl chloride (Aldrich) (7.83 g, 39.1 mmol) was added drop-wise over a period of 30 minutes. After the solution was stirred for 15 minutes at 0°C and then 15 minutes at room temperature, 100 mL of saturated aqueous NH₄Cl was added slowly. The organic layer was separated and washed with brine and dried over NaSO₄. The solvent was evaporated and the crude product recrystallized from ether-hexane yielding the product as a white solid, yield 10.03 g (78%). Spectra match those of the literature.[54]

5-Bromo-1,1-diphenyl-1-pentene. To a solution of 5-bromo-1,1-diphenyl-1-pentanol (10.03 g, 31.15 mmol) dissolved in 150 mL of benzene, p-toluenesulfonic acid (0.1 g, 0.58 mmol) was added. This solution was allowed to reflux for 6 hours. Upon cooling, the resulting solution was washed with 50 mL of saturated aqueous NaHCO₃, organic layer separated and solvent removal under reduced pressure gave the product as a yellow oil, 9.44 g (94%). Spectra match those of the literature.[54]

N,N-Dimethyl-5,5-diphenyl-4-pentenamine. 75 mL of 40% dimethylamine in water was added to a solution of 5-bromo-1,1-diphenyl-1-pentene (9.44 g, 31.0 mmol) in 100 mL of THF. The reaction was allowed to stir overnight, after which time, THF was removed under reduced pressure. This was followed by the addition of 100 mL of diethyl ether. The organic layer was separated and extracted with 50 mL of 10% aqueous HCl. The HCl extract was then neutralized with 10% aqueous NaOH causing the solution to cloud up. The solution was then extracted with 100 mL of ether and the organic layer separated and solvent removed under reduced pressure yielded a yellow oil as the crude

product. Column chromatography (silica, 9:2:0.5; CH3CN/MeCl2/TEA) afforded the product as a yellow oil, yield 6.4 g (78.2%). Spectra match the literature data. [54]

5-bromo-1-phenyl-1-pentanol. To an oven dried, nitrogen flushed flask charged with 100 mmol of phenylmagnesium bromide, 5-bromo-pentanal (Aldrich) (7.83 g, 39.1 mmol) of was added drop-wise over a period of 30 minutes. After the solution was stirred for 15 minutes at 0°C and then 15 minutes at room temperature, 100 mL of saturated aqueous NH_4Cl was added slowly. The organic layer was separated and washed with brine and dried over $NaSO_4$. The solvent was evaporated and the crude product recrystallized from ether-hexane yielding the product as a white solid, yield 10.03 g (92%). Spectra match the literature data. [54]

5-bromo-1-phenyl-4-pentene. The same method was used as that used in the synthesis of 5-Bromo-1,1-diphenyl-1-pentene substituting 5-bromo-1-phenyl-1-pentanol for 5-bromo-1,1-diphenyl-pentanol, yield 78%. Spectra match the literature data. [54]

N,N-dimethyl-5-phenyl-4-pentenamine. The same method of amination was used as in the synthesis of N,N-dimethyl-5,5-diphenyl-4-pentenamine substituting 5-bromo-1-phenyl-4-pentene in place of 5-bromo-1,1-diphenyl-4-pentenamine, yield 1.42 g (52%). [54]

N-methyl-5-phenyl-4-pentenamine. The exact synthesis of N,N-Dimethyl-5-phenyl-4-pentenamine was followed with the exception of using methylamine in place of dimethyl amine, yield 0.96 g (58%). Spectra match the literature data. [54]

N-methyl-5,5-diphenyl-4-pentenamine. The exact synthesis of N,N-Dimethyl-5,5-diphenyl-4-pentenamine was followed with the exception of using methyl amine in place of dimethylamine, yield 1.26 g (53%). Spectra match the literature data. [54]

N-(4-pyridyl)-methyl-N-methyl-5,5-diphenyl-4-pentenamine. N-methyl-5,5-

diphenyl-4-pentenamine (1 g, 25.7 mmol) was dissolved in 20 mL of methanol. To this

mixture was added pyridine-4-carboxaldehyde (3 g, 28.6 mmol) dissolved in 5 mL of

methanol. The solution was allowed to stir for 5 minutes. The pH of the solution was

brought to 6.5 with glacial acetic acid and allowed to stir for 5 minutes more.

$NaBH_3(CN)$ (3.075 g, 48.8 mmol) was then added turning the solution bright orange.

The mixture was allowed to stir overnight. After the night, the pH was brought to 2 with

acetic acid and the solvent removed in vacuum. The solid was dissolved in 100 mL water

and brought to pH 10. The solution was next washed with three portions of ethyl acetate.

The solvent removed and column chromatography (88:8:4 ethyl acetate:hexane:TEA)

yielded pure product as a yellow oil, yield 0.72 g (65%). ^{1}H NMR ($CDCl_3$, 300 MHz)

δ 8.49 (d, 2H), 7.35 (d, 2H), 7.22 (m, 10H), 6.08 (t, 1H), 3.43 (s, 2H), 2.37 (t, 2H), 2.16

(m, 2H), 2.14 (s, 3H), 1.65 (m, 2H). ^{13}C NMR ($CDCl_3$, 300 MHz) δ 149.50, 148.65,

142.57, 141.88, 140.05, 129.95, 129.78, 129.31, 128.07, 127.07, 126.83, 126.78, 123.69,

60.86, 56.99, 42.19, 27.57, 27.40 ppm.

N-(4-pyridyl)-methyl-N-methyl-5-phenyl-4-pentenamine. The same procedure

was used as for the synthesis of N-(4-pyridyl)-methyl-N-methyl-5,5-diphenyl-4-

pentenamine replacing N-methyl-5-phenyl-4-pentenamine for N-methyl-5,5-diphenyl-4-

pentenamine, yield 0.65 g (68%). ^{1}H NMR ($CDCl_3$, 300 MHz) δ 8.88 (d, 2H), 8.00 (d,

2H), 7.50 (m, 5H), 5.87 (t, 1H), 2.89 (s, 2H), 2.62 (t, 2H), 2.24 (m, 2H), 2.06 (m, 2H). [13]C

NMR ($CDCl_3$, 300 MHz) δ 151.5, 140.6, 136.8, 135.8, 133.3, 130.3, 123.6, 106.3, 101.7,

44.4, 42.8, 42.2, 33.4, 31.8 ppm.

N-pyridyl-4-methyl-pyrrollidine. Similar procedure as that of N-(4-pyridyl)-methyl-N-methyl-5,5-diphenyl-4-pentenamine was used except the yields were better when the reaction was performed neat with pyridine carboxaldehyde and pyrrollidine. Also the use of HCl in place of acetic acid increased the yield. Column chromatography gave 82% yield. ^{1}H NMR (CDCl$_3$, 300 MHz) δ 8.6 (d, 2H), 7.41 (d, 2H), 3.62 (s, 2H), 2.25 (t, 4H), 1.61 (t, 4H). ^{13}C NMR (CDCl$_3$, 300 MHz) δ 150.3, 146.5, 124.4, 59.1, 51.4, 23.5 ppm.

(bpy)Re(CO)$_3$Cl. 2.4053 g of Re(CO)$_5$Cl and 1.0458 g of bipyridine were dissolved in 250 mL of Toluene and refluxed for 1 hr. Filtration of the precipitate yielded 2.969 g of (bpy)Re(CO)$_3$Cl for 97% yield. Spectra match those of the literature data.[74]

(bpy)Re(CO)$_3$(CF$_3$SO$_3$). 1.007 g (bpy)Re(CO)$_3$Cl was dissolved in 50 mL of freshly distilled methylene chloride. The flask was degassed with argon and 1.6 mL of triflic acid was then added slowly. After 30 minutes, 100 mL of dry diethyl ether was added producing a bright yellow ppt. The solid was washed with diethyl ether and dried to give (bpy)Re(CO)$_3$(CF$_3$SO$_3$), yield 1.10 g (88 %). Spectra match those of the literature data.[74]

Re-A5, Re-A5mp, Re-bnz, Re-pyr. All final complexes were synthesized in the same fashion. A typical procedure for **Re-A5** is described: Compound **5a** (0.045 g, 0.17 mmol) was placed in a 50 mL round bottom flask and dissolved in 5 mL of freshly distilled, dry THF. Freshly prepared (bpy)Re(CO)$_3$(CF$_3$SO$_3$) (0.055 g, 0.1 mmol) and NH$_4$PF$_6$ (0.21 g, 1.3 mmol) were then added to the solution. TLC (10% CH$_3$CN/CH$_2$Cl$_2$, alumina) was used to monitor the reaction while it was stirred at room temperature under

a blanket of nitrogen for 12 hours. After 14 hours, the reaction mixture was filtered to remove excess NH_4PF_6 and the THF was evaporated under reduced pressure. The crude product was then dissolved in ca. 0.5 mL of CH_2Cl_2 and then precipitated by dropping the solution into 25 mL of diethyl ether with rapid stirring. The product was collect by filtration on a sintered glass funnel. Further purification by chromatography (10% CH_3CN/CH_2Cl_2, alumina) afforded the product as a yellow crystalline solid, yield 32 mg (40%). ^1H NMR (CDCl$_3$, 300 MHz) δ 9.07 (t, 2H), 8.58 (d, 2H), 8.31 (t, 2H), 7.92 (d, 2H), 7.72 (t, 2H), 7.41 (m, 12H), 6.04 (t,1H), 3.40 (s, 2H), 2.35 (t, 2H), 2.12 (m, 2H), 2.03 (s, 3H), 1.29 (m, 2H). ^{13}C NMR (CDCl$_3$, 300 MHz) δ 153.03, 152.41, 151.72, 146.32, 145.62, 140.28, 139.61, 137.82, 136.53, 135.80, 133.31, 131.18, 130.36, 129.65, 127.23, 123.62, 120.67, 116.76, 59.25, 55.67, 44.37, 32.66, 28.42 ppm.

Re-A5mp. Yield 46 mg (37%) ^1H NMR (CDCl$_3$, 300 MHz) δ 9.08 (d, 2H), 8.52 (d, 2H), 8.23 (t, 2H), 7.98 (m, 2H), 7.77, (t, 2H), 7.26 (m, 7H), 6.39 (m, 1H), 6.18 (m, 0.3H), 5.59 (m, 0.7H), 3.41 (s, 0.6H), 3.39 (s,1.4), 2.38 (m, 2H), 2.03 (m, 2.1H), 2.01 (s, 0.9H), 1.59 (m, 2H). ^{13}C NMR (CDCl$_3$, 300 MHz) δ 150.68, 149.72, 133.28, 131.24, 130.28, 130.12, 129.60, 129.36, 129.00, 127.72, 127.40, 126.76, 125.32, 124.60, 61.72, 57.48, 42.60, 30.88, 27.32 ppm.

Re-pyr. Yield 72 mg (62%) ^1H NMR (CDCl$_3$, 300 MHz) δ 9.22 (d, 2H), 8.39 (d, 2H), 8.28 (m, 2H), 8.14 (d, 2H), 7.78 (m, 2H), 7.25 (d, 2H), 3.59 (s, 2H), 2.43 (broad t, 4H), 1.71 (broad t, 4H) ^{13}C NMR (CDCl$_3$, 300 MHz) δ 156.8, 154.87, 152.68, 142.15, 129.83, 127.04, 125.73, 58.76, 54.76, 24.56 HRMS calc'd for $C_{23}H_{22}N_4O_3Re$, 589.125; observed 589.128.

CHAPTER 3
SYNTHESIS AND PHOTOPHYSICS OF BIPYRIDYL PLATINUM BISACETYLIDES

Introduction

Platinum Acetylides

Recently there has been much interest in the development of luminescent

materials based on platinum centers owing to the observation of luminescence from a

number of platinum(II) complexes. In 1989, the first report of luminescence from a

platinum species with an acetylide ligand was found by Demas and coworkers.[76] The

platinum complex, $[Pt_2(\mu\text{-}C\text{=}CHPh)(C\equiv CPh)(PEt_3)_3Cl]$ (Figure 3-1), was found to exhibit

red-orange luminescence in a 4:1 ethanol/methanol glass at 77 K (Figure 3-2), which was

initially attributed to the spin-forbidden metal-centered d-p phosphorescence because of

the similarity of the emission to the d-p phosphorescence of Pt d^8-d^8 and d^{10}-d^{10}

complexes.

1
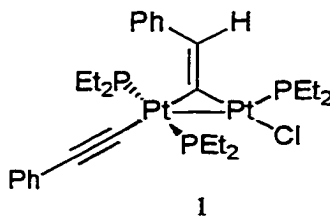
Figure 3-1: $[Pt_2(\mu\text{-}C\text{=}CHPh)(C\equiv CPh)(PEt_3)_3Cl]$ studied by Demas.
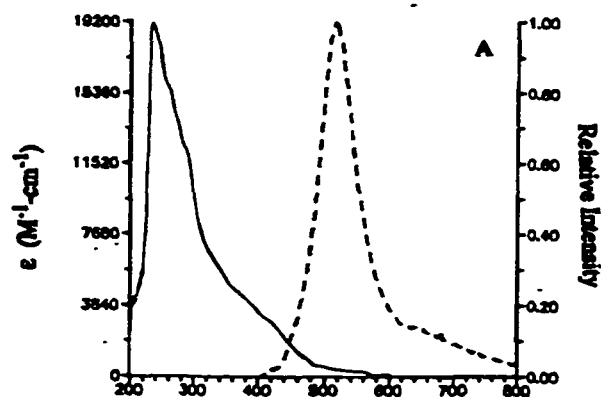
Figure 3-2: Absorption and emission spectra of complex **1**

Later, this same group reported that the emission was derived from a spin forbidden Pt_2-to-alkenylidene charge transfer transition.[77] In this species, however, the acetylide ligand was not directly involved in the lowest lying excited state.

The next set of platinum acetylide complexes, again, was discovered by Demas and coworkers (trans-[Pt(C≡CH)$_2$(PEt$_3$)$_2$] and trans-[Pt(C≡CPh)$_2$(PEt$_3$)$_2$]) (Figure 3-3).[78]
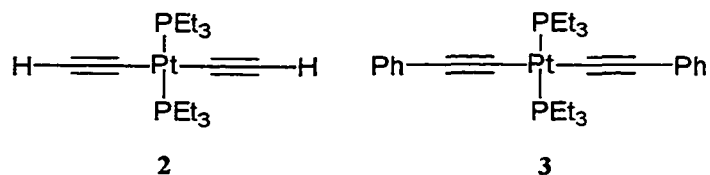
Figure 3-3: Platinum Bisacetylides studied by Demas.

These complexes exhibit intense vibronically structured emission in rigid glass at 77 K. It was observed that the emission spectra of these complexes show vibrational progressions in the ν(C≡C) mode. Also, additional progressions arising from phenyl-localized modes in the trans-[Pt(C≡CPh)$_2$(PEt$_3$)$_2$] complex were observed. These two observations along with the fact the parent cis- and trans-[PtCl$_2$(PEt$_3$)$_2$] are non-emissive

led the authors to assign the emissive state as Pt→π*(C≡C) MLCT in character. In a later report by Masai and coworkers,[79] the absorption bands of a series of trans-$[M(C≡CR)_2L_2]$ (M = Ni, Pd, Pt) were studied. In this report, the lowest lying band was believed to arise from a transition between the π(C≡CR) and π*(C≡CR) orbitals with large charge-transfer character resulting from the mixing of π*(C≡CR) and the metal $(n + 1)$p orbitals.

Platinum Acetylide Polymers and Oligomers

As discussed in chapter 1, there has been considerable interest in the photophysics of organometallic polymers of the type $[-M(PR_3)_2-C≡C-Ar-C≡C-]_n$, where M is Pt or Pd, and the development of these polymers as luminescent materials. These polymers are of interest because (1) the metal acetylide linkage is believed to provide π-conjugation along the polymer backbone and (2) the platinum or palladium center allows for the triplet excited state to be explored because the strong spin-orbit coupling of the metal renders the spin-forbidden emission from the triplet excited state partially allowed. Kohler and coworkers showed that by using spacers between the acetylenic units that act as acceptors and using electron rich platinum to act as a donor, the π,π* band can be lowered.[79] It is found that the donor-acceptor interation of thienopyrazine is enhanced lowering the optical gap from 3.0 eV to 1.7 eV and that the decoupling between the first and second excited state is srong enough to allow emission from the second excited state.

Later, Chawdhury and coworkers studied the effect the spacer in platinum polymers of the type shown in Figure 3-4 have on intersystem crossing and the spatial extent of singlet and triplet excitons.[80] By using electron rich thiophene as the spacer, it is reported that the conjugation is increased but intersystem crossing is reduced. The opposite is observed when pyridine is used as the space (i.e., intersystem crossing is

69

increased while effective conjugation is decreased). For all the systems studied,

calculations indicate that the T_0 triplet state is localized to less than one repeat unit while

the singlet excited state and a higher lying T_n triplet state extends over more than one

repeat unit.
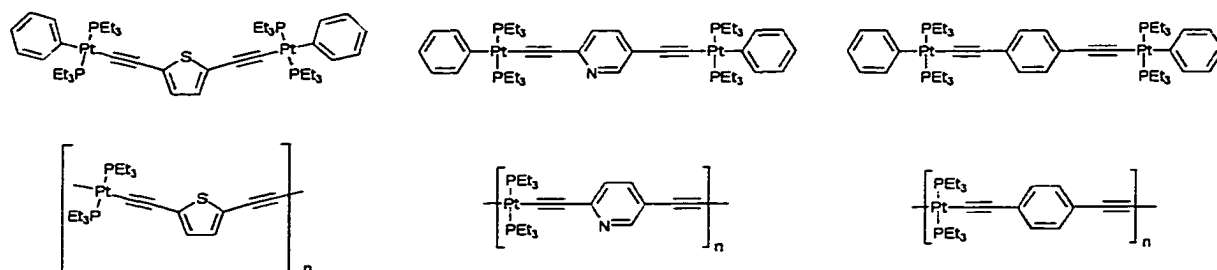
Figure 3-4: Polymers and Oligomers studied by Chawdhury

The previous study led to a study on the evolution of the lowest singlet and triplet

excited state by varying the number of thiophene rings in the spacer (Figure 3-5).[81] It is

found that by increasing the number of thiophene rings from 1 to 2 to 3, the vibronic

structure of the singlet emission becomes very similar to what is typical for

oligothiophenes. It is also found that the optical gap reduces as the number of the

thiophenes in the spacer increases. The singlet-triplet energy gap remains unaltered

while the amount of intersystem crossing from singlet to triplet decreases with increasing

number of thiophenes implying that the T_0 excited state is extended over several

thiophene rings.
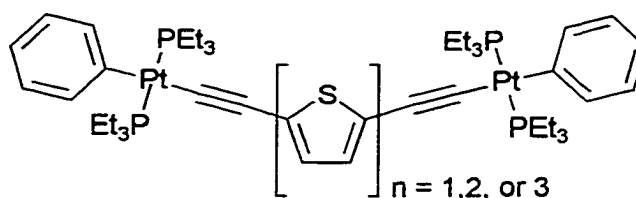
Figure 3-5: Structures that vary the number of thiophenes

Platinum Diimine Complexes

As is evident in virtually all of the previous examples given in the preceding sections, most work with platinum complexes has used various phosphines as the ancillary ligands. Various platinum diimines of the formula Pt(diimine)X_2 (Figure 3-6) that have been shown to be highly luminescent in solution, have been developed within the last ten years.[82] Eisenberg and coworkers have established the effect that changing X has on the energy and nature of the emitting state. It has been shown that when X is a dithiolate, the excited state arises from a charge transfer from an orbital of mixed metal/dithiolate character to a π^* orbital of the diimine. By changing X to CN, the excited state corresponds to a $^3(\pi,\pi^*)$ state owing to the higher energy and more structured emission.
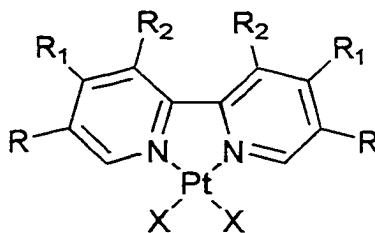
Figure 3-6: Platinum diimine complexes

Miskowski and Che studied the emission properties of a series of compounds of the formula (L_2)$PtCl_2$, where L_2 was tetramethylethylenediamine, 2,2'-bipyridinde, 4,4'-dimethylbipyridine, 5,5'-dimethyl bipyridine, 4,4'-di-t-butylbipyridine, 3,3'-dicarboxymethylbipyridine and 1,10-phenanthroline.[83] These complexes were studied both as solids and in glassy solution, and most show very broad, orange to red luminescence from a triplet ligand-field state (Table 3-1). There were, however, two exceptions: the "red" form of (bpy)$PtCl_2$ and (CH_3OCO)$_2$bpy$PtCl_2$. The (bpy)$PtCl_2$ crystallizes as two different polymorphs, a yellow form and a red form. The red form,

which crystallizes as linear chains with a significant Pt-Pt interaction, exhibits relatively narrow, vibronically structured red emission. The $(CH_3OCO)_2bpyPtCl_2$ exhibits a broad but structured orange emission. The emission from both these two complexes is assigned to triplet metal-to-ligand charge-transfer (^3MLCT) excited states. This study concluded with a detailed discussion of the excited-state energies, which is summarized in Figure 3-7.

Table 3-1: Photophysical Data for Pt Diimine complexes

formula	300 K		10 K	
	v_{max}/cm^{-1}	τ/ns	v_{max}/cm^{-1}	τ/ns
Pt(tmen)Cl_2	15500	< 20	1600	< 20
Pt((4,4'-Me_2bpy)Cl_2	15400	3340	15150	
Pt(4,4'-t-Bu_2bpy)Cl_2	15500	< 20	15500	~ 50
Pt(phen)Cl_2	15900	2400	15900	13300
Pt(bpy)Cl_2 yellow form	15600	500	15800	3500
Pt(bpy)Cl_2 red form	16300	250	15370	435
			13750 sh	
Pt(5,5'-Me_2bpy)Cl_2	15400	1140	15250	5100
Pt(3,3'-(CH_3OCO)_2bpy)Cl_2	18000 sh	350	18050	1100
	17050		16800	
	15000 sh		15500	
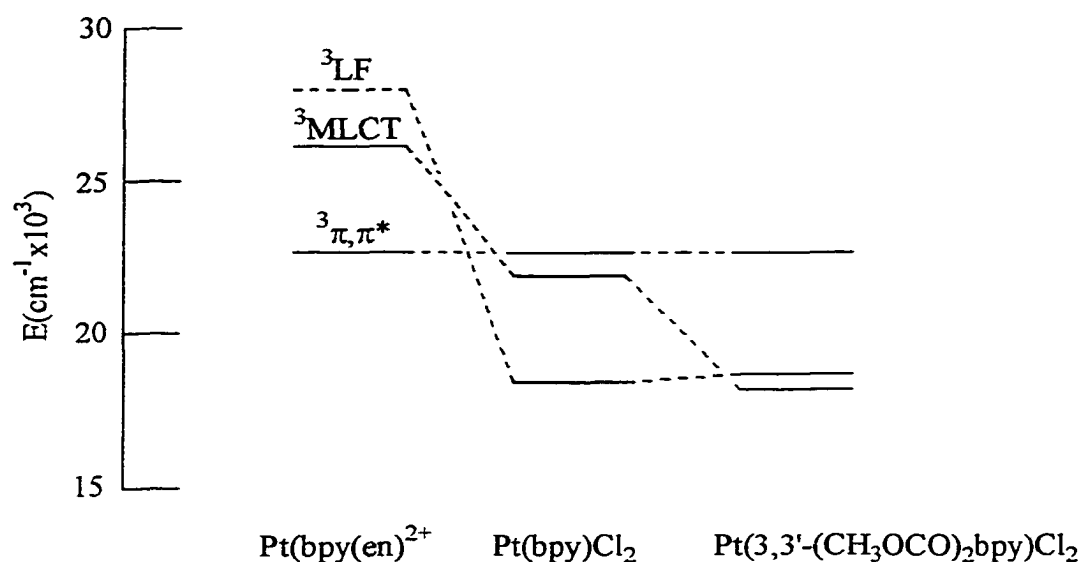
Figure 3-7: Estimates of the 0-0 energies of low lying excited states

Che later reported that with the diimine as a phenanthroline and changing X to phenylacetylide, the complex became brightly emissive with the excited state energy lying between the energies of the dithiolate and dicyanide complexes (Table 3-2, Figure 3-8).[84] Che proposed that the emissive state was ^{3}MLCT in nature. The interesting feature was the bright solution luminescence due to the fact that the analogous platinum phosphine acetylides studied by Demas (Figure 3-3) were only brightly emissive in a frozen glass or solid state and very weakly luminescent in solution.

Table 3-2: Photophysical data of $Pt(phen)(C{\equiv}CPh)_2$

Solvent	CH_2Cl_2	Me_2CO	CH_3CN	C_5H_5N	EtOH
E_{em} (nm)	578	581	581	585	583
E_{ab} (nm)	399	398	394	401	~400
τ_o (μs)	2.1	0.9	1	0.4	0.3
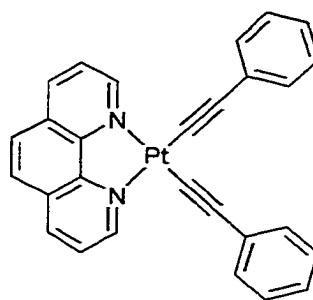
Figure 3-8: Structure of Pt(phen)(C≡CPh)$_2$

Fairly recently, Raithby and coworkers undertook a series of investigations in order to synthesize platinum acetylide polymers and their precursors which were stabilized by ancillary ligands other than phospines (Figure 3-9).[85,86] This was done in order to investigate whether the nature of the ancillary ligand had significant influence on the chemistry and electronic properties of these materials. One of the studies included

R = H, Me, or NO$_2$

R = H, Me, NO$_2$
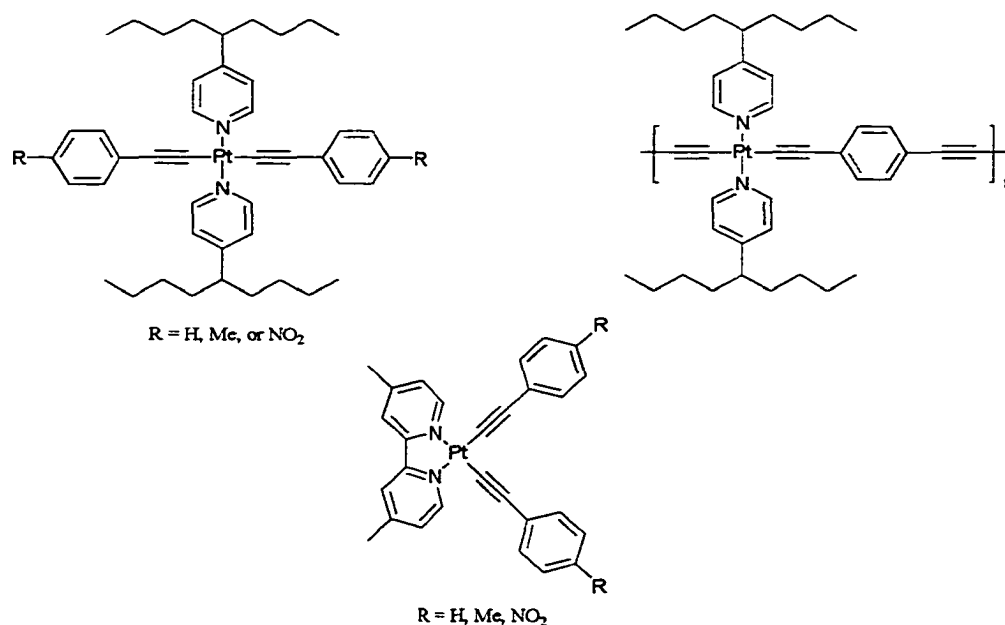
Figure 3-9: Complexes studied by James and Raithby

bipyridyl-stabilized platinum bisacetylides,[87] which showed that the absorption spectrum had two solvatochromatic bands at λ_{max}= 396 nm and 287 nm. The 396 nm band is

assigned to a MLCT transition due to the bipyridyl ligand. Any MLCT absorption due to the acetylide ligands (as observed in (PEt₃)₂Pt(C≡CPh)₂) is either absent or masked by absorptions due to the bpy ligand.

Adams and Raithby recently published a paper describing novel mixed metal acetylide complexes of the type [(t-bu₂bpy)Pt(C≡Ctolyl)₂M(SCN)] (M = Cu, Ag).[87] The cis-bisacetylides facilitate the synthesis of complexes with a second metal linked to the two acetylides via coordination to the two triple bonds. Crystal structure analysis comfirmed this assumption showing the copper and silver to be coordinated to both the acetylides with an η^2 interation. Electrochemistry shows a single fully reversible one-electron reduction at around −1.3 V vs Ag/AgCl which is consistent with the first reduction of the bipyridine, however, it is shifted slightly lower than the parent platinum bisacetylide complex.

Scope of Present Study

During completion of this study, a paper by Eisenberg and coworkers unfortunately reported very similar research as presented here.[88] Eisenburg's study characterized two series of platinum diimine bis(acetylide) complexes. The first series studied substituent effects using 5-substituted phenanthrolines as the diimine (Rphen; R = H, Me, Cl, Br, NO₂, or C≡CPh). The second series studied substituent effects of the acetylide ligand (acetylide = C≡CPhX; X = H, Me, F, OMe or NO₂). Photophysical results are listed in Table 3-3. It was shown that the MLCT absorption band shifts to lower energy as (1) the electron accepting properties of the phenanthroline increases and (2) as the electron donating properties of the acetylide substituent is increased. The complexes exhibit broad, asymmetric room temperature emission which shifts to lower

energy as the electron withdrawing ability of the diimine substituent increases and as the electron donating ability of the acetylide ligand increases.

Table 3-3: Photophysical Data from Eisenberg's Pt Acetylides

compound	λ_{abs} (nm)	λ_{em} (nm)	ϕ_{em}	τ_o (ns)
Pt(NO$_2$phen)(CCPh)$_2$	397	582	0.003	~ 400
Pt(Brphen)(CCPh)$_2$	395	605	0.036	366
Pt(Clphen)(CCph)$_2$	397	605	0.04	390
Pt(CH3phen)(CCPh)$_2$	396	575	0.098	972
Pt(PhCCphen)(CCPh)$_2$	396	590		5600
Pt(dbbpy)(CCPh)$_2$	386	570	0.11	691
Pt(dbbpy)(CCPhCH$_3$)$_2$	389	592	0.07	440
Pt(dbbpy)(CCPhOCH$_3$)$_2$	393	640	0.002	14
Pt(dbbpy)(CCPhF)$_2$	385	570	0.14	663
Pt(dbbpy)(CCPhNO$_2$)$_2$	371	570	0.04	4500

Note: All measuments performed in acetonitrile.

Although many studies on platinum acetylide polymers oligomers and monomers have been conducted, a thorough investigation of the photophysics of platinum diimine bisacetlyides has not been conducted (until recently). In an effort to further characterize and better understand the photophysics and orbital interactions of platinum diimine bisacetylides, a series of platinum complexes which vary the substituents on the diimine and the phenyl acetylide have been synthesized in order to systematically change the excited state properties (Figure 3-10). As mentioned above, while conducting this research, a paper by Eisenberg was published which presents very similar research and results, however, several other aspects of the photophysics are discussed in this chapter. Also, the comparison of the photophysically quite different phenanthroline and bipyridyl diimine, as in the Eisenberg paper, can cause some problems that are resolved in the present study by using all substituted bipyridyl diimines.

1a: R_1, R2 = Me
1b: R_1 = t-Butyl, R_2 = H
1c: R_1 = CONEt₂, R_2 = H → R_1 = $CONEt_2$, R_2 = H
1d: R_1 = COOEt, R_2 = H

2a: R = CF_3
2b: R = NO_2
2c: R = NMe_2
2d: R = OMe
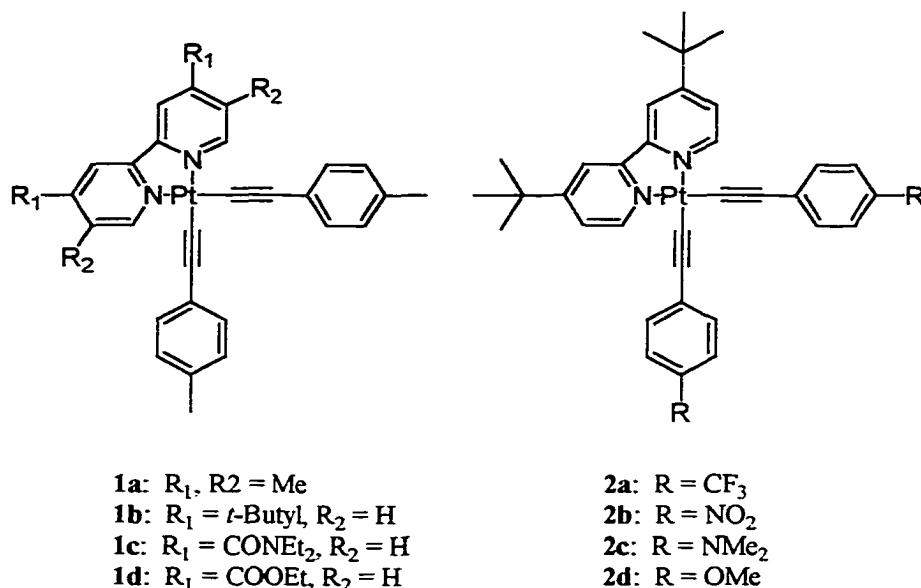
Figure 3-10: Complexes of this current study

Results and Discussion

Various photophysical parameters from many different measurements for the platinum-diimine complexes are presented table 3-4. The individual measurements are discussed later.

Table 3-4: Platinum diimine acetylide photophysics[a]

Comp.	λ_{abs} (nm)	λ_{em} (nm)	E_{00} (cm^{-1})[b]	Φ_{em}	τ_{em} (ns)	τ_{ta} (ns)[c]	k_r (x 10^5)[d]	k_{nr} (x 10^6)[e]
1a	396	553	18750	0.27	1300	1285	2.08	0.56
1b	405	570	17150	0.113	800	793	1.41	1.11
1c	417	642	15970	0.007	103	100	0.68	9.64
1d	450	670	14850	0.0046	20	22	2.3	49.8
2a	388	538	19400	0.207	607	600	3.41	1.31
2b	371	561	18350	0.09	3600	3720	0.25	0.253
2c	454	586	17700	0.0075	250	246[f]	0.3	3.97
2d	401	623	16800	0.019	60	51	3.17	16.4

a) All measurements performed in $MeCl_2$. b) Determined by spectral fitting of emission spectrum. c) Single component lifetime determined by analysis of the absorbance features of the TA spectrum. d) Calculated by $k_r = \Phi_{em}/\tau_{em}$. e) Calculated from $k_{nr} = 1/\tau_{em} \times (1 - \Phi_{em})$. f) Calculated from a very weak transient absorption spectrum.

Absorption Spectra

The absorption spectra of all the complexes are depicted in Figure 3-11 A-D. All spectra except for the nitro substituted phenyl acetylide complex show essentially two bands. The higher energy band (λ < 310 nm) with extinction coefficients between 40,000 and 58,000 $M^{-1}cm^{-1}$ is assigned to the π,π^* diimine and acetylide based intraligand transitions.
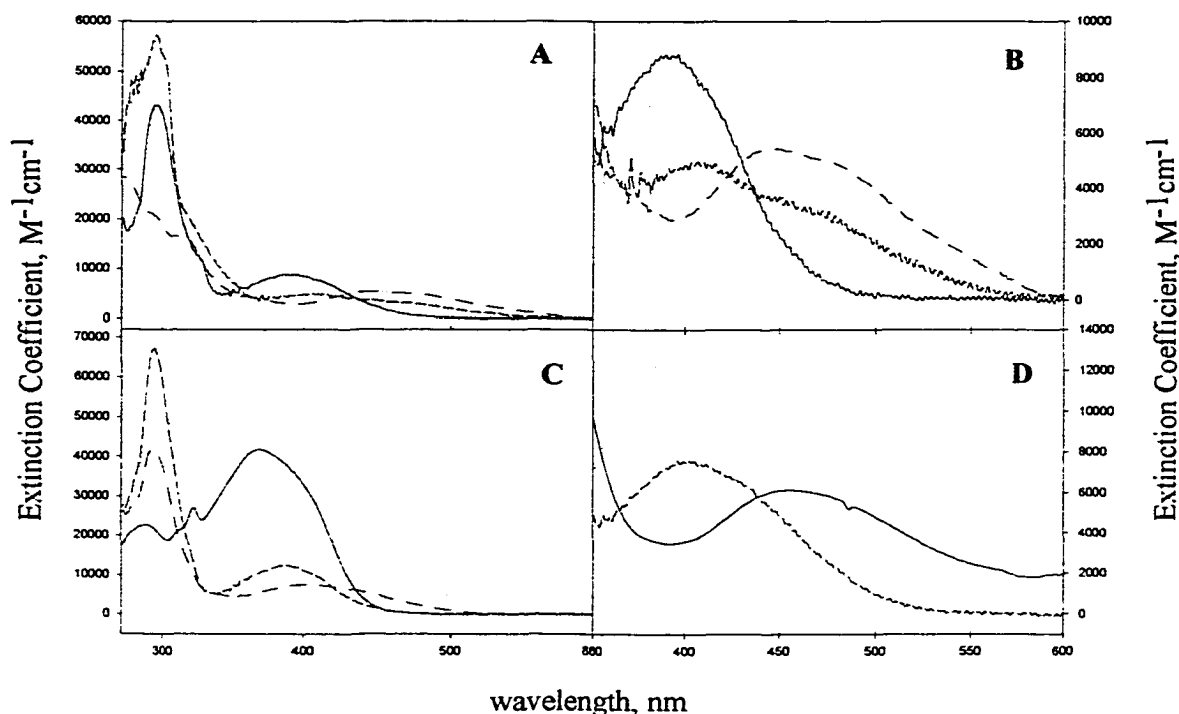
Figure 3-11: Absorption spectra of all platinum complexes in CH_2Cl_2. Spectra in **A** and **B** (—) **1a** (tmb)Pt(C≡Ctol)$_2$, (····) **1b** (tbbpy)Pt(C≡Ctol)$_2$, (---) **1c** (dea)Pt(C≡Ctol)$_2$, and (–·–) **1d** (dce)Pt(C≡Ctol)$_2$. Spectra in **C** (—) **2b** (tbbpy)Pt(C≡CPhNO$_2$)$_2$, (....) **2c** (tbbpy)Pt(C≡CPhNMe$_2$)$_2$, (---) **2a** (tbbpy)Pt(C≡CPhCF$_3$)$_2$, and (–·–) **2d** (tbbpy)Pt(C≡CPhOMe)$_2$. Spectra in **D** (—) **2c** (tbbpy)Pt(C≡CPhNMe$_2$)$_2$, (····) **2a** (tbbpy)Pt(C≡CPhCF$_3$)$_2$, and (---) **2d** (tbbpy)Pt(C≡CPhOMe)$_2$. The spectrum of **2b** (tbbpy)Pt(C≡CPhNO$_2$)$_2$ has been omitted from **D**.

The lower energy (λ_{max} ca. 400 nm) more interesting band has been assigned by Che and coworkers as a metal to ligand charge-transfer (MLCT) excitation from a filled metal d

orbital to a vacant π^* diimine orbital. By changing the substituents on the diimine or the acetylide ligand, we can study the dependence of the absorption maximum on the electron donating or withdrawing ability of the substituents. Altering the electron withdrawing abilities of the substituents on the diimine shows that the absorption band substantially shifts to lower energy and generally decreases in molar absorptivity as the withdrawing power of the substituent increases (COOEt > CONMe$_2$ > t-Butyl > Me$_4$). The absorption maximum shifts from 396 nm for the tetramethylbipyridine, **1a**, to 450 nm for the carboxyethylbipyridine, **1d**. Also of interest is the fact that this low energy band seems to actually be two overlapping bands, which is somewhat noticeable with the t-butyl substituent (**1b**) where a higher energy shoulder is seen. This becomes clearly evident in the spectra of the complexes with the strongest electron withdrawing substituents on the diimine (COOEt, **1d** and CONMe$_2$, **1c**) where two distinct bands are almost resolved. These two bands likely arise from 2 d orbital based transitions (d_{yz} and d_{xz} for instance). All of this behavior is consistent with charge transfer to the diimine.

Eisenberg noticed similar results with the Rphen platinum bisacetylides, however, it was found that the absoption maximum does not shift (Figure 3-12). Only a shoulder is resolved that shifts to lower energy as the electron withdrawing properties of the diimine substituents increases. For the current system, both the absorption maximum and the shoulder shift to lower energy as the electron withdrawing properties increase. The shift is expected because the π^* of the diimine should lower as the electron withdrawing power as the substituent increases.
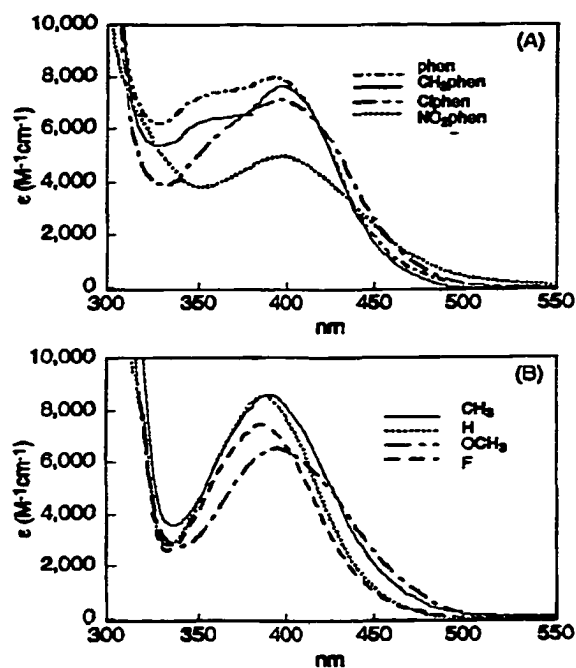
Figure 3-12: Absorption spectra of complexes studied by Eisenberg. A) Rphen series, B) C≡CPhX series

Altering the electron donating or withdrawing character of the acetylide ligand by changing the substituent, again, induces a shift in the lower energy band of the absorption spectra. The trifluoromethyl substituent (2a), being electron withdrawing, shows a shift to higher energy than that of the parent t-butylbipyridyl tolyl acetylide platinum complex (1b). Alternately, the two donating groups (OMe, 2d, and NMe_2, 2c) induce the absorption band to shift to lower energy. This shows that as the electron donating capability of the aryl acetylide substituent increases (NMe_2 > OMe > Me > CF_3), the energy of the absorption band decreases. The fact that the absorption band of interest is actually comprised of two bands is again evident in the spectra of the methoxy (2d) and dimethylamino (2c) substituted complexes, where a shoulder becomes apparent, although it is not as predominant as in the amide or ester species (1c and 1d, respectively).

Again, the work by Eisenberg shows similar trends. These results indicate that the HOMO is predominantly metal based. If this is the case, the non-bonding and weakly π bonding orbitals of the platinum should increase in energy as the donicity of the sustituent on the phenylacetylide increases, thus lowering the energy gap between the HOMO and LUMO. Conversely, as the electron withdrawing ability increases, the platinum orbitals should decrease in energy, thus increasing the energy gap between the HOMO and LUMO, and this is indeed the case.

The only spectrum that is substantially different than all the spectra of the other species is that of the nitrophenylacetylide complex (2b). The spectrum of this complex shows that the lowest energy absorption band is shifted to a higher energy as is expected due to the reduced donor ability of the ligand owing to the nitro groups electron withdrawing proficiency. However, the extinction coefficient is on the order of 40,000 $M^{-1}cm^{-1}$ which is much higher than the MLCT bands in the other complexes (6,000 - 10,000 $M^{-1}cm^{-1}$). Because of the increased extinction coefficient, the band is likely not MLCT based. Rather, the band is likely due to a π,π^*-based transition on the p-nitrophenylacetylide ligand. The expected MLCT band is probably hidden under the stronger band.

Emission Spectra

In an attempt to show the dependence of the emission of the diimine platinum acetylide complexes on the substituents of the diimine or acetylide ligand, both room temperature and temperature dependent emission spectra were obtained. The room temperature emission spectra were obtained from optically dilute methylene chloride solutions and are depicted in **Figure 3-13**. All complexes exhibit a broad emission band

that can likely be ascribed to the metal to ligand charge transfer state arising from promotion of a platinum d electron to a π^* orbital of the diimine. In the series **A**, which changes the diimine only and holds the tolylacetylide constant, a trend can be seen where the emission maximum shifts to lower energy as the donating ability of the substituent on the diimine decreases. The ester-substituted complex **1d** shows the lowest energy emission maximum followed by the amide **1c**, the t-butyl **1b** and finally the tetramethyl substituted complex **1a** shows the highest energy emission spectrum.
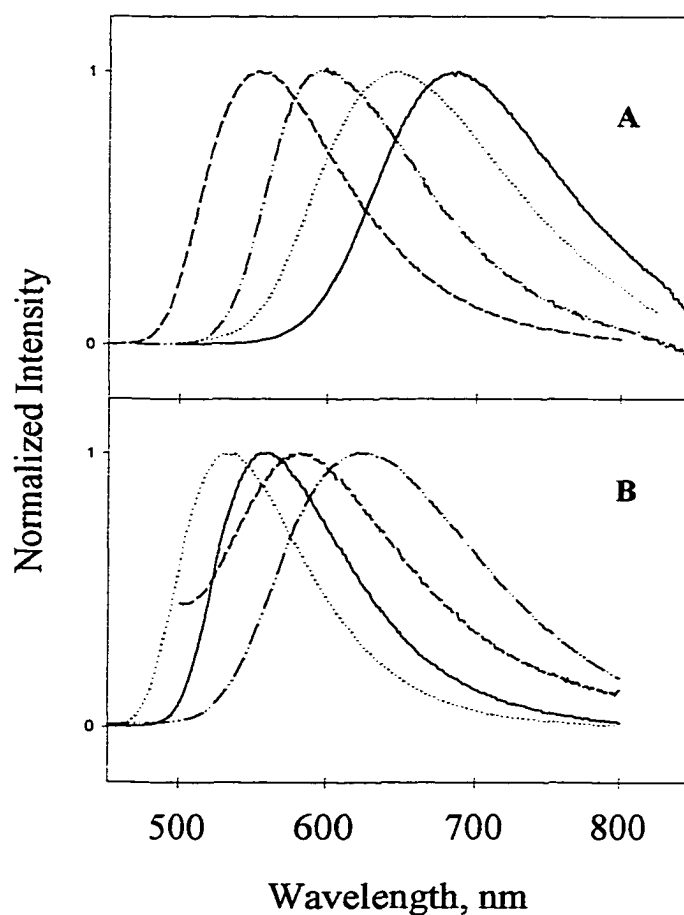
Figure 3-13: Room temperature emission of all complexes in CH_2Cl_2 (420 nm excitation). Spectra in **A** (—) **1d** (dce)Pt(C≡Ctol)$_2$, (⋯) **1c** (dea)Pt(C≡Ctol)$_2$, (‑‑‑) **1b** (tbbpy)Pt(C≡Ctol)$_2$, and (‑‑‑) **1a** (tmb)Pt(C≡Ctol)$_2$. Spectra in **B** (—) **2b** (tbbpy)Pt(C≡CPhNO$_2$)$_2$, (⋯) **2a** (tbbpy)Pt(C≡CPhCF$_3$)$_2$, (‑‑‑) **2c** (tbbpy)Pt(C≡CPhNMe$_2$)$_2$, and (‑‑‑) **2d** (tbbpy)Pt(C≡CPhOMe)$_2$.

For the series that changes the acetylide and holds the diimine constant as *t*-butylbipyridine, the similar such trends are not as evident. Both the complexes with donating groups (OMe **2d** and NMe$_2$ **2c**) show significantly broader emission spectra when compared to all others. Both complexes containing the donating methoxy (**2d**) and dimethylamine (**2c**) groups are expected to give spectra that are lower in energy than the parent t-butylbipyridine platinum bis(tolylacetylide) **1b**, however only the methoxy substituted complex shows a lower energy emission while the dimethylamine substituted complex shows higher energy. Also, it would be expected that the strongly withdrawing groups would increase the energy of the emission band, and this is indeed the case. However, normally the nitro-substituted complex **2b** would show the highest energy emission based on it having the strongest electron withdrawing ability, but the spectrum of the trifluoromethyl complex **2a** shows emission with the highest energy.

Emission spectra of each complex in an optically dilute 2-methyltetrahydofuran solution were taken as a function of temperature and are depicted in Figure 3-14. Each spectrum shows an increase in intensity and band structure as well as an expected blue shift in the emission maximum as the temperature decreases. Again, the diimine series shows the best defined trends. The amount to which the emission intensity increases as the temperature decreases follows the expected trend with the ester substituted complex showing the largest increase and tetramethyl substituted complex showing the smallest increase with decreasing temperature. Also, within the diimine series, the tetramethyl-substituted complex shows the greatest structure at the lowest temperature and the amount of structure decreases as the electron withdrawing ability increases (Me$_4$ > t-bbpy > COOEt > CONEt$_2$).

The temperature dependent emission spectra of the second series which changes the acetylide ligand do not show such simple and expected trends. The amino-substituted complex (top spectrum) shows a blue shoulder growing in as the temperature decreases. The methoxy-substituted complex shows the most "normal" spectra with slightly more structure in the lowest temperature spectrum as well as the expected blue shift of the emission maximum with decreasing temperature. The spectra obtained from
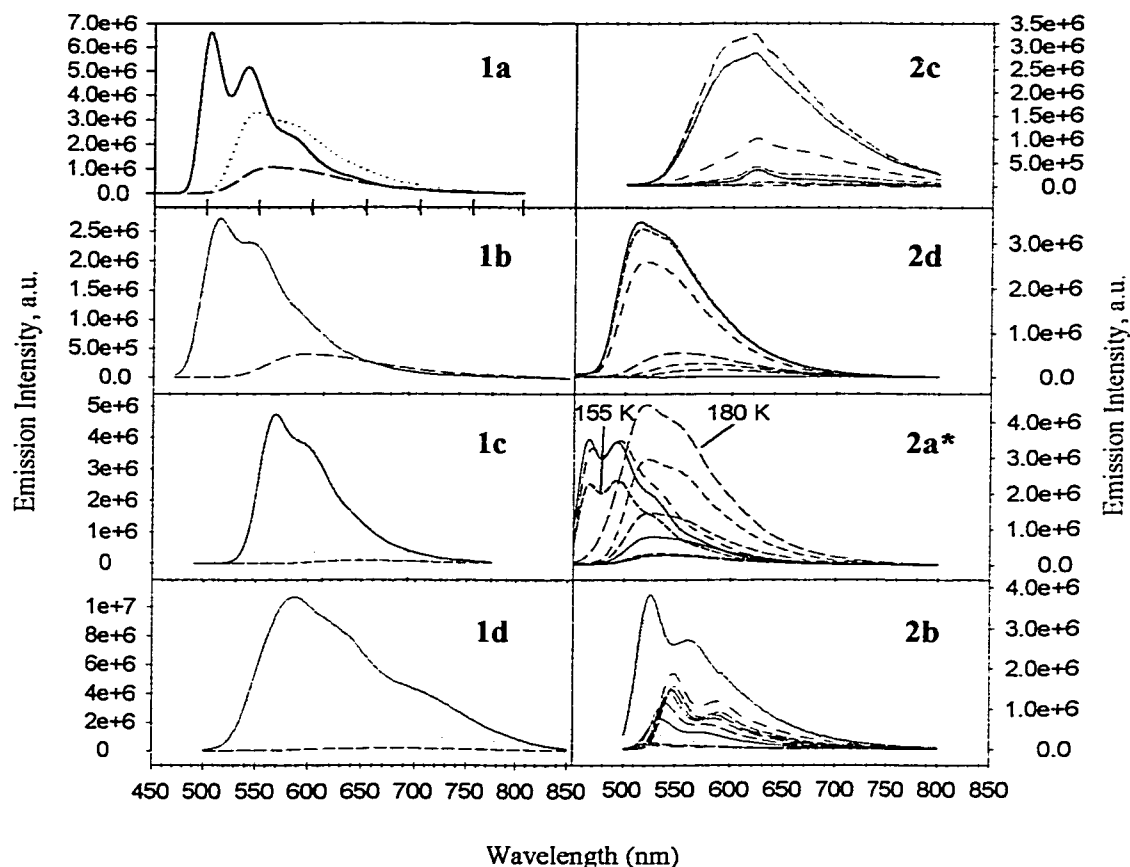
Figure 3-14: Variable temperature emission spectra of all complexes in 2-MTHF (420 nm excitation). Spectra are labeled according to complex number. Series 1 shows only 3 temperatures: (—) 80 K (····) 140 K and (---) 280 K. Series 2 shows multiple temperatures 280 K (weakest emission) incrementing by 25 K down to 80 K (most intense or bluest emission). *Highest intensity dashed line is 180 K and by 155 K, the band shape changes, blue shifts, and drops considerable in intensity (lowest shifted dotted line).

the trifluoromethyl-substituted complex show the expected blue shift and structure enhancement with decreasing temperature; however, the 0,1 band seems to grow in to be equal if not greater in intensity than the 0,0 band. Also, at around 155 K there is a drastic decrease in intensity. Finally, the nitro-substituted complex shows an odd series of temperature dependant spectra. The spectra show an increase in intensity and structure as the temperature decreases. However, from room temperature to about the glass temperature of the 2-methyltetrahydrofuran solvent, the emission maximum seems to red shift and then after the glass temperature there is a significant blue shift in the emission maximum.

Energy Gap Correlation

The emission decay lifetimes of each complex were recorded and are listed in Table 3-4. For the series changing the diimine substituents, the trend was observed which was in accord with the absorption and emission data discussed earlier. That is, as the electron withdrawing ability of the diimine substituent increased, the lifetime decreased from 1.3 microseconds for the tetramethyl substituted complex **1a** to 20 nanoseconds for the carboxyester substituted complex **1d**. Values for k_r and k_{nr} were calculated based on equations the following equations:

$$k_r = \Phi_{em}/\tau_{em} \tag{3-1}$$

$$k_{nr} = 1/\tau_{em} \times (1 - \Phi_{em}) \tag{3-2}$$

It is clear from the data that k_r decreases while k_{nr} increases as the electron withdrawing ability of the substituent on the diimine increase.

For the series that changes the substituent on the acetylide ligand, the trend is again less clear. The expected trend is that as the electron withdrawing ability increases, the lifetime increases. However, the lifetime seems to jump around with 60 and 250 nanoseconds for the methoxy- **2d** and dimethylamino- **2c** substituted complexes, respectively, and 3600 and 600 nanoseconds for the nitro- **2b** and trifluoromethyl- **2a** substituted complexes, respectively. The radiative and nonradiative decay rates show the same inconsistencies.

Finally, emission spectral fitting as discussed in the thesis introduction was conducted on each room temperature emission spectrum with the calculated parameters presented in Table 3-5. The hopes in doing so were to determine whether the complexes fit the energy gap law throughout both series, which can be accomplished by plotting $\ln(k_{nr})$ vs E_0 (Figure 3-15). Unfortunately, very little correlation was observed throughout the entire series. However, within the series that changes the diimine, a good correlation was found with a slope of -1.19×10^{-3} cm^{-1}. It was expected, based upon absorption, emission and lifetime data, that the complexes **2b** and **2c** (nitro and dimethylamino substituted, respectively) may not correlate well however it was unexpected that the methoxy and trifluoromethyl substituted complexes **2d** and **2a**, respectively would be so far off the line.

Table 3-5. Emission fitting parameters

CMPD	E_0 (cm^{-1})	$\hbar\omega$	S_m	$\Delta_{1/2}$
1a	18750	1300	1.45	1900
1b	17150	1300	1.15	1850
1c	15970	1300	1.2	2400
1d	14850	1300	0.85	3200
2a	19150	1300	0.12	1890
2b	18350	1300	1.6	1800
2c	17700	1300	1.4	3200
2d	16800	1300	1.6	2460
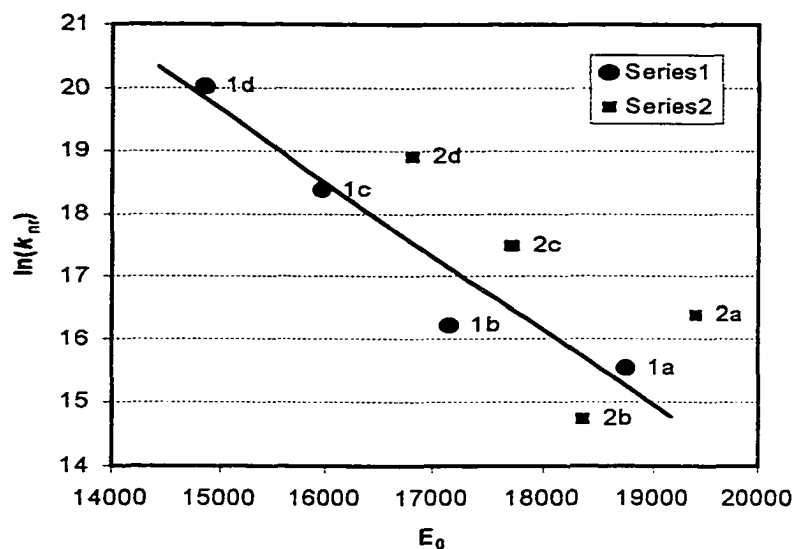
Figure 3-15. Energy gap plot. Series 1 correlates well, series 2 does not.

Silver Complexation

It was noticed in a paper by Raithby that diimine platinum bisacetylides show

complexation with Ag(SCN). In order to show the effects of Ag^+ complexation on the

emission lifetime and emission and absorption spectra, a quenching study was performed

by varying the $[Ag^+]$ in a solution of **1a**. Mono-exponential emission lifetime decays

were determined for various concentrations of silver triflate and are listed in Table 3-6. It

was found that there was an obvious decrease in the emission lifetime decay as the

concentration of silver triflate increased. The emission spectra were also determined for

the various concentrations of silver triflate and are depicted in Figure 3-17. Not only did

the emission intensity decrease with increasing amounts of silver triflate, a blue shift was

also observed. Finally, the same study was performed monitoring the absorption

spectrum and the results are depicted in Figure 3-16. It was found that as the

concentration of silver triflate increased, the MLCT absorption blue shifted while the

absorptivity increased.

Table 3-6. Lifetimes dependent on [AgOTf]

Sample #	[AgOTf] x 10^{-5}	Lifetime (ns)
1	0	691
2	0.20	682
3	0.40	666
4	0.80	626
5	1.60	584
6	3.20	554
7	4.80	530
8	7.80	507
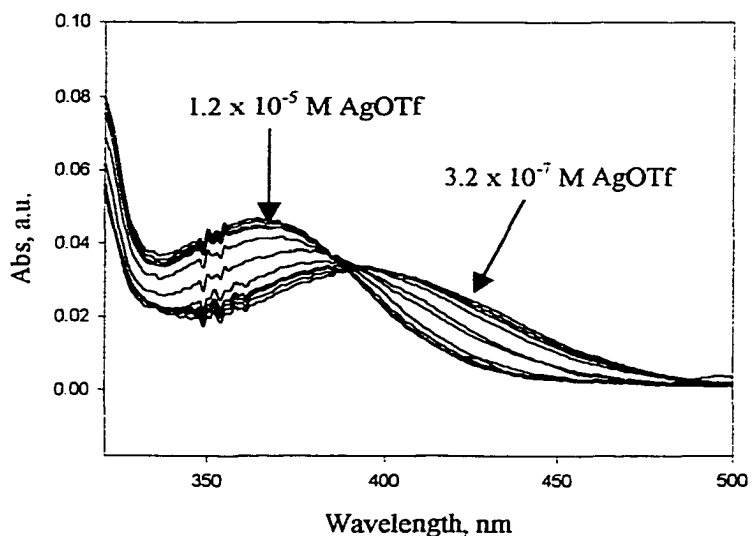
Figure 3-16: MLCT absorption spectrum of 1b (conc. = 3.5×10^{-5} M) as a function of AgOTf concentration in methylene chloride ranging from 0 M (most red) to 1.2×10^{-5} M (least intense).
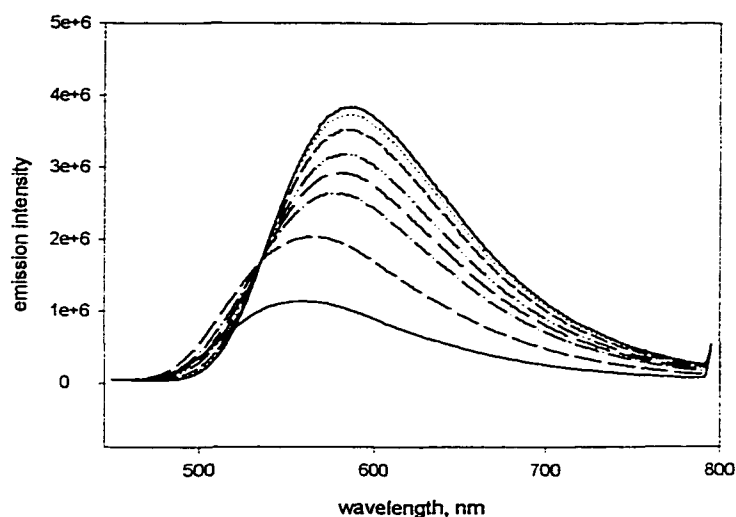
Figure 3-17: Emission spectrum of **1b** as a function of AgOTf concentration in methylene chloride ranging from 0 M (most intense) to 1.2 x 10^{-5} M (least intense).

These results can be explained as follows: The silver triflate has been shown to complex between the two cis-acetylide ligands. This silver coordination results in reducing the bonding between the acetylide and the platinum, thus reducing any effect the acetylide ligands imparted on the HOMO and/or LUMO. It has been shown that the acetylide ligand should increase the energy level of the platinum centered HOMO through π back-bonding. With the silver complexed between the two acetylides, the amount of π back-bonding is reduced, resulting in a lower energy metal-centered HOMO. This increases the energy gap between the HOMO and LUMO, resulting in higher energy absorption and emission and shorter lifetime.

Transient Absorption

The transient absorption spectra were recorded for all the platinum complexes and are depicted in Figure 3-18. Excited state lifetimes obtained from factor analysis and global decay fitting are listed in Table 3-4. Within each spectrum, equivalent first order

decays were obtained for all features of the transient absorption. For the series that

changes the diimine substituent, essentially two excited-state absorption bands are

observed. Each spectrum shows a band between ca. 310 and 430 nm. The second band

in each spectrum is much broader and seems to shift somewhat arbitrarily between

complexes. For all the spectra, the features are attributed to absorption of the MLCT

excited state except in the case of the nitro substituted complex **2b**. For tmbPtCCtol$_2$ the

second band is very broad from 510 nm reaching out to beyond 700 nm. For

tbbpyPtCCtol$_2$ the second band is not as broad arising between 600 and 720 nm. The

second band seen in the deaPtCCtol$_2$ complex appears at a higher energy ca. 450 to 570

nm. Finally the dcePtCCtol$_2$ complex shows the second band between 500 and 720 nm.

For the most part, the transient absorption spectra obtained from the second series,

which changes the substituent of the acetylide ligand, again shows two main absorption

bands. The spectrum obtained for the methoxy substituted complex has a high energy

band between 300 and 400 nm and the lower energy band is observed between 550 and

700 nm. The trifluoromethyl substituted complex shows a high energy band again

between 300 and 400 nm while the lower energy band is around 490 to 650 nm. The

major difference in this spectrum and the others is that the lower energy band shows

stronger absorption than the higher energy band. As was seen in the ground state

absorption spectrum, the nitro-substituted complex shows a markedly different transient

absorption spectrum than the other complexes. There is a bleaching of the ground state

π,π^* absorption between 300 and 420 nm followed by a broad excited state absorption

band extending into the near IR. This excited state lifetime obtained from this broad

band is, relative to the other complexes, very long (3.6 µs). This long lifetime is typical

for organic triplets and because of this long lifetime and the similarity to the spectrum

obtained from the phenylene-ethynylene oligomers studied in our group, this transient is

assigned to the $^3\pi,\pi^*$ excited state. Due to the very weak excited state absorption, the

spectrum of the dimethylamino substituted complex is omitted, however clearly shows

the same two bands as observed in the spectra of all the other complexes except the nitro

substituted complex.
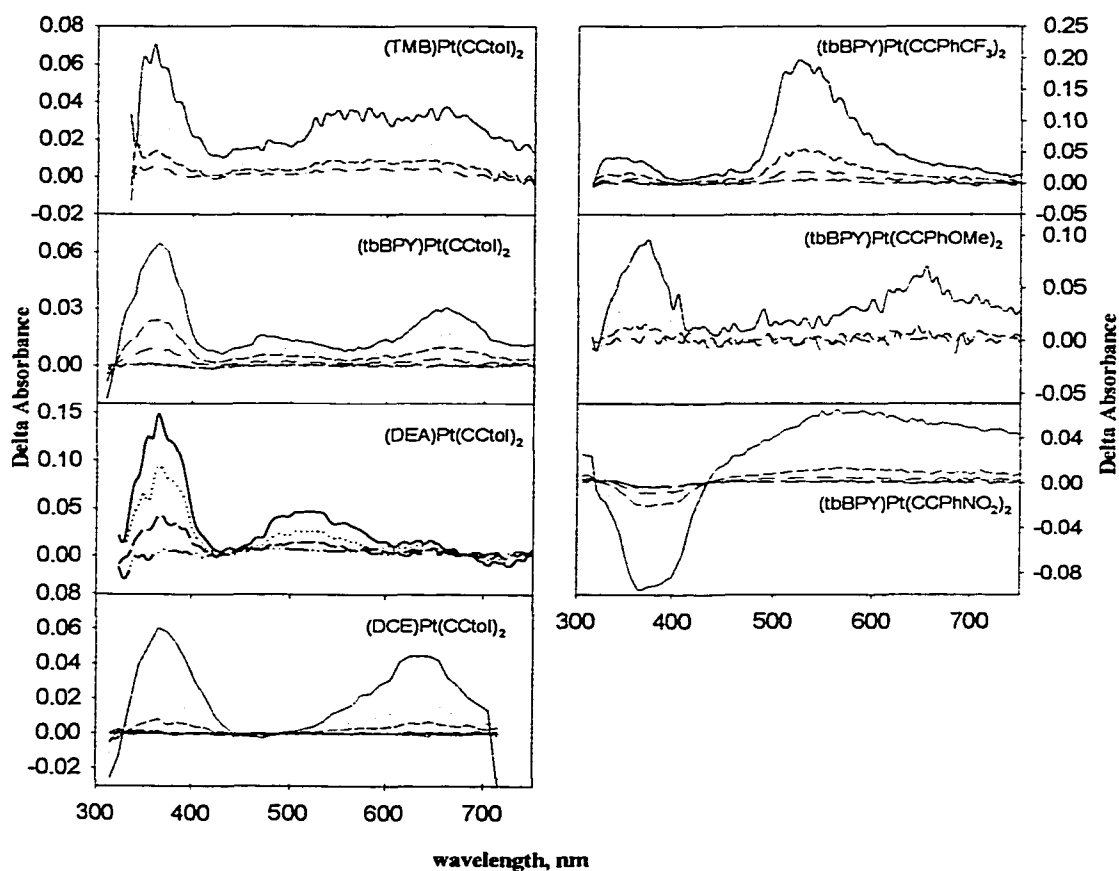
Figure 3-18: Transient Absoption spectra of all complexes. For **1c** and **1d**, transients were taken every 80 ns after the laser pulse. For **1a**, **1b**, **2a**, and **2d**, transients were taken every 320 ns after the laser pulse. For **2b**, transients were taken every 4 μs after the laser pulse.

Crystal Structure

The molecular structure of tbbpyPtCCtol2 was found to exist in two slightly different forms. Upon crystallization from methylene chloride and bezene or toluene, it was found that two types of crystals were formed; one yellow and one slightly orange, both depicted in Figure 3-19 and the crystal packing in Figure 3-20 and Figure 3-21. Important bond lengths and angles are given in Table 3-7, while complete tabulation of distances and angles are listed in the appendix. In both cases, the Pt-N and Pt-C distances lie within the range found in other complexes and are basically identical to the crystal structure of (phen)Pt(C≡CPh)$_2$ obtained by Eisenberg. The Pt-C-C angles are essentially linear and the C-Pt-C angle is almost 90°. The bipyridine is essentially planar while the phenyl rings are twisted out of the bipyridine plane (one almost perpindicular).
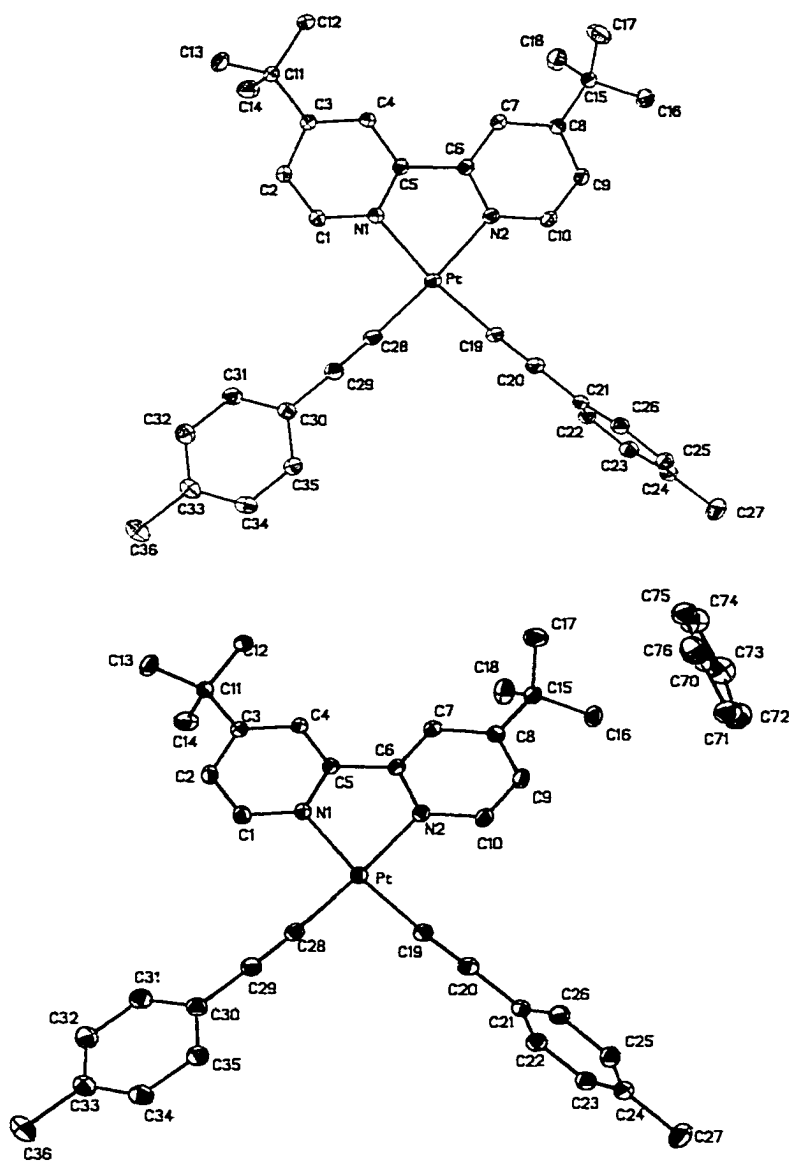
Figure 3-19: Crystal structure and atom numbering scheme for yellow (top) and orange (bottom) (tbbpy)Pt(C≡Ctol)₂.

Table 3-7. Selected bond lengths (Å) and Angles (deg) for orange (tbbpy)Pt(C≡Ctol)$_2$

Pt(1)-C(19)	1.945(3)	C(2)-C(3)	1.400(4)
Pt(1)-C(28)	1.954(3)	C(3)-C(4)	1.393(3)
Pt(1)-N(1)	2.051(2)	C(4)-C(5)	1.392(3)
Pt(1)-N(2)	2.065(2)	C(19)-C(20)	1.213(4)
N(1)-C(1)	1.353(3)	C(20)-C(21)	1.440(4)
N(1)-C(5)	1.352(3)	C(28)-C(29)	1.208(4)
C(1)-C(2)	1.380(4)	C(29)-C(30)	1.434(4)
C(19)-Pt(1)-N(1)	172.77(9)	C(28)-C(29)-C(30)	177.9(3)
C(19)-Pt(1)-N(2)	94.77(10)	N(1)-C(5)-C(6)	114.8(2)
C(19)-Pt(1)-C(28)	89.84(11)	N(1)-Pt(1)-N(2)	78.69(8)
C(19)-C(20)-C(21)	177.2(3)	Pt(1)-C(19)-C(20)	173.9(2)
C(28)-Pt(1)-N(1)	96.57(9)	Pt(1)-C(28)-C(29)	176.6(2)
C(28)-Pt(1)-N(2)	174.79(9)		

Selected bond lengths (Å) and Angles (deg) for yellow (tbbpy)Pt(C≡Ctol)$_2$

Pt(1)-C(19)	1.968(10)	C(2)-C(3)	1.364(13)
Pt(1)-C(28)	1.941(9)	C(3)-C(4)	1.357(13)
Pt(1)-N(1)	2.062(8)	C(4)-C(5)	1.432(12)
Pt(1)-N(2)	2.059(8)	C(19)-C(20)	1.151(14)
N(1)-C(1)	1.324(12)	C(20)-C(21)	1.486(14)
N(1)-C(5)	1.348(11)	C(28)-C(29)	1.231(13)
C(1)-C(2)	1.361(13)	C(29)-C(30)	1.429(12)
C(19)-Pt(1)-N(1)	175.2(3)	C(28)-C(29)-C(30)	174.1(10)
C(19)-Pt(1)-N(2)	96.3(4)	N(1)-C(5)-C(6)	115.5(8)
C(19)-Pt(1)-C(28)	87.8(4)	N(1)-Pt(1)-N(2)	79.0(3)
C(19)-C(20)-C(21)	174.7(13)	Pt(1)-C(19)-C(20)	177.1(10)
C(28)-Pt(1)-N(1)	97.0(3)	Pt(1)-C(28)-C(29)	172.9(9)
C(28)-Pt(1)-N(2)	175.1(3)		
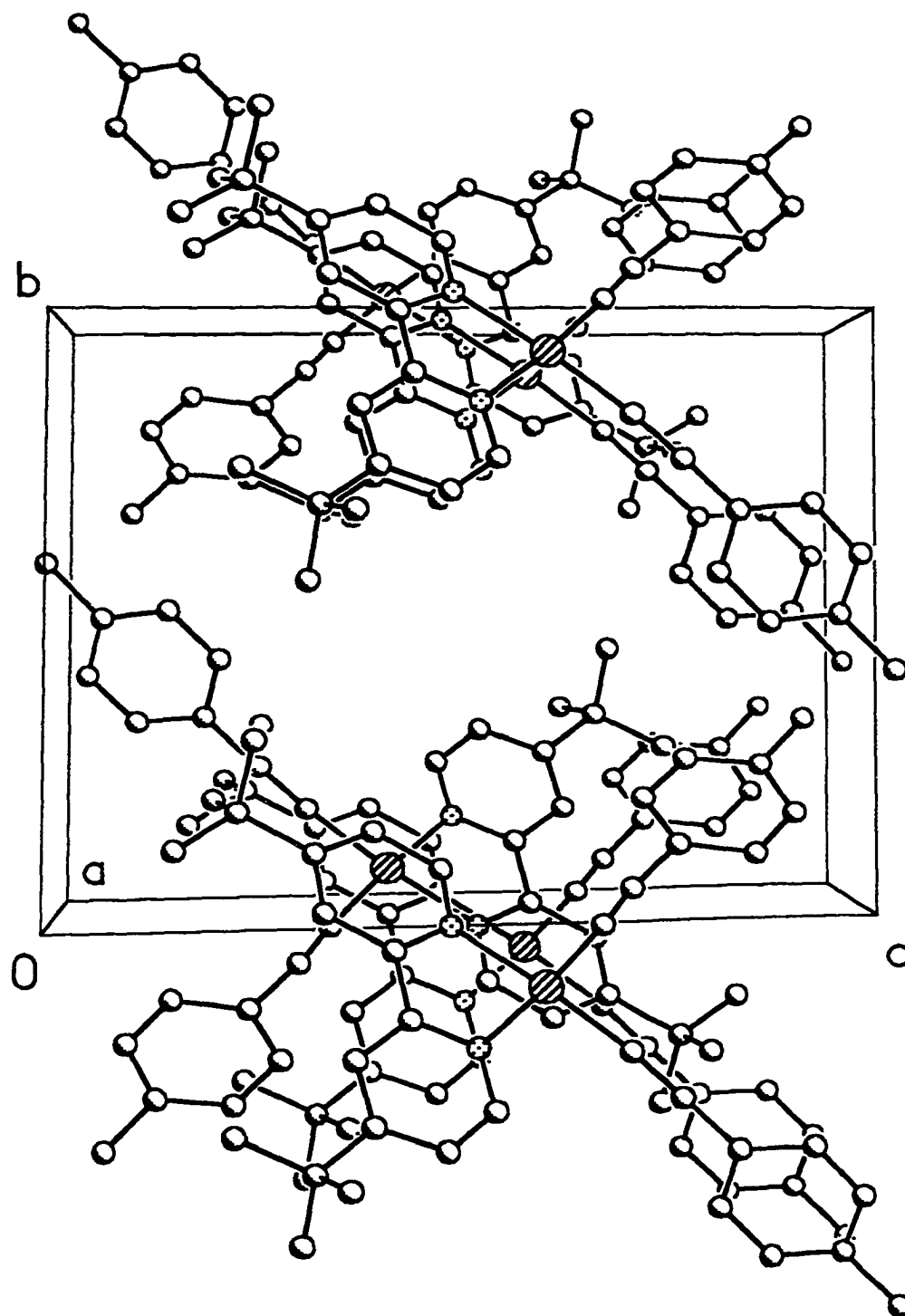
Figure 3-20. Crystal packing diagram for yellow (tbbpy)Pt(C≡Ctol)₂
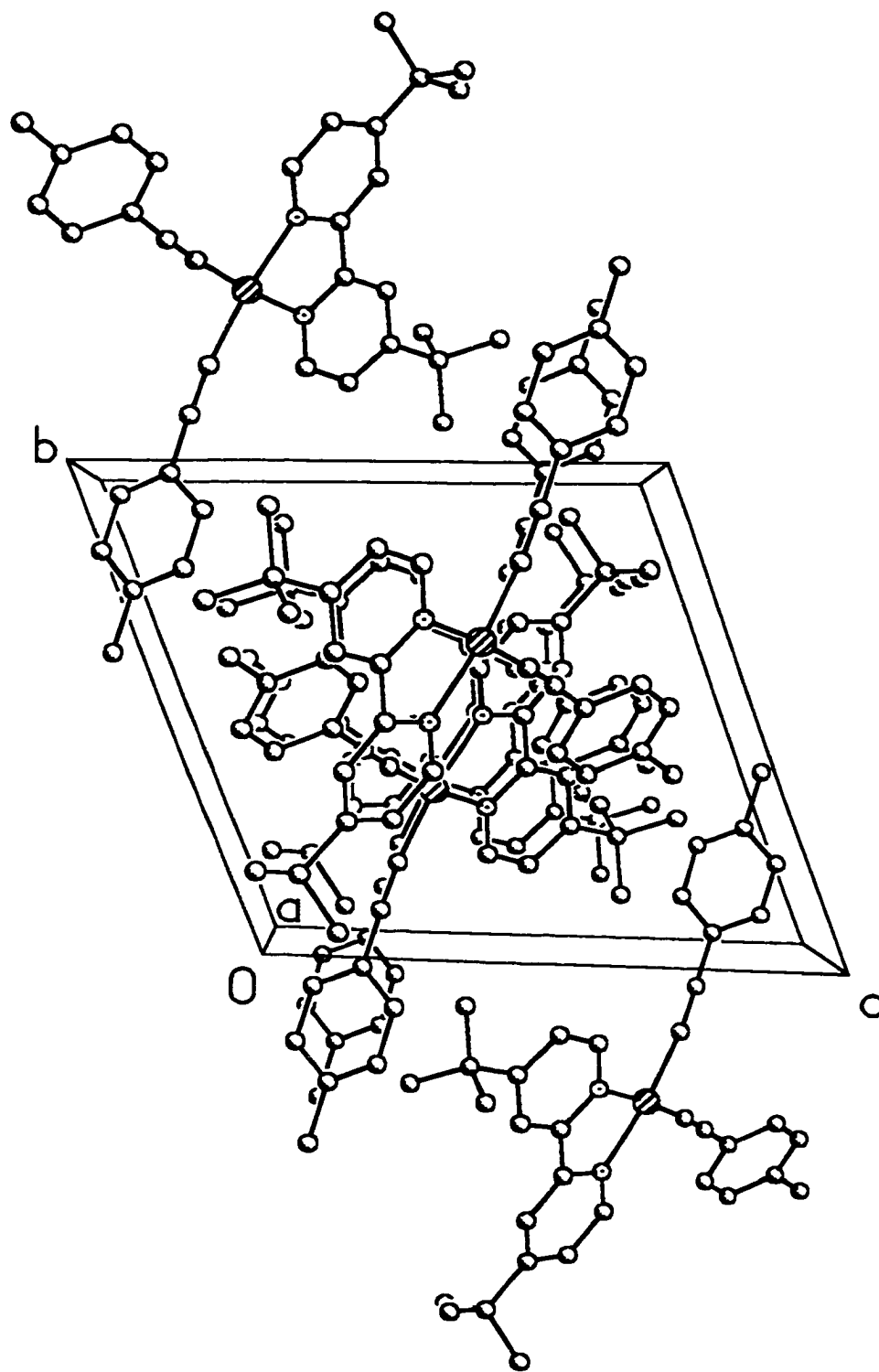
Figure 3-21. Crystal packing diagram for orange (tbbpy)Pt(C≡Ctol)$_2$

Differences between the single molecules are minimum, where the packing shows the major differences. The packing of each shows that the bipyridyl ligands lie directly under and over adjacent platinum atoms. It was hoped that the platinum-platinum distances would be close with stacking interactions in the case of the orange crystals as those seen in the red form of Pt(bpy)Cl$_2$. However, this was not the case as the platinum-platinum distances in each structure are well over 5 Å. The major difference between the two packed structures is that the yellow packing structure is close to being cubic, while the orange packing structure is more rhomboid like.

Conclusions

The work presented in this chapter is concerned with two series of relatively highly luminescent diimine platinum bisacetylides. The first group changes the electron-withdrawing ability of substituents on the diimine, while the second group changes the electron-withdrawing ability of the para-substituents of the aryl acetylide. Varying the substituent allows for a systematic way to determine the nature of the excited state in these systems has been investigated. As with other work in this area, the excited state has been defined as a ^{3}MLCT state. The first series has been shown to exhibit profound and systematic changes in the excited state properties with electron-withdrawing ability of the substituent on the diimine. The second series, however, does not demonstrate a systematic change in the excited state properties. Earlier work by Eisenburg suggests that variation of the arylacetylide leads only to minor changes in the Pt-based HOMO and thus only minor changes in the excited state properties. However, this has not been the case with series studied in this chapter. Although the changes are not systematic, they are strong and in one case (2b) quite profound. These species are well suited for application

in molecular photochemical devices owing to their relatively long-lived excited states and synthetic flexibility.

Experimental

Photophysical Measurements

All samples were studied in either dichloromethane or 2-methyltetrahydrofuran. All solvents were distilled according to typical laboratory practices. All photophysical studies were conducted in 1 cm square quartz cuvettes unless otherwise noted. All room temperature studies were conducted on argon degassed solutions, and all low temperature studies were conducted on solvent glasses degassed by four freeze pump thaw cycles (ca. 10^{-4} Torr). For emission studies, sample concentrations were adjusted to produce optically dilute solutions with absorptions less than 0.20. Transient absorption measurements were performed on solutions with absorptions at 355 ranging from 0.50 to 0.70 with concentration generally around 5×10^{-5} M.

Steady state absorption spectra were recorded on either an HP 8542A diode-array or Varian Cary 100 dual beam spectrophotometer. Corrected steady state emission measurements were conducted on a SPEX F-112 fluorimeter. Emission quantum yields were measured by relative actinometry with $Ru(bpy)_3[Cl^-]$ in degassed water (Φem = 0.055). Time resolved emission lifetime decays were observed with time correlated single photon counting (FLT, Photochemical Research Associates). Either a H_2 spark with a Schott UG-11 filter or a 405 nm IBH NanoLED-07 laser diode was used as the source with selected emission filters (P10-600 and P70-600). Lifetimes were determined from the observed decays with DECAN fluorescence lifetime deconvolution software. Low temperature emission measurements were conducted in 1 cm diameter glass tubes

contained in an Oxford Instruments cryostat connected to an Omega CYC3200 automatic temperature controller. Transient absorption spectra were obtained on the previously described instrumentation with the third harmonic of a Nd:YAG laser (Spectra Physics GCR-14, 355 nm, 10 ns fwhm, 5 mJ per pulse) as the excitation source. Primary factor analysis followed by first order (A->B) least square fits of the transient absorption data was accomplished with SPECFIT global analysis software.

X-ray Structure Analysis

Data were collected at 173 K on a Siemens SMART PLATFORM equipped with A CCD area detector and a graphite monochromator utilizing MoKα radiation (λ = 0.71073 Å). Cell parameters were refined using up to 8192 reflections. A hemisphere of data (1381 frames) was collected using the ω-scan method (0.3° frame width). The first 50 frames were remeasured at the end of data collection to monitor instrument and crystal stability (maximum correction on I was < 1 %). Absorption corrections by integration were applied based on measured indexed crystal faces.

The structure was solved by the Direct Methods in *SHELXTL5*, and refined using full-matrix least squares. The asymmetric unit consists of 2 molecules: the platinum complex and one toluene molecule. The non-H atoms were treated anisotropically, whereas the hydrogen atoms were calculated in ideal positions and were riding on their respective carbon atoms. A total of 424 parameters were refined in the final cycle of refinement using 7530 reflections with I > 2σ(I) to yield R_1 and wR_2 of 2.23% and 5.80%, respectively. Refinement was done using F^2.

Synthesis:

The general synthetic scheme is depicted in Figure 3-22.
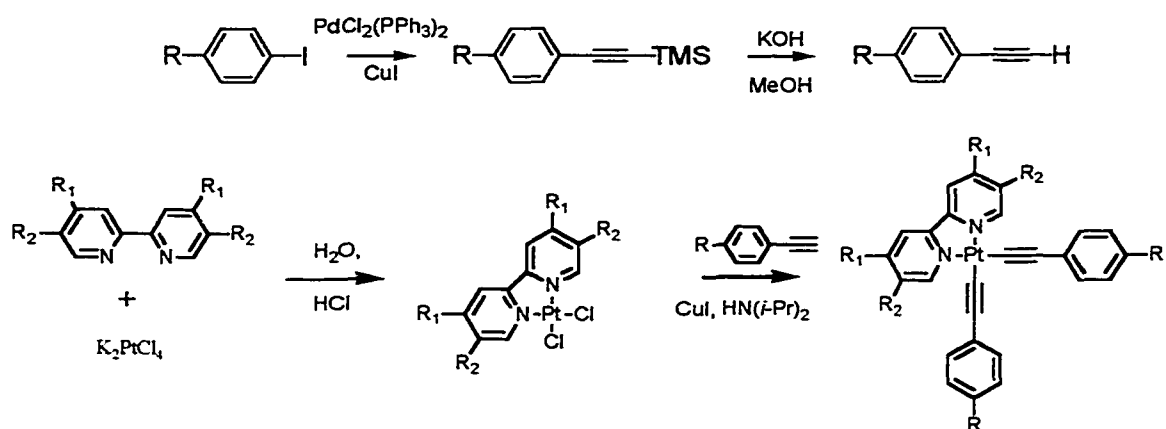
Figure 3-22: Generic synthetic scheme.

Organic Ligands:

Synthesis of the acetylide ligands proceeded via analogous procedures, so a representative procedure is given. All organic compounds have been previously prepared and the spectra obtained match the literature data.

p-nitrophenyl-trimethylsilylacetylene. *p*-Iodo-nitrobenzene (1 g, 4.02 mmol), 6 mole percent of Pd(PPh$_3$)Cl$_2$ (169 mg, 0.241 mmol) and 12 mole percent of copper iodide (91 mg, 0.482 mmol) were placed in a Schlenk flask, dissolved in a mixture of 50 mL of tetrahydrofuran and 15 mL diisopropylamine and then the flask was sealed with a septum. The solution was argon degassed for 45 minutes after which time 1.25 equivalents of trimethylsilylacetylene (492.5 mg, 5.025 mmol) was added via syringe to the stirred solution. A stream of argon was then flowed over the solution through the side arm while the septum was replaced with an argon line. The side arm stopcock was then closed and the flask was lowered into an oil bath set at 70°C. The solution was allowed to stir overnight. During this time the solution turned almost black and a large amount of

solid copper salts precipitated out of solution. The solution was then allowed to cool and then transferred to a round bottom flask using methylene chloride to wash out the reaction mixture Schlenk flask and then rotovapped to dryness. The solid was then purified via column chromatography (5 : 1, hexane : methylene chloride) affording 0.85 the pure product as a slightly yellow solid, yield 0.85 g (92.4%). NMR consistent with literature.[92]

p-nitrophenylacetylene. *p*-Nitrophenyltrimethylsilylacetylene (0.8 g, 3.65 mmol) was placed in a round bottom flask and dissolved 30 mL of methanol followed by addition of 1 mL of water. 15 equivalents of crushed solid potassium hydroxide (3 g, 54.8 mmol) were then added to the solution. The reaction was followed by thin layer chromatography (TLC, silica gel, 9:1 hexane/ether). After it was determined that the starting material was completely consumed (ca. 4 hrs), the methanol was removed via rotary evaporation. The wet solid was then dissolved in methylene chloride and washed 3 times with water, twice with a 5 % HCl solution, dried over sodium sulfate and then the solvent was removed by rotary evaporation. No further purification was needed. Yield 0.50 g (94%) ^{1}H NMR (CDCl$_3$, TMS) δ 8.91 (d, 2H), 7.63 (d, 2H), 3.36 (s, 1H)ppm; ^{13}C NMR (CDCl$_3$, TMS) δ 147.49, 132.93, 128.87, 123.53, 82.32, 81.56 ppm.[93]

p-iodo-N,N-dimethylaniline. Distilled N,N-dimethyl aniline (5 mL, 4.78 g, 39.5 mmol) was placed in a 50 mL round bottom flask. 35 mL of water and 5 g of NaHCO$_3$ were then added. The mixture was then cooled to 10°C. Iodine (10 g, 39.5 mmol) was then added in small portions making sure the temperature of the reaction did not rise above 15°C. Once all the iodine was added, the mixture was allowed to stir at 10° C for 30 minutes and then allowed to warm to room temperature. The mixture was then poured

into 500 mL of diethyl ether and washed consecutively with water, saturated sodium thiosulfate, and then water again (2x). The ether phase was dried with sodium sulfate and then the solvent was removed via rotary evaporation. The resulting residue was recrystallized with 10 : 1 hexane/ether affording *N,N*-dimethyl-4-iodoaniline as a white crystalline solid. Yield 9.2 g (94.2%). ^{1}H NMR (CDCl$_3$) δ 7.45 (d, 2H), 6.46 (d, 2H), 2.90 (s, 6H); ^{13}C NMR (CDCl$_3$) δ 149.91, 137.33, 135.92, 114.80, 40.23 ppm.[94]

1-(*p*-dimethylaminophenyl)-2-trimethylsilylacetylene. This compound was prepared following the same method described for (p-nitrophenyl)trimethylsilylacetylene and was purified via column chromatography (1 : 1, hexane : methylene chloride) affording the product as a white crystalline solid. Yield 1.3 g (42%) ^{1}H NMR (CDCl$_3$) d 7.34 (d, 2H), 6.60 (d, 2H), 2.97 (s, 6H) 0.25 (s, 9H); ^{13}C NMR (CDCl$_3$) d 149.65, 136.31, 118.72, 110.63, 85.21, 76.42, 41.45, 0.01 ppm.[95]

p-dimethylaminophenylacetylene. This compound was prepared following the same method described for p-nitrophenylacetylene and collected as a white crystalline solid. Yield 0.62 g (91.6%) ^{1}H NMR (CD$_3$Cl, TMS) δ 7.36 (d, 2H), 6.61 (d, 2H), 2.96 (s, 6H), 2.91 (s, 1H); ^{13}C NMR (CD$_3$Cl, TMS) δ 150.2, 133.0, 111.5, 108.5, 84.8, 74.7, 39.9 ppm.[96]

p-trifluoromethylphenyl-trimethylsilylacetylene. This compound was prepared following the same method described for (p-nitrophenyl)trimethylsilylacetylene and was purified via column chromatography (4 : 1, hexane : methylene chloride) yielding a pale yellow oil. Yield 0.232 g (87.3%). NMR consistent with literature.[97]

p-trifluoromethylphenylacetylene. This compound was prepared following the same method described for p-nitrophenylacetylene and collected as a pale yellow oil.

Yield 0.147 g (91%). ^{1}H NMR (CD$_3$Cl, TMS) δ 7.61 (s, 4H), 3.21 (s, 1H); ^{13}C NMR (CD$_3$Cl, TMS) δ 148.8, 136.5, 110.9, 107.9, 88.4, 76.2 ppm.[97]

***p*-methoxyphenyl-trimethylsilylacetylene.** This compound was prepared following the same method described for (p-nitrophenyl)trimethylsilylacetylene and was purified via column chromatography (4 : 1, hexane : methylene chloride) yielding a yellow oil. Yield 0.263 g (52%). ^{1}H NMR (CD$_3$Cl, TMS) δ 7.39 (d, 2H), 6.82 (d, 2H), 3.76 (s, 3H), 0.26 (s, 9H); ^{13}C NMR (CD$_3$Cl, TMS) δ 159.7, 115.21, 115.2, 113.7, 105.2, 92.3, 55.1, 0.0 ppm.[98]

***p*-methoxyphenylacetylene.** This compound was prepared following the same method described for p-nitrophenylacetylene and collected as a yellow oil. Yield 0.150 g (89%). ^{1}H NMR (CD$_3$Cl, TMS) δ 7.41 (d, 2H), 6.85 (d, 2H), 3.80 (s, 3H), 3.02 (s, 1H); ^{13}C NMR (CD$_3$Cl, TMS) δ 113.83, 160.0, 114.33, 114.5, 113.8, 85.0, 76.5, 55.32 ppm.[98]

4,4'-di-*t*-butyl-2,2'-bipyridine. 4-t-Butylpyridine (25 mL, 24.0 g, 177.8 mmol) was placed in a 50 mL round bottom flask. 1 gram of 10% Pd/C catalyst was added. The mixture was then refluxed for 24 hours. The mixture was allowed to cool to room temperature dissolved in diethyl ether and filtered. Rotary evaporation of the filtrate yielded a white solid, containing terpyridine and the desired bipyridine. The solid mixture was then sublimed to yield 40% 4,4'-di-t-butyl-2,2'-bipyridine. NMR are consistent with the literature.[97]

4,4'-di-carboxyethyl-2,2'-bipyridine. To a solution of potassium permanganate (55.0 g, 348 mmol) in water (950 mL), 4,4'-dimethyl-2,2'-bipyridine (4.0 g, 21.74 mmol) was added and heated to reflux until the solutions became colorless. The resulting solution was filtered and then washed with diethyl ether to remove unreacted 4,4'-

dimethyl-2,2'-bipyridine. Concentrated HCl was then added to the aqueous phase until acidic when a flocculent solid precipitated out of solution. The precipitate was collected by filtration, washed with water and dried under vacuum yielding 6.5 g of 4,4'-dicarboxy-2,2'-bipyridine.[97]

4,4'-dicarboxy-2,2'-bipyridine (3 g, 12.3 mmol) is placed in a 250 mL round bottom flask containing 55 mL of concentrated sulfuric acid and 120 mL of absolute ethanol. The solution was then refluxed overnight, cooled and then poured over ice. This solution was then neutralized by the addition of 20% NaOH solution. Upon neutralization the solution turned slight pind and a white precipitate formed. The precipitate was collected by filtration, washed with water and then recrystallized from 95% ethanol yielding 3 grams of long white fibrous crystals (mp = 158.5-160.5°C, Lit = 159- 160.5°C[97])

4,4'-bis-diethylamido-2,2'-bipyridine. The same method was used as for 4,4'-dicarboxyethyl-2,2'-bipyridine up to the 4,4'dicarboxy-2,2'-bipyridine. 4,4'-Dicarboxy-2,2'-bipyridine (3 g, 12.4 mmol)was refluxed in 30 mL of thionyl chloride for 3 hours producing a yellow solution. The excess thionyl chloride was removed under vacuum. 80 mL of dry benzene was then added followed by addition of diethyl amine (6 mL, 73.15 mmol). Upon this addition, a white precipitate was formed almost immediately. The mixture was then refluxed for 2 more hours, cooled, filtered and dried under vacuum. ^{1}H NMR (CD$_3$Cl, TMS) 8.98 (d, 2H), 8.77 (s, 2H), 8.15 (d, 2H), 3.47 (q, 4H), 1.24 (t, 3H).

4,4',5,5'-tetramethyl-2,2'-bipyridine. 2,3-dimethylpyridine (28.5 g, 30 mL, 266.4 mmol) was refluxed with Pd/C catalyst (10% Pd, Aldrich) for 8 days. Upon

cooling, a solid material was produced. A 1:1 toluene/chloroform mixture was added to dissolve the solid and the solution was filtered hot. The solution was then filtered and washed with a small amount of 1:1 toluene/chloroform followed by rotary evaporation of the filtrate yielding 6 g of the white solid product. ^{1}H NMR (CDCl$_3$, TMS) 8.25 (s, 2H), 7.75 (s, 2H), 2.34 (s, 3H), 2.25 (s, 3H).

Platinum Complexes

The synthesis of the diimine platinum bisacetylide complexes proceeded via similar procedures, thus only the full synthesis is described for **1b** t-bbpyPt(CCtol)$_2$. All new complexes were characterized by ^{1}H NMR, ^{13}C NMR, and Mass Spec, with the exception of the platinum dichlorides where ^{13}C NMR was not possible due to solubility restrictions. All previously made complexes spectra matched literature data.

4,4'-di-*t*-butyl-2,2'-bipyridyl platinum dichloride. 4,4'-di-t-Butyl-2,2'-bipyridine (200 mg, 0.746 mmol) and K$_2$PtCl$_4$ (300 mg, 0.741 mmol) were placed in a 100 mL round bottom flask. 60 mL of water was then added along with 4 drops of concentrated HCl. A condenser was placed on the round bottom flask and the mixture was then heated to 90°C in an oil bath for 2 hours with rapid stirring via magnetic stir bar. After the 2 hours, a large amount of yellow precipitate had formed. The mixture was then allowed to cool to room temperature and then filtered on a büchner funnel. The solid was then dissolved in methylene chloride and precipitated via addition of diethyl ether. After precipitation, the solid was filtered and washed with diethyl ether and then dried yielding 358 mg of the diimine platinum dichloride. ^{1}H NMR (CDCl$_3$,TMS) δ 9.58 (d, 2H), 7.84 (s, 2H), 7.52 (d, 2H), 1.43 (s, 18H).[88]

4,4'-di-t-butyl-2,2'-bipyridyl platinum bis(tolylacetylide). 4,4'-di-t-Butyl-2,2'-bipyridyl platinum dichloride (200 mg, 0.375 mmol) and 4-ethynyltoluene (86 mg, 0.75 mmol) were placed in a 100 mL round bottom flask and dissolved in 50 mL of dichloromethane and 3 mL of diisopropylamine. A septum was placed on the flask and then argon was bubbled through the solution for 30 minutes. With argon still flowing through the solution, the septum was removed and a catalytic amount of copper iodide (5 mg, 0.026 mmol) was added. The septum was then replaced and argon was bubbled through the solution for 10 more minutes. During the 10 minutes, the solution changed from a bright yellow solution to a slightly orange-yellow solution. The solution was allowed to stir overnight after which time the solvent was removed via rotary evaporator. The solid was purified via column chromatography on neutral alumina with methylene chloride as the eluent yielding 150 mg of the diimine platinum bis-acetylide. ^{1}H NMR (CDCl$_3$, TMS) δ 9.53 (d, 2H), 7.89 (s, 2H), 7.40 (dd, 2H), 7.15 (AB quartet, 8H), 2.41 (s, 6H), 1.34 (s, 18H).[88]

4,4',5,5'-tetramethyl-2,2'-bipyridyl platinum dichloride ^{1}H NMR (CDCl$_3$, TMS) δ 9.44 (s, 2H), 7.81 (s, 2H), 2.35 (s, 6H), 2.32 (s, 6H); HRMS: Calc'd for C$_{14}$H$_{16}$Cl$_2$N$_2$Pt: 477.034, found [M + H] 478.029.

4,4',5,5'-tetramethyl-2,2'-bipyridyl platinum bis(4-tolylacetylide) ^{1}H NMR (CDCl$_3$, TMS) δ 9.41 (s, 2H), 7.75 (s, 2H), 7.42 (d, 4H), 7.07 (d, 4H), 2.39 (s, 6H), 2.37 (s, 6H), 2.36 (s, 6H); ^{13}C NMR (CD$_2$Cl$_2$) δ 150.85, 139.96, 136.92, 132.31, 128.96, 124.10, 123.95, 120.82, 112.24, 102.03, 90.48, 21.83, 20.53, 17.43 ppm; HRMS: Calc'd for: C$_{32}$H$_{30}$N$_2$Pt 637.206; Found: 637.205 [M + H].

4,4'-dicarboxyethyl-2,2'-bipyridyl platinum dichloride ^{1}H NMR (CDCl$_3$,

TMS) δ 9.61 (d, 2H), 8.21 (s, 2H), 7.52 (d, 2H), 3.57 (q, 4H), 1.24 (t, 6H).

4,4'-dicarboxyethyl-2,2'-bipyridyl platinum bis(4-tolylacetylide) ^{1}H NMR

(CDCl$_3$, TMS) δ 9.98 (d, 2H), 8.62 (s, 2H), 8.07 (d, 2H), 7.36 (d, 4H), 7.07 (d, 4H), 4.47

(q, 4H), 2.35 (s, 6H), 1.43 (q, 6H); ^{13}C NMR (CD$_2$Cl$_2$, TMS) δ 163.88, 156.52, 152.55,

139.76, 135.56, 132.21, 128.72, 127.38, 125.13, 122.63, 85.85, 81.31, 63.21, 21.59, 14.40

ppm; HRMS: Calcd for C$_{34}$H$_{30}$N$_2$O$_4$Pt: 725.185; Found: 726.193 [M + H]

4,4'-dicarboxydiethylamido-2,2'-bipyridyl platinum dichloride ^{1}H NMR

(CDCl$_3$, TMS) δ 9.54 (d, 2H), 7.91 (s, 2H), 7.43 (d, 2H), 3.57 (q, 4H), 3.38 (q, 4H), 1.24

(t, 6H), 1.19 (t, 6H); HRMS: Calcd for C$_{20}$H$_{26}$Cl$_2$N$_4$O$_2$Pt: 619.108; Found: 620.218 [M +

H].

4,4'-dicarboxydiethylamido-2,2'-bipyridyl platinum bis(4-tolylacetylide) ^{1}H

NMR (CDCl$_3$, TMS) δ 9.63 (d, 2H), 7.95 (s, 2H), 7.41 (d, 2H), 7.38 (d, 4H), 7.06 (d, 4H),

3.54 (q, 4H), 3.33 (q, 4H), 2.35 (s, 6H), 1.24 (t, 6H), 1.09 (t, 6H); ^{13}C NMR (CD$_2$Cl$_2$) δ

166.91, 156.73, 151.35, 146.56, 135.25, 131.62, 128.68, 125.15, 124.24, 121.06, 101.94,

85.68, 43.38, 39.51, 21.31, 14.32, 12.67: HRMS: Calcd for C$_{38}$H$_{40}$N$_4$O$_2$Pt: 779.280;

Found: 780.288 [M + H].

4,4'-t-butyl-2,2'-bipyridyl platinum bis(4-methoxyphenylacetylide) ^{1}H NMR

(CDCl$_3$, TMS) δ 9.73 (d, 2H), 7.94 (s, 2H), 7.54 (dd, 2H), 7.47 (d, 4H), 6.80 (d, 4H), 3.80

(s, 6H), 1.44 (s, 18H); ^{13}C NMR (CD$_2$Cl$_2$) δ 163.05, 157.33, 156.15, 151.07, 133.16,

124.49, 121.00, 118.58, 113.14, 101.4, 83.60, 55.18, 35.74, 30.22; HRMS: Calcd for

C$_{36}$H$_{38}$N$_2$O$_2$Pt: 725.258; Found: 725.268. [88]

4,4'-t-butyl-2,2'-bipyridyl platinum bis(4-dimethylaminophenylacetylide) ^{1}H

NMR (CDCl$_3$, TMS) δ 9.78 (broad s, 2H), 7.92 (s, 2H), 7.51 (d, 2H), 7.43 (d, 4H), 6.64

(d, 4H), 2.93 (s, 12H), 1.43 (s, 18H); ^{13}C NMR (CD$_2$Cl$_2$) δ 162.80, 156.23, 151.20,

148.42, 132.90, 124.42, 118.50, 116.99, 112.13, 102.23, 82.39, 40.69, 35.70, 30.23 ppm;

HRMS: Calcd for C$_{38}$H$_{44}$N$_4$Pt: 751.3214; Found: 751.3227.

4,4'-t-butyl-2,2'-bipyridyl platinum bis(4-nitrophenylacetylide) ^{1}H NMR

(CDCl$_3$) δ 9.60 (d, 2H), 8.71 (s, 2H), 8.18 (d, 4H), 7.61 (d, 4H), 7.52 (d, 2H), 1.48 (s,

18H); HRMS: Calcd for C$_{34}$H$_{32}$N$_4$O$_4$Pt: 755.2071; Found: 756.2134 [M + H][88]

4,4'-t-butyl-2,2'-bipyridyl platinum bis(4-trifluoromethylphenylacetylide) ^{1}H

NMR (CDCl$_3$) δ 9.62 (d, 2H), 7.97 (s, 2H), 7.62 (m, 6H), 7.43 (d, 4H), 1.42 (s, 18H);

HRMS: Calcd for C$_{36}$H$_{32}$F$_6$N$_2$Pt: 801.212; Found: 802.2191 [M + H]

CHAPTER 4
PLATINUM MOLECULAR SQUARES

Introduction

Multi-Platinum Acetylides

As described in the previous chapter, there have been many various reports on

luminescent platinum complexes. Several publications have reported the photophysics of

platinum diimines with various ligands such as chloride, various alkyl groups, dithiolates

and aromatics (1-4, Figure 4-1).[91-98] Relatively few publications have reported on the

photophysics of platinum acetylides and those that have typically utilize phosphines as

the ancillary ligand (5, Figure 4-1). Even less work has been done on platinum

complexes that incorporate both diimines and acetylides (6, Figure 4-1). Most work in

the area of platinum acetylide chemistry has dealt with polymers that incorporate σ-

platinum acetylide bonds along the backbone in order to further extend the π-conjugation

(7, Figure 4-1). All of the listed work has been described in the previous chapter.
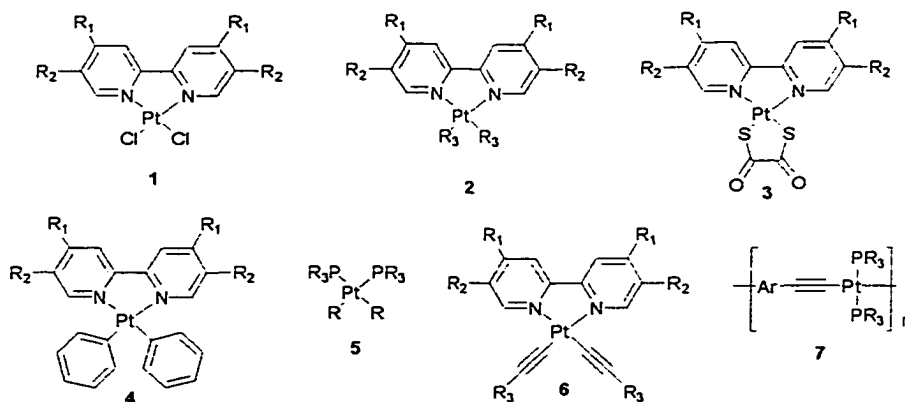
Figure 4-1. Various Platinum complexes

108

Other platinum acetylide macromolecules that have been studied are dendrimers of the type shown in Figure 4-2[101] and some macrocycles to be discussed in later sections. Dendrimers are nanosize compounds having a regularly branched structure and many functional end-groups. Most organometallic dendrimers contain only one metal either at the core or at the periphery with the remainder based solely on organic chemistry. This report, however, contains multiple platinum acetylide units with the dendrimer. The dendrimer is elegant, but no practical application was presented in the entirely synthetic paper and no photophysical data was reported.
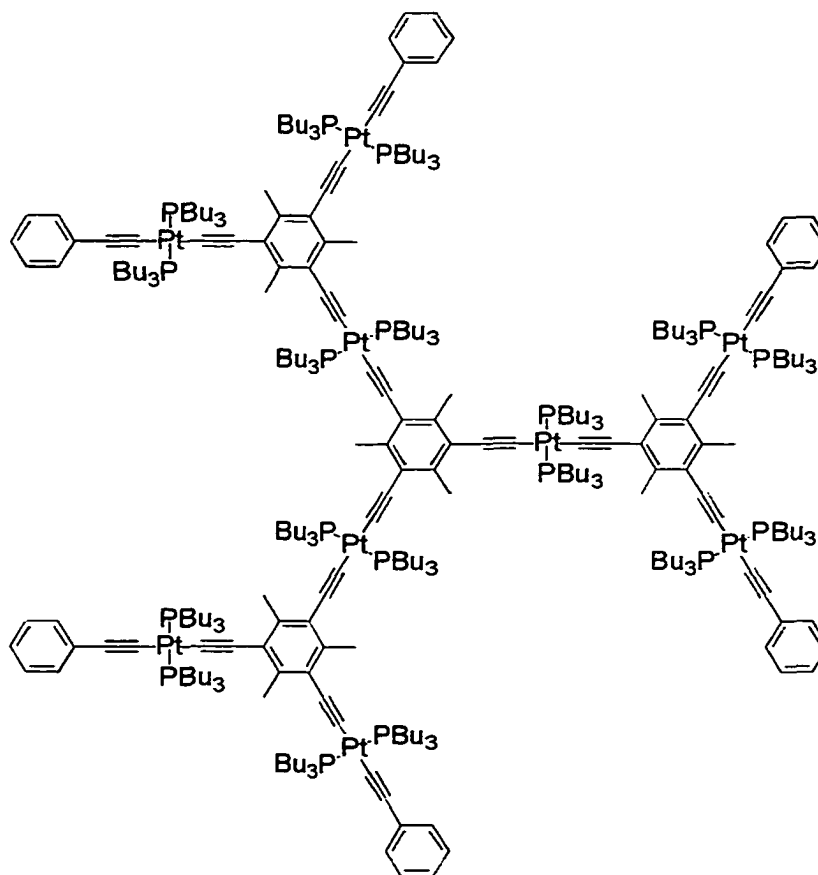
Figure 4-2. Platinum acetylide dendrimer

Transition Metal Macrocycles

Macrocycles that incorporate metals into the cycle have become of great interest as of late. The great interest stems from the great promise in host-guest, inclusion, and molecular recognition chemistry. The use of self-assembly has been utilized, most notably by Peter Stang[102-104] and Joseph Hupp,[105-107] in order to synthesize many different macrocycles and other nanostructures of various size and shape. Self-assembly proceeds via the simultaneous assembly of predetermined building blocks resulting in well-defined supramolecular architectures. The reason that this method typically works well is that the coordinative bonds are kinetically labile and can "self-heal" by the equilibrium of the desired product and constituents. The equilibrium finally yields the thermodynamic product that is typically the macrocycle or nanostructure of interest.

Maverick reported one of the first cyclic self-assembled transition metal containing macrocycles (Figure 4-3).[108] The complex was formed by the reaction of $Cu(NH_3)_4^{2-}$ and a bis-(b-diketone) ligand in aqueous solution. The interesting feature of this complex is its ability to act as a host, which was tested by measuring its binding constants with pyrazine, pyridine, quinuclidine, and diazabicyclo[2,2,2]octane (DABCO). DABCO was found to bind selectively over the other possible guests inside the complex with a binding constant of 220 M^{-1}. The internal coordination was established via x-ray crystallography of the inclusion complex.
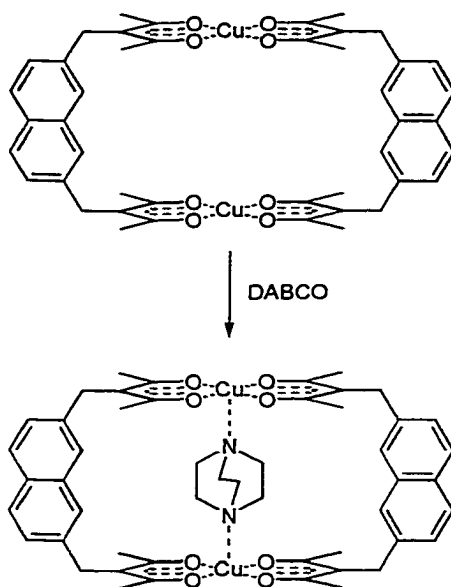
Figure 4-3. First cyclic self-assembled transition metal containing macrocycle

Fujita and coworkers used nonlinear spacers between two bipyridine rings to form several water soluble bi-nuclear macrocycles.[109] When the metal was palladium, it was shown that at room temperature the dinuclear palladium complex was in equilibrium with the catenane (Figure 4-4). It was determined that at low concentrations, the single ring assembly was favored, however, at higher concentrations, the two ring catenane was dominant. This is likely due to the benzene unit of one macrocycle serves as a guest to the other macrocycle via π–π interactions. When the metal is platinum, only the single ring system was produced. This was attributed to the stronger Pt-N bond strength as compared to the Pd-N bond. However, when the reaction mixture was heated to 100° C, the catenated two ring system was formed. When the reaction was cooled, isolation and crystallization allowed x-ray crystallography to confirm the catenane structure. Other complexes formed by analogous reactions are shown in Figure 4-5.[110,111]
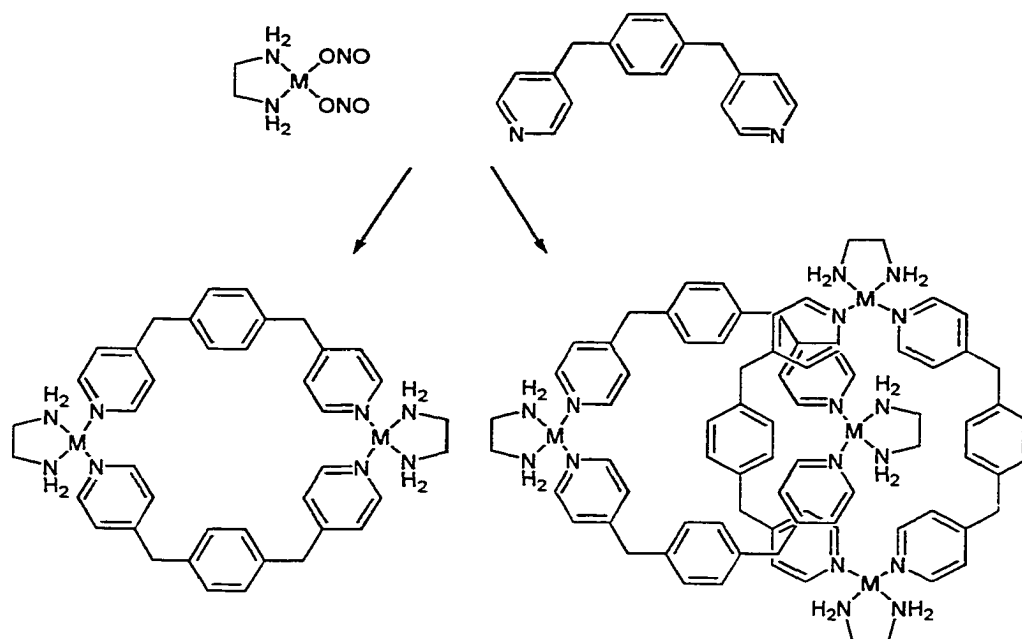
Figure 4-4. Structure of Fujita's macrocycles and catenane. ($M = Pt^{II}$ or Pd^{II})

Most if not all of the metal containing macrocycles described herein are intriguing, but have limited utility in the area of host guest chemistry because there is generally nothing built into the system to easily detect the guest inclusion. This problem has been addressed by a series of papers by Hupp and coworkers[106] where the incorporation of visible-light-addressable, luminescent rhenium-imine, rhenium-azine or porphyrin components with a square assembly is studied (Figure 4-6).
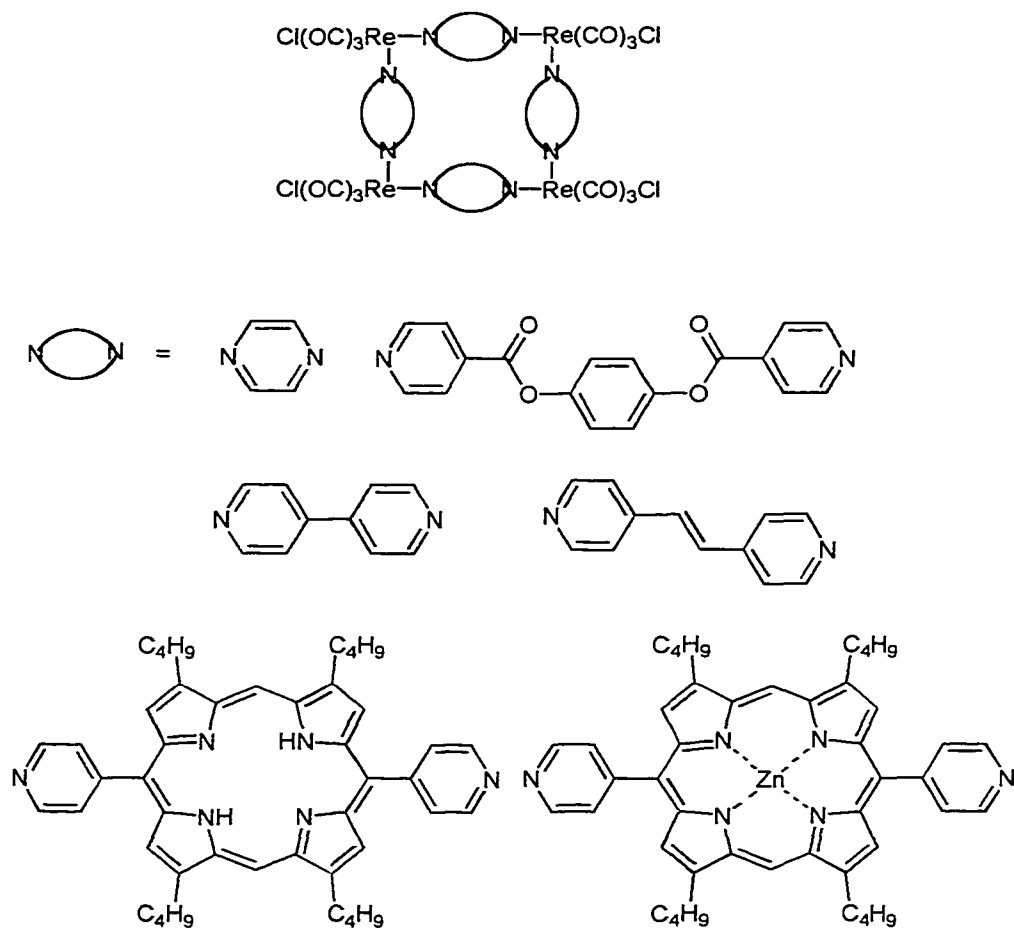
Figure 4-6. Structures of complexes studied by Hupp and coworkers

Platinum/Palladium Acetylide Macrocycles

Although much work has been presented which utilize platinum or palladium to form macrocycles, the majority has utilized the labile M-N bond between the metal and the imine (4,4'-bipyridine, bipyrazine, etc.) to form the macrocycle. Very little work has been done using different bidentate ligands such as diacetylides, dinitriles, and di-

isonitriles or combinations thereof as the side of the molecular assembly. Even fewer

have reported on the luminescence of such complexes.

There has been a desire to form mixed neutral-charged or heterobimetallic

molecular squares of the same topology. Stang[110] found that the simplest way to achieve

this was to use readily available Pd(II) and Pt(II) bistriflates 4-1 and 4-2 shown in Figure

4-7 for the charged portions of the assemblies along with specially designed monomeric

units which contain covalently linked neutral transition metal bisphosphane complexes

(4-3) also shown in Figure 4-6 . Reaction of 4-1 or 4-2 with 4-3 afforded molecular

squares 4-4 and 4-5. The structure of these compounds was confirmed via mass

spectrometric techniques as well as x-ray crystallography. The work on these compounds

was purely synthetic and no luminescence data was provided.

To further expand upon this idea, Stang[111] synthesized macrocycle 4-7 by reaction

of 4-3 with 4-6 (Figure 4-8). Unit 4-6 was prepared by from 4,4'diiodobiphenyl and

Pt(PPh₃)₄ via oxidative addition followed by the treatment of the product with AgOTf.

Self-assembly of macrocycle 4-7 occurred by the addition of 4-3 in dichloromethane.

The expected molecular weight was confirmed by MALDI and ESI-FTICR mass

spectrometric techniques. This macrocycle belongs to the class of ultra fine particles,

since their estimated dimensions are about 3.0 nm along the edge and 4.3 nm across the

diagonal. Again this study was purely synthetic in nature.

Four other macrocycles (4-8, 4-9, 4-10 and 4-11, Figure 4-9) based on metal

acetyl ides have been reported by Youngs[112,113] and Haley.[114] Macrocycles 4-8, 4-10 and

4-11 are monometallic in nature while 4-9 is bimetallic. 4-8 was prepared in one pot by

reaction of 4-12, 4-13, and 4-14 in diisopropylamine in the presence of copper iodide as

the catalyst. **4-9** was prepared by reacting 2 equivalents of cis-[PEt$_3$]$_2$PtCl$_2$ (**4-15**) with **4-16** in methylene chloride/diisopropylamine (1:4) with copper iodide catalyst. **4-10** was prepared by reacting **4-16** first with 2 equivalents of n-butyl lithium followed by addition of PtCl$_2$(tht)$_2$ in THF, and finally treatment with NBu$_4$Br in an isopropanol water mixture. Finally, **4-11** was prepared by addition of **4-17** to trans-(PEt$_3$)$_2$PtCl$_2$ in toluene with copper iodide as the catalyst. Again, all these studies were synthetic in nature showing little other utility.
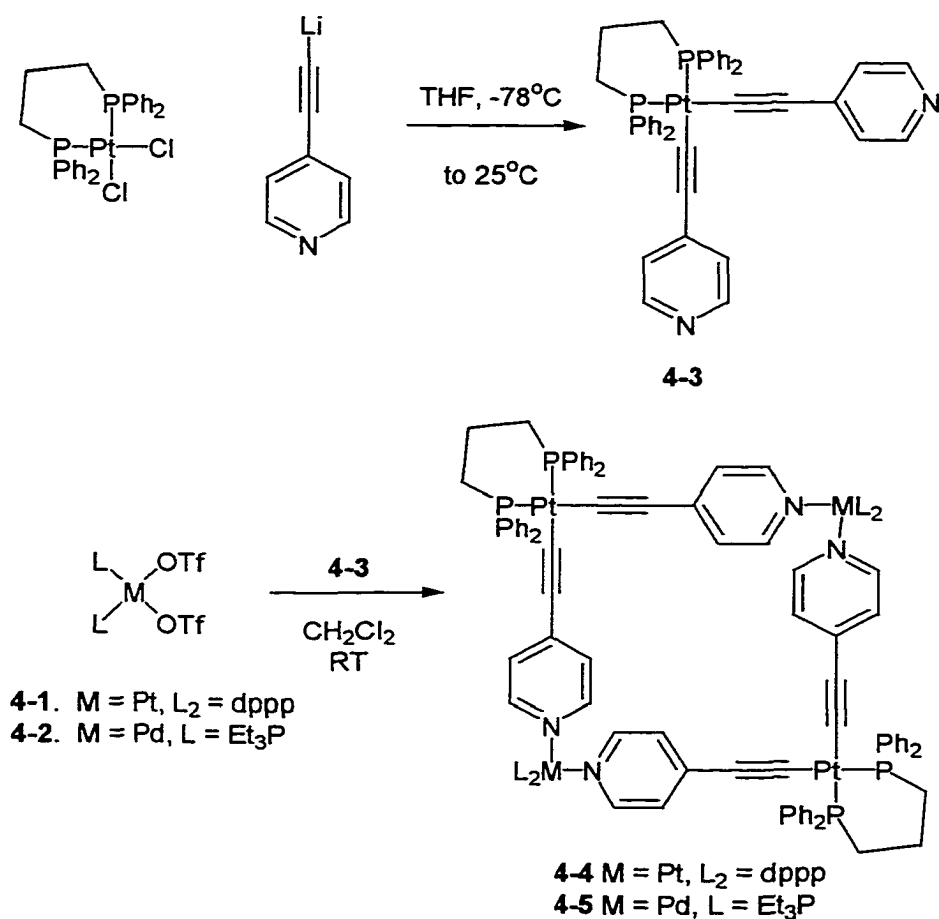
Figure 4-7. Stang's approach to macrocycles that contain metal acetylides
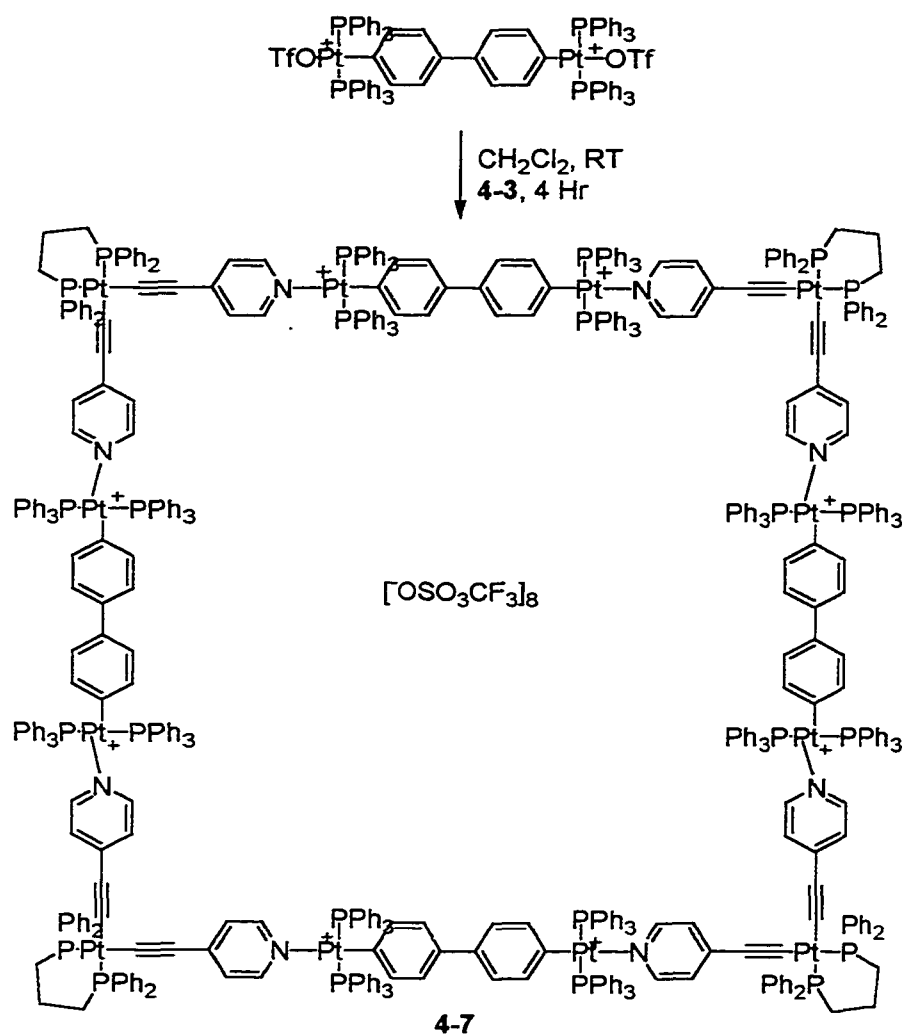
Figure 4-8. Large macrocycle containing platinum acetylide bonds
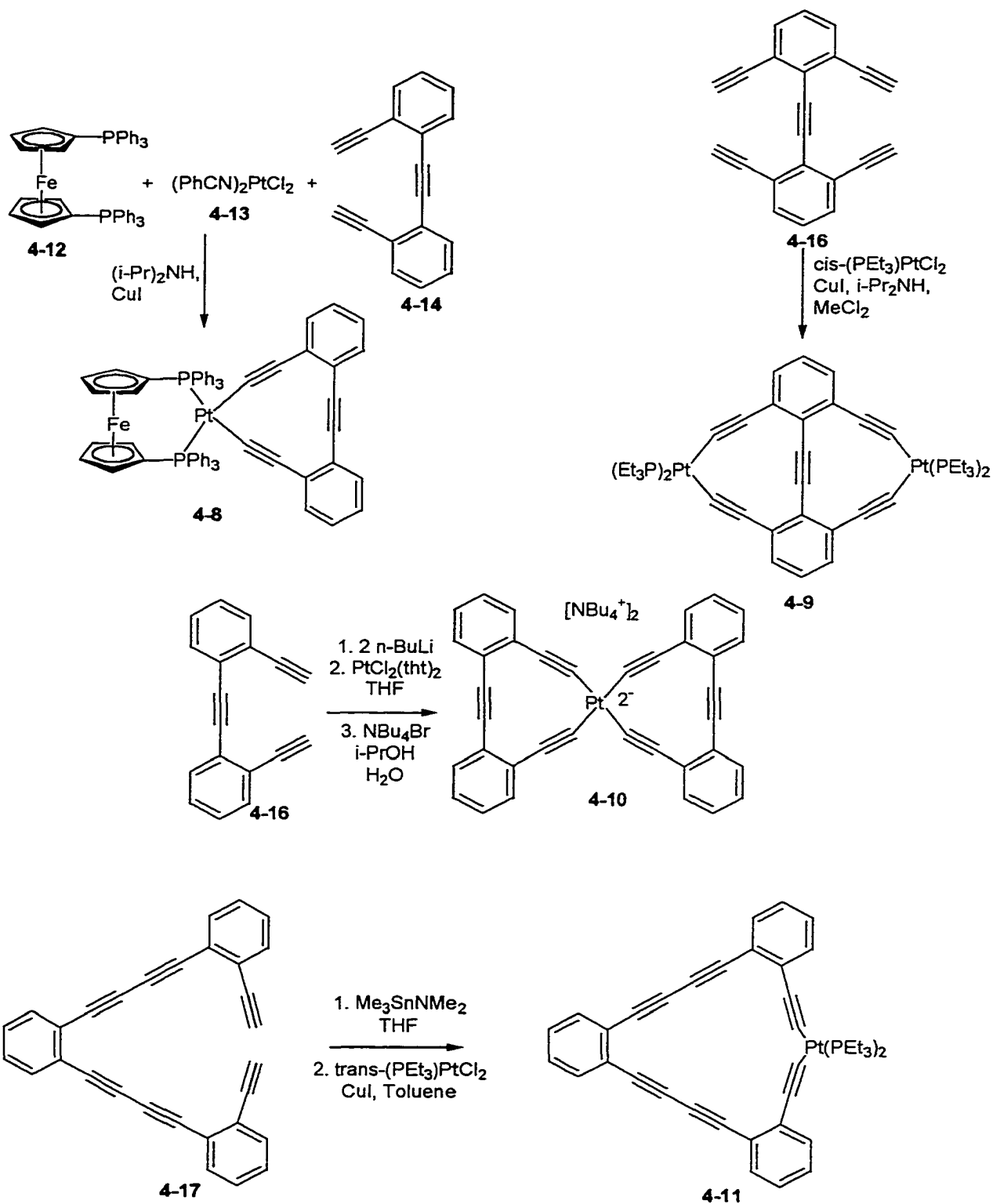
Figure 4-9. Other macrocycles containing platinum acetylide bonds

Only two studies have shown actual metal acetylide bond formation occurring in the self-assembly step (Figure 4-10).[113,114] The first used treatment of o-diethynylbenzene with equimolar amounts of (PEt₃)PtCl₂ in the presence of CuI catalyst to form macrocycle **4-18** in 33% yield. The cyclization proved to be fortuitous in that when the same procedure was performed with (PBu₃)PtCl₂, a mixture of oligomeric complexes resulted. This was likely due to the larger steric bulk of the butyl groups. Thus, this process was only useful when all the groups proved to be optimal. The final macrocycle **4-19** was formed by
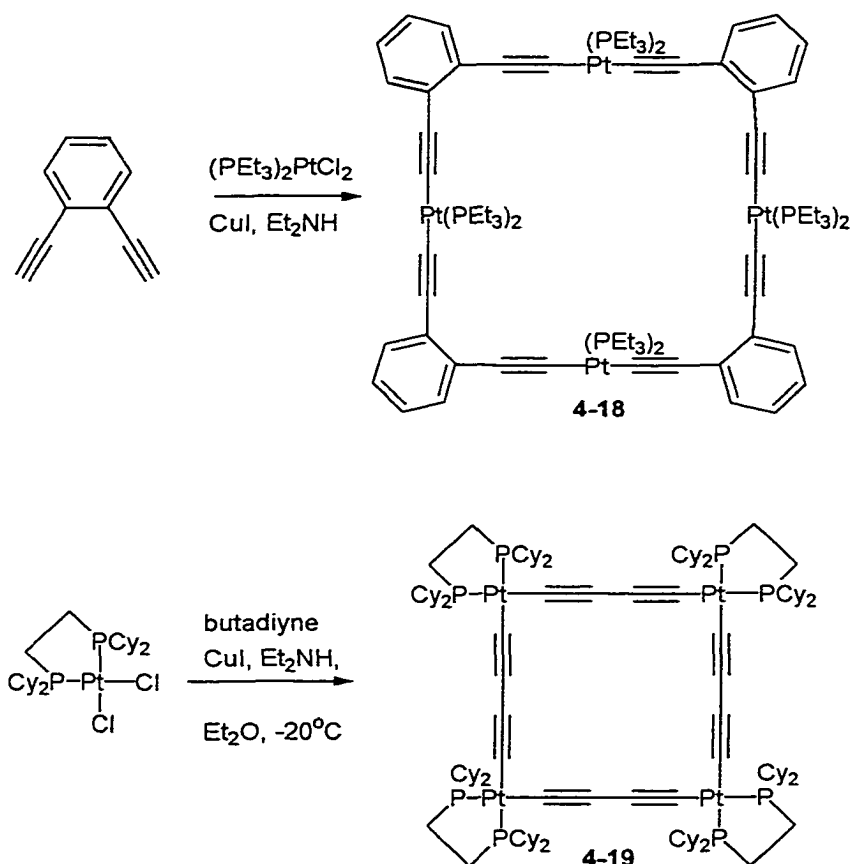
Figure 4-10. Only examples with metal acetylide bond formation during self-assembly

bubbling butadiyne into a suspension of [(C₆H₁₁)₂P)]₂PtCl₂, diethyalamine, diethyl ether, and a catalytic amount of CuI at –20° C. This gave the desired macrocycle in 95 % yield.

It is stated that further attempts at expanding this procedure to larger macrocycles is

underway, but have yet to be reported.

Scope of Current Project

As stated earlier, there has been considerable work in the area of transition metal

containing macrocycles. However, virtually all of the work done on these macrocycles

utilize imines such as pyrazine and 4,4'-bipyridine as the "sides" to form the macrocycle.

These are interesting, however their utility in the area of host/guest and inclusion

chemistry is somewhat limited in that there is usually no easy way to determine if and

how many guest molecules are held within the system.
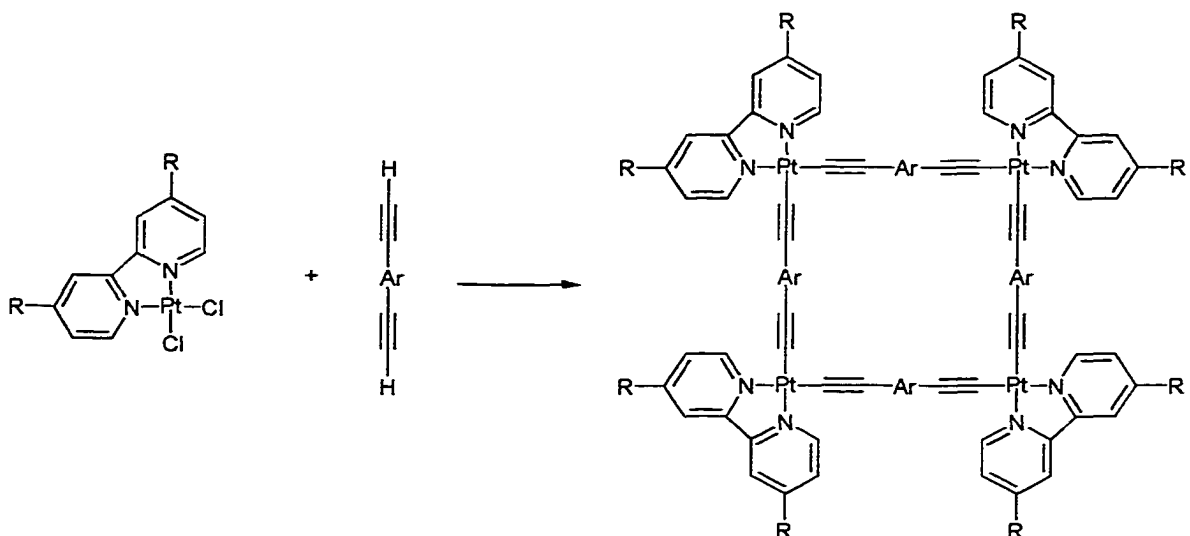
Figure 4-11. Theoretical platinum acetylide squares to be studied

The work described in Chapter 3 detailing the diimine platinum bisacetylides

showed that in some cases, long lived luminescent platinum diimine → MLCT states are

present and it has been theorized that there is some mixing with the acetylide orbitals. In

an attempt to utilize this luminescent feature of diimine platinum acetylides in the area of

macrocycles, work was performed to synthesize macrocycles that incorporate diimines

and acetylides. By using "sides" that have two terminal acetylenes, a macrocycle could theoretically be formed (Figure 4-11). This chapter will examine the synthesis, complete photophysical characterization and possible applications of two macrocyclic squares.

Results and Discussion

Synthesis and Structure

In order to synthesize a square macrocycle formed by platinum acetylide linkages, a side that has two terminal acetylenes is needed. Two methods that differ only in the first steps will be described and is depicted in Figure 4-12. The first method involves iodination of the readily available 1,4-dimethoxybenzene by treatment with iodine in acetic acid and sulfuric acid in the presence of potassium iodate. This is followed by cleavage of the methyl groups of the formed 2,5-diiodo-1,4-dimethoxybenzene by addition of boron tribromide to yield 2,5-diiododihydroquinone. The dihydroquinone could then be alkylated in a dimethylformamide/potassium hydroxide solution in the presence of 1-bromoheptane yielding 2,5-diiodo-1,4-diheptyloxybenzene. The difference in the second method is that instead of starting with the dimethoxybenzene, hydroquinone is first alkylated under similar conditions as the previously described alkylation method to yield diheptyloxybenzene. This dialkoxybenzene is then iodinated in a similar fashion as that describe for the iodination of dimethoxybenzene. Overall yields for the two methods are very similar, therefore, the second process is preferred because it contains less steps.

AcOH/H₂SO₄
KIO4, I₂

BBr₃

4-20

4-21

DMF/KOH
Br-C₇H₁₅

DMF/KOH
Br-C₇H₁₅

AcOH/H₂SO₄
KIO4, I₂

4-22

4-23

Pd(PPh₃)₂Cl₂, CuI
THF/(i-Pr)₂NH
1) TMSCCH
2) HOCH₂CCH

MeOH/THF
KOH

4-24a R = TMS

4-24b R = H

Pd(PPh₃)₂Cl₂, CuI
THF/(i-Pr)₂NH
4-23

MnO₂/KOH
MeCl₂

4-25a R' = CH₂OH

4-25b R' = H
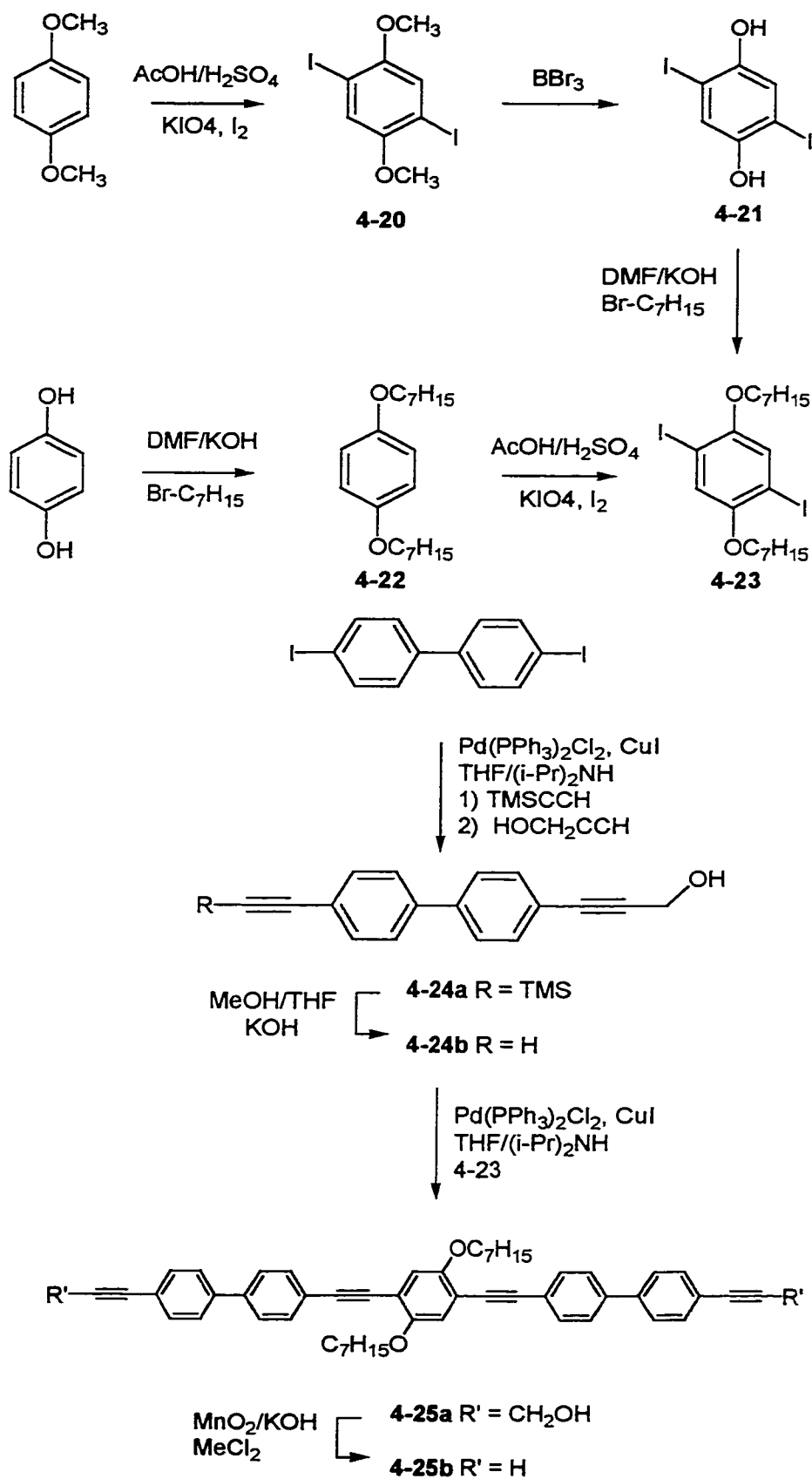
Figure 4-12. Synthesis of sides

In order to extend the conjugation, an unsymmetrically protected biphenyl-4,4'-diyne is needed. This synthesis was accomplished via a tandem Sonogashira coupling of 4,4'-diiodobiphenyl with trimethylsilylacetylene and propynol. The formation of three products is seen; diol, ditrimethylsilyl, and the desired asymmetrically protected diyne (Figure 4-13). These products are relatively easy to separate due to their polarity difference. This step has the lowest overall yield of the entire sequence, however, it was found to be the least time consuming method to form this species. With this product in hand, deprotection of the trimethylsilylacetylene could easily be performed by treatment of the product dissolved in THF/methanol with potassium hydroxide. The mono-protected product can then be used in another Sonogashira coupling with the diiodo-dialkoxybenzene 4-23. To form the final oligomer to be used in the synthesis of the square macrocycle, deprotection of the two final acetylenes was performed by oxidative cleavage using KOH and MnO₂. This final oligomer 4-25b will be termed "side" throughout the rest of the text as it comprises the side of the square.
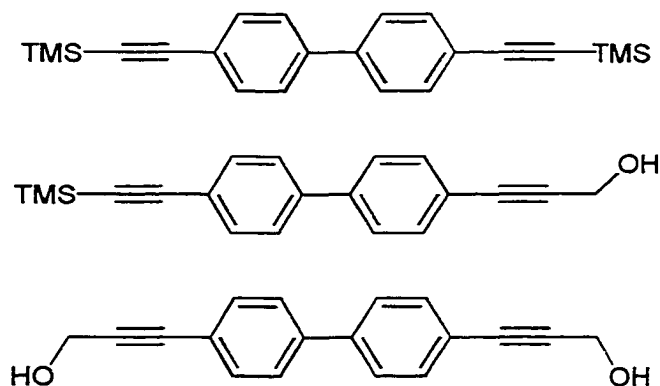
Figure 4-13. Three products formed upon tandem Sonogashira coupling.

After the synthesis of the terminal diacetylene side of the square macrocycle, the final step was formation of the macrocycle. This was accomplished under the same general conditions as those used to form the platinum diacetylides in Chapter 3. The side and one equivalent of (t-bbpy)PtCl$_2$ were dissolved in freshly distilled methylene chloride and diisopropylamine and the solution was thoroughly argon degassed. To this solution was added copper iodide and the reaction was allowed to stir for a week. During this time, the solution darkens to a darker yellow solution and solids start to form on the sides of the flask. This solid is believed to be insoluble long chain oligomers. Normally, as described in the previous chapter for the synthesis of the diimine platinum bisacetylides, the solution is rotovapped to dryness. Unfortunately, this was found to not be an effective procedure in this case. After evaporation of all the solvent, the resulting solid became completely insoluble in all organic solvents. Evaporation of the solvent until slightly more solid than was already present circumvented this problem of producing an insoluble material. The resulting solution was then filtered and the filtrate was added dropwise to rapidly stirred hexane or pentane to precipitate out the product mixture. The solid formed was then soluble in methylene chloride and was passed through a plug of neutral alumina collecting all the colored solvent. Again, complete evaporation results in insoluble material, therefore, the same procedure described above was used (evaporation of some of the solvent followed by precipitation from hexane or pentane). The resulting solid still had limited solubility, and initially only ^{1}H NMR (Figure 4-15) could then be used for characterization of the material (later a ^{13}C NMR was obtained by a polarization transfer technique).

Although only a ^{1}H NMR could be obtained, it was thought that the reaction produced a macrocycle because there were no endgroups and no peak broadening. There are essentially two possible outcomes of the synthesis described above: 1) long chain oligomers or polymers formation or 2) macrocycle formation. If the product was a long oligomer or polymer, the ^{1}H NMR spectrum would clearly show a definite broadening of the peaks and also there would be some evidence of end groups. Consider the peaks obtained from R-CH$_2$-O at $\delta = 4.08$; if the product were a polymer, these protons would no longer be equivalent, and would show either a very broad peak or possibly some discernibly different triplets. This would be the case for all the peaks in the spectrum as no two would be equivalent. Also, as stated above, there would be some sort of end group in the spectrum, whether it is a terminal acetylene proton or a bipyridine that is clearly different. Upon inspection of the ^{1}H NMR of the material, it is evident that the peak in the example above is clearly a triplet, as expected. All other peaks, as well, clearly show the expected multiplicity and no broadening. There also is no terminal acetylene proton evident and no differing bipyridyl peaks. The spectrum suggests a very symmetrical molecule, which can only occur if the compound is a macrocycle and the most likely and most stable cycle that can be formed is a square.

4-25b R = C₇H₁₅
4-31b R = CH₂CH₂N(Et)₂
4-26 R = C₁₈H₃₇

CuI, MeCl₂
HN(i-Pr)₂

4-27 R = C₇H₁₅
4-28 R = CH₂CH₂N(Et)₂
4-29 R = C₈H₃₇
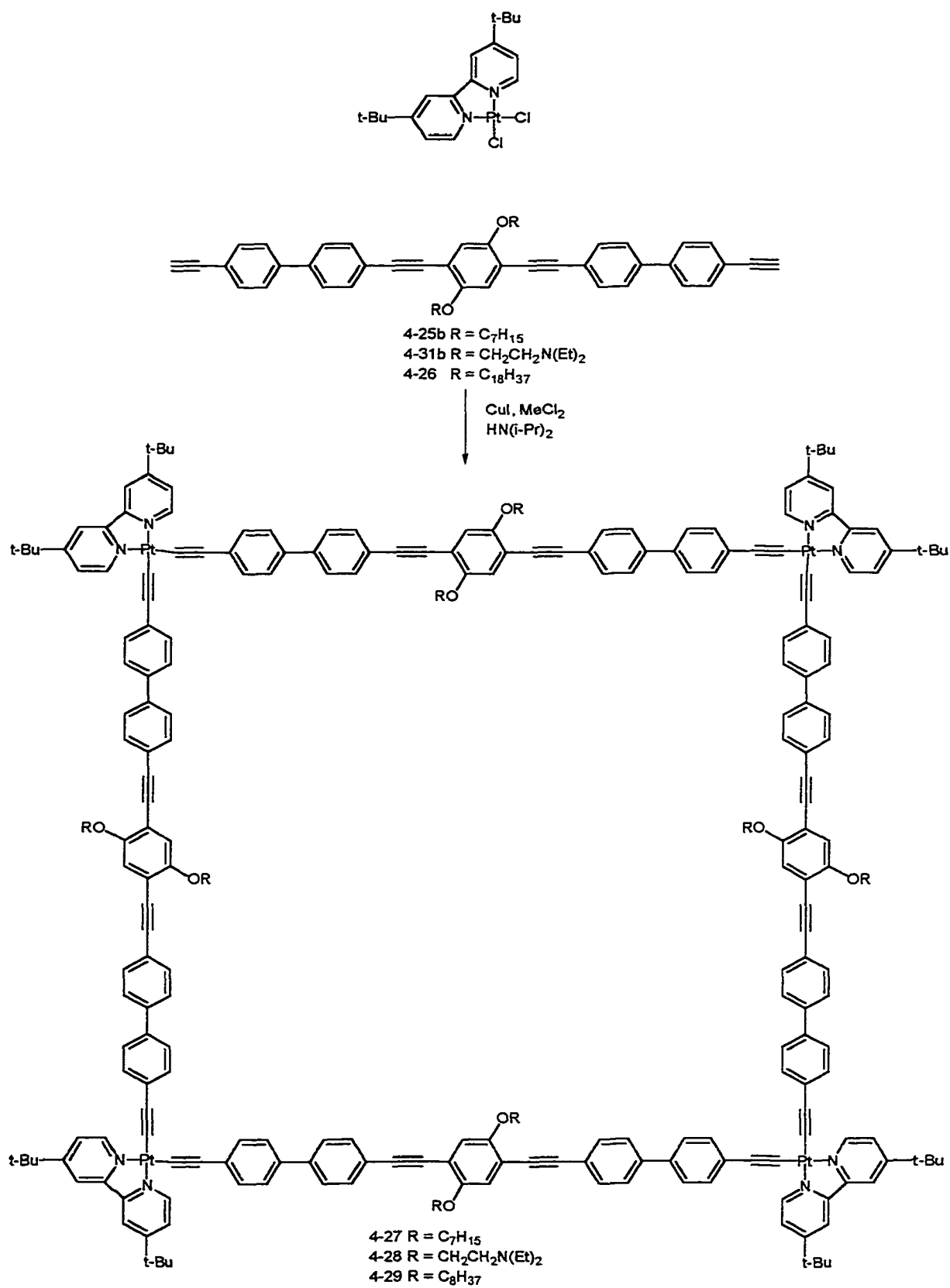
Figure 4-13. Synthesis of platinum squares

126
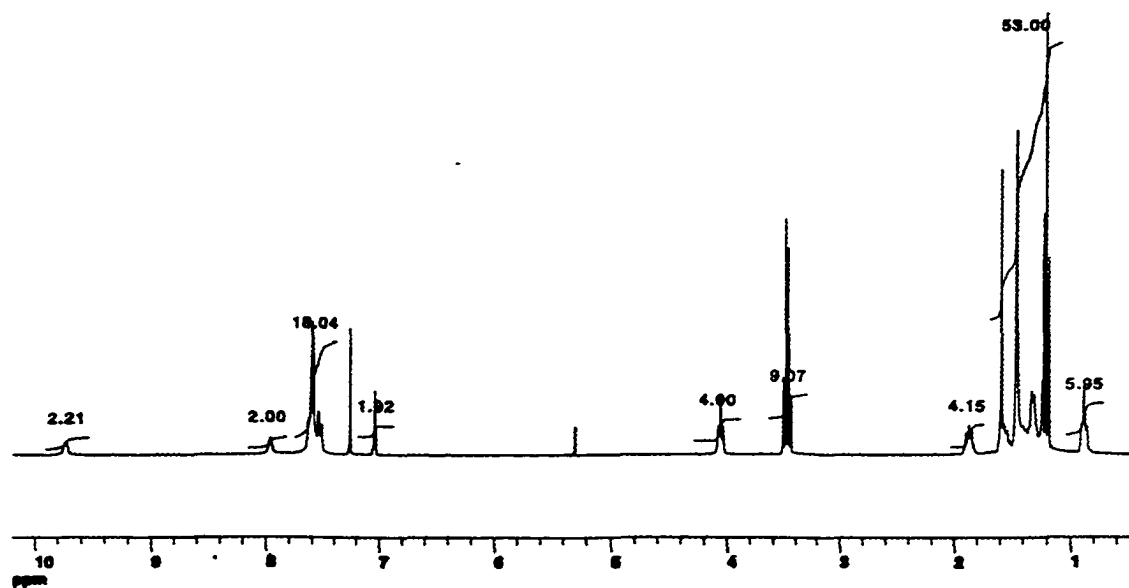
Figure 4-14. ^{1}H NMR spectrum of C7 platinum macrocycle
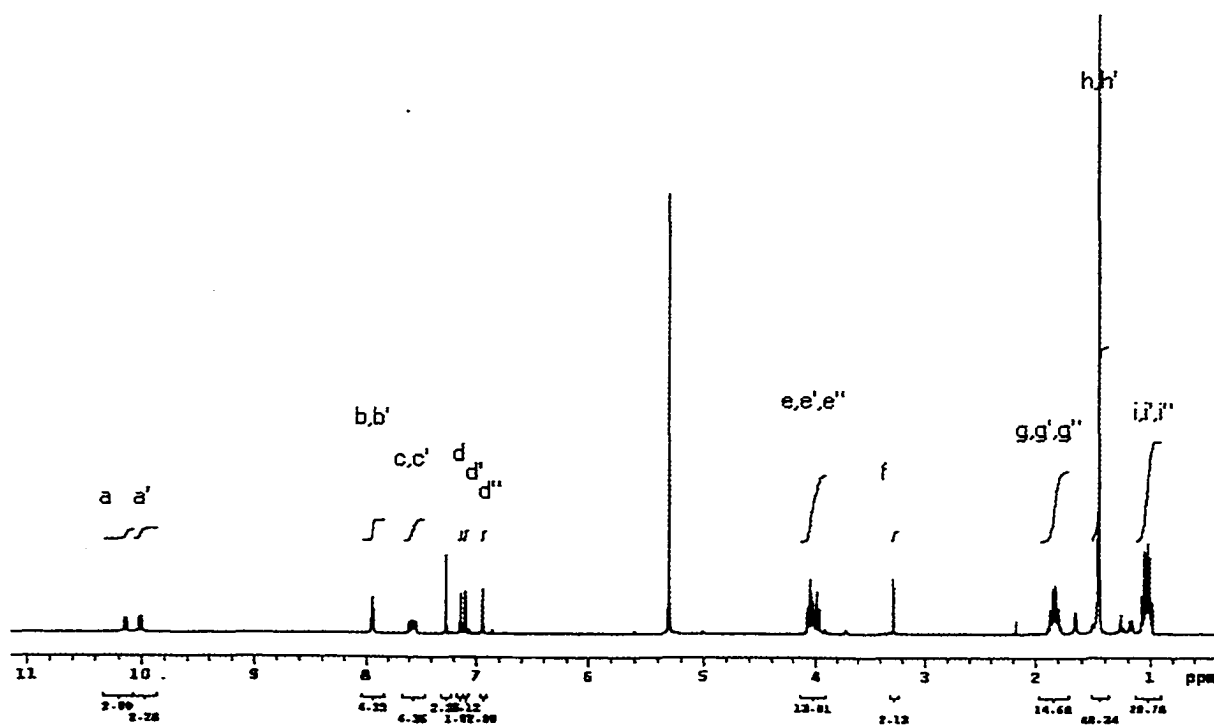
Figure 4-15. ^{1}H NMR spectrum of Platinum trimer
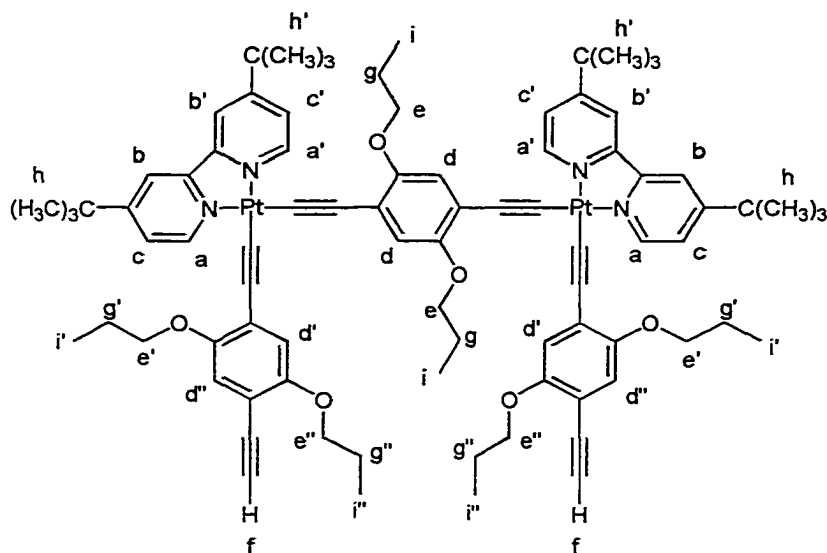
Figure 4-16. Structure and peak assignments of "trimer"

To further illustrate the idea that oligomers and polymers would show end groups and peak broadening or resolution of different peaks, one only need look at the ^{1}H NMR spectrum obtained from a trimer (WRT sides) formed when attempting to make a smaller square (Figures 4-15 and 4-16). The R-C$\underline{H}_2$-O signals at δ ~ 4.0 are clearly resolved showing that they are no longer equivalent. This is the case for all of the other peaks as well. There is also a peak resulting from the terminal acetylenes present in the spectrum.

Several attempts at obtaining a mass spectrum of the macrocyclic square were tried with little luck (MALDI-TOF with various matrixes, FAB, and electrospray). This was likely due to the large molecular weight, and multiple fragmentations that can occur in the mass spectrometer resulting in not detecting the parent ion. The only reasonable mass spectral results obtained were on square **4-29** where the alkoxy chain was changed to eighteen carbons instead of seven (done in hopes of increasing the solubility), where a mass that was equal to the parent ion with one of the C-18 side chains lost. This is good evidence that a square is being formed, however it is unfortunately not definitive. Later,

electrospray techniques revealed two multiply charged parent ions (M^{3+} and M^{4+}), This

leads us to believe that the macrocycles are indeed formed. Also, multiple attempts at

growing crystals for x-ray analysis using various solvents and various techniques proved

to be futile likely due to the limited solubility and the large void space in the molecule.

Because the problems in determining a mass spectrum of the molecular square

were possibly due to the large molecular weight, it was suggested that by adding a site

that could be protonated thus changing the mass to charge ratio could be useful.

Therefore, several attempts at designing a square with a protonatable site were tried. The

idea finally decided upon was one where the alkoxy side chains were changed from a

seven-carbon unit to diethylaminoethoxy groups. This only changed the synthesis in the

beginning steps. That is, in the first step of the second procedure above was to alkylate

the hydroxy groups with bromoheptane. This step was changed to alkylating with N,N-

diethylaminobromoethane. All other steps stayed unchanged yielding the amino

substituted square **4-20**. The ^{1}H NMR (Figure A-2 in the appendix) again showed no end

groups and very sharp peaks indicating no oligomers in the solution. Unfortunately, there

was again no luck in obtaining a mass spectrum of the product.

Photophysical Data

Various photophysical parameters from different measurements are presented for

squares 4-19 and 4-20 in Table 3-1. The individual measurements are discussed below.

Table 4-1. Various photophysical parameters

CMPD	λ_{abs}	λ_{em}	Φ_{em}	τ_{em} (μs)	τ_{ta} (μs)
(4-19)	386	597	0.087	126.4	103.8
(4-20)	386	594	0.075	108.8	76.26

a) Measurements were conducted on argon degassed $MeCl_2$ solutions

Absorption Spectra

The absorption spectra of each of the squares (**4-27** and **4-28**) were obtained in freshly distilled methylene chloride and are depicted in Figure 4-17 along with the absorption of the sides (**4-25b** and **4-31b**) for comparison. Each of the sides' absorption spectra are virtually identical and exhibit two absorption bands of approximately equal absorptivities at ca. 330 and 370 nm which can be attributed to the π,π^* absorption that are typical in phenylene ethynylenes of this type. The absorption spectra of the two squares, again, are virtually identical. They show the same two bands as the sides but are slightly red shifted in energy. The higher energy band of each square (ca. 333 nm) is partially resolved in to two bands and has decreased in absorptivity with respect to the lower energy band as compared to the sides.

The bands of each of the squares around 375-380 nm are increased in molar absorptivity with respect to the higher energy band as compared to the sides. An overall increase in molar absorptivity by a factor of about 4 is also seen in the squares with respect to the sides. This can be explained by that fact that there are now four equivalents of "side" per square. The shift to lower energy is indicative of increased conjugation. This is to be expected because in going from free sides to complexed macrocycle squares the platinum d-orbitals have been shown to increase conjugation length. The fact that the shift is only very slight is also somewhat expected because of the biphenyls being twisted somewhat out of plane with the system, thus breaking conjugation. This has been seen in previous work done by Kevin Ley, Keith Walters and Yiting Li of our group in studies of metal containing phenylene-ethynylene and biphenylene-ethynylene systems.
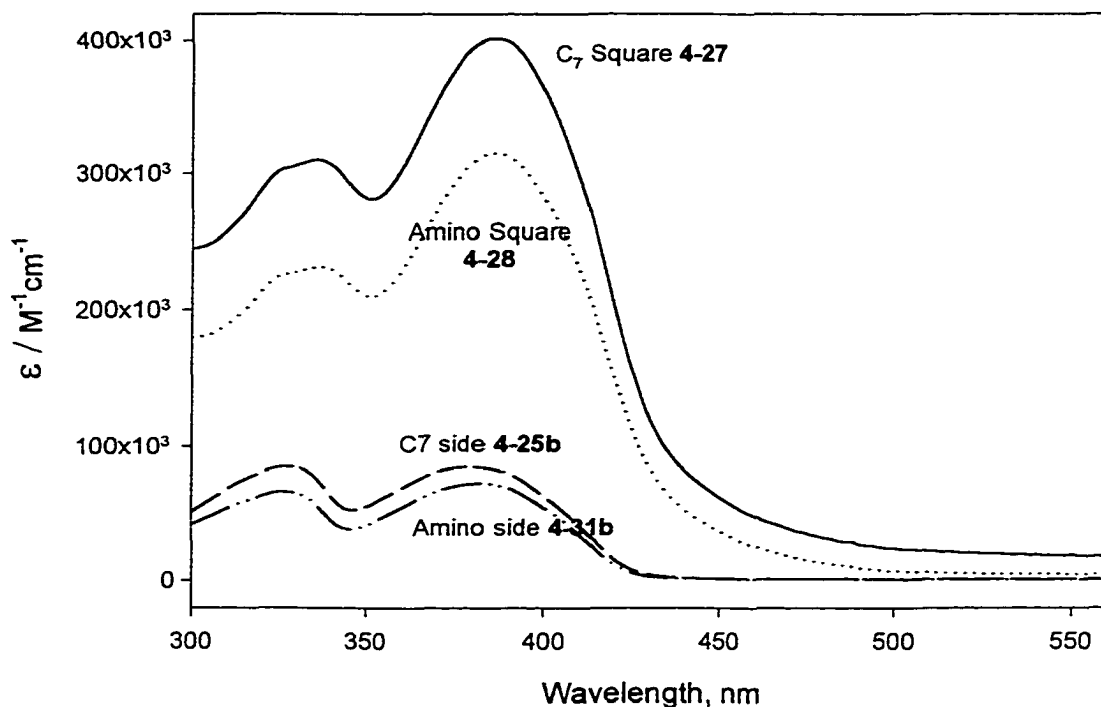
Figure 4-17. Absorption spectra of the sides and squares

Another interesting feature of the absorption spectra of the squares is the long tail

of the low energy peak. The absorption spectrum of (t-bbpy)Pt(C≡Ctol)$_2$ from Chapter 3

shows an absorption band in this region that we have attributed to a MLCT absorption

band. This tail likely arises from absorption of this same state.

Emission Spectra

The room temperature emission spectra of both of the squares (**4-27** and **4-28**) and

both sides (**4-25b** and **4-31b**) were obtained in freshly distilled methylene chloride and

the normalized spectra are depicted in Figure 4-18. The spectra obtained from both of the

sides show the typical emission characteristic of phenylene-ethynylene systems with a

maximum around 420 nm and is attributed to emission from the $^1\pi,\pi^*$ state. The spectra

obtained from both of the squares are virtually identical. They are both relatively sharp

and display vibronic structure with a shoulder around 645 nm and have a maximum

around 595 nm. At first thought, one might think that the emission comes from the same

^{3}MLCT state as with that of corner species (t-bbpy)Pt(C≡Ctol)$_2$, but the emission from

this complex is much broader and shows no vibronic structure. Because of its structure

and energy, the emission from the macrocycle is believed to arise from the $^3\pi,\pi^*$ state of

the side ligands.
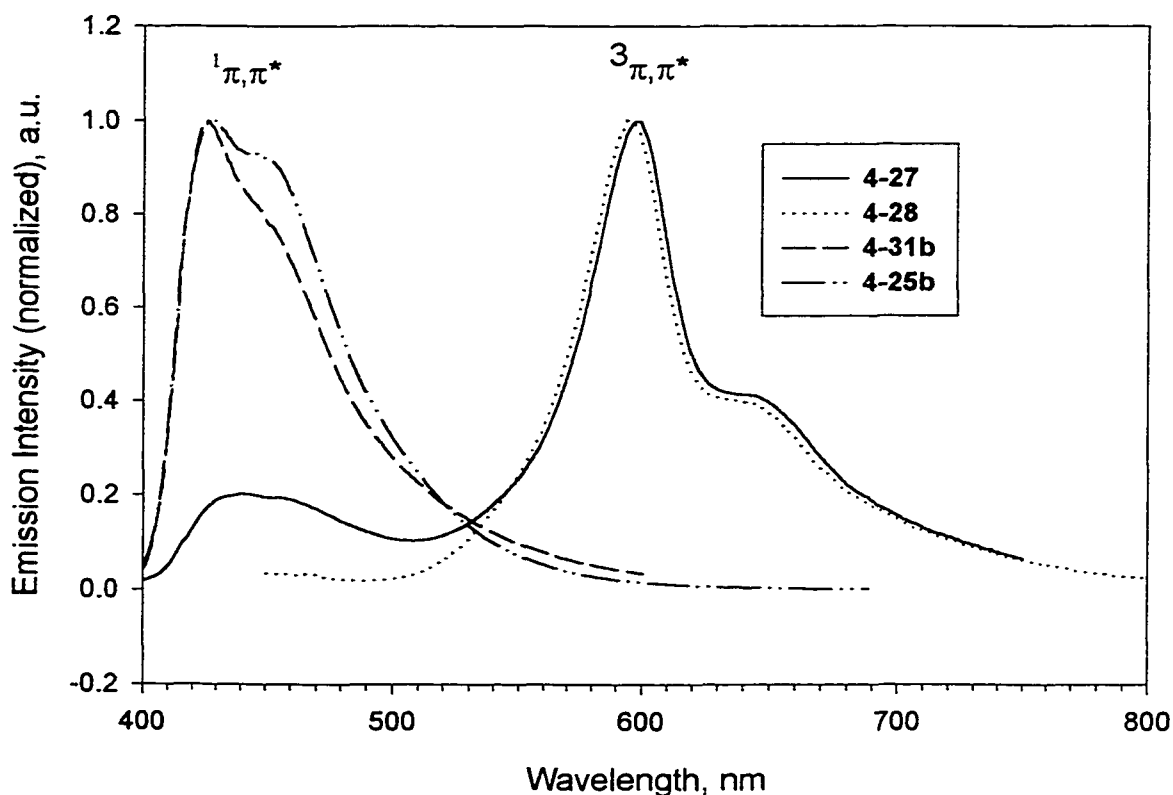
Figure 4-18. Emission spectra of the sides and squares (420 nm excitation)

A variable temperature emission study was performed on each of the squares in 2-methyltetrahydrofuran and the results are depicted in Figure 4-19. Both squares show the same expected trends. That is, the emission greatly increases with decreasing temperature. There is also little if any shifting to higher or lower energies as the temperature decreases.
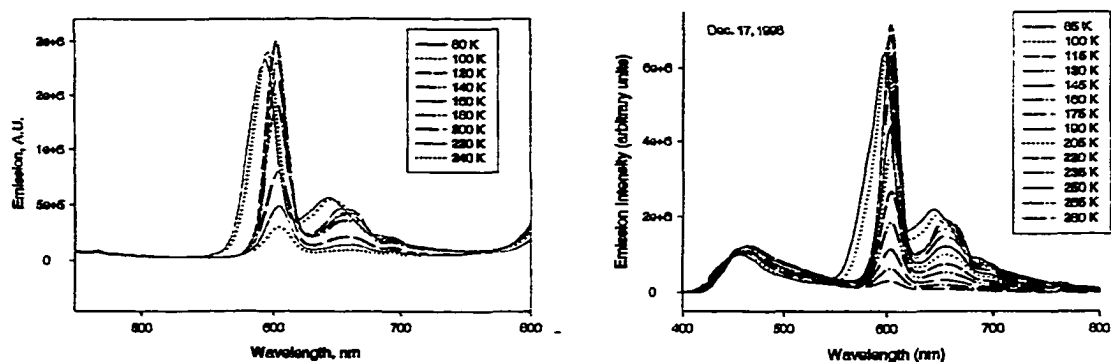
Figure 4-19. Variable temperature emission spectra of **4-27** (right side) and **4-28** (left side). In both cases, 420 nm excitation light was used.

Transient Absorption

The transient absorption spectrum of the macrocyclic squares in methylene chloride was recorded and is depicted in Figure 4-20. Generally, first order decays were observed for all spectral features. The spectrum is very similar to other metal containing phenylene-ethynylene complexes that our group has studied with a ground state bleach around 400 nm and a broad absorption band with a maximum around 680 nm. Bleaching is observed because there is a depopulation of the ground state absorption band in that region. Excited state lifetimes obtained through factor analysis and global decay fitting are listed in Table 4-1. Equivalent first order decays were observed for all features of

each transient absorption spectrum. The lifetimes do not exactly match those of obtained

via emission lifetime, which is due to problems in degassing the solution. The lifetime

obtained for the amine square **4-28** is somewhat shorter than that of **4-27**. This is likely

due to the amine lone pairs quenching the excited state.
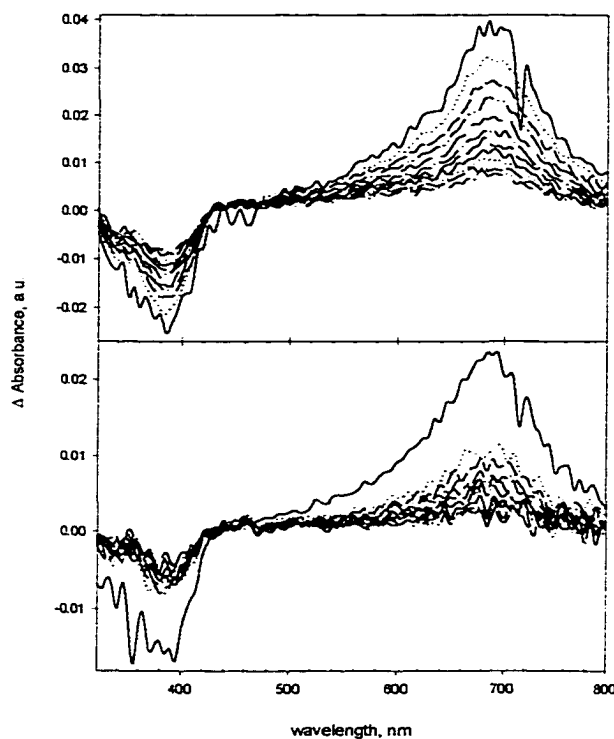
Figure 4-20. Transient absorption spectrum of squares in argon degassed methylene chloride(top, C7 square **4-27**; bottom, Amino square **4-28**). Transients are 80 ns after the laser excitation

Possible Application

In order to demonstrate an application of these macrocycles to show their

usefulness in sensing, the C7-substituted square **4-27** was tested with help from Joanne

Bedlek-Anslow to determine the oxygen sensing properties. The square was dissolved in

methylene chloride along with BMIM (butylmethyl-isobutylmethyl methacrylate)

polymer so that there was 0.5 % by weight square **4-27** with respect to the polymer

support. The solution was sprayed onto a glass plate (Figure 4-21) and allowed to cure.

The glass plate was then placed in a system designed to allow the plate to be exposed to

different pressures of air. The emission intensity was then tested at various air pressures

and a Stern-Volmer plot of the results is depicted in Figure 4-22. It can be seen that the

system studied is quite sensitive to air pressure. In fact, it is more sensitive than platinum

tetraphenylporphyrin which to date has been shown to be the most sensitive compound in

this same polymer support.
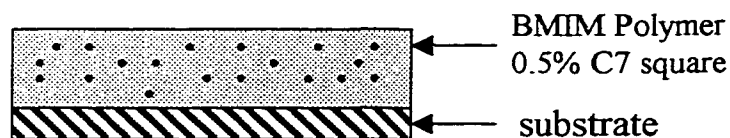
Figure 4-21. Polymer support containing 0.5% C7 square on glass plate
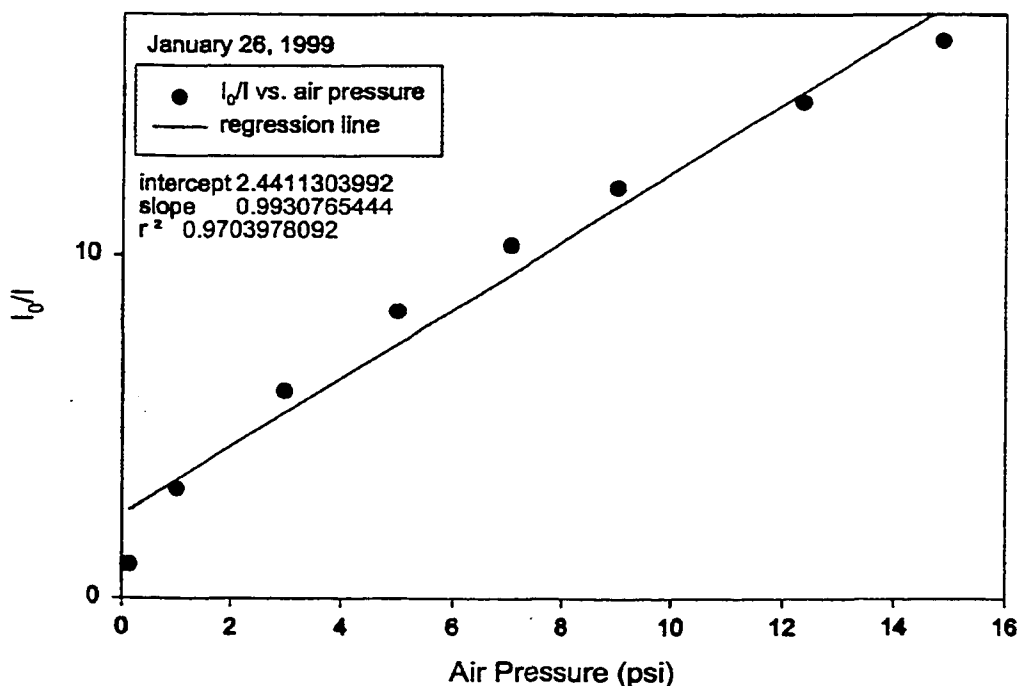
Figure 4-22. Stern-Volmer Plot illustrating oxygen sensing

Conclusion

Two highly luminescent molecular squares have been synthesized and the photophysics of each have been examined. A proposed simplified Jablonski diagram may help to understand all the data presented (Figure 4-23). For the simple non-ligated sides, the lowest energy absorption is to the $^1\pi,\pi^*$ state. Since intersystem crossing is generally forbidden for organic molecules of this type, this is the emissive state. For the squares, however, the lowest energy absorption is to the ^{1}MLCT state. This state can intersystem cross to the ^{3}MLCT state as is the case for (t-bbpy)Pt(C≡Ctol)$_2$, and at this state there must be strong orbital overlap with the $^3\pi,\pi^*$ state and thus the electron can move to the $^3\pi,\pi^*$, which can then emit a photon as it returns to the ground state. The idea that there is very good orbital overlap between the ^{3}MLCT state and the $^3\pi,\pi^*$ state is the only way to explain why there is no emission evident from the ^{3}MLCT.
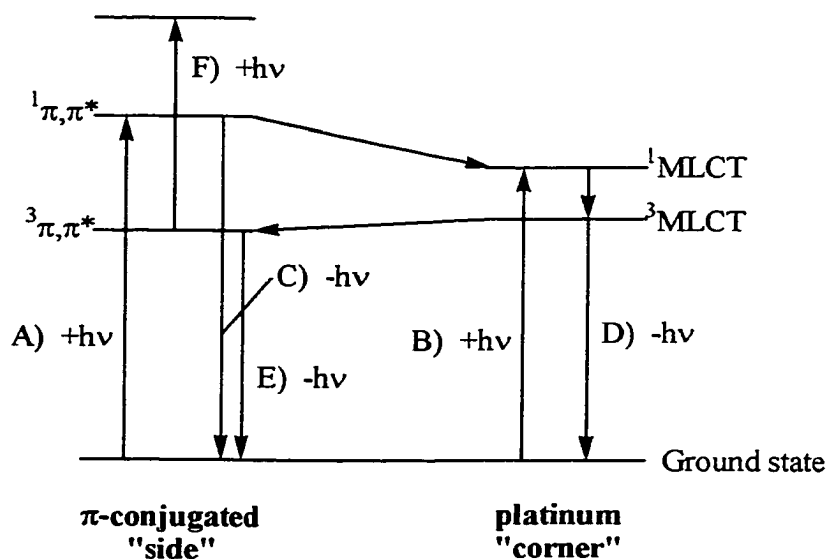
Figure 4-23. Jablonski Diagram. A) Absorption by the side ligand; B) Absorption into the ^{1}MLCT state; C) Emission from the side $^1\pi,\pi^*$ state; D) Emission from the 3MLCT state; E) Emission from the $^3\pi,\pi^*$ state; F) Absorption observed in TA.

Experimental

Photophysical Measurements

All sample solutions were studied in either methylene chloride or 2-methyl-

tetrahydrofuran. All solvents were distilled according to typical practices. All

photophysical studies were conducted with the same instrumentation and techniques

described in Chapter 3.

Synthesis

In addition to the synthesis shown in Figure 4-12, the synthesis of the sides of the

amino square **4-28** and "trimer" is shown in Figure 4-24.

Figure 4-24. Synthesis other substituted sides.

137

2,5-diiodo-1,4-dimethoxybenzene (4-20). 1,4-Dimethoxybenzene (6 g, 43.48 mmol) was dissolved in 150 mL of acetic acid, 10 mL of H_2SO_4, and 2 mL of water in a 500 mL round bottom flask equipped with a condenser. Iodine (25 g, 98.43 mmol) was added to the solution followed by 15 grams of potassium iodate (15 g, 65.22 mmol) and the mixture was allowed to reflux overnight. The reaction mixture was allowed to cool to room temperature and 200 mL of water was then added. Solid sodium thiosulfate was then added slowly with stirring until the iodine color disappeared. The water was then extracted 3 times with diethyl ether. The ether extract was dried over magnesium sulfate and removed in vacuo yielding a dark yellow viscous oil. The oil was chromatographed (silica, hexane as eluent). Spectra match those of the literature.

2,5-diiodohydroquinone (4-21). For complete synthesis see reference 76. Spectra match those of literature.

1,4-diheptyloxybenzene (4-22). Hydroquinone (7 g, 62.5 mmol) was placed in a round bottom flask and dissolved in 15 mL of freshly distilled DMF. Crushed solid KOH (4.2 g, 75.0 mmol) was then added to the solution. The mixture was then allowed to stir for 20 minutes, after which time, 4 equivalents of 1-bromoheptane (45 g, 250 mmol)was added. The reaction mixture was heated to reflux and allowed to stir for 4 hours. The reaction mixture was then allowed to cool to room temperature, dissolved in methylene chloride, washed 3 times with water and then dried over sodium sulfate. The solvent was removed yielding a yellow solid that was recrystallized from methanol yielding white crystals. Spectra match those of the literature

2,5-diiodo-1,4-diheptyloxybenzene (4-23). Method 1: Same method as used for **4-22**, substituting 2,5-diiodohydroquinone for hydroquinone. Method 2: Same method as used for **4-20** substituting 1,4-heptyloxybenzene for 1,4-dimethoxybenzene. Spectra match those of the literature.

(4-30). The same procedure was used as for **4-23** substituting N,N-diethylamino-bromoethane for bromoheptane. ^{1}H NMR (CD$_3$Cl, 300 MHz) δ 7.21 (s, 2H), 4.01 (t, 4H), 2.92 (t, 4H), 2.63 (q, 8H), 1.16 (t, 12H); ^{13}C NMR (CD$_3$Cl, 300 MHz) δ 152.47, 144.79, 138.52, 68.57, 48.75, 47.67, 25.84 ppm.

(4-32). The same procedure was used as for **4-23** substituting bromopropane for bromoheptane. ^{1}H NMR (CD$_3$Cl, 300 MHz) δ 7.08 (s, 2H), 3.98 (t, 4H), 1.82 (m, 4H), 1.12 (t, 6H); ^{13}C NMR (CD$_3$Cl, 300 MHz) δ 154.23, 146.52, 123.84, 67.84, 32.68, 16.79 ppm.

(4-24a). 4,4'-Diiodobiphenyl (5g, 0.123 mmol) was placed in a Schlenk flask and dissolved in 4:1 THF/(i-Pr)$_2$NH. 6 mole percent of Pd(PPh$_3$)$_2$Cl$_2$ (518 mg, 0.74 mmol) and 12 mole percent of copper iodide (280 mg, 1.4 mmol) were then added to the solution, which was then argon, degassed for 30 minutes. After this time, 1 equivalent of trimethylsilylacetylene (1.205 g, 12.3 mmol) was added to the rapidly stirred solution via syringe. Shortly after this addition, large amounts of precipitate formed. The solution was then heated on an oil bath at 70°C for 3 hours. Then, 1.2 equivalents of propynol (0.826 g, 14.76 mmol) were then added to the solution. Upon this addition, the solution turned black. The mixture was allowed to stir overnight at 70°C. The mixture was allowed to cool to room temperature, dissolved in methylene chloride, and then extracted twice each with 10% NH$_4$OH, then 10% HCl, and finally water. The organic phase was

dried over magnesium sulfate and evaporated to dryness. The solid was then purified via column chromatography (1:1 hexane/methylene chloride) giving the desired product in 28% yield as a pale yellow solid. ^{1}H NMR (CD$_3$Cl, 300 MHz) δ 7.52(m, 8H), 4.51 (d, 2H), 1.67 (t, 1H), 0.22 (s, 9H). All other spectra match the literature data.

(4-24b). 4-24a (2 g, 65.8 mmol) was dissolved in the minimum amount of THF, the 30 mL of methanol and 1 mL of water was added. Next, 10 equivalents of crushed KOH (36.8 g, 658 mmol) was added and the solution was allowed to stir at room temperature for 5 hours. The solution was then evaporated to dryness, dissolved in 100 mL of methylene chloride, and extracted with 5% HCl followed by extraction with water. The organic layer was dried over magnesium sulfate and the solvent removed yielding 1.2 grams of the desired product as a pale yellow solid that was used without further purification. ^{1}H NMR (CD$_3$Cl, 300 MHz) δ 7.56 (m, 8H), 4.51 (d, 2H), 3.18 (s, 1H), 1.71 (t, 1H). All other spectra match the literature data.

(4-24c). 4-24a (2 g, 65.8 mmol) was placed in a round bottom flask and dissolved in 50 mL of freshly distilled methylene chloride. To this solution was added 15 equivalents of crushed solid potassium hydroxide (55.2 g, 987 mmol) and 30 equivalents of MnO$_2$ (303.99 g, 1974 mmol). The mixture was argon degassed and allowed to stir at room temperature until it was determined by thin layer chromatography (TLC, Silica, MeCl$_2$) that the starting material was consumed (ca. 4 hours). The mixture was then passed through a bed of celite, evaporated to dryness and then purified by column chromatography (silica gel, 1:1 hexane/ether). ^{1}H NMR (CD$_3$Cl, 300 MHz) δ 7.57 (m, 8H), 3.17 (s, 1H), 0.23 (s, 9H). All spectra match the literature data.

(4-25a). To a Schlenk flask was added **4-23** (0.9 g, 1.607 mmol) and 4-17b (2.2

eq, 0.777 g, 3.53 mmol) followed by 50 mL of 3:1 freshly distilled THF/(i-Pr)$_2$NH. The

flask was sealed with a septum and argon degassed for 30 minutes. With the argon

needle still in the flask, the septum was removed and 6 mole percent of Pd(PPh$_3$)$_2$Cl$_2$

(67.6 mg, 0.096 mmol)and 12 mole percent of copper iodide (36.6 mg, 0.193 mmol) were

then added to the solution and the septum was replaced and then allowed to degas 15

minutes more. The solution darkened and precipitate fell out of solution. The reaction

was heated to 70°C and stirred overnight at that temperature. The solution was allowed

to cool to room temperature, transferred to a seperatory funnel using methylene chloride

to wash out the flask. The mixture was washed two times each with 10% NH$_4$OH, 10%

HCl, and water. Then the organic phase was dried over magnesium sulfate and the

solvent was removed. The crude material was purified by column chromatography

(silica, 1:1 ether/hexane). ^{1}H NMR (CD$_3$Cl, 300 MHz) δ 7.43 (m, 16H), 7.12 (s, 2H),

4.55 (d, 4H), 4.01 (t, 4H), 1.82 (t, 2H), 1.69 (t, 2H), 1.56 (m, 4H), 1.41-1.20 (m, 12H),

0.82 (t, 6H); ^{13}C NMR (CD$_3$Cl, 300 MHz) δ 151.87, 151.06, 139.15, 133.43, 131.13,

126.82, 126.76, 121.45, 121.28, 115.86, 114.89, 104.78, 94.23, 93.91, 84.25, 65.97,

64.75, 29.34, 29.10, 28.72, 26.03, 22.67, 14.13 ppm.

(4-25b). **4-25a** (1 g, 1.416 mmol) was placed in a round bottom flask and

dissolved in 50 mL of freshly distilled methylene chloride. To this solution was added 15

equivalents of crushed solid potassium hydroxide (1.19 g, 21.2 mmol) and 30 equivalents

of MnO$_2$ (8.49 g, 43.8 mmol). The mixture was argon degassed and allowed to stir at

room temperature until it was determined by thin layer chromatography (TLC, Silica,

MeCl$_2$) that the starting material was consumed (ca. 4 hours). The mixture was then

passed through a bed of celite, evaporated to dryness and then purified by column

chromatography (silica gel, MeCl$_2$). ^{1}H NMR (CD$_3$Cl, 300 MHz) δ 7.60 (m, 16H), 7.02

(s, 2H), 4.05 (t, 4H), 3.17 (s, 2H), 1.84 (m, 4H), 1.57 (m, 4H), 1.46-1.20 (m, 12H), 0.87 (t,

6H); ^{13}C NMR (CD$_3$Cl, 300 MHz) δ 151.87, 151.06, 139.15, 133.43, 131.13, 126.82,

126.77, 121.55, 121.25, 115.85, 114.99, 104.78, 94.23, 93.91, 84.25, 65.97, 29.34, 29.10,

28.72, 26.03, 22.67, 14.13 ppm.

(4-31a). The same procedure was used as for the synthesis of 4-25a except for

coupling 4-30 with 2 equivalents of 4-24c. ^{1}H NMR (CD$_3$Cl, 300 MHz) δ 7.59 (m, 16H),

7.02 (s, 2H), 4.17 (t, 4H), 2.99 (t, 4H), 2.68 (q, 8H), 1.08 (t, 12H), 0.22 (s, 18H); ^{13}C

NMR (CD$_3$Cl, 300 MHz) δ 153.99, 153.08, 140.17, 132.42, 132.10, 126.91, 126.67,

122.53, 122.32, 116.81, 113.88, 104.8, 95.22, 94.91, 86.83, 69.49, 42.71, 43.11, 31.86

ppm.

(4-31b). 4-31a (2 g, 2.34 mmol) was dissolved in the minimum amount of THF

(~ 10 mL), then 30 mL of methanol and 1 mL of water was added. Next, 10 equivalents

of crushed solid KOH (1.31 g, 23.4 mmol) was added and the solution was allowed to stir

at room temperature for 5 hours. The solution was then evaporated to dryness, dissolved

in 100 mL of methylene chloride, and extracted with 5 % HCl followed by extraction

with water. The organic layer was dried over magnesium sulfate and the solvent

removed yielding 1.2 grams of the desired product as a pale yellow solid. The crude

material was purified by column chromatography (silica, 3:1 ether/hexane). ^{1}H NMR

(CD$_3$Cl, 300 MHz) δ 7.59 (m, 16H), 7.03 (s, 2H), 4.18 (t, 4H), 3.17 (s, 2H), 2.99 (t, 4H),

2.68 (q, 8H), 1.08 (t, 12H); ^{13}C NMR (CD$_3$Cl, 300 MHz) δ 153.89, 153.06, 140.15,

132.43, 132.03, 126.82, 126.67, 122.53, 122.35, 116.85, 113.92, 104.8, 95.22, 94.91, 86.83, 69.57, 42.71, 43.03, 31.85 ppm.

(4-33a). The same procedure was used as for 4-25a coupling 4-32 with 2 equivalents of trimethylsilylacetylene. ^{1}H NMR (CD$_3$Cl, 300 MHz) δ 6.89 (s, 2H), 3.89 (t, 4H), 1.81 (m, 4H), 1.02 (t, 6H), 0.22 (s, 18H); ^{13}C NMR (CD$_3$Cl, 300 MHz) δ 141.18, 132.97, 123.91, 98.72, 90.87, 69.10, 28.85, 14.23 ppm.

(4-33b). The same procedure was used as for 4-25b. ^{1}H NMR (CD$_3$Cl, 300 MHz) δ 6.94 (s, 2H), 3.92 (t, 4H), 3.34 (s,2H), 1.82 (m, 4H), 1.02 (t, 6H); ^{13}C NMR (CD$_3$Cl, 300 MHz) δ 141.15, 133.48, 123.81, 104.8, 86.83, 68.79, 31.85, 14.14 ppm

Square Synthesis

(4-27) C7 square. Compound 4-25b (75 mg, 0.106 mmol) was placed into a round bottom flask and dissolved in 100 mL of CH$_2$Cl$_2$ and 5 mL of (i-Pr)$_2$NH. To this solution was added (t-bbpy)PtCl$_2$ (56.7 mg, 0.106 mmol). Once fully dissolved, the solution was argon degassed for 45 minutes. Next, with argon still streaming over the solution, CuI (1 mg, 0.005 mmol) was added. The solution was allowed to argon degas for 30 minutes more, during which time the solution changed from bright yellow to slightly orange-yellow. The vessel was then sealed with a septum and the solution was allowed to stir at room temperature for 6 days. Visual monitoring of the flask showed solids forming along the sides of the round bottom. The solution was then filtered and evaporated to a point where precipitates began to fall out of solution (ca. 15 mL, complete evaporation results in a completely insoluble solid material). Precipitation was induced by adding the solution drop wise to rapidly stirred beaker of hexane. The precipitate was recovered through centrifugation of the mixture followed by decanting off

the solvents. The precipitate was then dissolved in CH_2Cl_2 and purified by column chromatography (neutral alumina, CH_2Cl_2) where two yellow colored fractions were eluted off the column (product in the second colored fraction). Again, the second fraction was evaporated until precipitates began to appear (ca. 10 mL). Precipitation was then induced by adding the solution drop wise to rapidly stirred beaker of hexane (75 mL). The precipitate was collected by centrifugation of the hexane mixture followed by decanting off the solvents affording the product as a yellow/tan colored solid; yield 26 mg (21%). ^{1}H NMR (CD_3Cl, 300 MHz) δ 9.78 (d, 8H), 7.98 (s, 8H), 7.61 (m, 72H), 7.02 (s, 8H), 4.03 (t, 16H), 1.82 (m, 16H), 1.65-1.21 (m, 64H), 0.82 (t, 24H).

(4-28) Amino square. Synthesis of **4-28** followed the identical preparation as for **4-27**, coupling **4-31b** (75 mg, 0.105 mmol) and (tbbpy)$PtCl_2$ (56.5 mg, 0.105 mmol) and afforded the product as a brown/yellow solid; yield 32 mg (26%). ^{1}H NMR (CD_3Cl, 300 MHz) δ 9.78 (d, 8 H), 7.98 (s, 8H), 7.59 (m, 72H), 7.02 (s, 8H), 4.15 (t, 16H), 2.99 (t, 16H), 2.69 (q, 32H), 0.84 (t, 48H).

(4-29) C-18 square. Synthesis of **4-29** followed the identical preparation as for **4-27**, coupling the C-18 side (150 mg, 0.147 mmol) and (tbbpy)$PtCl_2$ (78.9 mg, 0.147 mmol) and afforded the product as a brown/yellow solid; yield 52 mg (22%). ESI: calc'd $C_{368}H_{464}N_8O_8Pt_4$: 5883.167 (M4$^+$ = 1475.87, M4$^+$ = 1967.82); found (M4$^+$) 1477.9, (M3$^+$)1970.0

CHAPTER 5
TEMPLATED MACROCYCLE SYNTHESIS AND CHARACTERIZATION

Introduction

As described in the previous chapter, macrocycles show quite interesting characteristics. Because of this, developments of methods that enhance the yield of the macrocycle need to be addressed. There have been two basic approaches to the synthesis of macrocycles. These two are the thermodynamic and the kinetic approach. High yields are typical via the thermodynamic method due to the use of the reversible reactions in the cyclizing steps that "fix" flaws in the cycle finally yielding the cyclic product of interest. Most often, the kinetic approach is used in the synthesis of macrocycles. In this approach, kinetically controlled irreversible reactions are used to construct the backbone or the pre-cycle. The yield of the final macrocycle is based on the probability of the two ends forming the final bond as opposed to forming a bond between another pre-cycle, thus forming a polymeric compound.

Thermodynamic Control

The thermodynamic control approach of forming macrocycles is relatively new and quite promising due to the high yields of the desired macrocycle. This is because the desired cyclic structure is typically the most stable and the cycle formation reaction is reversible, therefore the cycle will be formed as the major product. This concept is most often used in the formation of metallocyclic macrocycles via coordination chemistry.

Other than simple mononuclear metal containing macrocycles first developed in the

1970s, the first multinuclear metallocycle (5-1) was prepared in 1984 by Maverick and

Klavetter in 1984.[108] The use of only a cis-coordination site on the metal and linear

bridging lingands was first seen in work by Fujita in 1990 where an ethylenediamine

palladium dinitrite (acting as a corner) was reacted with 4,4'-bipyridine (acting as a side)

yielding a tetra-palladium square (5-2) in quantitative yield.[109]

5-1

8 NO$_3^-$

5-2
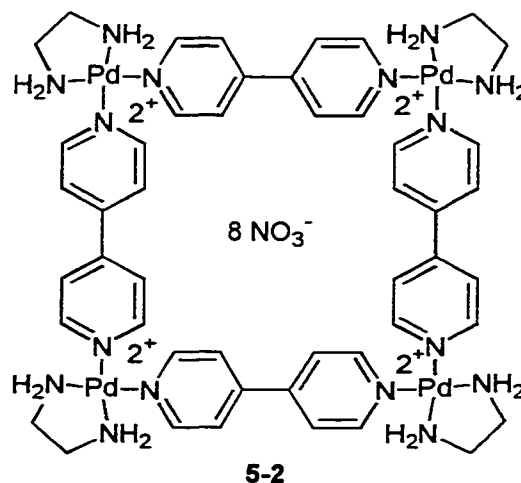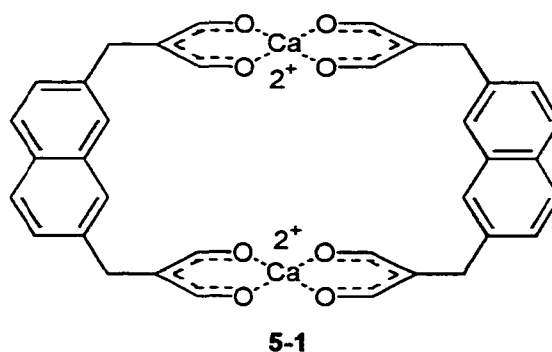
Figure 5-1. Examples of metal containing macrocycles

The use of this method can easily be envisioned to form any variety of polyhedral

macrocycles by simply reacting equal amounts of a linear linker ligand with a corner unit

that has the desired bond angle such as 90° for a square and 120° for a hexagon. The

macrocycles developed in this manner are typically stable and have been fully

characterized by all the usual methods and even, in some cases, by X-ray crystallography. The high yield can be attributed to the fact that in self-assembly processes there are a greater number of energetically favorable interactions per unit building block in the closed form as opposed to the oligomeric form therefore enthalpy favors the formation of macrocycles over the non-cyclized oligomers. Also, the macrocycle with the minimum number of subunits is favored for entropic reasons. Stang has also used this method in developing three-dimensional supramolecular assemblies such as 5-3.[110] The only problem seen with some such large macrocycles is that they often lie in equilibrium with other polygons.

5-3
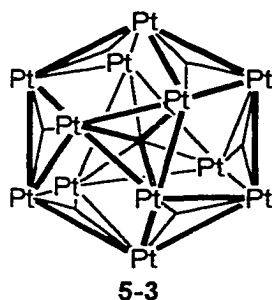
Figure 5-2. Stang's polyhedron via self-assembly

Kinetic Control

As mentioned above, kinetic control is the most used technique in making macrocycles. The kinetic approach involves connecting the building blocks of the macrocycle to a precursor of defined length, which then undergoes a ring closure reaction. In order to take a detailed look at such reactions, this section will focus mostly on phenylene-ethynyl backbones that lead to macrocycles.

The first very extreme method which involves the kinetic approach is seen in work by Staab in which a one-pot reaction was performed using the copper salt of m-iodo

phenylacetylene which was homocondensed yielding a large mixture of products, both cyclic and acyclic oligomers and polymers.[116] The oligomers and polymers were of varying lengths which, in a purely statistical reaction, is expected. The desired cyclic hexameric macrocycle was isolated in 4.6% yield by extraction of the less soluble oligomeric and polymeric material. This approach can prove to be problematic due to the low yield and fact that virtually all of the starting material is consumed especially if the starting material is costly and time consuming to make. Also, in this case, separation proved to be relatively easy, however; this may not always be the case and may even fail.
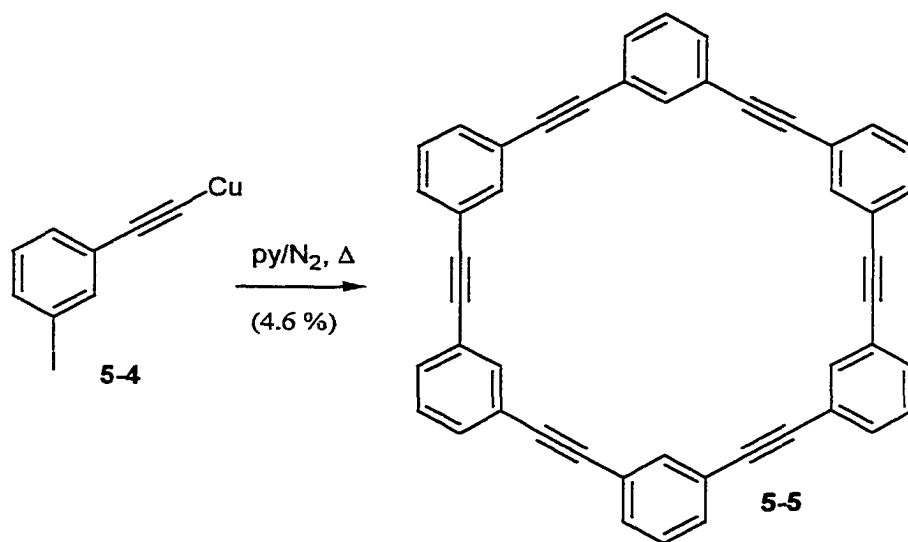
Figure 5-3. Staab's approach to macrocycle

In an attempt to increase the yield of this macrocycle, the Moore group went about the product formation in a slightly different approach.[117] Instead of performing the oligomerization and cyclization in a one-pot procedure, a multi-step synthesis that led to the oligomer **5-11** was first performed. The final cyclization step was an intramolecular palladium-catalyzed Hagihara coupling under pseudo high-dilution conditions yielding the desired macrocycle in 75% yield as the only product. This method has several

advantages over the method used by Staab. First, and most obvious is the increase in yield. Next, separation would not prove to be as difficult as it possibly could be in the Staab approach. Finally, due to the stepwise approach, it would be possible to include different monomers in a predefined location about the cycle. The main disadvantage is that the stepwise procedure can be quite time consuming.

Moore's work used pseudo high-dilution conditions in the final intramolecular cyclization step. The first use of high-dilution techniques to produce cyclic products as opposed to polymerization was seen in 1912 by Ruggli.[118] This is based on the fact that the ring-closure reaction is first order and thus the rate is proportional to the conc.
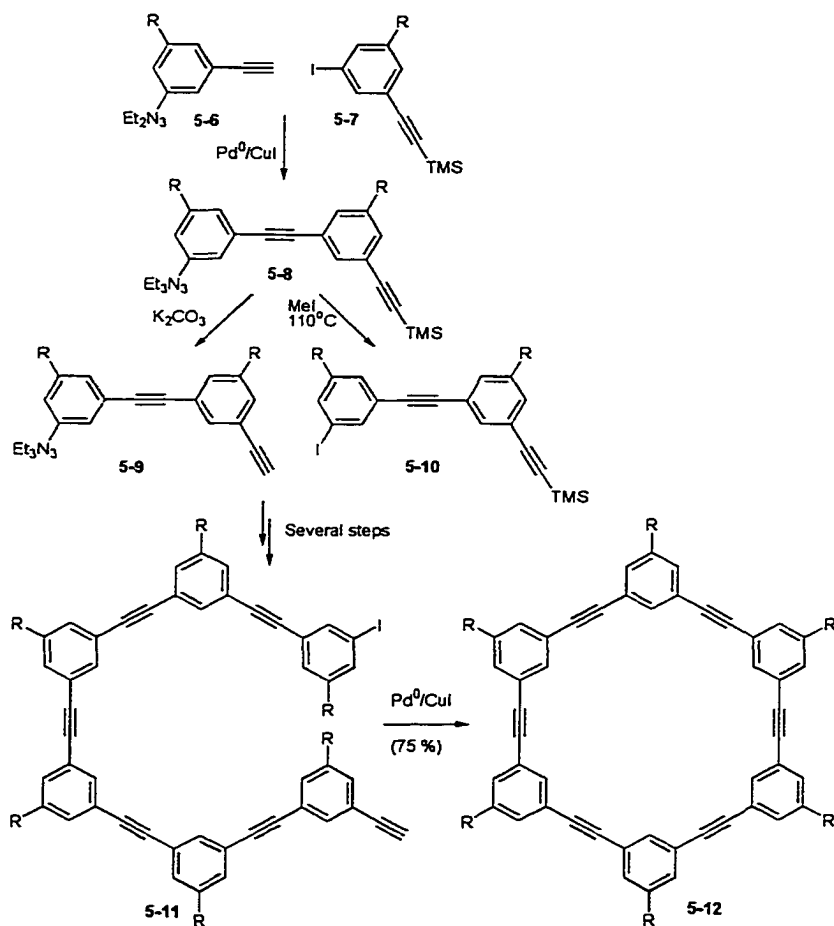
Figure 5-4. Moore's approach to macrocycle

while intermolecular condensation is second order and thus the rate is proportional to the square of the concentration. Because of this, the intramolecular ring-closure should be favored under high-dilution conditions. Typically, the reactant concentrations are less than 1 mM for high-dilution. This leads to the problem that large amounts of solvents need to be used, which is why pseudo high-dilution techniques were developed where the reactant is added to the reaction vessel at a rate that is slower than their consumption.

Cyclization from monomers and the stepwise techniques within the kinetic control approach to forming macrocycles have been employed by several groups in order to form various macrocycles as shown in Figure 5-5.[119-121] Some differences have been employed such as cyclization by coupling dimers and trimers instead of the simplest monomer as in the work Staab or the complete pre-cycle as Moore showed. The yield of macrocycle formation increases when one changes the starting material from monomer to dimer to trimer, however; the yields still do not approach that of cyclizing the pre-cycle. Thus, one is essentially left with either a poor yield from simple starting materials, or tedious and time-consuming multi-step syntheses to get to the pre-cycle to obtain high yields.

These two extremes were basically the only methods for forming macrocycles until 1990 when the Sanders group developed an ingenious method to increase the yield of cyclization.[122] When they tried to cyclize the relatively small porphyrin bisacetylene, 5-22, under oxidative conditions, a mixture of macrocycles of different sizes and oligomers were formed. However, upon performing the cyclization in the presence of the appropriate template, the yield of the desired macrocycles was increased substantially

(Figure 5-6). When the reaction was performed in the presence of 4,4'-bipyridine, the cyclic dimer was
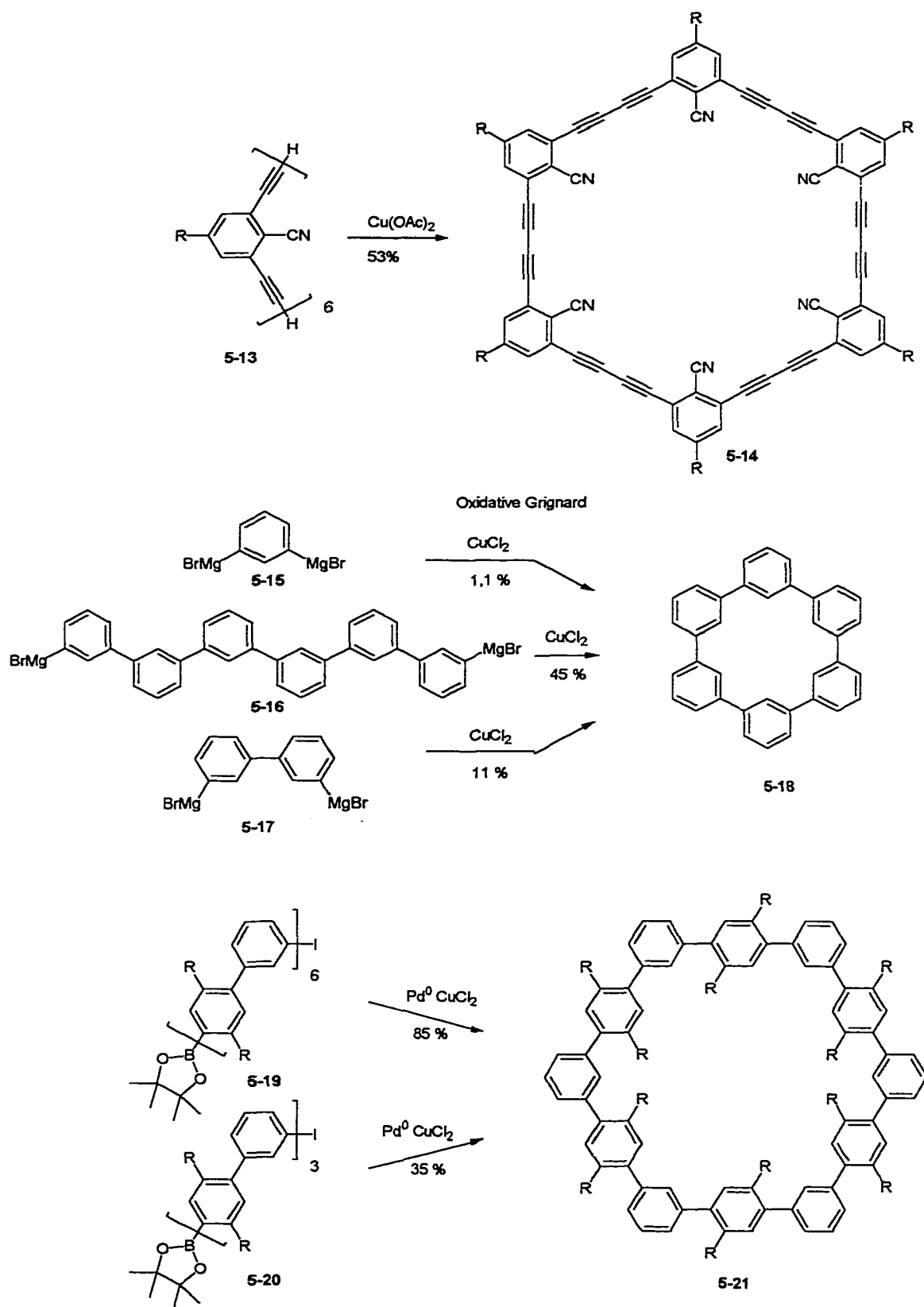
Figure 5-5. Various cyclization techniques
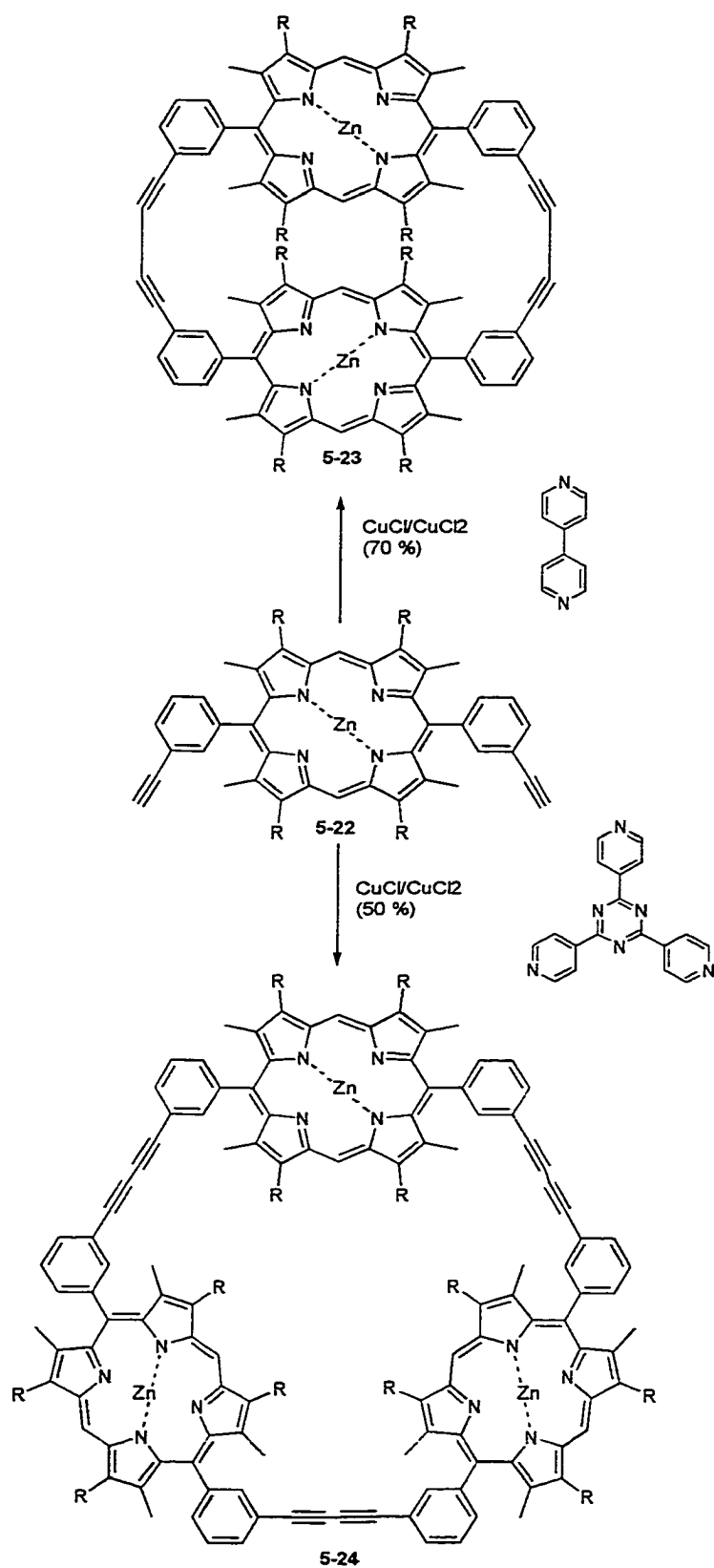
Figure 5-6. Non-covalent template method to macrocycles

formed in 70% yield. Conversely, when the reaction was performed in the presence of the terpyridyl unit the macrocyclic trimer was formed in 50% yield. The precursors are arranged around the pyridyl unit, which can be said to act as a template to hold the precursors close to one another to achieve a particular linkage.

Hoger and coworkers set out to develop a macrocyclic amphiphile with a switchable arrangement of the polar and non-polar functionalities via a Glaser coupling of bisacetylenes (Figure 5-7) under high dilution techniques and obtained yields of 60-65% (40-45% recovered).[123-125] The problem again was the time consuming repetitive synthetic approach of the half macrocycles. It was decided that making smaller building
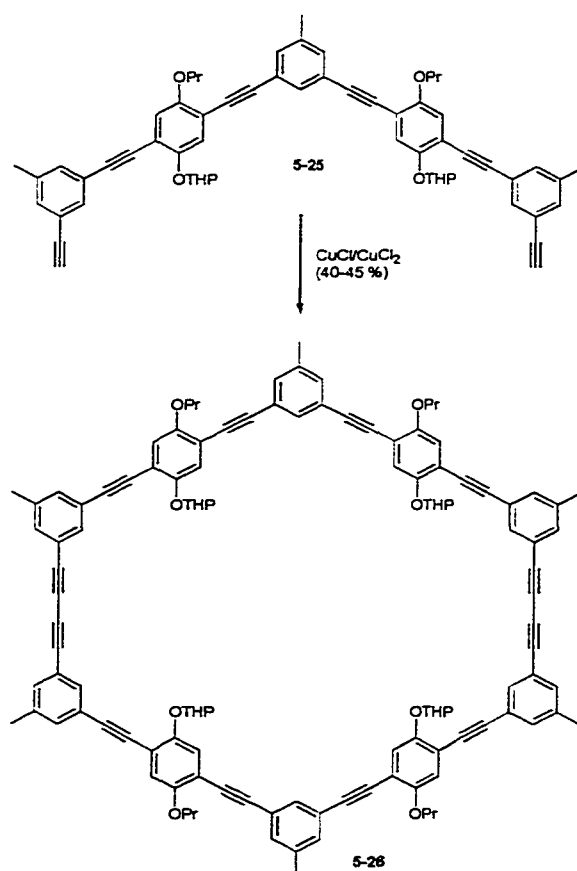
Figure 5-7. Hoger's switchable amphaphile macrocycle

154
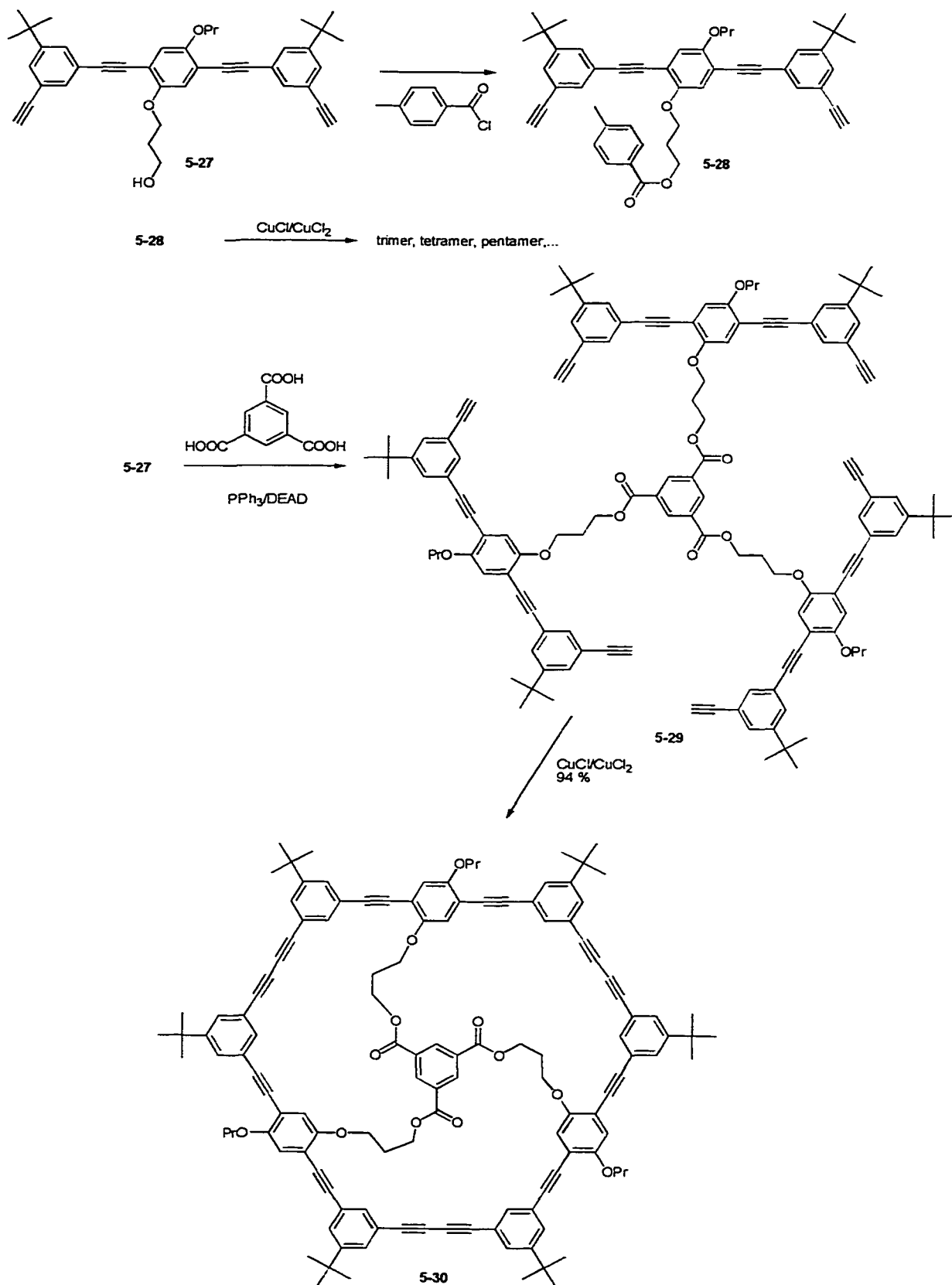
Figure 5-8. Template cyclization used by Hoger

155

blocks as discussed before would make the synthesis of the macrocycles easier and as

with other groups work this method lowered the yield of the desired macrocycle. During

this work, the polar alcohol group needs to be protected as a benzoate. An ingenious

method was then developed to increase the yield of the desired macrocycle. Instead of

protecting the alcohol with a benzoate, three of the sides were protected with trimesinic

acid prepared under Mitsunobu conditions. Cyclization of this template-bound hexa-

acetylene under Glaser conditions yielded the template-bound cyclic trimer in 95% yield.

It was assumed that the high yield was based on the fact that the tether length to the

"sides" was optimal. This was proved not to be the case when the length was extended to

eleven carbons and the yield was still 94%. Thus, the high yield is attributed to an

overall low concentration of reactive compounds and relatively high concentration of

close terminal acetylenes within the molecule.

Scope of Current Project

In the previous chapter it was found that during the formation of the tetra-

platinum macrocycle there was a large amount of insoluble oligomeric products formed.

The reaction technically falls under the thermodynamic control mechanism as defined in

introduction to this chapter. However, due to the poor reversibility of the platinum

acetylene bond formation, and the fact that as longer oligomers are formed, they become

insoluble and fall out of solution, the cyclization more closely resembles the kinetic

control mechanism discussed in the introduction. This would explain the low yield of

macrocycle product formation.

Much thought went into determining a way to "template" the reaction to increase

the yield. Finally it was decided that the method developed by Hoger would be ideal to

increase the yield of macrocycle, however, instead of a molecular square, a molecular triangle would result. This method proved to be successful and upon completion of the synthesis, full photophysical characterization of the templated macrocycle was performed.

Results and Discussion

Synthesis and Structure

The first attempt to use this templated method was carried out on a simple hexa-acetylene compound reacted with 4,4'-di-t-butyl-bypyridyl platinum dichloride, as shown in Figure 5-9. A simple reaction of 4-methoxyphenol with 3-bromopropanol followed by iodination then a Sonogashira coupling with trimethylsilylacetylene yielded the starting rod **5-34** in 82% overall yield. Reacting **5-35** under Mitsunobu conditions with benzene tricarboxylic acid yielded the templated macrocycle precursor **5-37**. Reaction of **5-37** with platinum dichloride **5-38**, yielded a product with a complex ^{1}H NMR spectrum that upon mass spectral analysis was concluded to likely be the uncyclized compound **5-39**, unfortunately not the macrocycle of interest. This result is likely attributed to the highly constrained structure that the macrocycle would need to adopt in order to form. That is, the relatively inflexible nature of the phenyl diacetylide side and the fact that geometry would predict a 60° angle at the platinum corners, which typically require 90°, explains the result.

The next attempt at forming a molecular triangle was more successful. Figure 5-10 shows a synthetic scheme for the entire process is. Again, simple reaction of 4-heptyloxyphenol with 3-bromopropanol followed by iodination and then a Sonogashira
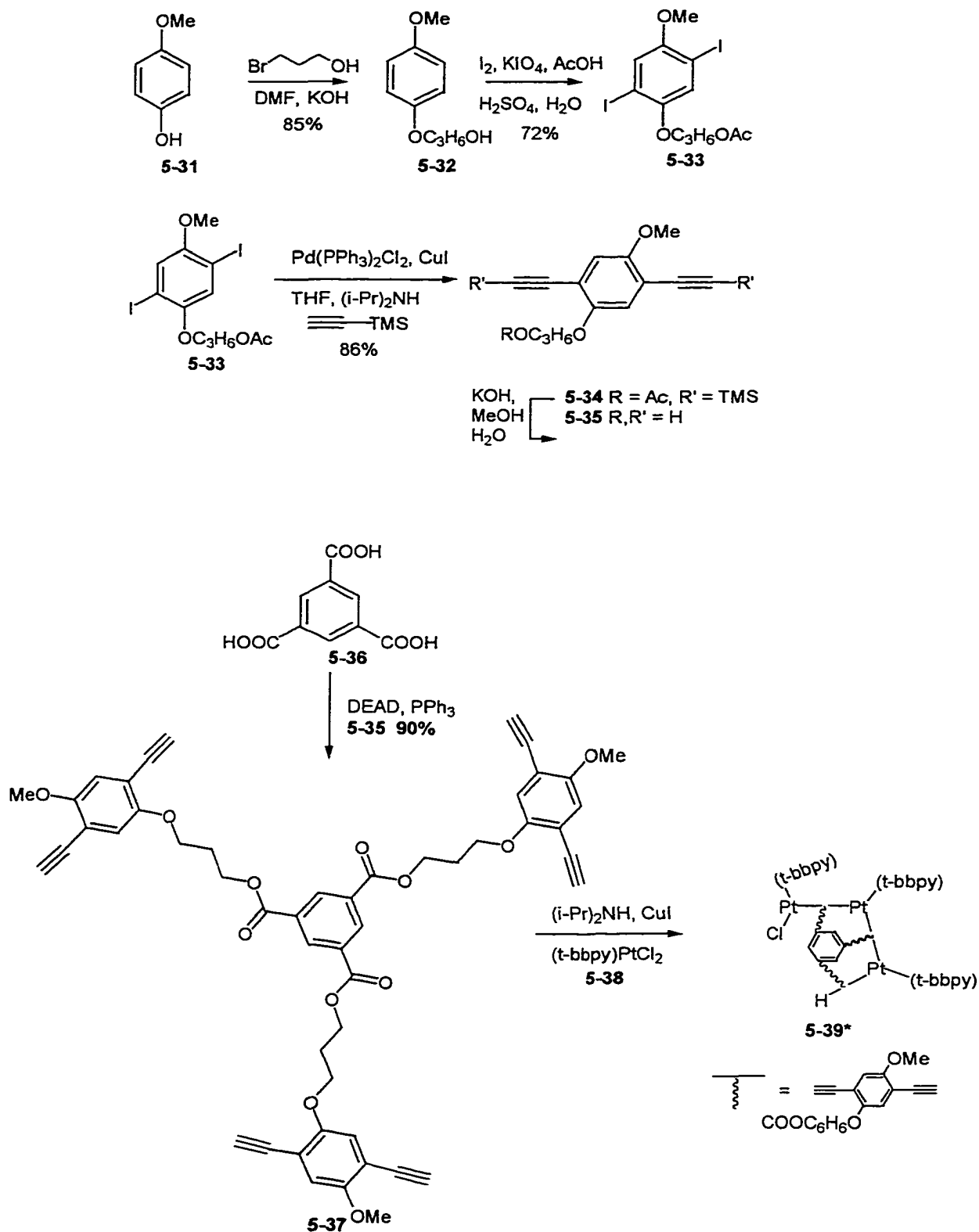
Figure 5-9. First failed synthetic attempt (* structure 5-39 is only proposed not proven).

OC$_7$H$_{15}$

OH

5-40

Br $\diagup\diagdown$ OH

DMF, KOH

91%

OC$_7$H$_{15}$

OC$_3$H$_6$OH

5-41

I$_2$, KIO$_4$, AcOH

H$_2$SO$_4$, H2O

83%

OC$_7$H$_{15}$

I

I

OC$_3$H$_6$OAc

5-42

I—Ar—I

1) Pd(PPh$_3$)$_2$Cl$_2$, CuI

2-propynol

2) ≡—TMS

R—≡—Ar—≡—TMS   28%

5-43a Ar =

5-43b Ar =

83% MnO$_2$ KOH

Ar =

5-44a R = CH$_2$OH

5-44b R = H

Ar =

5-45a R = CH$_2$OH

5-45b R = H

5-42

5-44b or 5-45b

Pd(PPh$_3$)$_2$Cl$_2$, CuI

84%

OC$_7$H$_{15}$

R—≡—Ar—≡—⟨⟩—≡—Ar—≡—R

R'OC$_3$H$_6$O

Ar =

Ar =

KOH,

88% MeOH

H$_2$O

5-46a R = TMS, R' = Ac

5-46b R, R' = H

5-47a R = TMS, R' = Ac

5-47b R, R' = H

COOH

HOOC **5-36** COOH

DEAD, PPh$_3$

5-46b, 76%

(iPr)NH$_2$, CuI

(tbbpy)PtCl$_2$

40%

(tbbpy)

Pt

Pt — Pt

5-49*

5-48

OC$_7$H$_{15}$

O

=⟨⟩=⟨⟩=⟨⟩=⟨⟩=

OC$_7$H$_{15}$

COOC$_6$H$_6$O

Figure 5-10. Successful templated macrocycle synthesis (*see Figure 5-11)
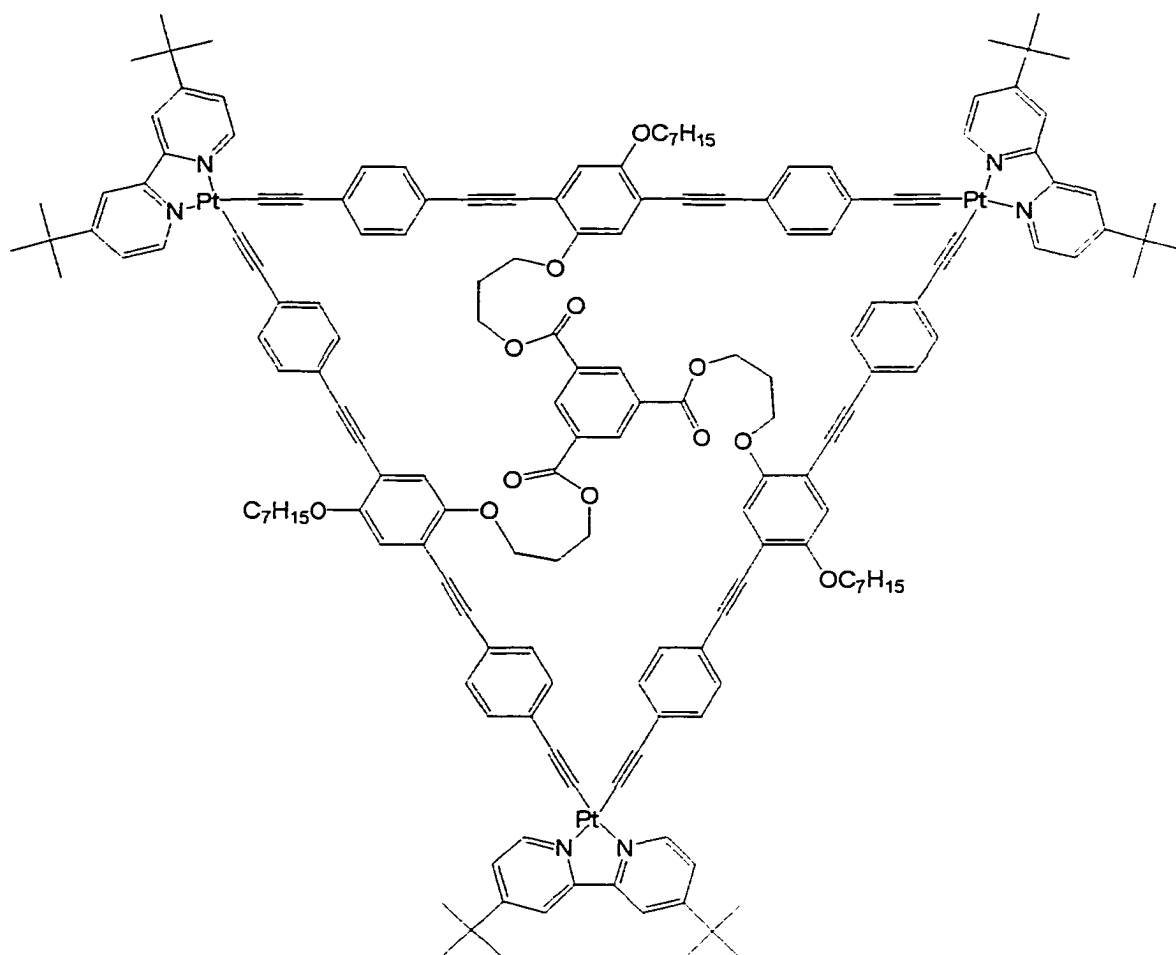
Figure 5-11. Full structure of templated triangle.

coupling with 4-(trimethylsilylethynyl)-pheynlacetylene **5-44b** yielded phenylene

ethynylene rod **5-46a**. Following deprotection and esterification under Mitsunobu

conditions, the hexa-acetylene macrocycle precursor **5-48** was formed in 67% overall

yield. The reaction of **5-48** with platinum dichloride **5-38** yielded a yellow solid product,

which had a complex ^{1}H NMR spectrum. The comparison of this spectrum with that of

the cycle obtained by Hoger (Figure 5-12) gave convincing, but not absolute evidence

that the macrocycle was indeed formed. The explanation for the complex ^{1}H NMR

spectrum is the restricted flexibility and because the asymmetric sides yields a mixture of

isomers.
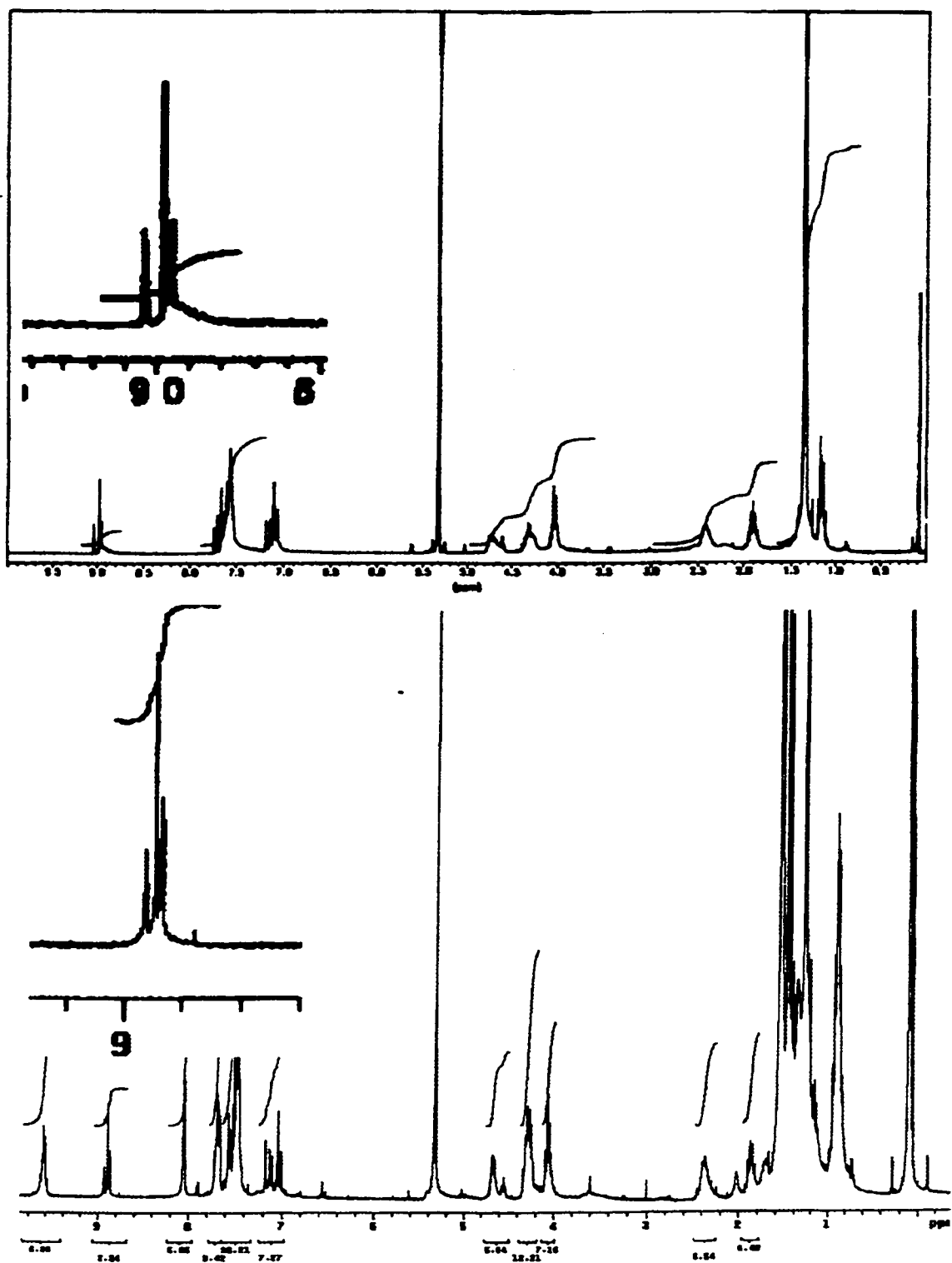
Figure 5-12. NMR of Hoger's macrocycle **5-30** (top) and macrocycle **5-49** (bottom). Inset corresponds to the signals from the three protons on central the phenyltricarboxylate.

The inset in Figure 5-12 shows the similarity between the two compounds where essentially three singlets are present with relative intensities that are very close between the two compounds. There is also great similarity between the peaks around $\delta = 6.9 - 7.4$ ppm which correspond to the protons on the central phenyl unit of the side.

Gel-permeation-chromatography (GPC) was performed on triangle complex **5-49** yielding a single peak with a short tail. Comparison to polystyrene standards revealed a molecular weight only 100 a.m.u. off the calculated molecular weight (calculated: 3082 a.m.u., obtained: 2983 a.m.u.), however; this may have just been fortuitous. Several attempts to obtain the more definitive mass spectral evidence were conducted. Finally, MALDI-TOF confirmed the molecular weight of the macrocycle and provided further evidence that the macrocycle of interest was indeed formed (spectrum and simulation Figure A-3).

The problems seen in the first attempt at forming the templated macrocycle is not a dilemma in this second case. It is known that even fairly short rigid rods are not rigid at all and have been shown to flex a great degree. Although the diethynylphenyl side of the first failed cycle can flex some, by extending the rod length by another two phenylene ethynylene units increases the flexibility dramatically. With this added flexibility, the final platinum acetylide linkage can be obtained and also come closer to reaching the 90° angle required for the square planar platinum (it is more likely between 70° and 80°).

Finally, this template method was tried with the objective of forming a "square" instead of a "triangle." The center template chosen was meso-tetracarboxyphenyl porphyrin. The synthesis followed along the same line as that use for the triangle with two small differences (Figure 5-12). It was determined through molecular mechanics

calculations that the sides used for the triangle would not be long enough in order to form the macrocycle, therefore the two outer phenylacetylenes of the side were replaced with biphenyl-acetylenes **5-47b**. With the new side **5-51** in hand, a simple esterification was performed. The Mitsunobu conditions used previously were found not to work, therefore a DCC coupling was used instead. With the pre-cycle in hand, insertion of the platinum corners was attempted. Unfortunately, this reaction yielded completely insoluble material. Again, molecular mechanics calculations showed the possible reason for this problem. Compound **5-51** was found to have the lowest conformational energy when the sides are perpendicular to the porphyrin plane (**Figure 5-13**). If this is indeed the case, the likelihood of two opposing sides coupling to the platinum is greater than that of two adjacent sides that would be required for a square to form. With this being the case, oligomerization can easily occur forming insoluble material.
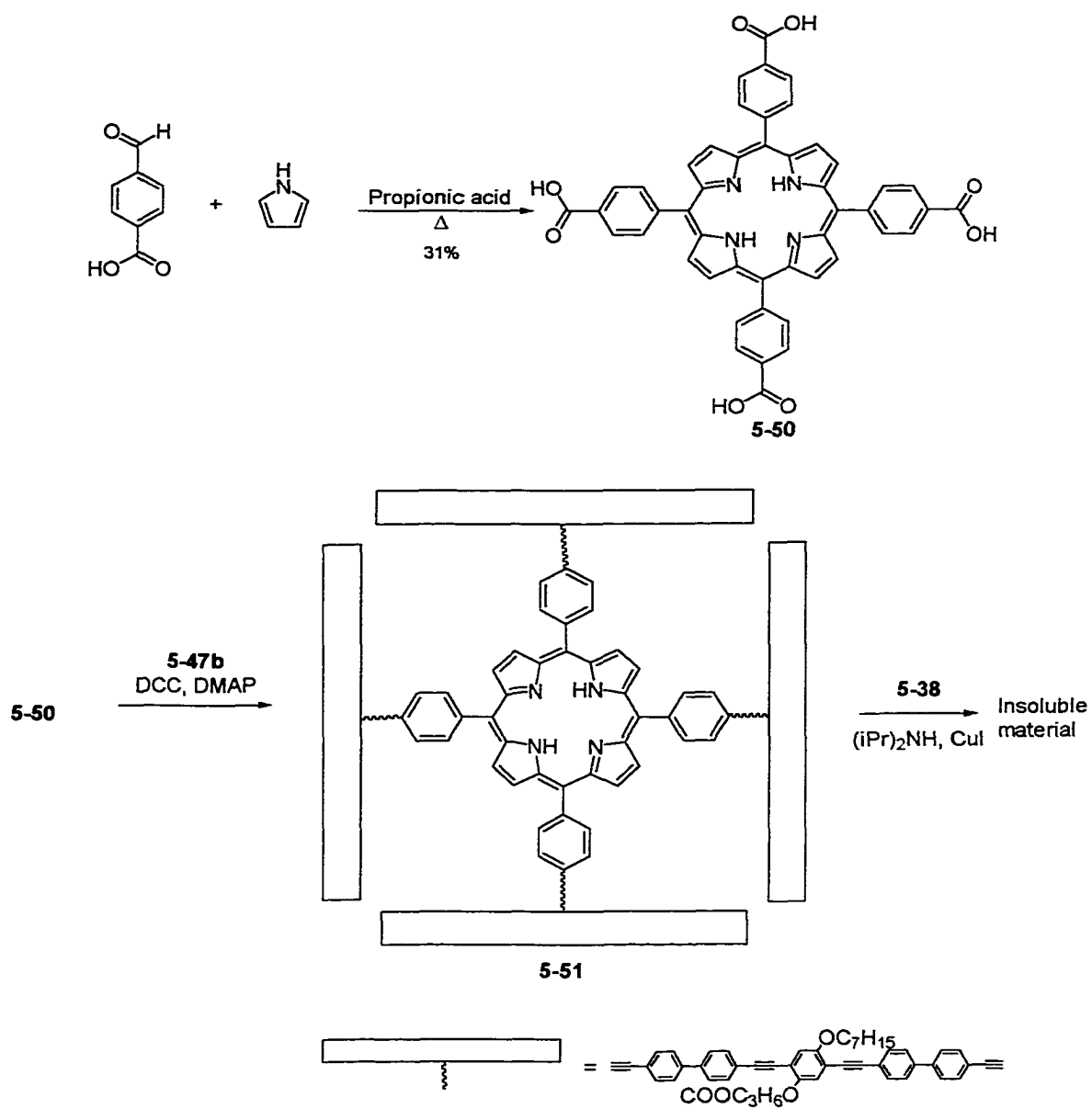
Figure 5-11. Failed templated "square" synthesis
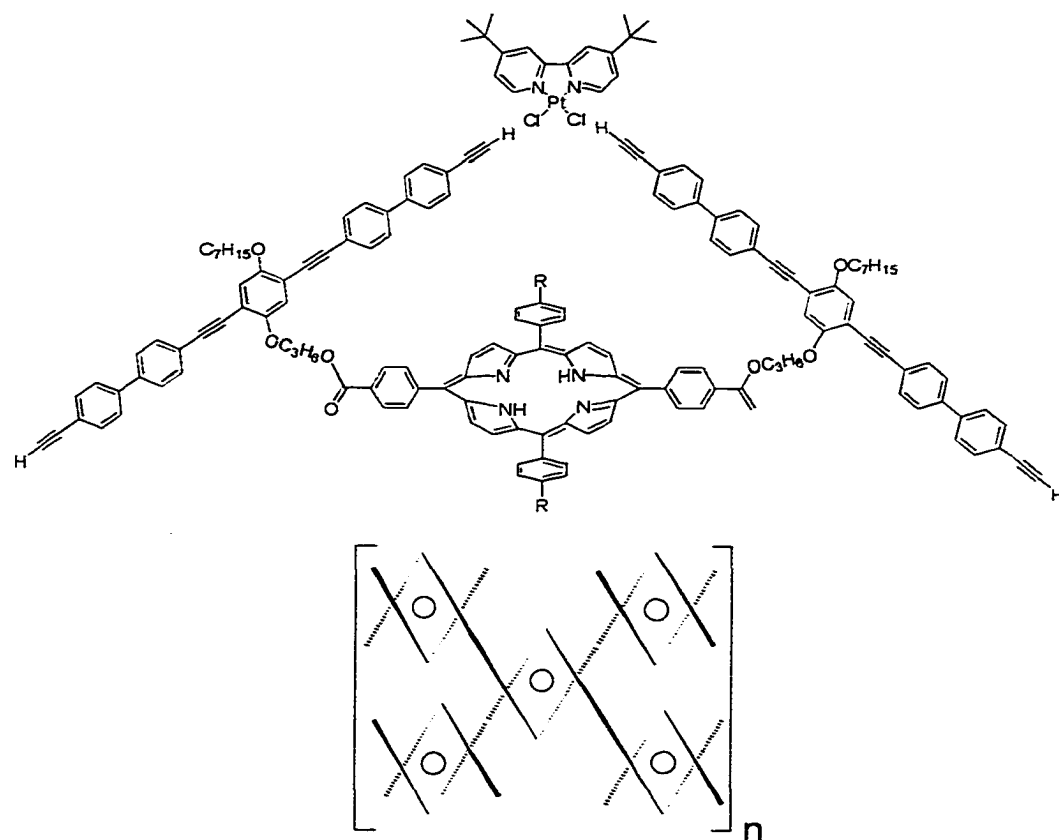
Figure 5-12. Opposing sides connecting finally yielding an insoluble polymer

Photophysical Experiments

Various photophysical experiments were carried out on triangle **5-49** and the

basic results of which are listed in Table 5-1. The detail of each experiment is described

in the following sections.

Figure 5-1: Photophysical data for templated triangle

CMPD	λ_{abs}	λ_{em}	Φ_{em}	τ_{em} (μs)	τ_{ta} (μs)	k_r (x 10^2 s^{-1})
5-49	410	591	0.113	124	106	9.11

Absorption Spectra

The absorption spectra of the macrocycle **5-49**, side **5-46b**, and the precursor **5-48**

are depicted in **Figure 5-14**. The absorption spectrum of both the side **5-46b** and the pre-

cycle **5-48** shows two strong bands at ca. 375 and 320 nm. The spectrum of macrocycle

triangle **5-49** again shows the same two strong bands, however, the extinction coefficient

is slightly larger and the lower energy band is red shifted to 382 nm. This indicates that

the conjugation is extended as predicted based on the fact that platinum has been shown

to extend π-conjugation through the metal d orbitals. There also is seen a tail that is

likely due to MLCT from the platinum to the diimine.
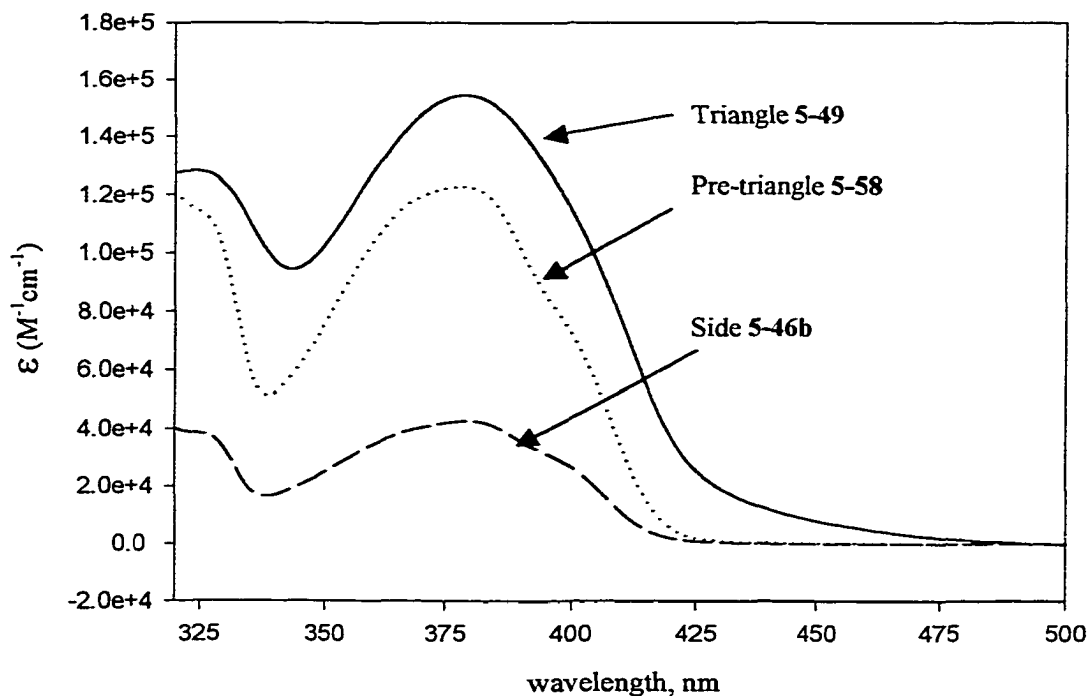
Figure 5-14. Absorption spectra in CH_2Cl_2. (—) Triangle **5-49**; (·····) Pre-triangle **5-58**; (---) Side **5-46b**.

Emission Spectra

The room temperature emission spectra of the side **5-46b**, precycle **5-48**, and the

macrocycle **5-49** are shown in Figure 5-15. Emission spectra from the side **5-46b** and

pre-cycle **4-48** are virtually identical with the exception that the pre-triangle is much

more intense (not evident by the normalized spectrum) and are very similar to work done

by Kevin Ley and Keith Walters from our group on phenylene-ethynylene systems. The

emission is attributed to emission from the $^1\pi,\pi^*$ state. Macrocycle **5-49** gives a

relatively intense, sharp, vibronically structured emission with a maximum at 594 nm and

shoulders of lesser intensity at 644 and 678 nm. Because of its structure and energy, the

emission is likely due to the $^3\pi,\pi^*$ excited state instead of the MLCT state as seen in the

platinum diimine bisacetylide spectra discussed in chapter 3. In order to obtain absolute

quantum yields, a freeze pump thaw method was used for degassing, as normal argon

degassing was difficult to reproduce due to the emission's sensitivity to oxygen. After

the degassing, the emission spectrum showed no triplet emission. The only conclusion

that could be made was that upon freezing the solution, the molecules aggregated which

has been shown to quench triplet emission through self-quenching (see thesis' of Keith

Walters and Kevin Lee). Because of this, only argon degassing could be used to

determine the quantum yield of 0.113 ± 0.004. This value is the average of four trials

that all gave very similar values however, is inherently limited and not absolute due to the

technique.
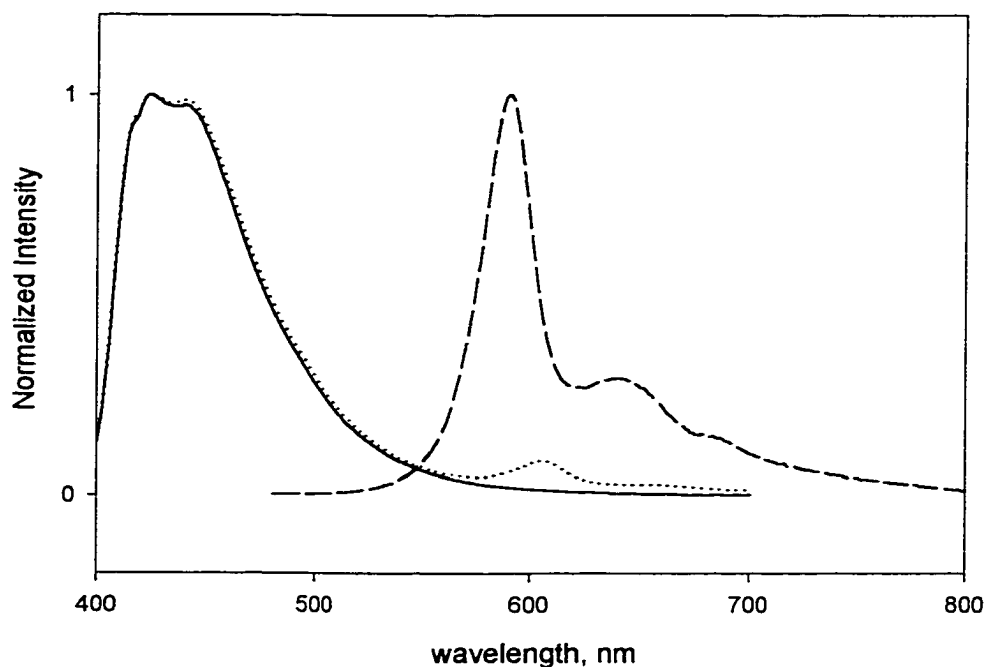
Figure 5-15. Room temperature emission of side **5-46b** (——), the pre-cycle **5-48** (⋯⋯) and triangle **5-49** (---) in CH_2Cl_2 (400, 400, and 420 excitation, respectively)

In order to investigate the assumption that aggregates form during freeze-pump-thaw degassing resulting in loss of the triplet emission, a solution of the macrocycle in 2-methyl-tetrahydrofuran was thoroughly argon degassed and a variable temperature emission study was performed. The initial results of this are shown in Figure 5-17. It can be seen that the emission greatly increases with decreasing temperature. There was also very little if any band shifting of the emission to higher or lower energies as the temperature decreases. These results were not too unexpected; however, upon warming the solution to room temperature and reacquiring the emission spectrum it is noticed that the emission was greatly decreased from the original room temperature emission on the

same solution. Subsequent freezing and warming of the solution, which mimics freeze

pump thaw degassing, further reduced the emission with respect to the original emission

spectrum (Figure 5-18). This was repeatedly seen until the emission was virtually

nonexistent. The observation that the emission decreases with repetitive freezing and

thawing cycles further supports the assumption made upon trying to determine the

absolute emission quantum yield that aggregation must be occurring. Molecular

mechanics indicate that the molecule is relatively flat and because of this, π-stacking can

easily occur as well as d-interactions between platinum centers of stacked triangles are

likely the source of the aggregation.
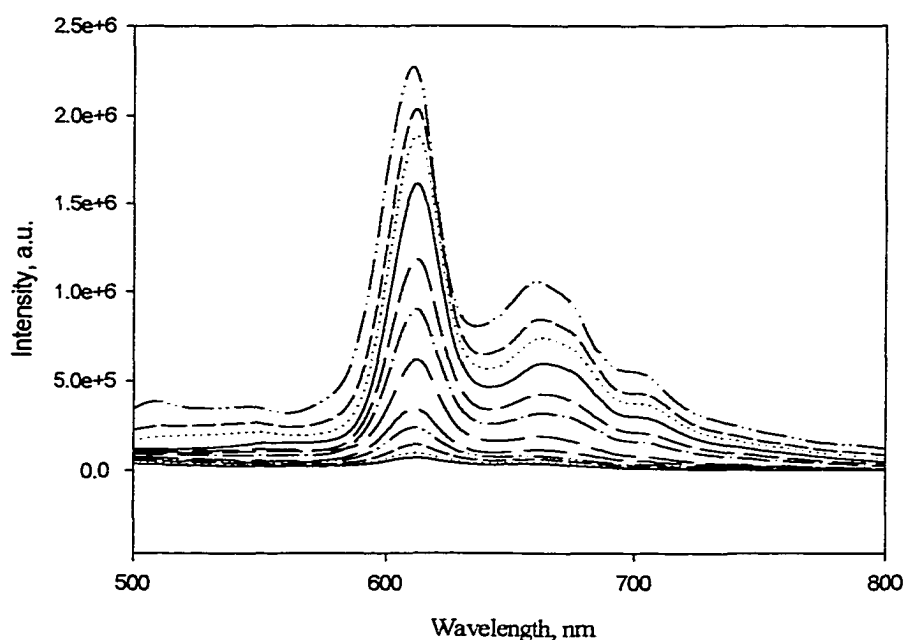
Figure 5-17. Emission spectrum of the triangle **5-49** in 2-MTHF (420 excitation) at temperatures varying from 285 to 80 K. Emission intensity decreases as temperature decreases. Spectra are in 20 K increments
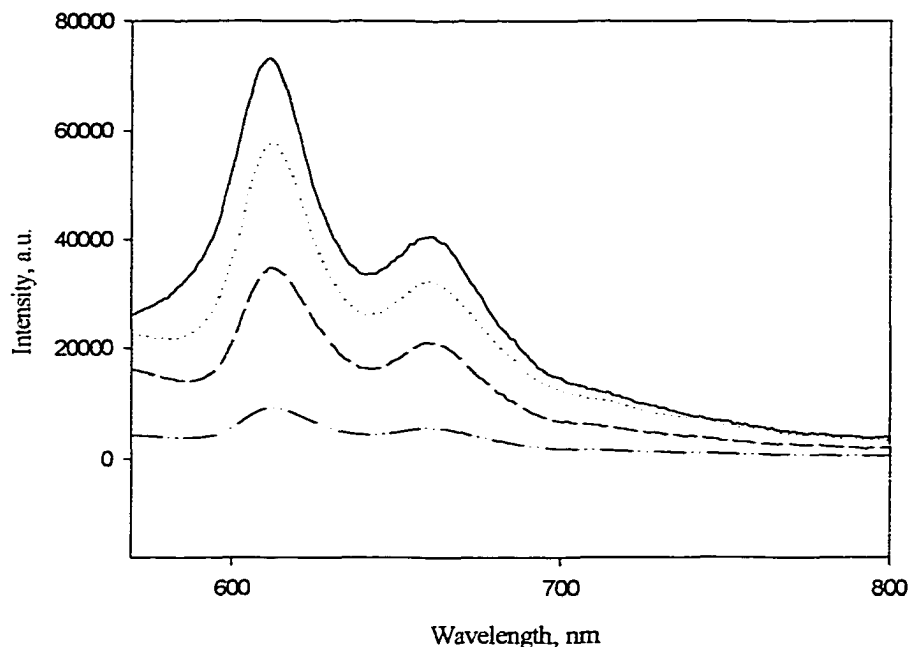
Figure 5-18. Emission spectra of triangle **5-49** in 2-MTHF (420 nm excitation), each at 285 K after repetitive freezing and thawing. Note the decrease in intensity from (——) not frozen; (·····) first freeze thaw cycle; (— — —) second freeze that cycle; (– ·· –) third freeze thaw cycle.

Transient Absorption

The transient absorption spectrum of the macrocycle **5-49** in methylene chloride was recorded and is depicted in Figure 5-19. Generally, first order decays were observed for all spectral features. The spectrum is very similar to other metal containing phenylene ethynylene complexes that our group has studied; with a ground state bleach around 400 nm and a broad absorption band with a maximum around 625 nm. As with the previous work of our group, this absorption is attributed to the same $^3\pi,\pi^*$ phosphorescent state of the phenylene-ethynylene sides.
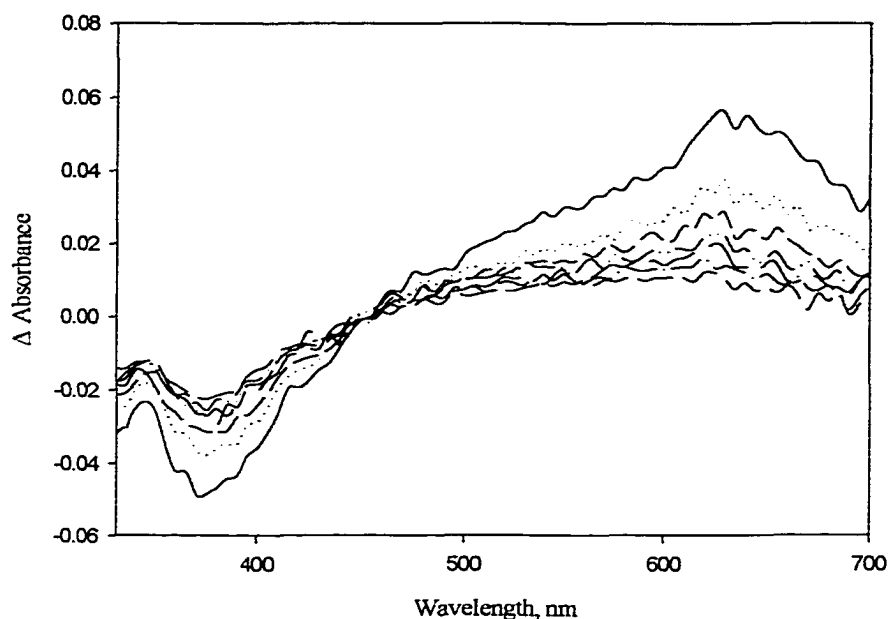
Figure 5-19. Transient absorption spectrum of the triangle **5-49** in argon degassed CH$_2$Cl$_2$ solutions. Arrows depict the spectral trend with increasing time after the laser excitation. Transients are 8000 ns increments after the laser excitation.

Conclusion

A new technique has been developed to synthesize platinum acetylide containing macrocycles of predetermined size in relatively high yields. The confirmation of the structure is based upon GPC data, MALDI-TOF and comparison of the ^{1}H NMR spectrum with that of a similar totally organic macrocycle. The successfully synthesized triangle exhibits unique photophysical behavior when compared to other platinum diimine complexes. Other platinum complexes exhibit primarily relatively weak MLCT based emission. The triangle as with the squares of the previous chapter have been shown to exhibit room temperature, long lived intense $^3\pi,\pi^*$ based emission. An interesting feature was shown where the molecules aggregate upon freezing and thawing

cycles with interactive forces strong enough to last several days if not longer which completely quenches the triplet emission.

Experimental

Photophysical Measurements

All sample solutions studied were in ether methylene chloride or 2-methyl-tetrahydrofuran. All solvents were distilled according to typical laboratory practices. All photophysical studies were conducted with the same instrumentation and techniques described in Chapter 3.

Synthesis

3-(4-heptyloxyphenoxy)-propanol (5-41). 4-Heptyloxyphenol (5 g, 24.4 mmol, Aldrich) was placed in a round bottom flask and dissolved in 10 mL of freshly distilled DMF. Solid KOH (3 g, 53.57 mmol) ground into a fine powder was then added to the solution. The mixture was then allowed to stir for 20 minutes, after which time, 3-bromopropanol (4 g, 32.26 mmol) was added and the reaction mixture was refluxed for 3 hours. The reaction mixture was then allowed to cool to room temperature, dissolved in methylene chloride, washed 3 times with water and then dried over sodium sulfate. The solvent was removed yielding an off white solid that was recrystallized from methanol affording 3-(4-heptyloxyphenoxy)-propanol as white crystals (5.9 g, 92%). ^{1}H NMR (CDCl$_3$, 300 MHz) δ 6.82 (s, 4H), 4.09 (t, 2H), 3.84 (m, 4H), 2.08 (m, 2H), 1.78 (m, 3H),

1.51-1.25 (m, 8H), 0.89 (t, 3H); ^{13}C NMR (CDCl$_3$, 300 MHz) 152.46, 151.78, 121.84, 121.81, 70.14, 67.65, 66.95, 31.74, 29.18, 28.81, 28.72, 22.69, 20.99, 14.14.

(2,5-diiodo-4-heptyloxyphenoxy)-propyl acetate (5-42). 3-(4-Heptyloxyphenoxy)-propanol (5 g, 18.8 mmol) was dissolved in a mixture of 150 mL of acetic acid, 10 mL of H$_2$SO$_4$ and 2 mL of water contained in a 500 mL round bottom flask. To the solution was added iodine (25 g, 98.43 mmol) and KIO$_3$ (15 g, 70.10 mmol) and the mixture was allowed to reflux overnight. (Caution: solid iodine crystallizes in the condenser and needs to be repeatedly scraped off with a long glass rod.) The reaction mixture was allowed to cool to room temperature whereupon 200 mL of water was then added. Solid Na$_2$S$_2$O$_4$ was then added slowly with rapid stirring until the iodine color disappears. The water was then extracted 3 times with diethyl ether. The combined ether extract was then dried over magnesium sulfate and removed in vacuo yielding a yellow solid that was recrystallized from methanol to afford (2,5-diiodo-4-heptyloxyphenoxy)-propyl acetate as a white solid, yield 8.7 g (83%). ^{1}H NMR (CDCl$_3$, 300 MHz) δ 7.21 (s, 1H), 7.18 (s, 1H), 4.36 (t, 2H), 4.05 (t, 2H), 3.95 (t, 2H), 2.17 (m, 2H), 2.07 (s, 3H), 1.81 (m, 2H), 1.49(m, 2H), 1.41-1.23(m, 6H), 0.89(t, 3H); ^{13}C NMR (CDCl$_3$, 300 MHz) δ 171.15, 153.11, 152.39, 126.71, 126.53, 122.84, 122.70, 70.32, 66.63, 62.97, 31.73, 29.09, 28.92, 28.54, 25.96, 22.57, 20.98, 14.07.

1-(4-trimethylsilylethynylphenyl)-1-propyn-3-ol (5-44a). 1,4-Diiodobenzene (5 g, 12.30 mmol) was placed in a Schlenk flask and dissolved in 4:1 THF/(i-Pr)$_2$NH. 6 mole percent of Pd(PPh$_3$)$_2$Cl$_2$ (0.522 g, 0.739 mmol) and 12 mole percent of CuI (0.281 g, 1.48 mmol) were then added to the solution that was then argon degasses for 30 minutes. After this time, 1 equivalent of trimethylsilylacetylene (1.20 g, 12.3 mmol) was

then added to the rapidly stirred solution via syringe. Shortly after this addition, large

quantities of precipitate formed. The solution was then heated on an oil bath at 80°C for

3 hours. 1.2 equivalents of 2-propynol (0.827, 14.76 mol) were then added to the

solution. Upon this addition, the solution turned almost black. The mixture was allowed

to stir overnight at 80°C. The mixture was allowed to cool to room temperature,

dissolved in methylene chloride, and then extracted twice each with 10% NH_4OH, then

10% HCl, and finally water. The organic phase was dried over magnesium sulfate and

then evaporated to dryness. The solid was then dissolved in the minimum amount of 1:1

hexane/methylene chloride and purified via column chromatography (1:1

hexane/methylene chloride) yielding the product as an off white powder, yield 0.841 g

(30%) in 30% yield. ^1H NMR ($CDCl_3$, 300 MHz) δ 7.38 (m, 4H), 4.49 (d, 2H), 1.63 (t,

1H), 0.22 (s, 9H).

(4-trimethylsilylethynylphenyl)-acetylene (5-44b). 1-(4-

Trimethylsilylethynylphenyl)-1-propyn-3-ol (1 g, 4.38 mmol) was dissolved in freshly

distilled dichloromethane. 15 equivalents of MnO_2 (5.72g, 65.7 mmol) and 5 equivalents

of crushed solid KOH (1.23 g, 21.90 mmol) was then added. The mixture was stirred

rapidly and the progress of the reaction was followed by TLC (2:1 hexane/CH_2Cl_2).

When it was determined that the reaction was complete (ca. 4 hrs), the solution was

filtered through a bed of celite. The solution was then washed 3 times with water, dried

over sodium sulfate and the solvent removed via rotary evaporation. The resulting solid

was dissolved in hexane and passed through a short silica column with hexane as the

eluent. Evaporation of the solvent yielded the product; yield 0.72 g (83 %). ^1H NMR

(CDCl₃, 300 MHz) δ 7.39 (m, 4H), 3.18 (s, 1H), 0.22 (s, 9H); ^{13}C NMR (CDCl₃, 300

MHz) δ 132.17, 132.08, 123.84, 122.36, 104.61, 96.71, 83.45, 79.21, 0.14.

(5-46a). To a Schlenk flask was added **5-42** (0.9 g, 1.61 mmol) and **5-44b** (2.2

eq, 0.7 g, 3.54 mmol) followed by 50 mL of 3:1 freshly distilled THF/(i-Pr)₂NH. The

flask was sealed with a septum and the degassed for 30 minutes with argon. With the

needle still in the flask, the septum was removed and 6 mole % of Pd(PPh)₂Cl₂ (68.3 mg,

0.0966 mmol) and 12 mole % of CuI (36.8 mg, 0.1932 mmol) was then added and the

septum replaced. The solution darkened and precipitate fell out of solution. The reaction

was heated to 70°C and stirred overnight. The solution was allowed to cool to room

temperature, transferred to a seperatory funnel using methylene chloride to wash out the

Schlenk flask. The mixture was washed two times each with 10% NH₄OH, 10% HCl,

and water, then dried over sodium sulfate. The solvent was removed on a rotary

evaporator. The crude material was purified by column chromatography (silica, 2:1

hexane/ether) affording a pale yellow solid, yield 0.94 g (84%). ^{1}H NMR (CDCl₃, 300

MHz) δ 7.45 (m, 8H), 7.01 (s, 1H), 7.00 (s, 1H), 4.34 (t, 2H), 4.12 (t, 2H), 4.02 (t, 2H),

2.17 (m, 2H), 2.05 (s, 3H), 1.85 (m, 2H), 1.53 (m, 2H), 1.42-1.32 (m, 6H), 0.88 (t, 3H),

0.257 (s, 9H), 0.255 (s, 9H); ^{13}C NMR (CDCl₃, 300 MHz) δ 171.00, 153.92, 153.10,

131.91, 131.86, 131.35, 131.31, 123.41, 123.01, 116.94, 116.86, 114.06, 113.91, 104.64

(2C), 96.36 (2C), 94.78, 94.75, 87.74, 87.57, 69.58, 66.03, 61.23, 31.81, 29.28, 29.04,

28.73, 25.99, 22.58, 20.04, 14.07, 0.09.

(5-46b). Compound **5-46a** (0.9 g, 1.29 mmol) was dissolved in the minimum

amount of THF (about 5 mL), then 30 mL of methanol and 1 mL of water was added.

Next, 10 equivalents of ground up solid KOH (0.72 g, 12.9 mmol) was added, and the

solution was allowed to stir at room temperature. The reaction was monitored by TLC (1:1 hexane/ether). When it was determined that the reaction was complete (about 4 hours), the solution was evaporated to dryness, redissolved in methylene chloride and extracted with 5% HCl followed by water. The organic layer was dried over magnesium sulfate and then evaporated to dryness. The crude material was purified by column chromatography (silica, 1:1 ether/hexane) affording the product as a pale yellow solid; yield 0.58 g (88%). ^{1}H NMR (CDCl$_3$, 300 MHz) δ 7.47 (m, 8H), 7.03 (s, 1H), 7.01 (s, 1H), 4.22 (t, 2H), 4.01 (t, 2H), 3.92 (q, 2H), 3.19 (s, 1H), 3.17 (s, 1H), 2.12 (m, 2H), 1.82 (m, 2H), 1.54 (m, 2H), 1.42-1.22 (m, 6H), 0.87 (t, 3H); ^{13}C NMR (CDCl$_3$, 300 MHz) δ 154.18, 153.17, 134.74, 132.26, 132.23, 131.62, 131.59, 123.99, 123.80, 116.94, 114.23, 114.04, 94.82 (2C), 88.00, 87.80, 83.46 (2C), 79.24 (2C), 76.32, 69.69, 66.13, 62.84, 32.02, 29.49, 29.26, 28.95, 26.20, 22.79, 14.30.

(5-47a). A similar procedure was used as for molecule 5-46a. Yield 0.78 g (84%) ^{1}H NMR (CDCl$_3$, 300 MHz) δ 7.59 (m, 16H), 7.07 (s, 1H), 7.06 (s, 1H), 4.38 (t, 2H), 4.16 (t, 2H), 4.03 (t, 2H), 2.21 (m 2H), 2.01 (m, 2H), 1.85 (m, 2H), 1.61-1.22 (m, 8H), 0.84 (t, 3H), 0.23 (s, 9H), 0.21 (s, 9H); ^{13}C NMR (CDCl$_3$, 300 MHz) δ 171.02, 153.89, 153.06, 140.15, 140.01, 132.43, 132.03, 126.67, 126.67, 122.53, 122.35, 116.86, 113.92, 104.80 (2C), 95.22 (2C), 94.91 (2C), 86.82 (2C), 69.57, 65.97, 61.27, 31.85, 29.34, 29.10, 28.76, 26.03, 22.63, 21.00, 14.13, -0.004, -0.13 ppm.

(5-47b). A similar procedure was used as for molecule 5-46b. Yield 0.6 g (93%) ^{1}H NMR (CDCl$_3$, 300 MHz) δ 7.59 (m, 16H), 7.06 (s, 1H), 7.05 (s, 1H), 4.25 (t, 2H), 4.06 (t, 2H), 3.97 (q, 2H), 3.18 (s, 1H), 3.17 (s, 1H), 2.77 (t, 1H), 2.16 (m, 2H), 1.84 (m, 2H), 1.55 (m, 2H), 1.42-1.22 (m, 6H), 0.87 (t, 3H); ^{13}C NMR (CDCl$_3$, 300 MHz) δ

154.02, 152.95, 140.64, 140.60, 140.09, 139.97, 132.61 (2C), 132.13, 132.07, 126.98,

126.85, 126.82 (2C), 122.77, 122.34, 121.34 (2C), 116.90, 116.07, 114.06, 113.67, 95.29,

94.97, 86.87, 86.50, 83.42 (2C), 78.04 (2C), 69.65, 69.04, 61.87, 31.84, 31.79, 29.35,

29.08, 26.02, 22.60, 14.11 ppm.

(5-48). Compound **5-46b** (260 mg, 0.506 mmol) was dissolved in 10 mL of

freshly distilled THF. Benzenetricarboxylic acid (34 mg, 0.162 mmol) and

triphenyphosphine (250 mg, 0.962 mmol) were then added and the solution was allowed

to stir at room temperature for 20 minutes. Next, diethyldiazodicarboxylate (176 mg,

0.946 mmol) was added to the solution. This mixture was allowed to stir overnight under

nitrogen and then poured into 100 mL of ether and 50 mL of water. The organic layer

was extracted with water and brine, dried over magnesium sulfate and evaporated to

dryness. The crude material was purified by column chromatography (silica gel, 1:3

hexane/MeCl$_2$) affording **5-48** as a pale yellow solid, yield 210 mg (76%). ^{1}H NMR

(CDCl$_3$, 300 MHz) δ 8.79 (s, 3H), 7.42 (m, 24H), 7.02 (s, 3H), 6.99 (s, 3H), 4.63 (t, 6H),

4.19 (t, 6H), 4.0 (t, 6H), 3.19 (s, 3H), 3.18 (s, 3H), 2.38 (m, 6H), 1.82 (m, 6H), 1.53 (m,

6H), 1.42-1.23 (m, 18H), 0.84 (t, 9H); ^{13}C NMR (CDCl$_3$, 300 MHz) δ 164.99, 154,16,

153.16, 134.72, 132.24, 132.21, 131.59, 131.33, 123.96, 123.79, 122.11, 117.05, 116.93,

114.23, 114.03, 94.80 (2C), 88.00, 87.78, 83.44 (2C), 79.25, 79.19, 69.68, 66.143,

62.837, 32.00, 29.46, 29.24, 28.93, 26.17, 22.77, 14.28.

3-(4-methoxyphenoxy)-propanol (5-32). This compound was prepared by a

similar procedure to that used for **(5-41)**; yield 2.48 g (85%). ^{1}H NMR (CDCl$_3$, 300

MHz) δ 6.82 (m, 4H), 4.07 (t, 2H), 3.82 (m, 2H), 3.78 (s, 3H), 2.02 (m, 2H), 1.91 (t, 1H);

^{13}C NMR (CDCl$_3$, 300 MHz) δ 153.50, 152.53, 122.98, 121.43, 66.67, 61.22, 57.14, 28.57.

3-(2,5-diiodo-4-methoxyphenoxy)-propyl acetate (5-33). This compound was prepared by a similar procedure to that used for **(5-42)**; yield 3.17 g (72%). ^{1}H NMR (CDCl$_3$, 300 MHz) δ 7.21 (s, 1H), 7.19 (s, 1H), 4.33 (t, 2H), 4.02 (t, 2H), 3.81 (s, 3H), 2.16 (m, 2H), 2.08 (s, 3H); ^{13}C NMR (CDCl$_3$, 300 MHz) δ 171.15, 153.11, 152.39, 122.84, 122.70, 86.26, 86.22, 70.32, 66.63, 62.43, 28.43.

(5-34). This compound was prepared by a similar procedure to that used for **(5-46a)**, yield 2.23 g (86%). ^{1}H NMR (CDCl$_3$, 300 MHz) δ 6.93 (s, 1H), 6.90 (s, 1H), 4.29 (t, 2H), 4.05 (t, 2H), 3.82 (s, 3H), 2.15 (m, 2H), 2.03 (s, 3H), 0.23 (s, 9H), 0.21 (s, 9H); ^{13}C NMR (CDCl$_3$, 300 MHz) δ 174.06, 153.87, 152.82, 117.45, 116.62, 112.99, 112.56, 85.47, 84.18, 79.87, 79.62, 68.71, 61.49, 55.72, 32.06.

(5-35). This compound was prepared by a similar procedure to that used for **(5-46b)**; yield 1.06 g (78%). ^{1}H NMR (CDCl$_3$, 300 MHz) δ 7.00 (s, 1H), 6.97 (s, 1H), 4.18 (t, 2H), 3.88 (m, 2H), 3.83 (s, 3H), 2.48 (t, 1H), 2.16 (m, 2H); ^{13}C NMR (CDCl$_3$, 300 MHz) δ 154.87, 153.82, 117.55, 116.00, 113.34, 112.87, 83.47, 83.13, 79.78, 79.74, 68.71, 61.49, 56.65, 31.96.

(5-37). This compound was prepared by a similar procedure to that used for **(5-48)**; yield 0.324 g (90%). ^{1}H NMR (CDCl$_3$, 300 MHz) δ 8.83 (s, 3H) 7.02 (s, 3H), 6.99 (s, 3H), 4.61 (t, 6H), 4.18 (t, 6H), 3.82 (s, 9H), 3.38 (s, 3H), 3.36 (s, 3H) 2.29 (m, 2H); ^{13}C NMR (CDCl$_3$, 300 MHz) δ 170.89, 154.86, 153.73, 117.51, 116.25, 113.24, 112.81, 83.51, 83.24, 79.91, 79.82, 68.68, 61.52, 59.81, 32.15.

Pt Triangle (5-49). Compound **5-48** (100 mg, .0588 mmol) and (tbbpy)PtCl$_2$ (95 mg, 0.176 mmol) are placed in a 250 mL round bottom flask and dissolved in 180 mL of freshly distilled MeCl$_2$ and 5 mL of diisopropylamine. The solution is sealed with a septum and argon degassed for 30 minutes. The septum is removed and with the argon needle still in the solution, CuI (1 mg, 0.0052 mmol) is added. The flask is then sealed again with the septum and argon degassed for another 30 minutes. The reaction mixture was then allowed to stir at room temperature for 7 days. During this time, the solution darkened to an orange/red hue. After the seven days, the solution was evaporated until roughly 5 mL of solvent remained and the solution was added drop wise to 40 mL of rapidly stirred hexane. The precipitate was collected by centrifugation and then chromatographed on alumina using methylene chloride for the eluent until a first yellow band comes off the column. Then, 2% methanol/MeCl$_2$ is added as the eluent and the product is flushed off the column, yield 40 mg (22%). For ^{1}H NMR see Figure 5-12. ^{1}H NMR (CD$_2$Cl$_2$, 300 MHz) 9.62 (m, 6H), 8.83 (m, 3H), 8.03 (s, 6H), 7.67-7.41 (m, 30H), 7.18-6.91 (m, 6H), 4.62 (m, 6H), 4.28 (m, 12H), 4.06 (m, 6H), 2.37 (m, 6H), 1.82 (m, 6H), 1.61-1.24 (m), 0.82 (m). MALDI-TOF: calc'd for C$_{171}$H$_{168}$N$_6$O$_{12}$Pt$_3$ 3082.16; observed 3086.02 (isotope analysis indicates 3085.51 as the most abundant peak for the above formula).

APPENDIX

Table A-1. Crystal data and structure refinement for yellow (tbbpy)Pt(CCtol)$_2$.

Identification code	edw2
Empirical formula	C43 H46 N2 Pt
Formula weight	785.91
Temperature	173(2) K
Wavelength	0.71073 Å
Crystal system	Triclinic
Space group	P-1
Unit cell dimensions	a = 12.0096(5) Å α= 105.6470(10)°.
	b = 12.6647(5) Å β= 106.1540(10)°.
	c = 13.1835(5) Å γ = 102.6230(10)°.
Volume	1758.74(12) Å^3
Z	2
Density (calculated)	1.484 Mg/m^3
Absorption coefficient	4.021 mm^{-1}
F(000)	792
Crystal size	0.26 x 0.19 x 0.15 mm^3
Theta range for data collection	1.72 to 27.50°.
Index ranges	-14$\leq$h$\leq$15, -16$\leq$k$\leq$16, -17$\leq$l$\leq$9
Reflections collected	11955
Independent reflections	7849 [R(int) = 0.0312]
Completeness to theta = 27.50°	97.2 %
Refinement method	Full-matrix least-squares on F^2
Data / restraints / parameters	7849 / 0 / 424
Goodness-of-fit on F^2	1.037
Final R indices [I>2sigma(I)]	R1 = 0.0223, wR2 = 0.0580 [7530]

179

| R indices (all data) | $R1 = 0.0235$, $wR2 = 0.0590$ |
| Largest diff. peak and hole | 1.026 and -0.967 e.Å^{-3} |

$R1 = \Sigma(||F_o| - |F_c||) / \Sigma|F_o|$

$wR2 = [\Sigma[w(F_o^2 - F_c^2)^2] / \Sigma[wF_o^{2\,2}]]^{1/2}$

$S = [\Sigma[w(F_o^2 - F_c^2)^2] / (n-p)]^{1/2} w = 1/[\sigma^2(F_o^2)+(0.0370*p)^2+0.31*p]$, $p = [\max(F_o^2,0)+ 2* F_c^2]/3$

Table A-2. Atomic coordinates (x 10^4) and equivalent isotropic displacement parameters ($\mathring{A}^2$x 10^3)for yellow (tbbpy)Pt(CCtol)$_2$. U(eq) is defined as one third of the trace of the orthogonalized U^{ij} tensor.

	x	y	z	U(eq)
Pt	7520(1)	6491(1)	5842(1)	23(1)
N1	6543(2)	4954(2)	4509(2)	24(1)
N2	6023(2)	6879(2)	5035(2)	24(1)
C1	6905(2)	4007(2)	4264(2)	29(1)
C2	6256(2)	3055(2)	3290(2)	30(1)
C3	5166(2)	3020(2)	2518(2)	25(1)
C4	4792(2)	3992(2)	2796(2)	25(1)
C5	5498(2)	4944(2)	3771(2)	23(1)
C6	5201(2)	6035(2)	4058(2)	22(1)
C7	4213(2)	6231(2)	3383(2)	26(1)
C8	4042(2)	7316(2)	3665(2)	25(1)
C9	4874(3)	8146(2)	4688(2)	30(1)
C10	5830(2)	7905(2)	5337(2)	29(1)
C11	4465(2)	1985(2)	1419(2)	28(1)
C12	3236(2)	2074(2)	773(2)	32(1)
C13	4227(3)	861(2)	1679(3)	40(1)
C14	5243(3)	1956(3)	669(3)	44(1)
C15	3004(2)	7554(2)	2879(2)	31(1)
C16	3166(3)	8847(2)	3217(3)	41(1)
C17	1801(3)	6901(3)	2936(4)	54(1)
C18	2983(4)	7129(3)	1671(3)	50(1)
C19	8334(2)	8032(2)	6978(2)	27(1)
C20	8797(2)	9032(2)	7610(2)	30(1)
C21	9374(2)	10230(2)	8322(2)	26(1)
C22	10115(2)	10996(2)	8009(2)	30(1)
C23	10659(2)	12151(2)	8687(2)	32(1)
C24	10507(2)	12584(2)	9707(2)	31(1)
C25	9775(2)	11820(2)	10030(2)	30(1)
C26	9215(2)	10671(2)	9352(2)	29(1)
C27	11110(3)	13839(3)	10449(3)	45(1)

C28	8918(2)	6015(2)	6479(2)	28(1)
C29	9772(2)	5685(2)	6816(2)	30(1)
C30	10756(2)	5252(2)	7205(2)	28(1)
C31	10945(3)	4333(2)	6474(2)	33(1)
C32	11882(3)	3901(3)	6858(3)	36(1)
C33	12668(2)	4369(3)	7977(3)	33(1)
C34	12493(3)	5282(3)	8704(2)	35(1)
C35	11555(3)	5722(2)	8333(2)	33(1)
C36	13683(3)	3897(3)	8402(3)	47(1)
C70	1901(3)	9293(3)	7065(3)	38(1)
C71	2752(3)	10291(3)	7191(3)	48(1)
C72	2697(4)	10691(3)	6298(4)	58(1)
C73	1786(4)	10092(4)	5266(3)	55(1)
C74	942(4)	9065(4)	5119(3)	55(1)
C75	994(3)	8679(3)	6008(3)	44(1)
C76	1895(3)	8890(3)	8032(3)	48(1)

Table A-3. Bond lengths [Å] and angles [°] for yellow (tbbpy)Pt(CCtol)₂.

Pt-C19	1.945(3)
Pt-C28	1.954(3)
Pt-N2	2.051(2)
Pt-N1	2.065(2)
N1-C5	1.352(3)
N1-C1	1.353(3)
N2-C10	1.344(3)
N2-C6	1.365(3)
C1-C2	1.380(4)
C1-H1A	0.9500
C2-C3	1.400(4)
C2-H2A	0.9500
C3-C4	1.393(3)
C3-C11	1.530(3)
C4-C5	1.392(3)
C4-H4A	0.9500
C5-C6	1.479(3)
C6-C7	1.386(3)
C7-C8	1.401(3)
C7-H7A	0.9500
C8-C9	1.395(4)
C8-C15	1.527(3)
C9-C10	1.375(4)
C9-H9A	0.9500
C10-H10A	0.9500
C11-C12	1.531(4)
C11-C14	1.536(4)
C11-C13	1.538(4)
C12-H12A	0.9800
C12-H12B	0.9800
C12-H12C	0.9800
C13-H13A	0.9800
C13-H13B	0.9800
C13-H13C	0.9800

C14-H14A	0.9800
C14-H14B	0.9800
C14-H14C	0.9800
C15-C18	1.528(4)
C15-C16	1.529(4)
C15-C17	1.532(4)
C16-H16A	0.9800
C16-H16B	0.9800
C16-H16C	0.9800
C17-H17A	0.9800
C17-H17B	0.9800
C17-H17C	0.9800
C18-H18A	0.9800
C18-H18B	0.9800
C18-H18C	0.9800
C19-C20	1.213(4)
C20-C21	1.440(4)
C21-C22	1.396(4)
C21-C26	1.404(4)
C22-C23	1.385(4)
C22-H22A	0.9500
C23-C24	1.388(4)
C23-H23A	0.9500
C24-C25	1.397(4)
C24-C27	1.507(4)
C25-C26	1.381(4)
C25-H25A	0.9500
C26-H26A	0.9500
C27-H27A	0.9800
C27-H27B	0.9800
C27-H27C	0.9800
C28-C29	1.208(4)
C29-C30	1.434(4)
C30-C35	1.402(4)
C30-C31	1.403(4)
C31-C32	1.387(4)

C31-H31A	0.9500
C32-C33	1.388(4)
C32-H32A	0.9500
C33-C34	1.387(4)
C33-C36	1.508(4)
C34-C35	1.390(4)
C34-H34A	0.9500
C35-H35A	0.9500
C36-H36A	0.9800
C36-H36B	0.9800
C36-H36C	0.9800
C70-C71	1.377(5)
C70-C75	1.390(5)
C70-C76	1.498(5)
C71-C72	1.392(5)
C71-H71A	0.9500
C72-C73	1.370(6)
C72-H72A	0.9500
C73-C74	1.391(6)
C73-H73A	0.9500
C74-C75	1.378(5)
C74-H74A	0.9500
C75-H75A	0.9500
C76-H76A	0.9800
C76-H76B	0.9800
C76-H76C	0.9800
C19-Pt-C28	89.84(11)
C19-Pt-N2	94.77(10)
C28-Pt-N2	174.79(9)
C19-Pt-N1	172.77(9)
C28-Pt-N1	96.57(9)
N2-Pt-N1	78.69(8)
C5-N1-C1	117.9(2)
C5-N1-Pt	115.92(16)
C1-N1-Pt	125.97(17)

C10-N2-C6	117.8(2)
C10-N2-Pt	125.93(17)
C6-N2-Pt	116.12(16)
N1-C1-C2	122.3(2)
N1-C1-H1A	118.9
C2-C1-H1A	118.9
C1-C2-C3	121.0(2)
C1-C2-H2A	119.5
C3-C2-H2A	119.5
C4-C3-C2	116.0(2)
C4-C3-C11	122.8(2)
C2-C3-C11	121.2(2)
C5-C4-C3	120.8(2)
C5-C4-H4A	119.6
C3-C4-H4A	119.6
N1-C5-C4	122.0(2)
N1-C5-C6	114.8(2)
C4-C5-C6	123.1(2)
N2-C6-C7	121.5(2)
N2-C6-C5	114.3(2)
C7-C6-C5	124.1(2)
C6-C7-C8	120.9(2)
C6-C7-H7A	119.5
C8-C7-H7A	119.5
C9-C8-C7	116.0(2)
C9-C8-C15	123.2(2)
C7-C8-C15	120.8(2)
C10-C9-C8	120.8(2)
C10-C9-H9A	119.6
C8-C9-H9A	119.6
N2-C10-C9	122.8(2)
N2-C10-H10A	118.6
C9-C10-H10A	118.6
C3-C11-C12	111.9(2)
C3-C11-C14	108.3(2)
C12-C11-C14	108.3(2)

C3-C11-C13	109.8(2)
C12-C11-C13	108.5(2)
C14-C11-C13	110.1(2)
C11-C12-H12A	109.5
C11-C12-H12B	109.5
H12A-C12-H12B	109.5
C11-C12-H12C	109.5
H12A-C12-H12C	109.5
H12B-C12-H12C	109.5
C11-C13-H13A	109.5
C11-C13-H13B	109.5
H13A-C13-H13B	109.5
C11-C13-H13C	109.5
H13A-C13-H13C	109.5
H13B-C13-H13C	109.5
C11-C14-H14A	109.5
C11-C14-H14B	109.5
H14A-C14-H14B	109.5
C11-C14-H14C	109.5
H14A-C14-H14C	109.5
H14B-C14-H14C	109.5
C8-C15-C18	109.9(2)
C8-C15-C16	111.5(2)
C18-C15-C16	107.6(3)
C8-C15-C17	107.8(2)
C18-C15-C17	109.9(3)
C16-C15-C17	110.1(3)
C15-C16-H16A	109.5
C15-C16-H16B	109.5
H16A-C16-H16B	109.5
C15-C16-H16C	109.5
H16A-C16-H16C	109.5
H16B-C16-H16C	109.5
C15-C17-H17A	109.5
C15-C17-H17B	109.5
H17A-C17-H17B	109.5

C15-C17-H17C	109.5
H17A-C17-H17C	109.5
H17B-C17-H17C	109.5
C15-C18-H18A	109.5
C15-C18-H18B	109.5
H18A-C18-H18B	109.5
C15-C18-H18C	109.5
H18A-C18-H18C	109.5
H18B-C18-H18C	109.5
C20-C19-Pt	173.9(2)
C19-C20-C21	177.2(3)
C22-C21-C26	117.6(2)
C22-C21-C20	120.8(2)
C26-C21-C20	121.6(2)
C23-C22-C21	120.8(2)
C23-C22-H22A	119.6
C21-C22-H22A	119.6
C22-C23-C24	121.4(3)
C22-C23-H23A	119.3
C24-C23-H23A	119.3
C23-C24-C25	118.0(2)
C23-C24-C27	121.4(3)
C25-C24-C27	120.6(3)
C26-C25-C24	120.9(3)
C26-C25-H25A	119.5
C24-C25-H25A	119.5
C25-C26-C21	121.2(2)
C25-C26-H26A	119.4
C21-C26-H26A	119.4
C24-C27-H27A	109.5
C24-C27-H27B	109.5
H27A-C27-H27B	109.5
C24-C27-H27C	109.5
H27A-C27-H27C	109.5
H27B-C27-H27C	109.5
C29-C28-Pt	176.6(2)

C28-C29-C30	177.9(3)
C35-C30-C31	117.5(3)
C35-C30-C29	121.3(3)
C31-C30-C29	121.2(3)
C32-C31-C30	121.1(3)
C32-C31-H31A	119.5
C30-C31-H31A	119.5
C31-C32-C33	121.1(3)
C31-C32-H32A	119.5
C33-C32-H32A	119.5
C34-C33-C32	118.2(3)
C34-C33-C36	120.4(3)
C32-C33-C36	121.4(3)
C33-C34-C35	121.4(3)
C33-C34-H34A	119.3
C35-C34-H34A	119.3
C34-C35-C30	120.7(3)
C34-C35-H35A	119.6
C30-C35-H35A	119.6
C33-C36-H36A	109.5
C33-C36-H36B	109.5
H36A-C36-H36B	109.5
C33-C36-H36C	109.5
H36A-C36-H36C	109.5
H36B-C36-H36C	109.5
C71-C70-C75	117.9(3)
C71-C70-C76	122.2(3)
C75-C70-C76	119.8(3)
C70-C71-C72	121.4(3)
C70-C71-H71A	119.3
C72-C71-H71A	119.3
C73-C72-C71	120.3(4)
C73-C72-H72A	119.8
C71-C72-H72A	119.8
C72-C73-C74	118.8(4)
C72-C73-H73A	120.6

C74-C73-H73A	120.6
C75-C74-C73	120.5(3)
C75-C74-H74A	119.7
C73-C74-H74A	119.7
C74-C75-C70	120.9(3)
C74-C75-H75A	119.5
C70-C75-H75A	119.5
C70-C76-H76A	109.5
C70-C76-H76B	109.5
H76A-C76-H76B	109.5
C70-C76-H76C	109.5
H76A-C76-H76C	109.5
H76B-C76-H76C	109.5

Symmetry transformations used to generate equivalent atoms:

Table A-4. Anisotropic displacement parameters (Å^2x 10^3) for yellow (tbbpy)Pt(CCtol)$_2$. The anisotropic displacement factor exponent takes the form: $-2\pi^2$[h^2 a*^{2}U^{11} + ... + 2 h k a* b* U^{12}]

	U^{11}	U^{22}	U^{33}	U^{23}	U^{13}	U^{12}
Pt	22(1)	22(1)	20(1)	5(1)	4(1)	6(1)
N1	24(1)	23(1)	25(1)	8(1)	8(1)	8(1)
N2	25(1)	23(1)	21(1)	7(1)	7(1)	7(1)
C1	29(1)	27(1)	30(1)	10(1)	6(1)	12(1)
C2	31(1)	25(1)	33(1)	7(1)	8(1)	12(1)
C3	23(1)	22(1)	27(1)	6(1)	7(1)	6(1)
C4	22(1)	23(1)	27(1)	8(1)	6(1)	6(1)
C5	23(1)	21(1)	24(1)	8(1)	8(1)	6(1)
C6	23(1)	20(1)	23(1)	7(1)	9(1)	5(1)
C7	24(1)	22(1)	26(1)	5(1)	6(1)	6(1)
C8	24(1)	25(1)	27(1)	10(1)	9(1)	8(1)
C9	34(1)	22(1)	30(1)	6(1)	9(1)	11(1)
C10	32(1)	22(1)	26(1)	2(1)	6(1)	7(1)
C11	25(1)	24(1)	28(1)	4(1)	6(1)	8(1)
C12	26(1)	28(1)	31(1)	3(1)	2(1)	6(1)
C13	46(2)	22(1)	37(2)	6(1)	2(1)	8(1)
C14	36(2)	49(2)	37(2)	2(1)	14(1)	10(1)
C15	27(1)	25(1)	34(1)	9(1)	3(1)	10(1)
C16	44(2)	29(1)	46(2)	14(1)	5(1)	16(1)
C17	30(2)	46(2)	86(3)	34(2)	10(2)	12(1)
C18	67(2)	47(2)	34(2)	13(1)	6(2)	29(2)
C19	25(1)	27(1)	23(1)	5(1)	5(1)	7(1)
C20	26(1)	30(1)	28(1)	9(1)	5(1)	8(1)
C21	23(1)	26(1)	25(1)	7(1)	2(1)	9(1)
C22	29(1)	35(1)	24(1)	9(1)	7(1)	10(1)
C23	28(1)	32(1)	36(1)	15(1)	10(1)	7(1)
C24	28(1)	26(1)	33(1)	9(1)	6(1)	8(1)
C25	33(1)	29(1)	27(1)	8(1)	10(1)	11(1)
C26	27(1)	28(1)	29(1)	10(1)	7(1)	7(1)
C27	50(2)	27(1)	50(2)	6(1)	19(2)	6(1)

C28	29(1)	25(1)	22(1)	7(1)	3(1)	4(1)
C29	28(1)	30(1)	29(1)	10(1)	7(1)	7(1)
C30	23(1)	30(1)	32(1)	13(1)	10(1)	7(1)
C31	32(1)	37(1)	27(1)	9(1)	8(1)	10(1)
C32	38(2)	40(2)	37(2)	15(1)	18(1)	17(1)
C33	28(1)	40(1)	40(2)	23(1)	15(1)	13(1)
C34	31(1)	41(2)	31(1)	14(1)	6(1)	10(1)
C35	32(1)	33(1)	29(1)	7(1)	7(1)	11(1)
C36	41(2)	62(2)	55(2)	31(2)	20(2)	29(2)
C70	38(2)	43(2)	40(2)	13(1)	21(1)	22(1)
C71	40(2)	54(2)	40(2)	8(2)	13(1)	7(1)
C72	60(2)	54(2)	61(2)	19(2)	33(2)	8(2)
C73	63(2)	65(2)	45(2)	23(2)	26(2)	22(2)
C74	54(2)	64(2)	38(2)	12(2)	15(2)	12(2)
C75	40(2)	44(2)	42(2)	9(1)	15(1)	9(1)
C76	51(2)	56(2)	48(2)	24(2)	20(2)	26(2)

193

Table A-5. Hydrogen coordinates (x 10⁴) and isotropic displacement parameters (Å^2x 10³) for yellow (tbbpy)Pt(CCtol)₂.

	x	y	z	U(eq)
H1A	7631	3996	4779	35
H2A	6553	2415	3142	36
H4A	4046	4005	2314	30
H7A	3645	5620	2718	31
H9A	4778	8886	4938	36
H10A	6377	8490	6030	35
H12A	2804	1386	89	48
H12B	3375	2765	564	48
H12C	2741	2129	1252	48
H13A	3679	861	2107	59
H13B	5003	810	2124	59
H13C	3847	197	970	59
H14A	6052	1946	1086	65
H14B	5330	2644	453	65
H14C	4842	1261	-12	65
H16A	3157	9140	3982	62
H16B	2497	8972	2688	62
H16C	3948	9258	3198	62
H17A	1720	6078	2742	81
H17B	1114	6998	2400	81
H17C	1799	7211	3701	81
H18A	3779	7504	1652	76
H18B	2344	7321	1179	76
H18C	2814	6289	1409	76
H22A	10249	10721	7321	36
H23A	11147	12659	8448	38
H25A	9662	12095	10728	36
H26A	8713	10169	9585	35
H27A	11886	14136	10355	67
H27B	11266	13913	11240	67
H27C	10571	14284	10236	67

H31A	10422	4001	5703	40
H32A	11988	3276	6347	43
H34A	13025	5614	9472	42
H35A	11454	6347	8850	40
H36A	14277	4031	8033	71
H36B	13341	3065	8231	71
H36C	14090	4289	9220	71
H71A	3388	10716	7902	57
H72A	3295	11381	6405	69
H73A	1731	10374	4661	66
H74A	325	8626	4399	66
H75A	401	7984	5898	53
H76A	2687	9286	8652	72
H76B	1750	8053	7787	72
H76C	1245	9066	8292	72

10

195

Table A-6. Torsion angles [°] for yellow (tbbpy)Pt(CCtol)₂.

C19-Pt-N1-C5	-22.9(8)
C28-Pt-N1-C5	-175.27(18)
N2-Pt-N1-C5	2.52(17)
C19-Pt-N1-C1	151.3(7)
C28-Pt-N1-C1	-1.1(2)
N2-Pt-N1-C1	176.7(2)
C19-Pt-N2-C10	-1.1(2)
C28-Pt-N2-C10	-153.1(9)
N1-Pt-N2-C10	-178.0(2)
C19-Pt-N2-C6	173.89(18)
C28-Pt-N2-C6	21.9(10)
N1-Pt-N2-C6	-3.01(17)
C5-N1-C1-C2	0.9(4)
Pt-N1-C1-C2	-173.1(2)
N1-C1-C2-C3	-1.5(4)
C1-C2-C3-C4	0.0(4)
C1-C2-C3-C11	177.9(3)
C2-C3-C4-C5	2.0(4)
C11-C3-C4-C5	-176.0(2)
C1-N1-C5-C4	1.1(4)
Pt-N1-C5-C4	175.72(18)
C1-N1-C5-C6	-176.3(2)
Pt-N1-C5-C6	-1.7(3)
C3-C4-C5-N1	-2.6(4)
C3-C4-C5-C6	174.6(2)
C10-N2-C6-C7	1.5(4)
Pt-N2-C6-C7	-173.93(18)
C10-N2-C6-C5	178.5(2)
Pt-N2-C6-C5	3.0(3)
N1-C5-C6-N2	-0.9(3)
C4-C5-C6-N2	-178.2(2)
N1-C5-C6-C7	176.0(2)
C4-C5-C6-C7	-1.4(4)
N2-C6-C7-C8	1.7(4)

C5-C6-C7-C8	-175.0(2)
C6-C7-C8-C9	-3.8(4)
C6-C7-C8-C15	175.8(2)
C7-C8-C9-C10	2.9(4)
C15-C8-C9-C10	-176.6(3)
C6-N2-C10-C9	-2.4(4)
Pt-N2-C10-C9	172.5(2)
C8-C9-C10-N2	0.2(4)
C4-C3-C11-C12	-8.6(4)
C2-C3-C11-C12	173.6(2)
C4-C3-C11-C14	110.8(3)
C2-C3-C11-C14	-67.1(3)
C4-C3-C11-C13	-129.1(3)
C2-C3-C11-C13	53.1(3)
C9-C8-C15-C18	131.8(3)
C7-C8-C15-C18	-47.7(3)
C9-C8-C15-C16	12.5(4)
C7-C8-C15-C16	-167.0(3)
C9-C8-C15-C17	-108.5(3)
C7-C8-C15-C17	72.0(3)
C28-Pt-C19-C20	143(2)
N2-Pt-C19-C20	-35(2)
N1-Pt-C19-C20	-10(3)
Pt-C19-C20-C21	-56(7)
C19-C20-C21-C22	1(6)
C19-C20-C21-C26	-179(100)
C26-C21-C22-C23	-0.8(4)
C20-C21-C22-C23	179.2(2)
C21-C22-C23-C24	1.2(4)
C22-C23-C24-C25	-0.6(4)
C22-C23-C24-C27	179.3(3)
C23-C24-C25-C26	-0.4(4)
C27-C24-C25-C26	179.7(3)
C24-C25-C26-C21	0.8(4)
C22-C21-C26-C25	-0.2(4)
C20-C21-C26-C25	179.8(2)

C19-Pt-C28-C29	-144(4)
N2-Pt-C28-C29	8(5)
N1-Pt-C28-C29	32(4)
Pt-C28-C29-C30	-70(10)
C28-C29-C30-C35	-119(8)
C28-C29-C30-C31	60(8)
C35-C30-C31-C32	0.5(4)
C29-C30-C31-C32	-178.7(3)
C30-C31-C32-C33	-0.3(4)
C31-C32-C33-C34	-0.1(4)
C31-C32-C33-C36	179.5(3)
C32-C33-C34-C35	0.3(4)
C36-C33-C34-C35	-179.3(3)
C33-C34-C35-C30	-0.1(4)
C31-C30-C35-C34	-0.2(4)
C29-C30-C35-C34	179.0(3)
C75-C70-C71-C72	1.1(5)
C76-C70-C71-C72	-175.9(3)
C70-C71-C72-C73	0.1(6)
C71-C72-C73-C74	-1.9(6)
C72-C73-C74-C75	2.5(6)
C73-C74-C75-C70	-1.3(6)
C71-C70-C75-C74	-0.5(5)
C76-C70-C75-C74	176.6(3)

Symmetry transformations used to generate equivalent atoms:

Table A-7. Crystal data and structure refinement for orange (tbbpy)Pt(CCtol)$_2$.

Identification code	edw1t	
Empirical formula	C42 H44 N2 Pt	
Formula weight	674.34	
Temperature	173(2) K	
Wavelength	0.71073 Å	
Crystal system	Triclinic	
Space group	P-1	
Unit cell dimensions	a = 9.3578(5) Å	$\square$= 88.1280(10)°.

	$b = 12.3344(7)$ Å	$\square = 79.8700(10)°.$
	$c = 15.5305(8)$ Å	$\square = 83.4010(10)°.$
Volume	$1752.80(16)$ Å^3	
Z	2	
Density (calculated)	1.278 Mg/m^3	
Absorption coefficient	2.048 mm^{-1}	
F(000)	698	
Crystal size	? x ? x ? mm^3	
Theta range for data collection	1.66 to $27.50°.$	
Index ranges	$-12 \leq h \leq 9$, $-16 \leq k \leq 16$, $-20 \leq l \leq 19$	
Reflections collected	11853	
Independent reflections	7804 [R(int) = 0.0778]	
Completeness to theta = 27.50°	97.0 %	
Refinement method	Full-matrix least-squares on F^2	
Data / restraints / parameters	7804 / 0 / 415	
Goodness-of-fit on F^2	1.069	
Final R indices [I>2sigma(I)]	R1 = 0.0711, wR2 = 0.2129 [7405]	
R indices (all data)	R1 = 0.0735, wR2 = 0.2167	
Extinction coefficient	0.130(9)	
Largest diff. peak and hole	1.694 and -0.985 e.Å^{-3}	

$R1 = \Sigma(||F_o| - |F_c||) / \square|F_o|$

$wR2 = [\Sigma[w(F_o^2 - F_c^2)^2] / \Sigma[wF_o^{2\,2}]]^{1/2}$

$S = [\Sigma[w(F_o^2 - F_c^2)^2] / (n-p)]^{1/2}$ $w = 1/[\square^2(F_o^2)+(0.0370*p)^2+0.31*p]$, $p = [max(F_o^2,0)+ 2* F_c^2]/3$

Table A-8. Atomic coordinates (x 10^4) and equivalent isotropic displacement parameters (Å^2x 10^3) for orange (tbbpy)Pt(CCtol)$_2$. U(eq) is defined as one third of the trace of the orthogonalized U^{ij} tensor.

	x	y	z	U(eq)
Pt	12772(1)	10806(1)	4088(1)	26(1)
N2	12484(8)	9855(6)	5207(5)	63(2)
N1	13816(8)	11619(6)	4891(5)	67(2)
C19	11759(10)	9934(8)	3398(6)	64(2)
C28	13030(10)	11808(7)	3098(6)	66(2)
C7	12940(9)	9598(7)	6674(6)	65(2)
C5	13827(9)	11174(7)	5695(6)	67(2)
C30	13036(10)	13364(8)	1874(6)	73(2)
C3	15083(10)	12643(7)	6100(6)	66(2)
C6	13088(9)	10178(7)	5877(6)	63(2)
C9	11559(10)	8405(8)	6119(6)	71(2)
C10	11750(10)	9008(7)	5325(6)	69(2)
C34	13702(11)	14069(9)	432(6)	79(2)
C29	13105(10)	12531(8)	2532(6)	74(2)
C20	11145(11)	9401(9)	3026(8)	83(3)
C4	14481(9)	11699(7)	6312(6)	69(2)
C8	12185(9)	8704(8)	6801(6)	67(2)
C15	12020(12)	8034(9)	7666(6)	78(2)
C33	12724(11)	15022(8)	630(7)	75(2)
C21	10428(10)	8753(8)	2470(8)	80(3)
C35	13825(11)	13277(8)	1037(7)	78(2)
C11	15759(11)	13252(8)	6752(7)	74(2)
C1	14469(10)	12516(7)	4699(6)	73(2)
C2	15097(10)	13039(7)	5269(7)	73(2)
C16	12867(12)	6881(9)	7475(7)	86(3)
C26	9563(11)	8014(9)	2837(7)	78(2)
C17	12654(13)	8595(9)	8382(7)	83(3)
C12	15660(12)	12677(10)	7620(7)	86(3)
C18	10346(11)	7892(11)	7960(8)	102(4)
C32	11968(12)	15143(9)	1446(8)	91(3)

C31	12106(12)	14338(8)	2060(7)	84(2)
C14	17366(12)	13353(10)	6361(7)	91(3)
C13	14885(14)	14399(8)	6886(9)	99(3)
C25	8877(12)	7409(11)	2321(9)	103(4)
C23	9975(15)	8301(13)	1040(10)	100(4)
C24	9093(12)	7518(11)	1409(8)	98(3)
C22	10645(13)	8915(11)	1547(8)	92(3)
C71	5670(20)	9938(17)	9101(12)	123(5)
C61	9494(16)	6019(13)	5419(11)	117(5)
C36	12557(14)	15925(11)	-69(9)	108(4)
C62	8959(14)	5653(13)	4629(10)	109(4)
C60	10436(15)	5291(13)	5744(9)	115(4)
C27	8390(16)	6797(14)	841(14)	153(7)
C70	6360(20)	9413(14)	9702(14)	147(6)
C72	4350(20)	10538(14)	9355(13)	133(5)

201

Table A-9. Bond lengths [Å] and angles [°] for orange (tbbpy)Pt(CCtol)₂.

Pt-C28	1.941(9)
Pt-C19	1.968(10)
Pt-N2	2.059(8)
Pt-N1	2.062(8)
N2-C10	1.306(12)
N2-C6	1.359(11)
N1-C1	1.324(12)
N1-C5	1.348(11)
C19-C20	1.151(14)
C28-C29	1.231(13)
C7-C8	1.368(13)
C7-C6	1.404(12)
C5-C4	1.432(12)
C5-C6	1.474(12)
C30-C35	1.378(14)
C30-C31	1.406(14)
C30-C29	1.429(12)
C3-C4	1.357(13)
C3-C2	1.364(13)
C3-C11	1.540(13)
C9-C8	1.376(13)
C9-C10	1.413(13)
C34-C35	1.342(14)
C34-C33	1.412(15)
C20-C21	1.486(14)
C8-C15	1.547(14)
C15-C16	1.558(14)
C15-C17	1.563(15)
C15-C18	1.582(14)
C33-C32	1.342(15)
C33-C36	1.544(14)
C21-C26	1.336(15)
C21-C22	1.422(16)
C11-C12	1.497(15)

C11–C14	1.537(14)
C11–C13	1.552(14)
C1–C2	1.361(13)
C26–C25	1.393(16)
C32–C31	1.366(14)
C25–C24	1.399(18)
C23–C22	1.382(17)
C23–C24	1.39(2)
C24–C27	1.547(18)
C71–C70	1.33(3)
C71–C72	1.37(3)
C61–C60	1.33(2)
C61–C62	1.50(2)
C62–C60#1	1.337(19)
C60–C62#1	1.337(19)
C70–C72#2	1.50(2)
C72–C70#2	1.50(2)
C28–Pt–C19	87.8(4)
C28–Pt–N2	175.1(3)
C19–Pt–N2	96.3(4)
C28–Pt–N1	97.0(3)
C19–Pt–N1	175.2(3)
N2–Pt–N1	79.0(3)
C10–N2–C6	118.8(8)
C10–N2–Pt	125.7(7)
C6–N2–Pt	115.5(6)
C1–N1–C5	117.6(8)
C1–N1–Pt	127.0(7)
C5–N1–Pt	115.4(6)
C20–C19–Pt	177.1(10)
C29–C28–Pt	172.9(9)
C8–C7–C6	121.3(8)
N1–C5–C4	119.6(8)
N1–C5–C6	115.5(8)
C4–C5–C6	124.8(8)

C35-C30-C31	116.0(8)
C35-C30-C29	123.9(9)
C31-C30-C29	120.1(9)
C4-C3-C2	117.4(9)
C4-C3-C11	122.6(9)
C2-C3-C11	120.0(9)
N2-C6-C7	120.3(8)
N2-C6-C5	114.7(8)
C7-C6-C5	125.0(8)
C8-C9-C10	119.3(9)
N2-C10-C9	123.0(9)
C35-C34-C33	120.6(10)
C28-C29-C30	174.1(10)
C19-C20-C21	174.7(13)
C3-C4-C5	120.8(8)
C7-C8-C9	117.3(8)
C7-C8-C15	122.7(8)
C9-C8-C15	120.0(9)
C8-C15-C16	108.0(8)
C8-C15-C17	111.2(9)
C16-C15-C17	109.5(9)
C8-C15-C18	107.8(8)
C16-C15-C18	108.0(9)
C17-C15-C18	112.2(9)
C32-C33-C34	118.7(9)
C32-C33-C36	120.5(11)
C34-C33-C36	120.8(10)
C26-C21-C22	119.4(10)
C26-C21-C20	119.9(11)
C22-C21-C20	120.7(11)
C34-C35-C30	122.1(10)
C12-C11-C14	109.9(9)
C12-C11-C3	111.8(8)
C14-C11-C3	108.7(8)
C12-C11-C13	108.4(9)
C14-C11-C13	110.5(9)

C3-C11-C13	107.5(8)
N1-C1-C2	124.3(9)
C1-C2-C3	120.1(9)
C21-C26-C25	120.3(11)
C33-C32-C31	120.3(11)
C32-C31-C30	122.3(10)
C26-C25-C24	122.2(12)
C22-C23-C24	121.5(14)
C23-C24-C25	116.7(11)
C23-C24-C27	121.6(13)
C25-C24-C27	121.6(14)
C23-C22-C21	119.8(13)
C70-C71-C72	119.7(18)
C60-C61-C62	115.2(14)
C60#1-C62-C61	118.9(14)
C61-C60-C62#1	125.4(15)
C71-C70-C72#2	119.2(18)
C71-C72-C70#2	121.0(16)

Symmetry transformations used to generate equivalent atoms:
#1 -x+2,-y+1,-z+1   #2 -x+1,-y+2,-z+2

Table A-10. Anisotropic displacement parameters ($\text{Å}^2 \times 10^3$) for orange (tbbpy)Pt(CCtol)$_2$. The anisotropic displacement factor exponent takes the form: $-2\pi^2[$ $h^2 a^{*2}U^{11} + \ldots + 2 h k a^* b^* U^{12}]$

	U^{11}	U^{22}	U^{33}	U^{23}	U^{13}	U^{12}
Pt	28(1)	25(1)	24(1)	4(1)	-7(1)	-2(1)
N2	63(4)	56(4)	69(4)	0(3)	-11(3)	-2(3)
N1	62(4)	68(4)	68(4)	1(3)	-12(3)	-1(3)
C19	67(5)	65(5)	60(4)	-2(4)	-18(4)	3(4)
C28	69(5)	66(5)	67(5)	5(4)	-20(4)	-8(4)
C7	65(4)	68(5)	63(4)	3(3)	-14(3)	-7(3)
C5	60(4)	69(5)	68(5)	5(4)	-8(3)	-2(3)
C30	79(5)	75(5)	71(5)	17(4)	-25(4)	-21(4)
C3	64(4)	63(4)	71(5)	4(4)	-15(4)	-4(3)
C6	60(4)	65(4)	62(4)	-1(3)	-8(3)	-4(3)
C9	74(5)	64(5)	76(5)	11(4)	-15(4)	-14(4)
C10	67(5)	68(5)	73(5)	1(4)	-16(4)	-6(4)
C34	83(6)	92(7)	66(5)	13(4)	-20(4)	-21(5)
C29	78(5)	75(5)	70(5)	3(4)	-10(4)	-21(4)
C20	68(5)	80(6)	99(7)	-8(5)	-19(5)	3(4)
C4	61(4)	73(5)	69(5)	5(4)	-10(3)	0(4)
C8	60(4)	66(5)	73(5)	7(4)	-16(4)	1(3)
C15	83(6)	85(6)	64(5)	-3(4)	-11(4)	-5(5)
C33	80(5)	77(5)	72(5)	14(4)	-22(4)	-15(4)
C21	63(5)	75(6)	103(7)	-23(5)	-25(5)	5(4)
C35	76(5)	77(6)	83(6)	-2(5)	-23(4)	-2(4)
C11	71(5)	73(5)	81(6)	-4(4)	-18(4)	-11(4)
C1	74(5)	72(5)	75(5)	7(4)	-14(4)	-15(4)
C2	67(5)	63(5)	91(6)	7(4)	-11(4)	-13(4)
C16	88(6)	80(6)	84(6)	27(5)	-12(5)	4(5)
C26	71(5)	78(6)	86(6)	3(5)	-17(4)	-7(4)
C17	103(7)	82(6)	66(5)	12(4)	-21(5)	-16(5)
C12	83(6)	103(8)	78(6)	-12(5)	-18(5)	-23(5)
C18	75(6)	128(9)	97(7)	40(7)	-9(5)	-4(6)
C32	84(6)	90(7)	100(8)	13(6)	-19(5)	-7(5)

C31	94(6)	84(6)	72(5)	7(5)	-11(5)	-11(5)
C14	89(6)	104(8)	88(7)	2(6)	-25(5)	-28(6)
C13	109(8)	65(5)	131(10)	-12(6)	-43(7)	-8(5)
C25	69(6)	117(9)	123(10)	-14(7)	-18(6)	-7(6)
C23	91(8)	113(10)	102(9)	-20(8)	-32(7)	-15(7)
C24	81(6)	120(9)	99(8)	-29(7)	-34(6)	-2(6)
C22	89(7)	108(8)	82(7)	4(6)	-28(5)	-4(6)
C71	130(13)	142(14)	101(10)	22(10)	-31(9)	-25(11)
C61	102(9)	116(11)	120(11)	-1(8)	-5(8)	19(8)
C36	100(8)	114(9)	114(9)	39(7)	-31(7)	-18(7)
C62	82(7)	125(11)	115(10)	-21(8)	-3(7)	-6(7)
C60	96(8)	146(12)	101(9)	-27(9)	4(7)	-31(8)
C27	96(9)	153(14)	220(20)	-48(14)	-58(11)	-7(9)
C70	164(16)	112(12)	159(16)	-30(11)	4(14)	-37(11)
C72	148(14)	117(12)	143(15)	17(10)	-53(12)	-14(10)

Table A-11. Hydrogen coordinates ($\times 10^4$) and isotropic displacement parameters ($\mathring{A}^2 \times 10^{3}$) for orange (tbbpy)Pt(CCtol)$_2$.

	x	y	z	U(eq)
H7A	13374	9831	7135	78
H9A	11004	7801	6181	85
H10A	11326	8786	4856	83
H34A	14279	13986	-135	94
H4A	14494	11382	6877	82
H35A	14477	12637	884	94
H1A	14500	12814	4124	88
H2A	15546	13680	5087	88
H16A	12364	6479	7107	129
H16B	12910	6481	8027	129
H16C	13862	6956	7170	129
H26A	9415	7900	3453	94
H17A	13716	8571	8211	124
H17B	12423	8209	8942	124
H17C	12220	9356	8442	124
H12A	14642	12756	7922	129
H12B	16269	12997	7975	129
H12C	16002	11900	7533	129
H18A	9795	8605	8108	153
H18B	10224	7406	8473	153
H18C	9981	7576	7481	153
H32A	11333	15792	1597	110
H31A	11555	14439	2632	101
H14A	17859	13607	6811	137
H14B	17416	13876	5871	137
H14C	17848	12639	6152	137
H13A	13842	14337	6918	149
H13B	15218	14879	6394	149

H13C	15041	14707	7431	149
H25A	8242	6904	2598	124
H23A	10121	8418	425	120
H22A	11249	9444	1280	111
H71A	6100	9896	8499	148
H61A	9182	6717	5670	140
H36A	13473	15918	-489	162
H36B	12327	16637	214	162
H36C	11766	15793	-377	162
H62A	8204	6086	4398	131
H60A	10699	5458	6284	138
H27A	8294	7174	286	230
H27B	7423	6656	1152	230
H27C	9010	6103	725	230
H70A	7294	9012	9534	176
H72A	3882	10929	8927	159

Table A-12. Torsion angles [°] for orange (tbbpy)Pt(CCtol)$_2$.

C28-Pt-N2-C10	143(3)
C19-Pt-N2-C10	-3.6(8)
N1-Pt-N2-C10	177.0(8)
C28-Pt-N2-C6	-35(3)
C19-Pt-N2-C6	178.4(6)
N1-Pt-N2-C6	-1.0(6)
C28-Pt-N1-C1	-2.4(8)
C19-Pt-N1-C1	173(3)
N2-Pt-N1-C1	-179.6(8)
C28-Pt-N1-C5	177.9(6)
C19-Pt-N1-C5	-7(4)
N2-Pt-N1-C5	0.6(6)
C28-Pt-C19-C20	-165(18)
N2-Pt-C19-C20	13(18)
N1-Pt-C19-C20	20(20)
C19-Pt-C28-C29	119(7)
N2-Pt-C28-C29	-28(9)
N1-Pt-C28-C29	-61(7)
C1-N1-C5-C4	2.3(12)
Pt-N1-C5-C4	-177.9(6)
C1-N1-C5-C6	-180.0(8)
Pt-N1-C5-C6	-0.2(9)
C10-N2-C6-C7	0.9(13)
Pt-N2-C6-C7	179.1(6)
C10-N2-C6-C5	-177.0(8)
Pt-N2-C6-C5	1.2(9)
C8-C7-C6-N2	-0.3(13)
C8-C7-C6-C5	177.3(8)
N1-C5-C6-N2	-0.7(11)
C4-C5-C6-N2	176.9(8)
N1-C5-C6-C7	-178.5(8)
C4-C5-C6-C7	-0.9(13)
C6-N2-C10-C9	-0.2(14)
Pt-N2-C10-C9	-178.2(7)

C8-C9-C10-N2	-1.0(15)
Pt-C28-C29-C30	-71(13)
C35-C30-C29-C28	-118(10)
C31-C30-C29-C28	61(10)
Pt-C19-C20-C21	-169(11)
C2-C3-C4-C5	-2.9(13)
C11-C3-C4-C5	178.2(8)
N1-C5-C4-C3	0.4(12)
C6-C5-C4-C3	-177.0(8)
C6-C7-C8-C9	-0.9(14)
C6-C7-C8-C15	179.1(8)
C10-C9-C8-C7	1.6(14)
C10-C9-C8-C15	-178.4(8)
C7-C8-C15-C16	-113.4(10)
C9-C8-C15-C16	66.6(12)
C7-C8-C15-C17	6.7(13)
C9-C8-C15-C17	-173.3(9)
C7-C8-C15-C18	130.2(10)
C9-C8-C15-C18	-49.9(12)
C35-C34-C33-C32	2.9(15)
C35-C34-C33-C36	-178.8(10)
C19-C20-C21-C26	173(11)
C19-C20-C21-C22	-8(12)
C33-C34-C35-C30	-1.3(15)
C31-C30-C35-C34	-0.7(14)
C29-C30-C35-C34	178.3(9)
C4-C3-C11-C12	-0.1(13)
C2-C3-C11-C12	-178.9(9)
C4-C3-C11-C14	121.4(10)
C2-C3-C11-C14	-57.4(12)
C4-C3-C11-C13	-119.0(10)
C2-C3-C11-C13	· 62.2(12)
C5-N1-C1-C2	-2.7(14)
Pt-N1-C1-C2	177.6(7)
N1-C1-C2-C3	0.1(15)
C4-C3-C2-C1	2.7(14)

·

C11-C3-C2-C1	-178.4(9)
C22-C21-C26-C25	-0.1(15)
C20-C21-C26-C25	179.5(9)
C34-C33-C32-C31	-2.5(16)
C36-C33-C32-C31	179.3(10)
C33-C32-C31-C30	0.4(17)
C35-C30-C31-C32	1.2(15)
C29-C30-C31-C32	-177.9(10)
C21-C26-C25-C24	2.1(18)
C22-C23-C24-C25	2(2)
C22-C23-C24-C27	-177.5(12)
C26-C25-C24-C23	-3.0(18)
C26-C25-C24-C27	176.7(11)
C24-C23-C22-C21	0(2)
C26-C21-C22-C23	-0.7(17)
C20-C21-C22-C23	179.7(11)
C60-C61-C62-C60#1	-7(2)
C62-C61-C60-C62#1	8(2)
C72-C71-C70-C72#2	2(3)
C70-C71-C72-C70#2	-2(3)

Symmetry transformations used to generate equivalent atoms:
#1 -x+2,-y+1,-z+1   #2 -x+1,-y+2,-z+2
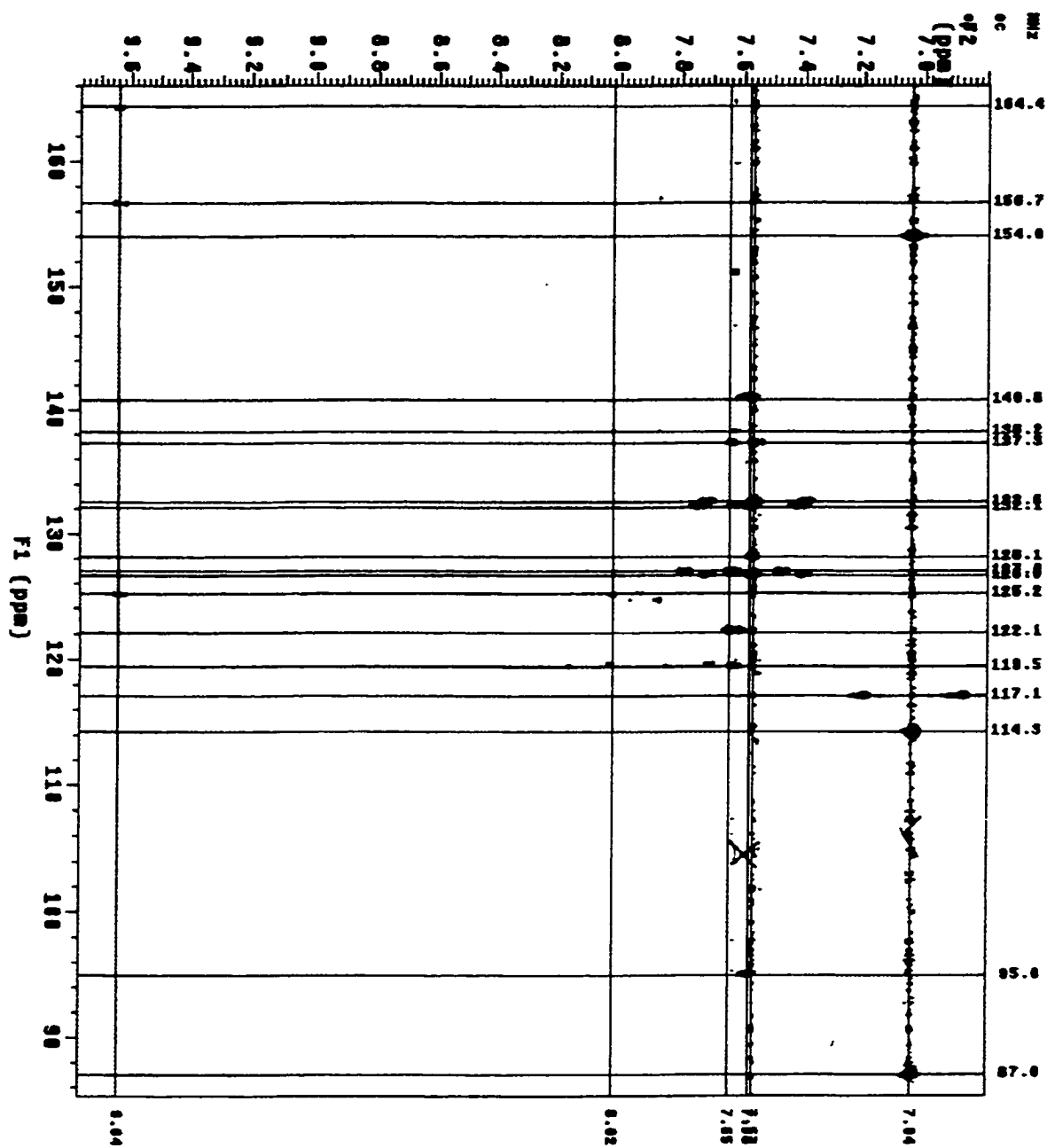
Figure A-1. Indirect ^{13}C NMR of square **4-27**
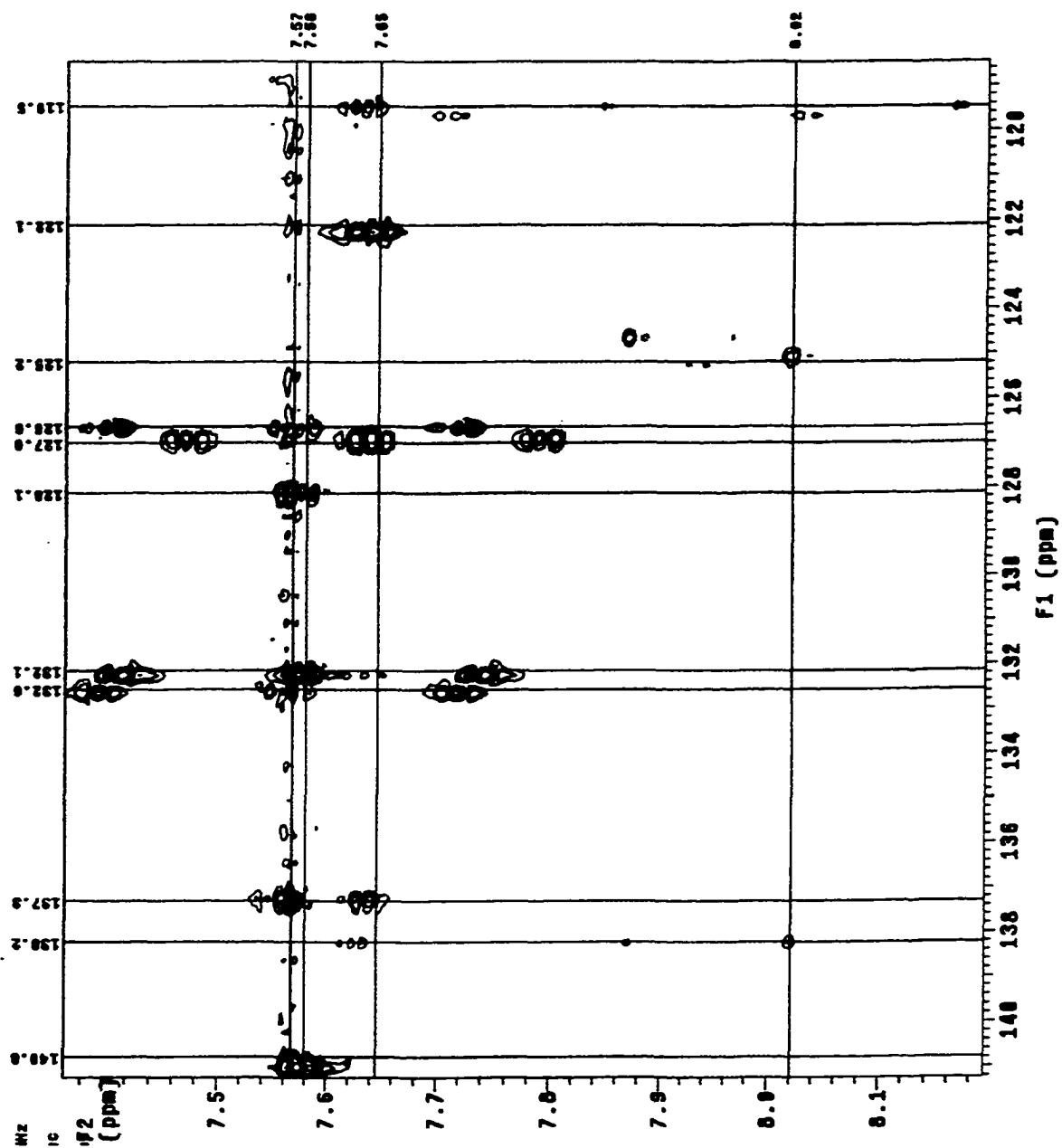
Figure A-2. Indirect ^{13}C NMR of square **4-27**
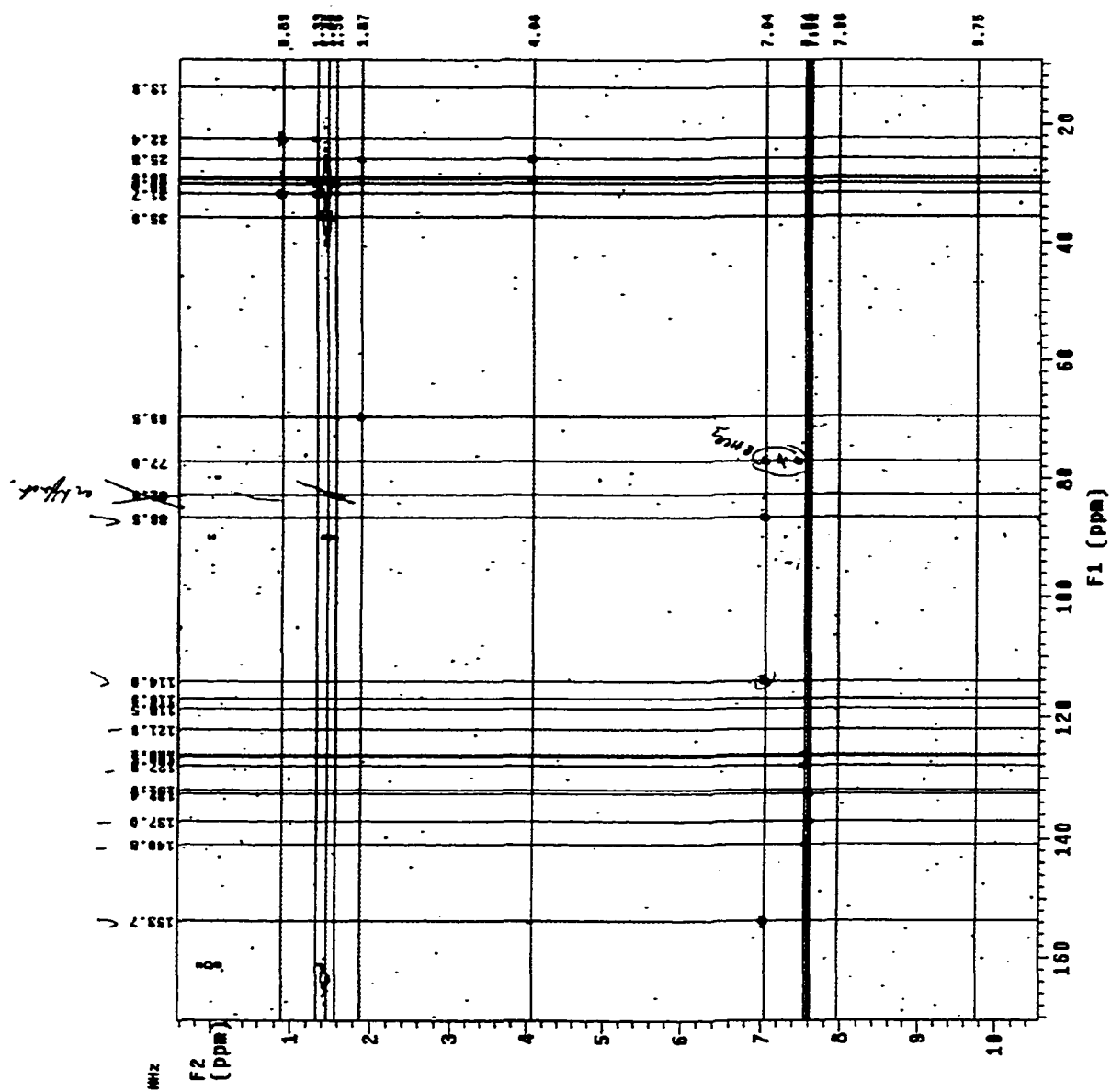
Figure A-3. Indirect ^{13}C NMR of square **4-27**
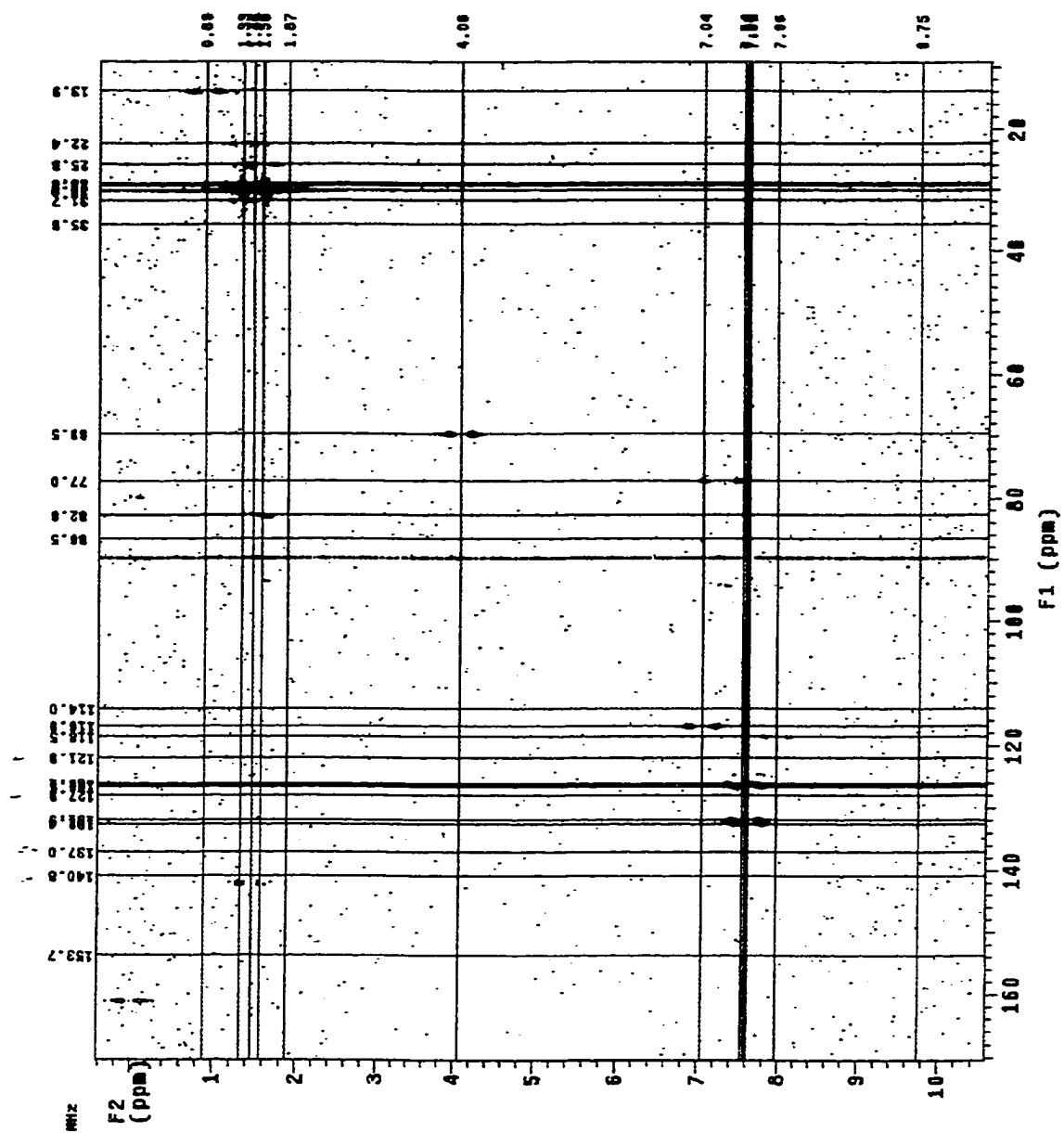
Figure A-4. Indirect ^{13}C NMR of square **4-27**
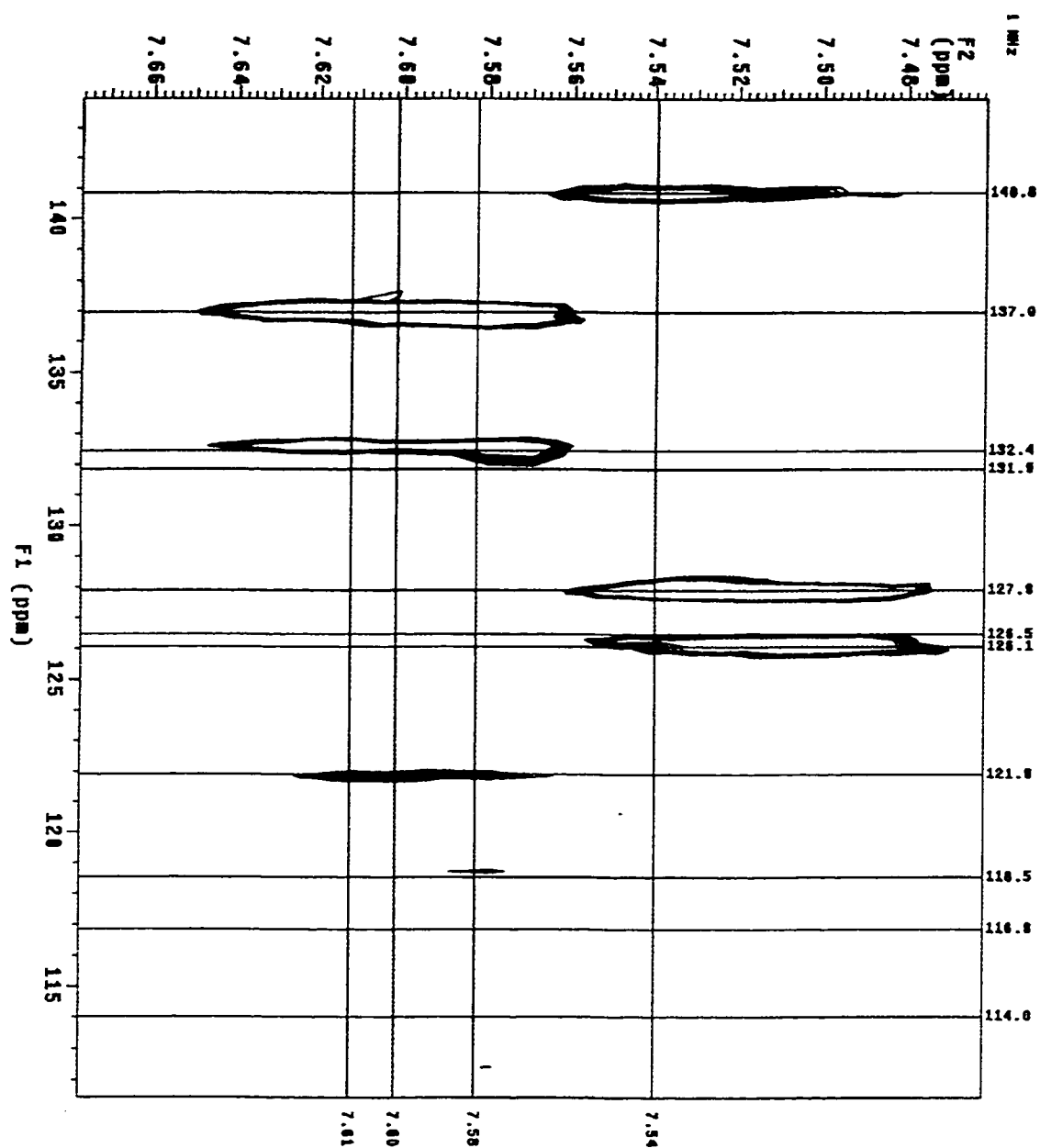
Figure A-5. Indirect ^{13}C NMR of square **4-27**
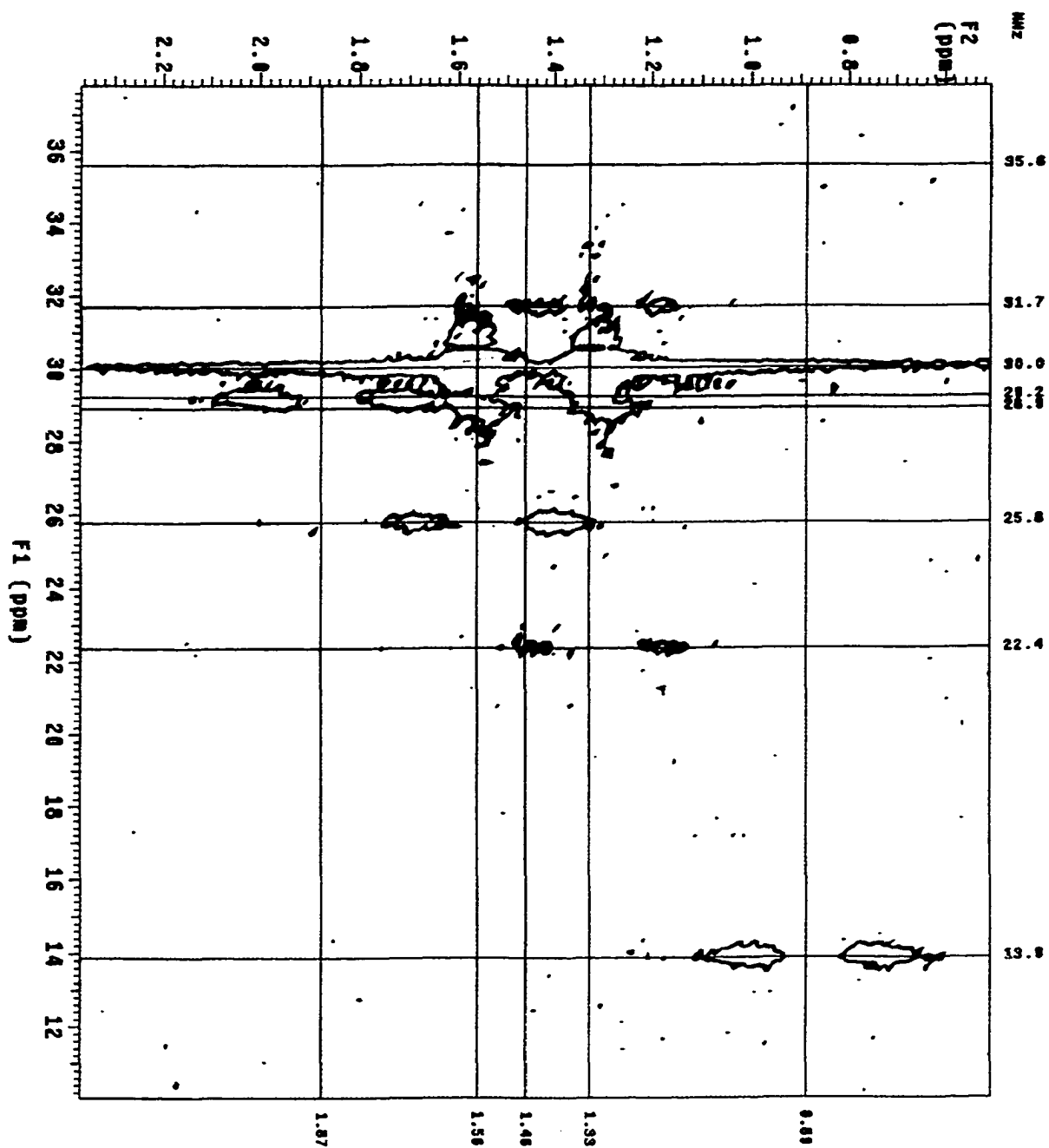
Figure A-6. Indirect ^{13}C NMR of square **4-27**
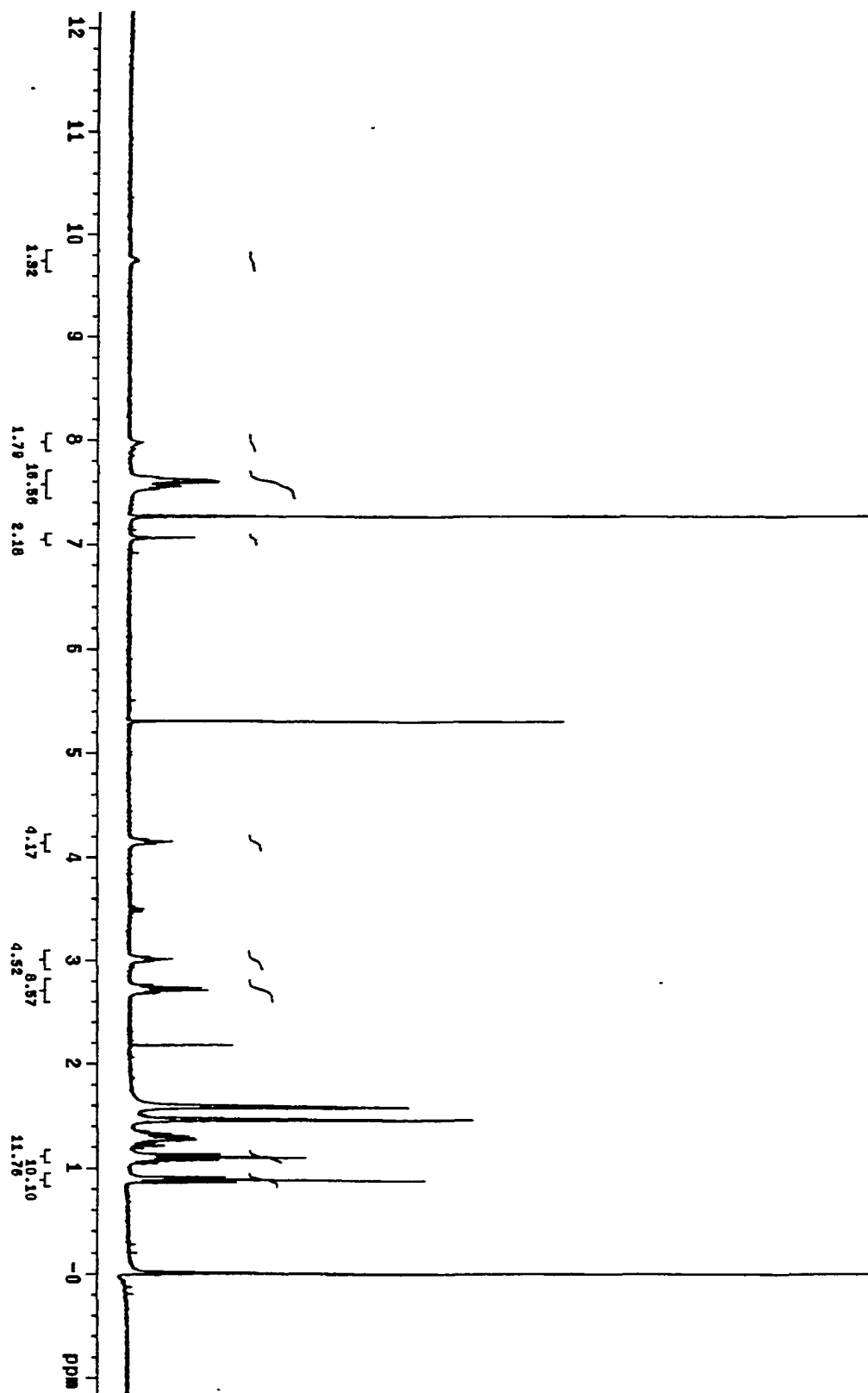
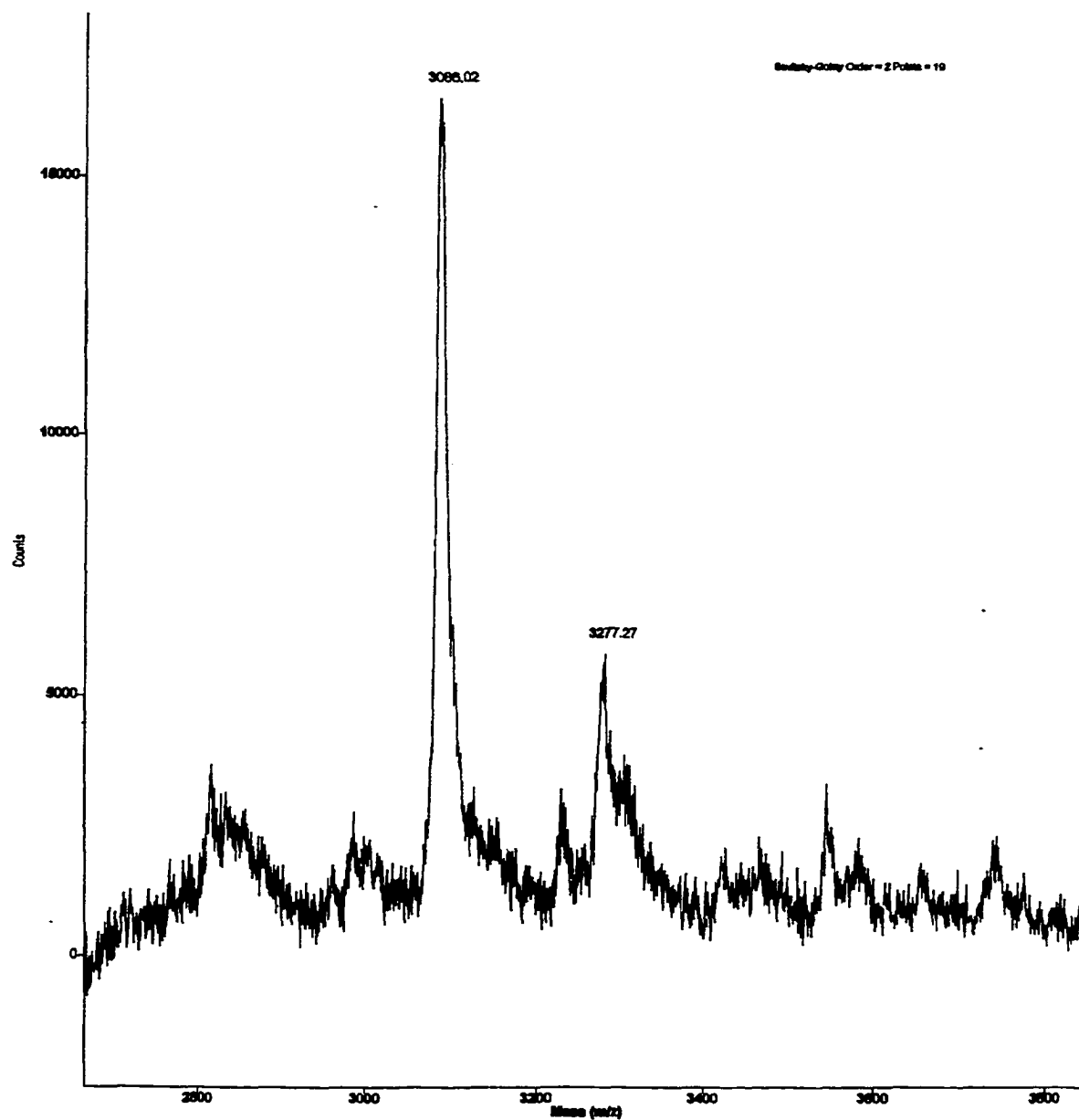**Figure A-7.** ^{1}H NMR of Amino square **4-28**.

Figure A-8. MALDI-TOF of triangle **5-49**.
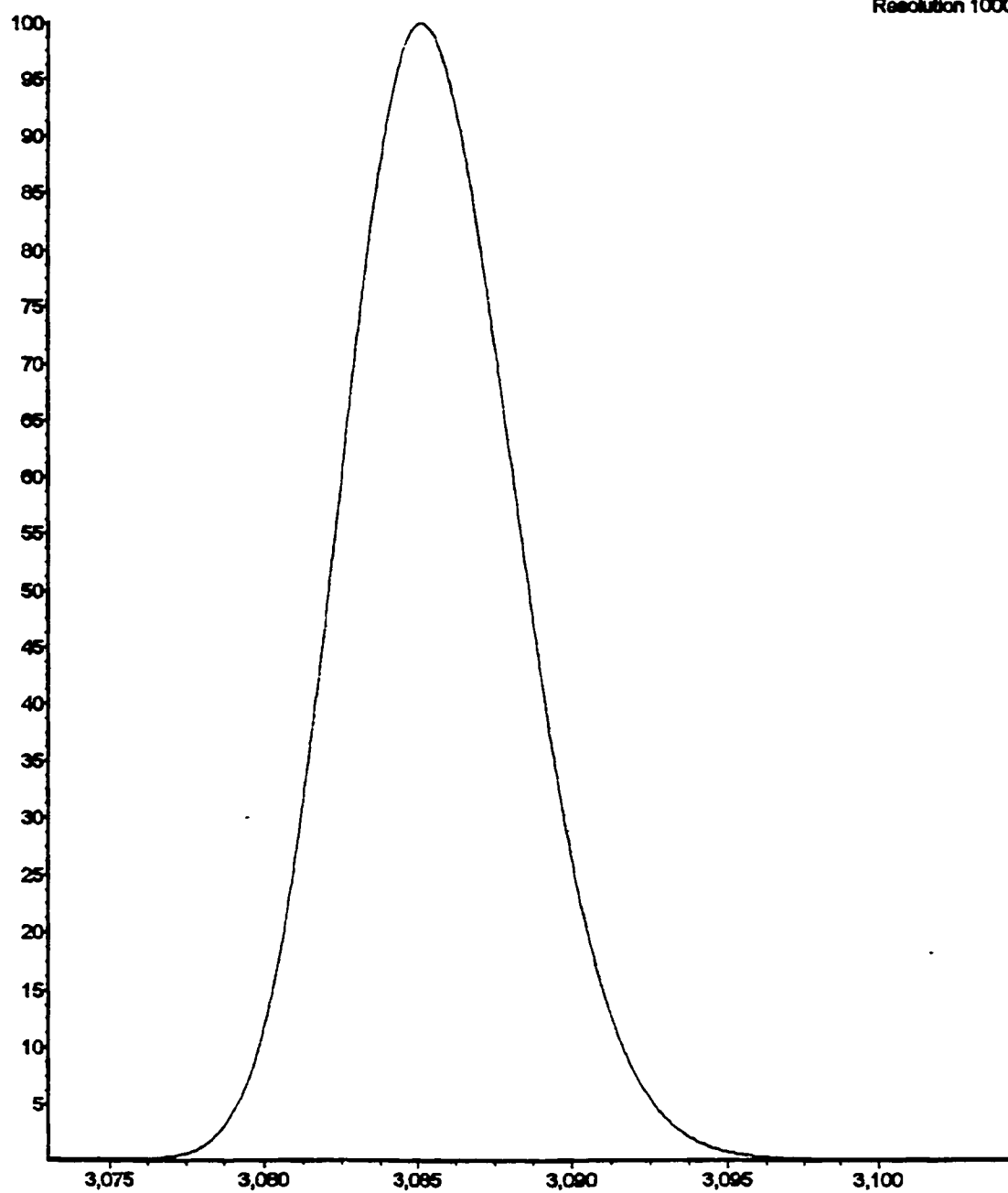
C171 H169 N6 O12 Pt3
Resolution 1000

Figure A-9. Generated isotope pattern

LIST OF REFERENCES

1.   Hudson, Alvin; Nelson, Rex. *Universe & Physics;* Harcourt Brace Jovanovich: New York, **1982**.

2.   Rurro, Nicholas J. *Modern Molecular Photochemistry;* Benjamin Cummings: Menlo Park **1978**.

3.   Fox, M. A.; Chanon, M. *Photoinduced Electron Transfer;* Elsivier: New York, **1988**.

4.   Pine, Stanley H. *Organic Chemistry;* McGraw Hill: New York, 1987.

5.   Seekamp, C. S. *Ann Chim. Phys.* **1805**, *56,* 142.

6.   Calven J.G., Pifts, J.N., Jr. *Photochemistry;* Wiley-Interscience: New York, 1966.

7.   Balzani, Vincenzo; Scandola, Franco. *Supramolecular Photochemistry;* Ews Harwood: New York, **1991**.

8.   Kurreck, Harry; Huber, Martina. *Angew. Chem. Int. Ed. Engi.* **1995**, *34*, 849.

9.   Gust, Devens; Moore, Thomas A.; Liddell, Paul A.; Nemeth, Gregory A.; Makings, Lewis R.; Moore, Ana L.; Barren Donna; Pessiki, Peter J.; Bensasson, Ren6 V.; Rouge, Michel; Chachaty, Claude; DeSchryver, F.C.; Van der Auweraer, M.; Holzwarth, Alfred R.; Connolly, John S. *J Am. Chem. Soc.* **1987**, *109*, 846.

10.   Marcus, KA. *J Chem. Phys.* **1956**, *24,* 966.

11.   Marcus, KA. *J Chem. Phys.* **1956**, *24,* 979.

12.   Marcus, KA. *Faraday Discuss. Chem. Soc.* 1960, *29,* 2 1.

13.   Hush, N.S. *J. Chem. Phys.* **1958**, *28,* 962.

14.   Marcus, KA.; Sutin, N. *Biochim. Biophys. Acta* **1985**, *811*, 265.

221

15. Sutin, N.; Bnmschwig, B.S. *ACS Symp. Ser.* **1982,** *198,*_105.

16. Sutin, *N. Acc. Chem. Res.* **1982,** *15,*_275.

17. Newton, M.D.; Sutin, *N. Annu. Rev. Phys. Chem.* **1984,** *35,* 437.

18. Suppan, Paul. *Topics in Current Chemistry*; Springer-Veriag: New York, **1992,** p. 65.

19. Sutin, N. *J Phys. Chem.* **1986,** 90, 3465.

20. PatWasiewlewski Michael R. *Chem. Rev.* **1992,** 92. 43 **5.**

21. Wasielewski, Michael R.; Niemczyk. M.P.; Svee, W.A.; Pewitt, E.B. J *Am. Chem. Soc.* **1985,***107,* 1080.

22. Winstein, S.; Clipinger, E.; Fainberg, A. H.; Robinson, G. C. J *Am. Chem. Soc.* **1954,** *76,*_2597.

23. Patil, A. Ao.; Heeger, A. J.; Wudl, F. *Chem. Rev.* **1988,** *88,* 183.

24. Davey, A. P.; Elliott, S.; O-Connor, O.; Blau, W. *Chem. Commun.* **1995,** *1433.*

25. Skotheim, T. A.; Elsenbaumer, R. L.; Reynolds, J. R. *Handbook of Conducting Polymers*; 2nd ed.; Marcel-Dekker; New York, **1988.**

26. Bredas, J. L.; Silbey, R. *Conjugated Polymers: The Novel Science and Technology of Highly Conducting and Nonliniear Aptically Active Materials*; Kluwer: Boston, **1991.**

27. Moroni, M.; Le Moigne, J.; Luzzati, S. *Macromol.* **1994,** *27,* 562.

28. Bjornholm, T.; Greve, D. R.; Geisler, T.; Peterson, J. C.; Jayaraman, M.; McCullough, R. D. *Synth. Met.* **1997,** *84,* 531.

29. Burroughs, J. H.; Bradley, D. D. C.; Brown, A. R.; Marks, R. N.; Mackay, K.; Friend, R. H.; Burn, P. L.; *Nature* **1990,** *347,* 539.

30. Baigent, D. R.; Hamer, P. J.; Friend, R. H.; Moratti, S. C.; Holmes, A. B.; *Synth. Met.* **1995,** *71,* 2175.

31. Green, .; Leditzky, G.; Ullrich, B.; Leising, G. *Adv. Mater.* **1992,** *4,* 36.

32.   Greenham, N. C.; Brown, A. R.; Bradley, D. D. C.; Friend, R. H. *Synth Met.* **1996**, *55-57*, 4134.

33.   Joshi, N. V. *Photoconductivity Art, Science, and Technology*; Marcel Dekker: New York, **1990**.

34.   Takiguchi, T.; Park, D. H.; Ueno, H.; Yoshino, K. *Synth. Met.* **1987**, *17*, 657.

35.   Lee, C. H.; Yu, G.; Moses, D.; Pakbaz, K.; Zhang, C.; Sariciftci, N. S.; Heeger, A. J.; Wudl, F. *Phys. Rev. B* **1993**, *48*, 15425.

36.   Moerner, W. E.; Silence, S. M. *Chem. Rev.* **1994**, *94*, 127.

37.   Yu, L; Chan, W. K.; Bao, Z. *Acc. Chem. Res.* **1996**, *29*, 13.

38.   Zhou, Q.; Swager, T. M. *J. Am. Chem. Soc.* **1995**, *117*, 12593.

39.   Zhu, S. S.; Carroll, P. J.; Swager, T. M. *J. Am. Chem. Soc.* **1996**, *118*, 8713

40.   Wang, B. Wasielewski, M. R. *J. Am. Chem. Soc.* **1997**, *119*, 12.

41.   Jones, L.; Pearson, D. L.; Tour, J. M. *Pure & Appl. Chem.* **1996**, *68*, 145.

42.   Tour, J. M. *Chem. Rev.* **1996**, *96*, 537.

43.   Rothberg, L. J.; Yan, M.; Papadimitrakopoulos, F.; Galvin, M. E.; Kwock, E. W.; Miller, T. M. *Synth Met.* **1996**, *80*, 41.

44.   Monkman, A. P.; Burrows, H. D.; Miguel, M. d. G.; Hamblett, I. *Chem. Phys. Lett.* **1999**, *307*, 303.

45.   Chandross, M.; Mazumdar, S. *Phys. Rev. B.* **1997**, *55*, 1497.

46.   Chen, L. Z.; Jager, W. J. H.; Niemczyk, M. P.; Wasielewski, M. R. *J. Phys. Chem. A* **1999**, *103*, 4341.

47.   Wautlet, P.; Moroni, M.; Oswald, L.; Le Moigne, J.; Pahm, A.; Bigot, J. Y. *Macromol.* **1996**, *29*, 446.

48.   Swager, T. M.; Gil, C. J.; Wrighton, M. S. *J. Phys. Chem.* **1995**, *99*, 4886.

49.   Xu, B.; Holdcraft, S. *J. Am. Chem. Soc.* **1993**, *115*, 8447.

50. Xu, B.; Holdcraft, S. *Adv. Mater.* **1994**, *6*, 325.

51. Ley, K. D.; Whittle, C. E.; Bartberger, M. D.; Schanze, K. S. *J. Am. Chem. Soc.* **1997**, *119*, 3423.

52. Ley, K. D.; Schanze, K. S. *Coord. Chem. Rev.* **1998**, *171*, 287.

53. Esker, J. L.; Newcomb, M. In *Advances in Heterocyclic Chemistry*; Katritzky, A. R., Ed.: Academic: San Diego, **1993**.

54. Newcomb, M.; Deeb, T. M.; Marquardt, D. J. *Tetrahedron* **1990**, *46*, 2317.

55. Bowman, W. R.; Clark, D. N.; Marmon, R. J. *Tetrahedron Lett.* **1991**, *32*, 6441.

56. Beckwith, A. L. J.; Maxwell, B. J.; Tsanaktsidis, J. *Aust. J. Chem.* **1991**, *44*, 1809.

57. Murphy, J. A.; Dickinson, J. M. *Tetrahedron* **1992**, *48*, 1317.

58. Dowd, P.; Choi, S.-C. *Tetrahedron* **1991**, *47*, 4847.

59. Maeda, Y.; Ingold, K. U. *J. Am. Chem. Soc.* **1980**, *102*, 328.

60. Newcomb, M.; Horner, J. H. Shahin, H. *Tetrahedron Lett.* **1993**, *35*, 5523.

61. Musa, A. M.; Horner, J. H.; Shahin, H.; Newcomb, M. *J. Am. Chem. Soc.* **1996**, *118*, 3862.

62. Coehn, S. G.; Parola, A. H.; Parsons, G. H., Jr. *Chem. Rev.* **1973**, *73*, 141.

63. Parker, V. D.; Tilset, M. *J. Am. Chem. Soc.* **1991**, *113*, 8778.

64. Goez, M.; Sartorius, I. *J. Am. Chem. Soc.* **1993**, *115*, 11123.

65. Anne, A.; Hapiot, P.; Moiroux, J.; Neta, P.; Saveant, J. M. *J. Am. Chem. Soc.* **1992**, *114*, 4694.

66. Horner, J. H.; Martinez, F. N.; Musa, O. M.; Newcomb, M.; Shahin, H. *J. Am. Chem. Soc.* **1995**, *117*, 11124.

67. Della Ciana, L.; Hamachi, I.; Meyer, T. J. *J. Org. Chem.* **1989**. *54*, 1731.

68.   Sullivan, B. P.; Abruan, H.; Finklea, H. O.; Salmon, D. J.; Nagle, J. K.; Meyer, T. J.; Sprintschnik, H. *Chem. Phys. Lett.* **1978**, *58*, 389.

69.   Root, M. J.; Deutsch, E.; Sullivan, J. C.; Meisel, D. *Chem. Phys. Lett. 1983*, *101*, 353.

70.   Westmoreland, T. D.; Le Bozec, H.; Murray, R. W.; Meyer, T. J. *J. Am. Chem. Soc.* **1983**, *105*, 3932.

71.   Chen, P.; Danielson, E.; Meyer, T. J. *J. Phys. Chem.* **1988**, *92*, 3701.

72.   Chen, P.; Curry, M.; Meyer, T. J. *Inorg. Chem.* **1989**. *28*, 2271.

73.   Meyer, T. J. Prog. *Inorg Chem.* **1983**, *30*, 389.

74.   Perkins, T. A.; Humer, W.; Netzel, T. L.; Schanze, K. S. *J. Phys. Chem.* **1990**, *94*, 2229.

75.   MacQueen, D. B.; Schanze, K. S. *J. Am. Chem. Soc.* **1991**, *113*, 7470.

76.   Baralt, E.; Boudreaux, E. A.; Demas, J. N.; Lenhert, P. G.; Lukehart, C. M.; McPhail, D. R.; Myers, J. B.; Sacksteder, L.; True, W. R. *Organometallics* **1989**, *8*, 2417-2430.

77.   Sacksteder, L.; Baralt, E.; DeGraff, B. A.; Lukehart, C. M.; Demas, J. N. *Inorganic Chemistry* **1991**, *30*, 3955-3957.

78.   Sacksteder, L.; Baralt, E.; DeGraff, B. A.; Lukehart, C. M.; Demas, J. N. *Inorganic Chemistry* **1991**, *30*, 2460-2476.

79.   Kohler, A.; Younus, M.; Al-Mandhary, M. R. A.; Raithby, P. R.; Khan, M. S.; Friend, R. H. *Synthetic Metals* **1999**, *101*, 246-247.

80.   Chawdhury, N.; Kohler, A.; Friend, R. H.; Younus, M.; Long, N. J.; Raithby, P. R.; Lewis, J. *Macromolecules* **1998**, *31*, 722-727.

81.   Chawdhury, N.; Kohler, A.; Friend, R. H.; Wong, W.-Y.; Lewis, J.; Younus, M.; Raithby, P. R.; Corcoran, T. C.; Al-Mandhary, M. R. A.; Khan, M. S. Journal of *Chemical Physics* **1999**, *110*, 10, 4963-4970.

82.   Miskowski, V. M.; Houlding, V. H. *Coordination Chemistry Reviews* **1991**, *111*, 145. B) Che, C. M.; Wan, K. T.; He, L. Y.; Poon, C. K.; Yan, V. W. W. *Chemical Communications* **1989**, 943. C) Wan, K. T.; Che, C. M. Chemical Communications 1990, 140. D) Wan, K. T.; Cho, K. C. *Journal of the Chemical Society, Dalton Transactions* **1991**, 1077. E) Zuleta, J. Al; Burberry, M. S.;

Eisenberg, T. *Coordination Chemistry Reviews* **1990**, *97*, 47. F) Maestri, M.; Deuschel-Cornioley, C.; von Zelewsky, A. *Coordination Chemsitry Reviews* **1991**, *111*, 117. G) Kunkley, A.; Vogler, A. *Journal of the American Chemical Society* **1990**, *112*, 5625.

83.   Miskowski, V. M.; Houlding, V. H.; Che, C.-M.; Wang, Y. *Inorganic Chemistry* **1993**, *32*, 2518-2524.

84.   Chan, C.-W.; Cheng, L.-K.; Che, C.-M. *Coordination Chemistry Reviews*, **1994**, *132*, 87-97.

85.   Adams, C. J.; James, S. L.; Raithby, P. R. *Chemical Communications* **1997**, 2155-2166.

86.   James, S. L.; Younus, M.; Raithby, P. R.; Lewis, J. *Journal of Organometallic Chemistry* **1997**, *543*, 233-235.

87.   Adams, C. J.; Raithby, P. R. *Journal of Organometallic Chemistry* **1999**, *578*, 178-185.

88.   Hissler, M.; Connick, W. B.; Geiger, D. K.; McGarrah, J. E.; Lipa, D.; Lachicotte, R. L.; Eisenberg, R. *Inorganic Chemistry* **2000**, *39*, 447-457.

89.   Szewczyk, J.; Gryff-Keller, A. *Journal of Organometallic Chemistry* **1992**, *424*, 41-47.

90.   Hegishi, E.; Kotora, M.; Xu, C. *Journal of Organic Chemistry* **1997**, *62*, 25, 8957, 8960.

91.   La Clair, J. J. *Journal of the American Chemical Society* **1997**, *119*, 33, 7676-7684.

92.   Leonard, K.; Nelen, M.; Raghu, M.; Detty, M. R. *Journal of Heterocyclic Chemistry* **1999**, *36*, 3, 707-718.

93.   Michel, P.; Gennet, D.; Rassat, A. *Tetrahedron Letters* **1999**, *40*, 49, 8575-8578.

94.   Crisp, G. T.; Flynn, B. L. *Journal of Organic Chemsitry* **1993**, *58*, 24, 6614-6619.

95.   Soderquist, J. A.; Rane, A. M.; Matos, K.; Ramos, J. *Tetrahedron Letters* **1995**, *36*, 38, 6847-6850.

96.   Carran, J.; Waschbuesch, R.; Marinetti, A.; Savignac, P. *Synthesis* **1996**, *12*, 1494-1498.

97. Belser, P.; Zelewsky, A. V. *Helvetica Chimica Acta* **1980**, *63*, 6, 1675-1702.

98. Patterson, B. T.; Keene, F. R. *Australian Journal of Chemistry* **1998**, *51*, 11, 999-1002.

99. Elliot, C. M.; Hershenhart, E. J. *Journal of the American Chemical Society* **1982**, *104*, 26, 7519-7526.

100. Lehn, J.-M.; Ziessel, R. *Helvetica Chimica Acta* **1988**, *71*, 1511-1516.

101. Ohshiro, N.; Takei, F.; Onitsuka, K.; Takahashi, S. J. Organometallic Chem. 1998, 569, 195.

102. Stang, P. J.; Zhdankin, V. V. *Chem. Rev.* **1996**, *96*, 1123.

103. Stang, P. J.; Chen, K. *J. Am. Chem. Soc.* **1995**, *117*, 1667.

104. Stang, P. J.; Chen, K.; Arif, A. M. *J. Am. Chem. Soc.* **1995**, *117*, 8793.

105. Slone, R. V.; Hupp, J. T.; Stern, C. L.; Albrecht-Schmitt, T. E. *Inorg. Chem.* **1996**, *35*, 4096.

106. Slone, R. V.; Benkstein, K. D.; Belanger, S.; Hupp, J. T.; Guzie, I. A.; Rheinghold, A. L. *Coord. Chem. Rev.* **1998**, *171*, 221.

107. Slone, R. V.; Yoon, D. I.; Calhoun, R. M.; Hupp, J. T. *J. Am. Chem. Soc.* **1995**, *117*, 11813.

108. Maverick, A. W.; Buckingham, S. C.; Yao, Q.; Bradbury, J. R. Stanley, G. G. *J. Am. Chem. Soc.* **1986**, *108*, 7430.

109. Fujita, M.; Ibukuro, F.; Hagihara, H.; Ogura, K. *Nature* **1994**, *367*, 720.

110. Whiteford, J. A.; Rachlin, E. M.; Stang, P. J. *J. Am. Chem. Soc.* **1997**, *119*, 2524.

111. Manna, J.; Kuehl, C. J.; Whiteford, J. A.; Stang, P. J. Muddiman, D. C.; Hofstadler, S. A.; Smith, R. D. *J. Am. Chem. Soc.* **1997**, *119*, 11611.

112. Bradshaw, J. D.; Guo, Li, Tessier, C. A.; Youngs, W. J. *Organometallics* **1996**, *15*, 2582.

113. Zhang, D.; McConville, D. B.; Tessier, C. A.; Youngs, W. J. *Organometallics*, **1997**, *16*, 824.

114. ALQaisi, S. M.; Galat, K. J.; Chai, M.; Ray, D. G.; Rinaldi, P. L.; Tessier, C. A.; Youngs, W. J. *J. Am. Chem. Soc.* **1998**, *120*, 12149.

115. Onitsuka, K.; Yamamoto, S.; Takahashi, S. *Angew. Chem. Int. Ed.* **1999**, *38*, 174.

116. Staab, H. A.; Neuhoeffer, K. *Synthesis*, **1974**, 424.

117. Moore, J. S.; Zhang, J. *Angew. Chem. Int. Ed.* **1992**, *31*, 292.

118. Ruggli, P. *Liebigs. Ann. Chem.* **1912**, *392*, 92.

119. Tobe, Y.; Utsumi, N.; Nagano, A.; Naemura, K. *Angew. Chem. Int. Ed.* **1998**, *37*, 1285.

120. Staab, H.; Binning, F. *Chem. Ber.* **1967**, *100*, 293.

121. Hensel, V.; Lutzow, K.; Jakob, J.; Gessler, K.; Saenger, W.; Schluter, A.-D. *Angew. Chem. Int. Ed.* **1997**, *36*, 2654.

122. Anderson, H. L.; Sanders, J. K. M. *Angew. Chem. Int. Ed.* **1990**, *29*, 1400.

123. Hoger, S,; Enkelmann, V. *Angew. Chem. Int. Ed.* **1995**, *34*, 2713.

124. Hoger, S.; Meckenstock, A.-D.; Bonrad, K. *Chem. Eur. J.* **1999**, *5*, 1686.

125. Hoger, S. Meckenstock, A.-D.; Pellen, H. *J. Org. Chem.* **1997**, *62*, 4556.

BIOGRAPHICAL SKETCH

Born in Knoxville, TN as Carl Edgar Whittle, I have always gone by Ed. I am not sure why. I think it is a southern thing. Six months after I was born, my family moved to Bowling Green, KY where I spent the next 25 years. I began my education at T.C. Cherry Elementary School. I spent two years there and then my family moved to another school district, and was transferred to McNeil elementary, which was followed by Bowling Green Junior High School and then Bowling Green High. Memories of the times before high school are few and far between. In Junior High School, I played football, or should I say, I was on the team. When I asked the coach why I never played, his response was that I was too small and slow. Oh, well. In High School, I again was on the football team and again was too small to play. I took it upon myself to become big enough to play through weight training. By my senior year, I was the strongest on the offensive line.

I graduated from high school in the top 10% of my class, which was pretty good considering I never cracked a book. Schoolwork seemed to come easy to me. I decided to stay in my home town and attend Western Kentucky University as a pre-vet major. This changed relatively quickly. I thought that since schoolwork came easy to me in high school, it had to come easy to me in college as well. In my first chemistry class I received a D. Oh my, this stuff wasn't easy to me. This proceeded to be the case for the first two years of college.
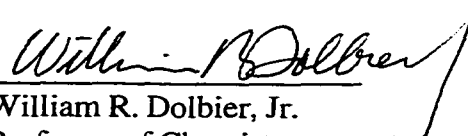
I retook freshman chemistry, got through it, and then got into sophomore organic chemistry. This stuff was very interesting and finally something in college did come easy to me. I credit that mostly to my excellent professor, Dr. Robert Holman. He saw that I liked organic chemistry and asked if I would join his research group. I began research with him and quickly developed a love of the research. I spent all my free time in the lab making new compounds, causing fires, and all the fun things that come with doing research. During this time I met my now wife Kelley Moran. We became good friends first and then started dating. Shortly after that time, she graduated and left for graduate school at the University of Florida. After I graduated, I wasn't sure what I wanted to do, so Dr. Holman suggested that I stay a couple more years at Western and obtain a Master's Degree. During this time, Kelley and I kept in constant contact. I would drive down to see her in Florida fairly regularly. I finished my M.S. and decided that I wanted to continue my education and I also wanted to be with my girlfriend. For these reasons, I followed her lead to the University of Florida.

After I applied to UF, Dr. Kirk Schanze contacted me. He apparently liked what I put in my application, I guess. His work seemed very interesting and I came to UF in the summer to start research with him. After that summer, I decided officially to join his research group and have never regretted that decision. My work at UF has been very challenging and interesting. Now as I am about to finish my career here, I am looking forward to finding employment and continue my education for I still have a lot to learn.
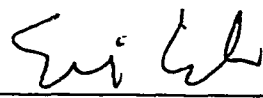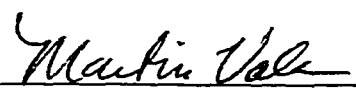
I certify that I have read this study and that in my opinion it conforms to acceptable standards of scholarly presentation and is fully adequate, in scope and quality, as a thesis for the degree Doctor of Philosophy.

Kirk S. Schanze, Chairman
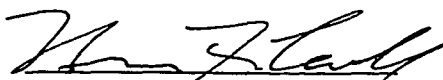Professor of Chemistry

I certify that I have read this study and that in my opinion it conforms to acceptable standards of scholarly presentation and is fully adequate, in scope and quality, as a thesis for the degree Doctor of Philosophy.

William R. Dolbier, Jr.
Professor of Chemistry

I certify that I have read this study and that in my opinion it conforms to acceptable standards of scholarly presentation and is fully adequate, in scope and quality, as a thesis for the degree Doctor of Philosophy.

Eric J. Enholm
Professor of Chemistry

I certify that I have read this study and that in my opinion it conforms to acceptable standards of scholarly presentation and is fully adequate, in scope and quality, as a thesis for the degree Doctor of Philosophy.

Martin T. Vala
Professor of Chemistry

I certify that I have read this study and that in my opinion it conforms to acceptable standards of scholarly presentation and is fully adequate, in scope and quality, as a thesis for the degree Doctor of Philosophy.

Bruce Carroll
Professor of Aerospace
Engineering, Mechanics, &
Engineering Sciences

This dissertation was submitted to the Graduate Faculty of the Department of Chemistry in the College of Liberal Arts and Sciences and to the Graduate School and was accepted as partial fulfillment of the requirements for the degree of Doctor of Philosophy.

May 2001

Dean, Graduate School